Spine: 5 mm

Volume 73 • Issue 3 • July-September 2024

Journal of The Anatomical Society of India • Volume 73 • Issue 3 • July-September 2024 • Pages 197-296

ISSN : 0003-2778

Scopus
Indexed

JOURNAL OF THE ANATOMICAL SOCIETY OF INDIA

An International Journal

An Official Publication of Anatomical Society of India

Full text online at **https://journals.lww.com/joai**
Submit articles online at **https://review.jow.medknow.com/jasi**

Editor-in-Chief
Dr. Vishram Singh

Wolters Kluwer

Medknow

Journal of the Anatomical Society of India

Print ISSN: 0003-2778

GENERAL INFORMATION

About the Journal

Journal of the Anatomical Society of India (ISSN: Print 0003-2778) is peer-reviewed journal. The journal is owned and run by Anatomical Society of India. The journal publishes research articles related to all aspects of Anatomy and allied medical/surgical sciences. Pre-Publication Peer Review and Post-Publication Peer Review Online Manuscript Submission System Selection of articles on the basis of MRS system Eminent academicians across the globe as the Editorial board members Electronic Table of Contents alerts Available in both online and print form. The journal is published quarterly in the months of January, April, July and October.

Scope of the Journal

The aim of the *Journal of the Anatomical Society of India* is to enhance and upgrade the research work in the field of anatomy and allied clinical subjects. It provides an integrative forum for anatomists across the globe to exchange their knowledge and views. It also helps to promote communication among fellow academicians and researchers worldwide. The Journal is devoted to publish recent original research work and recent advances in the field of Anatomical Sciences and allied clinical subjects. It provides an opportunity to academicians to disseminate their knowledge that is directly relevant to all domains of health sciences.

The Editorial Board comprises of academicians across the globe.

JASI is indexed in Scopus, available in Science Direct.

Abstracting and Indexing Information

The journal is registered with the following abstracting partners:

Baidu Scholar, CNKI (China National Knowledge Infrastructure), EBSCO Publishing's Electronic Databases, Ex Libris – Primo Central, Google Scholar, Hinari, Infotrieve, Netherlands ISSN center, ProQuest, TdNet, Wanfang Data

The journal is indexed with, or included in, the following:

SCOPUS, Science Citation Index Expanded, IndMed, MedInd, Scimago Journal Ranking, Emerging Sources Citation Index.

Impact Factor® as reported in the 2023 Journal Citation Reports® (Clarivate Analytics, 2024): 0.2

Information for Authors

Article processing and publication charges will be communicated by the editorial office. All manuscripts must be submitted online at https://review.jow.medknow.com/jasi.

Subscription Information

A subscription to JASI comprises 4 issues. Prices include postage. Annual Subscription Rate for non-members-		
Rates of Membership (with effect from 1.1.2022)		
	India	**International**
Ordinary membership	INR 1500	US $ 100
Couple membership	INR 2250	
Life membership	INR 8000	US $ 900
Subscription Rates (till 31st August)		
Individual	INR 6000	US $ 650
Library/Institutional Trade discount of 10% for agencies only	INR 12000	US $ 1000
Subscription Rates (after 31st August)		
Individual	INR 6500	US $ 700
Library/Institutional	INR 12500	US $ 1050
The Journal of Anatomical Society of India (ISSN: 0003-2778) is published quarterly **Subscriptions** are accepted on a prepaid basis only and are entered on a calendar year basis. Issues are sent by standard mail Priority rates are available upon request.		

Information to Members/Subscribers

All members and existing subscribers of the Anatomical Society of India are requested to send their membership/existing subscription fee for the current year to the Treasurer of the Society on the following address: Prof (Dr.) Punit Manik, Treasurer, ASI, Department of Anatomy, KGMU, Lucknow - 226003. Email: punitamanik@yahoo.co.in. All payments should be made through an account payee bank draft drawn in favor of the **Treasurer, Anatomical Society of India,** payable at **Lucknow** only, preferably for **Allahabad Bank, Medical College Branch, Lucknow.** Outstation cheques/drafts must include INR 70 extra as bank collection charges.

All complaints regarding non-receipt of journal issues should be addressed to the Editor-in-Chief, JASI at editorjasi@gmail.com. The new subscribers may, please contact wkhlrpmedknow_subscriptions@wolterskluwer.com.

Requests of any general information like travel concession forms, venue of next annual conference, etc. should be addressed to the General Secretary of the Anatomical Society of India.

For mode of payment and other details, please visit www.medknow.com/subscribe.asp

Claims for missing issues will be serviced at no charge if received within 60 days of the cover date for domestic subscribers, and 3 months for subscribers outside India. Duplicate copies cannot be sent to replace issues not delivered because of failure to notify publisher of change of address. The journal is published and distributed by Wolters Kluwer India Pvt. Ltd. Copies are sent to subscribers directly from the publisher's address. It is illegal to acquire copies from any other source. If a copy is received for personal use as a member of the association/society, one cannot resale or give-away the copy for commercial or library use.

The copies of the journal to the subscribers are sent by ordinary post. The editorial board, association or publisher will not be responsible for non receipt of copies. If any subscriber wishes to receive the copies by registered post or courier, kindly contact the publisher's office. If a copy returns due to incomplete, incorrect or changed address of a subscriber on two consecutive occasions, the names of such subscribers will be deleted from the mailing list of the journal. Providing complete, correct and up-to-date address is the responsibility of the subscriber.

Nonmembers: Please send change of address information to subscriptions@medknow.com.

Advertising Policies

The journal accepts display and classified advertising. Frequency discounts and special positions are available. Inquiries about advertising should be sent to Wolters Kluwer India Pvt. Ltd, advertise@medknow. com.

The journal reserves the right to reject any advertisement considered unsuitable according to the set policies of the journal.

The appearance of advertising or product information in the various sections in the journal does not constitute an endorsement or approval by the journal and/or its publisher of the quality or value of the said product or of claims made for it by its manufacturer.

Copyright

The entire contents of the JASI are protected under Indian and international copyrights. The Journal, however, grants to all users a free, irrevocable, worldwide, perpetual right of access to, and a license to copy, use, distribute, perform and display the work publicly and to make and distribute derivative works in any digital medium for any reasonable non-commercial purpose, subject to proper attribution of authorship and ownership of the rights. The journal also grants the right to make small numbers of printed copies for their personal non-commercial use.

Permissions

For information on how to request permissions to reproduce articles/information from this journal, please visit https://journals.lww.com/joai.

Disclaimer

The information and opinions presented in the Journal reflect the views of the authors and not of the Journal or its Editorial Board or the Publisher. Publication does not constitute endorsement by the journal. Neither the JASI nor its publishers nor anyone else involved in creating, producing or delivering the JASI or the materials contained therein, assumes any liability or responsibility for the accuracy, completeness, or usefulness of any information provided in the JASI, nor shall they be liable for any direct, indirect, incidental, special, consequential or punitive damages arising out of the use of the JASI. The JASI, nor its publishers, nor any other party involved in the preparation of material contained in the JASI represents or warrants that the information contained herein is in every respect accurate or complete, and they are not responsible for any errors or omissions or for the results obtained from the use of such material. Readers are encouraged to confirm the information contained herein with other sources.

Addresses

Editorial Office

Dr. Vishram Singh, Editor-in-Chief, JASI
B5/3 Hahnemann Enclave, Plot No. 40, Sector 6, Dwarka Phase – 2,
New Delhi - 110 075, India.
Email: editorjasi@gmail.com

Published by

Wolters Kluwer India Pvt. Ltd
A-202, 2nd Floor, The Qube,
C.T.S. No.1498A/2 Village Marol, Andheri (East),
Mumbai - 400 059, India.
Phone: 91-22-66491818
Website: www.medknow.com

Printed at

Nikeda Art Printers Pvt. Ltd.,
Building No. C/3 - 14,15,16, Shree Balaji Complex, Vehele Road,
Village Bhatale, Taluka Bhiwandi, District Thane - 421302, India.

Journal of the Anatomical Society of India

Print ISSN: 0003-2778

EDITORIAL BOARD

Editor-in-Chief

Dr. Vishram Singh
MBBS, MS, PhD (hc), FASI, FIMSA
Adjunct Professor, Department of Anatomy, KMC, Mangalore, MAHE, Manipal, Karnataka

Joint-Editor

Dr. Murlimanju B.V
Associate Professor, Department of Anatomy, KMC, Mangalore, MAHE, Manipal, Karnataka

Managing Editor

Dr. C. S. Ramesh Babu
Associate Professor, Department of Anatomy, Muzaffarnagar Medical College, Muzaffarnagar, Uttar Pradesh

Associate Editor

Dr. D. Krishna Chaitanya Reddy
Assistant Professor, Department of Anatomy, KAMSRC, Hyderabad, Telangna

Section Editors

Clinical Anatomy
Dr. P. Vatasalaswamy, Director Academics,
D.Y. Patil, Medical College, Pune

Histology
Dr. G.P. Pal, Prof & Head,
Department of Anatomy, MDC & RC, Indore, India

Gross and Imaging Anatomy
Dr. Srijit Das, Department of Human and Clinical Anatomy,
College of Medicine and Health Sciences, Sultan Qaboos
University, Muscat, Oman

Neuroanatomy
Dr. T.S. Roy,
Prof & Head, Department of Anatomy,
NDMC Medical College, New Delhi

Medical Education
Dr. Anu Sharma, Professor of Anatomy DMCH, Ludhiana

Embryology
Dr. Deepti Shastri, Deputy Dean and Professor of
Anatomy, Vinayaka Mission K V Medical College,
Tamil Nadu

Genetics
Dr. Rima Dada,
Prof, Department of Anatomy, AIIMS, New Delhi, India

Dental Sciences
Dr. Rashi Singh, Professor
Department of Pediatric and Preventive
Dentistry SDC, GZB. NCR - New Delhi

National Editorial Board

Dr. M. Natrajan, Mumbai
Dr. Rajanigandha Vadagaonkar, Mangalore
Dr. Navneet Chauhan, Lucknow
Dr. Prashant Natekar, Goa
Dr. Daksha Dixit, Belgaum
Dr. S.K. Jain, Moradabad
Dr. P.K. Sharma, Lucknow
Dr. S. Senthil Kumar, Chennai
Dr. G. M. Mahesh, Chitradurga
Dr. Ruchira Sethi, Jaunpur,U.P.
Dr. Renu Chauhan, Delhi
Dr. Ashok Sahai, Agra
Dr. Anshu Sharma Chandigarh
Dr. T.C. Singel, Ahmedabad
Dr. Ajay Nene, Rajasthan
Dr. S.L. Jethani, Dehradun
Dr. Surajit Ghatak, Jodhpur
Dr. Brijendra Singh, Rishikesh
Dr. Ashok Nirvan, Ahemdabad

International Editorial Board

Dr. Yun-Qing Li, China
Dr. In-Sun Park, Korea
Dr. K.B. Swamy, Malaysia
Dr. Syed Javed Haider, Saudi Arabia
Dr. Pasuk Mahakknaukrauh, Thailand
Dr. Tom Thomas R. Gest, USA
Dr S. K. Saxena, USA
Dr. Chris Briggs, Australia
Dr. Petru Matusz, Romania
Dr. Min Suk Chung, South Korea
Dr. Veronica Macchi, Italy
Dr. Gopalakrishnakone, Singapore
Dr. Sunil Upadhyay, UK
Dr. SPd Singh UK

Journal of the Anatomical Society of India

Volume 73 | Issue 3 | July-September 2024

CONTENTS

continued...

CASE REPORTS

Neuroanatomical Basis of Dementia

Dementia is an umbrella term used for the loss of memory, thinking, and reasoning to such an extent that it interferes with a person's daily life and activities.

The common symptoms of dementia include:
- Memory problem, particularly in remembering recent events
- Increasing confusion
- Reduced concentration
- Personality and behavior changes
- Apathy and withdrawal or depression
- Loss of ability to do everyday tasks
- Struggling to follow conversation or find right word.

A little knowledge of learning, memory, and associated parts of the brain is essential to understand dementia better.

Learning is an acquisition of new facts while memory is the storage and recall of these facts.

Types of Memory

The memory is of two types as under:[1]

a. Short-term memory: Here, the information of new facts is stored only for a few seconds to a few minutes. It is readily available up to 30 s
b. Long-term memory: It stores the memory for a longer period. Here, the information from short-term memory is stored or consolidated in the brain. Thus, long-term memory can hold an unlimited amount of memory and one can remember the events that have happened a long time ago.

The short-term memory formed in the hippocampus and later gets stabilized in the long-term memory in fast learning hippocampus and also slow in learning neocortex.

Loss of memory is called amnesia. One often confuses amnesia with dementia; hence, it is essential to know the difference between amnesia and dementia as given below.

The amnesia is simply a memory loss while dementia in addition to the memory loss (i.e. amnesia) has some other associated cognitive problems, namely thinking and reasoning, which effect a person's ability to carry out the daily activities.

There are two types of amnesia:

a. Retrograde amnesia (RA), one cannot recall memories from his past, i.e., before the onset of amnesia. However, he can form new memories, i.e., he can remember new information
b. In anterograde amnesia (AA), one cannot form new memories. However, he/she can still remember events/things of past before the onset of amnesia.

Regions of the Brain Involved in Amnesia

- Regions of the brain involved in RA are structures forming the hippocampal complex/formation consisting of amygdala, hippocampus, parahippocampus, entorhinal cortex, etc., present in the medical temporal lobe. Damage to the hippocampus only causes little or no effect on RA
- Regions of the brain involved in AA are the hippocampus, mamillary bodies, and fornix, but the hippocampus seems to play a key role in AA.

Etiology

Dementia is not a single disease but a disease complex caused by various diseases. Hence, its etiology varies according to the disease that causes it and classified accordingly.[2]

Classification

Dementia is classified into the following types:
- Alzheimer's dementia (60%–80%)
- Vascular dementia (15%–20%)
- Dementia with Lewy bodies (10%–15%)
- Fronto – temporal dementia
- Mixed dementia
- Rare types of dementia.
  - Hutington's dementia
  - Parkinson's dementia
  - Normal pressure hydrocephalus (NPH) etc.

Causes of Various Types of Dementia

Alzheimer's dementia

It is the most common type and is responsible for 60%–80% cases of dementia. The Alzheimer's disease is a neurodegenerative disease caused by the deposition of ß-Amyloid plaques in and around synapses and the deposition of neurofibrillary tangles made up of tau protein in the nerve cell bodies, especially in the region of the hippocampus.

Vascular dementia

It is the second most common cause and responsible for 15%–20% of cases.

It is caused by the reduced blood supply to the brain leading to the damage and eventually to the death of brain cells due to lack of oxygen supply.

The reduced blood supply occurs due to:
- Narrowing and blockages of small blood vessels inside the brain
- A single big stroke which cuts off blood supply to the part of the brain

© 2024 Journal of the Anatomical Society of India | Published by Wolters Kluwer - Medknow

- Lot of mini-strokes, which cause tiny but widespread damage to the brain.

The areas commonly affected by vascular ischemia are arterial border zones, pyramidal cells in the hippocampus (CA1 area) etc.

Dementia with Lewy Bodies

It occurs due to buildup of proteins called Lewy bodies. The Lewy bodies are the tiny clumps of *alpha-synuclein* and *ubiquitin* proteins present as inclusion bodies within the nerve cell bodies and killing them. The Lewy bodies are mainly seen in limbic system and cerebral cortex. These proteins are also associated with Parkison's disease, in which DLB occurs very late.

Fronto-temporal dementia

This occurs due to abnormal clumping of tau and TDP-43 proteins in the neurons of frontal and temporal lobes, which not only damage but eventually kills the nerve cells. This ultimately leads to brain shrinkage. The frontotemporal dementia is one of the most common dementias which strike young people.

Mixed dementia

In this, the person suffers from more than one type of dementias at a time. For example, vascular dementia and Alzheimer's disease often occur together.

Rare types of dementia

These include a number of diseases, namely Hutington's disease, Parkinson's disease, NPH, etc. In these conditions, nerve cells across the brain break down over time. As a result, the person does not develop amnesia but cognitive decline.

Risk Factors

The risk factors responsible for dementia include:[3] Age (strongest risk factor as dementia mostly effects people of 65 years and older), hypertension, depression, excessive smoking and alcohol intake, atherosclerosis, mild cognitive impairment, family history, diabetes, and high level of low-density lipoprotein, etc.

Treatment

The various modes of treatment are as under[4]

- *Medication* - by giving cognitive-enhancing drugs, namely acetylcholinesterase inhibitors, etc.
- *Rehabilitation* - by various therapies, namely cognitive therapy, physiotherapy, occupational therapy, and psychological therapies
- *Life style changes* - such as increasing physical activities, eating a healthy diet, quitting cigarette smoking, and excessive drinking.

Vishram Singh, Rashi Singh[1], Gaurav Singh[2]

Department of Anatomy, Kasturba Medical College, Mangalore, Manipal Academy of Higher Education, Manipal, Karnataka, [1]Department of Pediatric and Preventive Dentistry, Santosh Dental College and Hospital, [2]British Medical Journal, Noida, NCR Delhi, India

Address for correspondence: *Dr. Vishram Singh, B5/3 Hahnemann Enclave, Plot No. 40, Sector 6, Dwarka Phase - 2, New Delhi - 110 075, India.*
E-mail: drvishramsingh@gmail.com

References

1. Morris R. Learning and memory. In: Neuroscience in the 21st Century: From Basic to Clinical. Cham: Springer International Publishing; 2022. p. 2945-85.
2. Coope B, Richards FA, editors. ABC of Dementia. West Sussex, PO19 8SQ, UK: John Wiley & Sons; 2020.
3. van den Kieboom R, Snaphaan L, Mark R, Bongers I. The trajectory of caregiver burden and risk factors in dementia progression: A systematic review. J Alzheimers Dis 2020;77:1107-15.
4. Kuo CY, Stachiv I, Nikolai T. Association of late life depression, (Non-) modifiable risk and protective factors with dementia and Alzheimer's disease: Literature review on current evidences, preventive interventions and possible future trends in prevention and treatment of dementia. Int J Environ Res Public Health 2020;17:7475.

This is an open access journal, and articles are distributed under the terms of the Creative Commons Attribution-NonCommercial-ShareAlike 4.0 License, which allows others to remix, tweak, and build upon the work non-commercially, as long as appropriate credit is given and the new creations are licensed under the identical terms.

Article Info

Received: 12 August 2024
Revised: 12 August 2024
Accepted: 14 August 2024
Available online: 25 September 2024

Access this article online	
Quick Response Code:	**Website:** https://journals.lww.com/joai
	DOI: 10.4103/jasi.jasi_121_24

How to cite this article: Singh V, Singh R, Singh G. Neuroanatomical basis of dementia. J Anat Soc India 2024;73:197-8.

Original Article

Aberrant Origin of Left Vertebral Artery – Multidetector Computed Tomography Study

Abstract

Background: The vertebral arteries originating from respective subclavian arteries are the major source of oxygenated blood to posterior cerebral circulation and supply the upper spinal cord, brain stem, cerebellum, and occipital lobes of the cerebrum. Paucity of radiological studies prompted us to undertake this study which aims to analyze the variations in origin of left vertebral artery (LVA). **Materials and Methods:** This is a retrospective cross-sectional study of contrast-enhanced computed tomography chest scans of 710 subjects retrieved from the archives of a single imaging center. **Observations and Discussion:** Normal origin of LVA from the left subclavian artery (LSA) in the root of the neck was noted in 90.56% and variant origin in 9.44% of cases. Four-branched aortic arch (AA) with direct AA origin of LVA was observed in 6.76% of cases. An atypical three-branched pattern with LVA origin between the bovine trunk (common trunk of brachiocephalic trunk [BCT] and left common carotid artery [LCCA]) and LSA was seen in 0.84% of cases. Common origin of both LVA and LSA from a vertebro-subclavian trunk (VST) is found in 0.98% of cases. LVA as the last branch of arch distal to LSA and LVA of arch origin associated with aberrant right subclavian artery were noted in 0.14% of cases each. A rare but important observation is the presence of two common trunks (bovine trunk (BCT + LCCA) and VST (LVA + LSA) in an atypical two-branched fashion found in 0.56%. **Conclusion:** Critical knowledge of variations of the origin of LVA is clinically relevant as such variations are more prone to vascular pathologies. Variations of the LVA are thought to alter cerebral hemodynamics and can produce cerebral dysfunction. Preprocedural knowledge of such variations aids in the successful accomplishment of catheterization of LVA and avoids complications during neuroradiological interventions and surgical procedures.

Keywords: *Aberrant left vertebral artery, aortic arch origin, contrast-enhanced computed tomography, vertebro-subclavian trunk*

Vinay Sharma, C. S. Ramesh Babu, O. P. Gupta[1]

Department of Anatomy, Muzaffarnagar Medical College, Muzaffarnagar, [1]Dr. O. P. Gupta Imaging Centre, Meerut, Uttar Pradesh, India

Introduction

The vertebral arteries originating from respective subclavian arteries at the root of the neck supply 28% of oxygenated blood to cerebral circulation and supply the upper spinal cord, brain stem, cerebellum, and occipital lobes of the cerebrum.[1] Normally, the vertebral arteries arise from respective subclavian arteries at the root of the neck medial to scalenus anterior muscle. Variations in the origin of the vertebral arteries are common and left vertebral artery (LVA) variations are more frequent than right vertebral artery (RVA) and unilateral variants common than bilateral.[1] A recent meta-analysis included 31 studies and 12,456 left vertebral arteries and estimated a prevalence of subclavian origin as 94.1%. The same meta-analysis also reported a prevalence of 4.81% for the aortic arch (AA) origin of LVA after studying 15,848 cases from 35 studies.[1]

Imaging studies analyzing the variations of AA branching patterns in Indian subjects are few. After examining the contrast-enhanced computed tomography (CECT) chest scans of 1116 patients, Krishnan *et al*. reported that 78.6% of cases had normal branching pattern of AA and 5.4% of cases exhibited AA origin of LVA between left common carotid artery (LCCA) and left subclavian artery (LSA).[2] Another study of 4000 CECT chest scans found the prevalence of variations of AA as 0.675% (only in 27 cases out of 4000) and found only 1 case of "bovine origin of LVA from the arch."[3] Variation in the origin and anomalous proximal course of LVA in the superior mediastinum is dangerous during surgery of the mediastinum and lower neck region. Moreover, it is suggested that the initial segment of the vertebral artery is more

This is an open access journal, and articles are distributed under the terms of the Creative Commons Attribution-NonCommercial-ShareAlike 4.0 License, which allows others to remix, tweak, and build upon the work non-commercially, as long as appropriate credit is given and the new creations are licensed under the identical terms.

For reprints contact: WKHLRPMedknow_reprints@wolterskluwer.com

How to cite this article: Sharma V, Babu CS, Gupta OP. Aberrant origin of left vertebral artery – Multidetector computed tomography study. J Anat Soc India 2024;73:199-203.

Article Info

Received: 29 June 2024
Accepted: 11 August 2024
Available online: 25 September 2024

Address for correspondence:
Dr. Vinay Sharma, Muzaffarnagar Medical College, N.H. 58, Opp. Begrajpur Industrial Area, Muzaffarnagar - 251 203, Uttar Pradesh, India.
E-mail: vinay_sharma1979@yahoo.com

Access this article online

Website: https://journals.lww.com/joai

DOI: 10.4103/jasi.jasi_97_24

Quick Response Code:

prone to atherosclerotic changes, especially close to its origin.[4] Variations of the LVA are thought to alter cerebral hemodynamics and can produce cerebral dysfunction. Preprocedural knowledge of such variations aids in the successful accomplishment of catheterization of LVA and avoids complications during neuroradiological interventions and surgical procedures. Paucity of radiological studies on Indian subjects has prompted the present study to focus on the variations in the origin of LVA.

Materials and Methods

Retrospective cross-sectional study of CECT chest scans of 710 subjects (male 435 and female 275) obtained from a single imaging center. All subjects were referred to undergo CECT chest for suspected mediastinal and lung pathologies. The images were retrieved from the archives of the imaging center. The imaging center routinely obtains informed consent from the patients before administration of the contrast medium. The scans of the patients with malignancies likely to distort the anatomy of AA, poorly enhanced scans, and those with thoracic aortic disease were excluded from the study.

All patients underwent contrast-enhanced multi-detector CT (MDCT) by a 64-channel scanner (GE Optima 660, 2011, Tokyo, Japan) and received 90–100 mL of nonionic iohexol contrast (Omnipaque 350 mg I/mL; GE Healthcare, Shanghai, China) at the rate of 5 mL/s intravenously. Sections of 0.625 mm thickness were obtained from the lower part of the neck to the upper part of the abdomen and analyzed in a separate workstation (GE: AW Volume share 4.5). After analyzing axial, coronal, and sagittal scans, volume-rendered and maximum intensity projections were obtained. We specifically looked for variations in the origin of the LVA.

Observations

Typical three-branched patterns of the AA with brachiocephalic trunk (BCT), LCCA, and left subclavian (LSA) arteries were seen in 72.95% of cases and variant branching pattern of the arch was noted in 27.05% of cases. Normal origin of LVA from LSA in the root of the neck is noted in 90.56% (643/710) and variant origin in 9.44% (67/710) of cases. Four-branched AA with direct AA origin of LVA between LCCA and LSA was observed in 6.76% [48/710; male/female = 33/15; Figure 1] and this pattern is the second most common variant branching pattern of the arch of aorta. An atypical three-branched pattern with LVA origin between the "brachiocephalicocarotid trunk (the so-called "bovine trunk," the common trunk of BCT and LCCA) and LSA was seen in 0.84% of cases [6/710 cases; male/female = 6/0; Figure 2]. Common origin of both LVA and LSA from a vertebro-subclavian trunk (VST) is found in 0.98% of cases [7/710; male/female = 6/1; Figure 3]. LVA as the last branch of arch distal to LSA [Figure 4] and LVA of arch origin associated with aberrant right subclavian artery (ARSA) with a branching sequence of RCCA, LCCA, LVA, LSA, and ARSA [Figure 5] were noted in

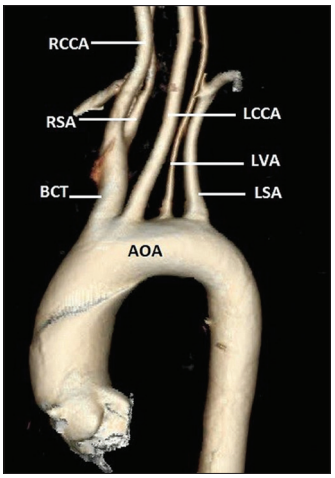

Figure 1: Volume rendered image. Direct aortic arch origin of left vertebral artery between left common carotid artery and left subclavian artery seen in 48 cases (6.76%; male/female = 33/15)

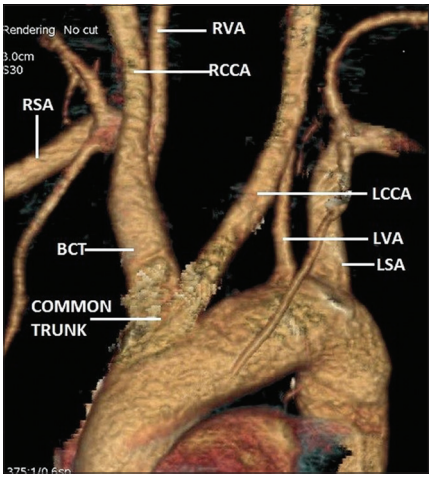

Figure 2: Volume rendered image. Direct aortic arch origin between common trunk ("Bovine trunk" - brachiocephalic trunk + left common carotid artery) and left subclavian artery seen in 6 cases (0.84%; male/female = 6/0)

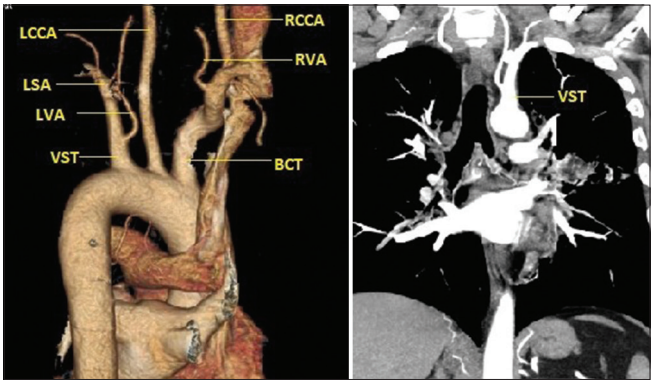

Figure 3: Vertebro-subclavian trunk (VST) common trunk of left vertebral artery (LVA) and left subclavian artery (LSA) seen in 7 cases (0.98%; male/female 6/1) (a) Volume rendered scan posterior view; (b) Coronal section

0.14% of cases each (1/710 each; both cases males). A rare but important observation is the presence of two common trunks, brachiocephalicocarotid trunk (BCT + LCCA) and VST (LVA + LSA) in an atypical two-branched fashion was found in 0.56% [4/710; male/female + 2/2; Figures 6 and 7]. Overall, variant origin of LVA was noted in 6.90% of cases in males (49/710) and 2.54% of cases in females (18/710).

Discussion

Development

The arch of the aorta and its branches are the derivatives of six pairs of pharyngeal arch arteries. Normally, the left third arch artery connected to the left horn of the aortic sac elongates to form LCCA and the left horn of the aortic sac itself will form that part of the arch of the aorta between the origins of BCT and LCCA. The right horn of the aortic sac will develop into BCT. The common trunk of origin of BCT and LCCA (the so-called "bovine trunk") may be due to the regression or slower growth rate of the left horn of the aortic sac such that the left third arch artery (LCCA) gets connected to the right horn of aortic sac (BCT). Normally, the first part of LVA develops from the dorsal branch of the left 7th intersegmental artery which itself forms the LSA and the second part develops from longitudinal postcostal anastomosis between 6th and 1st intersegmental arteries. Proximal portions of the upper six intersegmental arteries arising from the dorsal aorta normally disappear [Figure 8]. Failure of the formation of the dorsal branch of the seventh and persistence of the proximal portion of the sixth intersegmental artery results in AA origin of LVA between the origins of LCCA and LSA.[5] Incorporation of the proximal left 7th intersegmental artery into the developing arch of the aorta could also result in LVA originating directly from the AA.[6] The origin of LVA distal to LSA as the last branch of the arch is due to the persistence of 8th intersegmental artery. It is suggested that the persistence of the sixth intersegmental artery and absorption of a portion of the left fourth arch artery into the developing LSA could result in the origin of LVA from the root of LSA, the so-called VST.[6]

Branching pattern variations of AA attracted little attention in radiological literature because many of these variants are isolated and remain asymptomatic. Increased application of several surgical and endovascular interventional procedures has revived interest in the study of variations of the AA branching pattern. Normal three-branched AA with the sequence of BCT, LCCA, and LSA is reported to occur in 64.9%–94.3% of the population by some systematic reviews.[7-9] The most common variation reported is two-branched pattern with a "brachiocephalico-carotid trunk" (common trunk of BCT and LCCA, the so-called "bovine trunk" a misnomer) and LSA with a prevalence of 2.6%–27.4%[10-12] The recent meta-analysis reported a prevalence of 11.95%.[7] The second most common

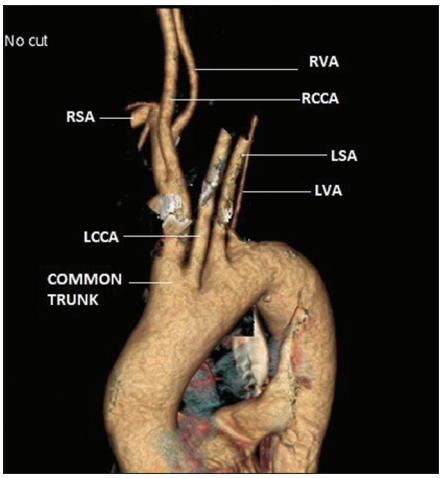

Figure 4: Volume rendered image. Direct aortic arch origin of left vertebral artery distal to left subclavian artery as last branch seen in 1 case (0.14%-male/female = 1/0)

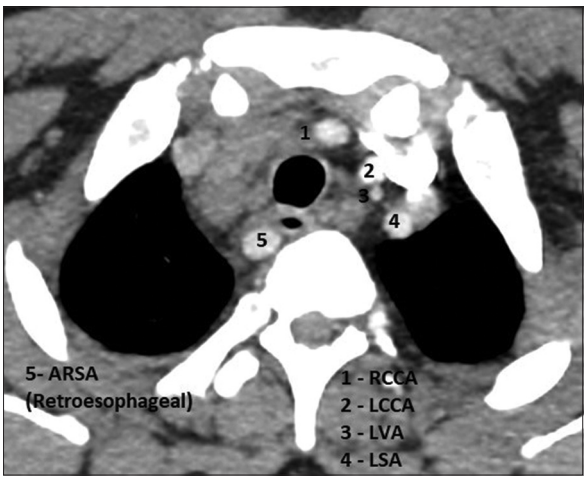

Figure 5: Axial scan showing 5 branches from arch in order from right to left – 1-RCCA; 2-Left common carotid artery; 3-Left vertebral artery; 4-Left subclavian artery and 5- aberrant right subclavian artery (ARSA). Note the retroesophageal course of ARSA seen in 1 case (0.14%)

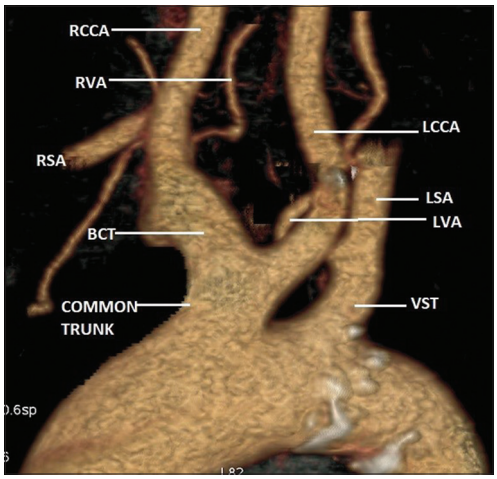

Figure 6: Volume rendered image. Two common trunks. Vertebro-subclavian trunk gives off left vertebral artery and left subclavian artery. Common trunk ("Bovine trunk") gives off left common carotid artery and brachiocephalic trunk seen in 4 cases (0.56%; male/female = 2/2)

variation observed is the direct AA origin of LVA between the origins of LCCA and LSA with a prevalence of 6.76% in the present study, 3.66% by Tsiouris *et al*.,[7] 2.9% by Popieluszko *et al*.,[8] 5.4% by Krishnan *et al*.[2] and 4.1% by Uchino *et al*.[13] AA origin of LVA along with "bovine trunk" (BCT + LCCA trunk) was noted in 0.84% of cases in the present study and 0.31% by Tsiouris *et al*.,[7] 0.4% by Popieluszko *et al*.[8]

Yuan collected data on the aberrant origin of vertebral arteries from 214 articles with 1286 cases (955 patients and 331 cadavers) and found single aberrant origin of LVA in 1056 out of 1233 cases.[5] It was also observed that there were more left than right and more unilateral than bilateral aberrant vertebral arteries. Analyzing MDCT images of 830 Indian patients, Sankhe *et al*.[14] observed LVA of AA origin in 26 patients (3.1%). They also observed a five-branched arch in 1 case (0.12%) with a sequence of RCCA, LCCA, LVA, LSA, and aberrant RSA as the last branch similar to our observation in 1 case (0.14%). Choi *et al*.[15] studied CT angiographic images of 3460 patients and noted AA origin of LVA between LCCA and LSA in 151 patients (4.36%) and LVA origin distal to LSA as the last branch in 2 cases (0.06%).

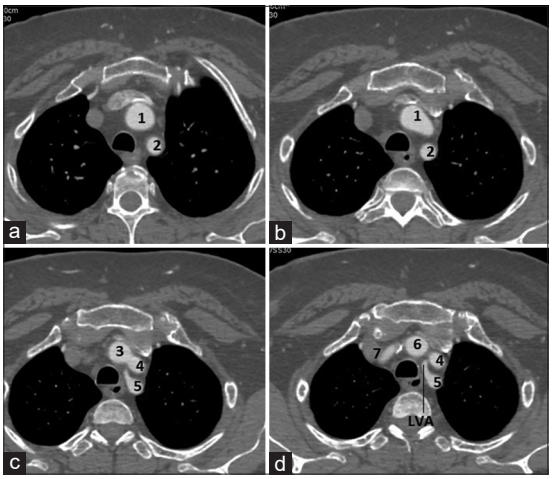

Figure 7: (a-d) Serial axial scans in a caudal to cranial direction showing two common trunks (a and b) 1-Brachiocephalicocarotid trunk ("bovine trunk") and 2-Vertebrosubclavian trunk (c) 3-Brachiocephalic trunk; 4-Left common carotid artery; 5-Left subclavian artery giving off left vertebral artery (d) 4-Left common carotid artery; 5-Left subclavian artery; 6-Right common carotid artery; and 7-Right subclavian artery. LVA: Left vertebral artery

The common trunk of origin of LVA and LSA referred as VST has been reported sporadically in cadaveric case reports without any other associated branching variation.[6,16,17] The LVA may arise from the root of LSA immediately above the arch or arise as a branch of LSA in the superior mediastinum few mm above the arch with a short course along the left border of the esophagus. The VST was found in 0.98% of cases in the present study, 0.027% by Tsiouris *et al*.,[7] and 1.6% of cases by Uchino *et al*.[13] Occurrence of two common trunks from the arch, "bovine trunk" (common trunk of BCT + LCCA) and VST (common trunk of LVA + LSA) was very rare and reported earlier in two cadaveric case reports.[18,19] Recently another cadaveric case report presented two common trunks as the bulbous origin from the AA.[20] Anomaly of two common trunks was reported in 0.005% of cases in the recent meta-analysis.[7] In the present study, we observed two common trunks in 0.56% of cases.

Clinical significance

Of the two vertebral arteries, the LVA appears dominant in nearly half of the cases and is catheterized for investigating the posterior cerebral circulation. In the presence of aberrant LVA of AA or VST origin, the transfemoral route for catheterization is easier technically in comparison to the transradial route. It was noted that LVA of AA origin entered the transverse foramen of either C4 or C5 vertebrae resulting in a longer course through mediastinum and neck.[13] Such a long course in front of the lower cervical vertebrae makes it susceptible to damage in surgical procedures involving the vertebrae. In contrast to RVA or LVA of subclavian origin, the LVA of arch origin exhibited

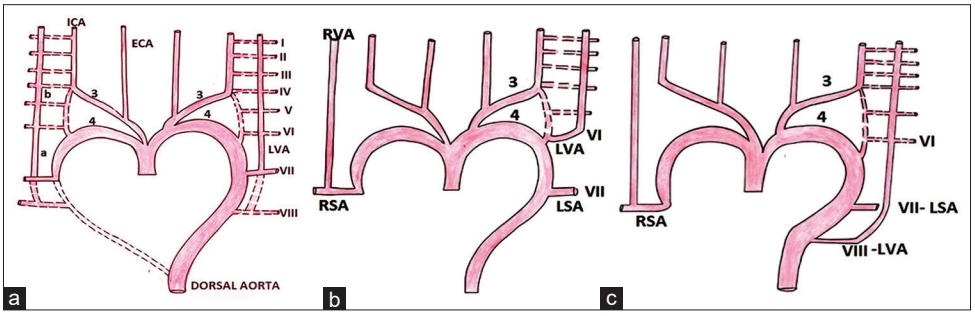

Figure 8: Development of left vertebral artery (a) Shows normal development of left vertebral artery (LVA) from left subclavian (LSA). Series of intersegmental arteries (I–VII) arise from dorsal aorta and are interconnected by a vertical postcostal anastomosis. Third (3) and fourth (4) pharyngeal arch arteries are connected to dorsal aorta. Left fourth arch artery and left dorsal aorta distal to VII intersegmental artery develop into arch of aorta; left VII intersegmental artery form left subclavian. Normal VA (both RVA and LVA) develops from dorsal branch of VII intersegmental (a) And vertical postcostal anastomosis between VII and I intersegmental arteries (b) Roots of origin of I to VI intersegmental arteries disappear. Other parts which disappear during fetal life are indicated by dotted lines (b) If root of left VI intersegmental artery persists and dorsal branch of VII does not develop then LVA will arise from aortic arch between the origins of left common carotid (3 – third pharyngeal arch) and left subclavian (left VII intersegmental artery) (c) Aortic arch origin of LVA distal to origin of LSA will develop due to persistence of VIII intersegmental artery. ICA: Internal carotid artery, ECA: External carotid artery

a higher incidence of arterial dissection.[21] Although the exact reason for arterial dissection of aberrant LVA remains to be elucidated, the longer extracranial course makes it vulnerable to shear stress due to high pressure which might cause dissection. The presence of two common trunks, though very rare, has to be kept in mind because any pathology affecting these vessels leads to severe cerebrovascular stroke.

Conclusion

Our observations on the aberrant origin of LVA are based on the examination of chest scans only which limits our observation to mediastinum. Very careful examination is essential to delineate the VST because in some cases, the common trunk may show a bulbous appearance giving an impression of arch origin of LVA. Variation in the origin and anomalous proximal course of LVA in the superior mediastinum is dangerous during surgery of the mediastinum and lower neck region. Moreover, it is suggested that LVA is more prone to atherosclerotic changes, especially close to its origin. Variations of the LVA are thought to alter cerebral hemodynamics and can produce cerebral dysfunction. Preprocedural knowledge of such variations aids in the successful accomplishment of catheterization of LVA and avoids complications during neuroradiological interventions and surgical procedures.

Financial support and sponsorship

Nil.

Conflicts of interest

There are no conflicts of interest.

References

1. Tudose RC, Rusu MC, Hostiuc S. The vertebral artery: A systematic review and a meta-analysis of the current literature. Diagnostics (Basel) 2023;13:2036.
2. Krishnan VK, Narayan V, Ibrahim N, Mathew J, James SM. Imaging spectrum and prevalence of variant branching pattern of aortic arch. Int J Res Med Sci 2019;7:1313-8.
3. Pandalai U, Pillay M, Moorthy S, Sukumaran TT, Ramakrishnan S, Gopalakrishnan A, *et al.* Anatomical variations of the aortic arch: A computerized tomography-based study. Cureus 2021;13:e13115.
4. Gluncic V, Ivkic G, Marin D, Percac S. Anomalous origin of both vertebral arteries. Clin Anat 1999;12:281-4.
5. Yuan SM. Aberrant origin of vertebral artery and its clinical implications. Braz J Cardiovasc Surg 2016;31:52-9.
6. Nelson ML, Sparks CD. Unusual aortic arch variation: Distal origin of common carotid arteries. Clin Anat 2001;14:62-5.
7. Tsiouris C, Lazaridis N, Piagkou M, Duparc F, Antonopoulos I, Antonitsis P, *et al.* The left-sided aortic arch variants: Prevalence meta-analysis of imaging studies. Surg Radiol Anat 2022;44:673-88.
8. Popieluszko P, Henry BM, Sanna B, Hsieh WC, Saganiak K, Pękala PA, *et al*. A systematic review and meta-analysis of variations in branching patterns of the adult aortic arch. J Vasc Surg 2018;68:298-306.e10.
9. Natsis KI, Tsitouridis IA, Didagelos MV, Fillipidis AA, Vlasis KG, Tsikaras PD. Anatomical variations in the branches of the human aortic arch in 633 angiographies: Clinical significance and literature review. Surg Radiol Anat 2009;31:319-23.
10. Celikyay ZR, Koner AE, Celikyay F, Denız C, Acu B, Firat MM. Frequency and imaging findings of variations in human aortic arch anatomy based on multidetector computed tomography data. Clin Imaging 2013;37:1011-9.
11. Boyaci N, Dokumaci DS, Karakas E, Yildiz S, Cece H, Kocarslan A, *et al*. Multidetector computed tomography evaluation of aortic arch and branching variants. Turk J Thorac Cardiovasc Surg 2015;23:51-7.
12. Uchino A, Saito N, Okada Y, Kozawa E, Nishi N, Mizukoshi W, *et al.* Variation of the origin of the left common carotid artery diagnosed by CT angiography. Surg Radiol Anat 2013;35:339-42.
13. Uchino A, Saito N, Takahashi M, Okada Y, Kozawa E, Nishi N, *et al.* Variations in the origin of the vertebral artery and its level of entry into the transverse foramen diagnosed by CT angiography. Neuroradiology 2013;55:585-94.
14. Sankhe AP, Ukirde V, Gomes CW, Pai S, Kulkarni S. MDCT evaluation of variations in branching patterns of aortic arch: Study of 830 Indian patients. Int J Biomed Adv Res 2016;7:329-36.
15. Choi Y, Chung SB, Kim MS. Prevalence and anatomy of anomalous left vertebral artery originated from aorta evaluated by computed tomographic angiography. Surg Radiol Anat 2018;40:799-806.
16. Bayat PD, Ghanbari A, Esmaeili S, Esmaeili K. Abnormal originating of vertebral artery in the superior mediastinum: A case report. Eur J Anat 2011;15:117-20.
17. Sateesha BN, Sirasanagandla SR, Surekha DS, Deepthinath R, Sudarshan S, Raghu J. Variant origin of the left vertebral artery from a vertebro-subclavian trunk associated with an unusual branch arising from the brachiocephalic trunk. J Surg Acad 2014;4:73-5.
18. Yazar F, Yalcin B, Ozan H. Variation of the aortic arch branches: Two main trunks originating from the aortic arch. Gazi Med J 2003;14:181-4.
19. Babu CS, Sharma V. Two common trunks arising from arch of aorta: Case report and literature review of a very rare variation. J Clin Diagn Res 2015;9:D05-7.
20. Tessema CB. Two bulbous origins of the aortic arch branches and compartmentalized left interscalene triangle. Int J Anat Var 2021;14:120-2.
21. Komiyama M, Morikawa T, Nakajima H, Nishikawa M, Yasui T. High incidence of arterial dissection associated with left vertebral artery of aortic origin. Neurol Med Chir (Tokyo) 2001;41:8-11.

Original Article

Prevention of Neuronal Damage in Brains of Chronic Stress-induced Male Wistar Rats Administering *Centella asiatica* (L) Urban

Saravanan Jagadeesan, Prarthana Kalerammana Gopalakrishna[1], Sreenivasulu Sura[2,3], Barani Karikalan[4], Krishna Chaitanya Reddy Dandala[2], Gandrakota Ravindranadh[2], Mohamad Aris Mohd Moklas[3], Thirupathirao Vishnumukkala[1,3]

Department of Anatomy, School of Medicine, Taylors University, [1]Human Biology Division, School of Medicine, IMU University, Kuala Lumpur, Departments of [2]Anatomy and [4]Pathology, Faculty of Medicine, MAHSA University, [3]Department of Human Anatomy, Faculty of Medicine and Health Sciences, Universiti Putra Malaysia, Serdang, Malaysia

Abstract

Introduction: Physiological and psychological response of an organism to repetitive stimulus leads to chronic stress which results in depression. This affects the neuro-endocrine axis causing hypersecretion of glucocorticoids which damages the hippocampal neurons in brain through oxidative stress. The body responds by producing Catalase (CAT) an antioxidant found on peroxisomes, which splits the hydrogen peroxide produced by oxidative stress into water and oxygen which are nontoxic, thus offering a protective effect. The synaptic function of the hippocampal neurons is dependent on acetylcholinesterase (AChE) and oxidative stress affects the levels of AChE. The available anti-depressants have the late onset of action and increased toxicity. *Centella asiatica* (CA), an herb with neuroprotective properties, is known as neuro-tonic and has less toxicity and has been used in ancient traditional medicines. This study aims to examine the neuroprotective effects of crude extract of CA on hippocampal neurons using Nissls stain and levels of AChE and expression of mRNA CAT in the brain tissues of chronic unpredictable mild stress (CUMS)-induced male Wistar rats. **Materials and Methods:** Thirty-six Male Wistar rats aged 8–10 weeks were held in six groups. One group assigned as control, whereas the other groups were administered CUMS by various stressors, namely restrain, forced swimming in cold water, overnight food and water deprivation, wet bedding, cage tilt at 45°, tail pinching, overcrowding the cages, and change of cage mates randomly for a period of 64 days. One of the stress-induced groups was retained as model group and others were administered crude extracts of CA at the doses of 200, 400, 800, and fluoxetine (Flx) 10 mg/kg body weight. At the end of 64 days, the rats were euthanized and the brain tissue was collected for Nissls staining of the hippocampus, measure levels of AChE using ELISA and expression of mRNA CAT levels using RT-PCR. **Results:** The rats of the model group exhibited reduced number of viable neurons in the hippocampus as observed in Nissls stain, reduced levels of AChE, and reduced expression of mRNA CAT in the brain tissue while the rat groups receiving CA showed increase in the number of viable neurons, increase in level of AChE, and increase in the expression of mRNA CAT in the brain tissues. The results were comparable to that of Flx. **Conclusion:** CA effectively attenuates CUMS-induced neuronal loss in the hippocampus of the rat's brain, normalizes AChE levels, and also the expression of mRNA CAT antioxidant levels. CA could be used in the long-term prevention of chronic stress-induced depression.

Keywords: *Catalase, Centella asiatica, chronic stress, fluoxetine, hippocampus, neuronal damage*

Introduction

Depression is a pervasive disorder in humans that is linked to experiencing stressful life events. The American Psychiatric Association defines it as a condition marked by feelings of sadness, emptiness, or irritability, as well as physical and cognitive changes that greatly hinder a person's ability to function normally.[1] Depression is a prominent contributor to disability, impacting almost 280 million individuals globally.[2] This condition leads to significant emotional distress, substantial financial detriment, and notable societal strain. Stress is a phenomenon in which stressors, including physical and psychological demands on an individual, hinder the individual or organism's ability to cope with subsequent challenges effectively.[3] The numerous stressors can be categorized into three types: (a) acute and chronic, (b) significant and small, and (c) desirable and undesired. These categories help to highlight the varied components of stress in life. Chronic stress is characterized by the ongoing presence of stressors or the repeated occurrence of a stressful event.[4] Chronic stress is a significant factor in causing depression.

This is an open access journal, and articles are distributed under the terms of the Creative Commons Attribution-NonCommercial-ShareAlike 4.0 License, which allows others to remix, tweak, and build upon the work non-commercially, as long as appropriate credit is given and the new creations are licensed under the identical terms.

For reprints contact: WKHLRPMedknow_reprints@wolterskluwer.com

How to cite this article: Jagadeesan S, Gopalakrishna PK, Sura S, Karikalan B, Dandala KS, Ravindranadh G, *et al*. Prevention of neuronal damage in brains of chronic stress-induced male wistar rats administering *Centella asiatica* (L) urban. J Anat Soc India 2024;73:204-13.

Article Info

Received: 08 June 2024
Revised: 08 July 2024
Accepted: 11 August 2024
Available online: 25 September 2024

Address for correspondence:
Dr. Thirupathirao Vishnumukkala, Human Biology Division, School of Medicine, IMU University, Bukit Jalil, Kuala Lumpur, Malaysia.
E-mail: thirusree.rao56@gmail.com

Access this article online

Website: https://journals.lww.com/joai
DOI: 10.4103/jasi.jasi_80_24
Quick Response Code:

© 2024 Journal of the Anatomical Society of India | Published by Wolters Kluwer - Medknow

Researchers can subject the rats to chronic unpredictable mild stress (CUMS) to produce the animal models of depression.[5] Research conducted on both people and rodents has shown that the hippocampus has a role in the development and progression of depression. Given the hippocampus's role in learning and memory, impairments in these cognitive functions are a significant characteristic of depression.[6] Depression leads to hippocampal atrophy and a decrease in volume, as evidenced by experiments conducted on rat models of depression. These experiments have shown that depression causes neuron loss, neurogenesis inhibition, and retraction of dendritic processes in the hippocampus. Conversely, successful treatment of depression in rat models has been found to promote the growth of new neurons in the hippocampus, a process known as neurogenesis.[7,8] The degree of reduction in hippocampus volume is correlated with the early onset and duration of depression. Similar alterations have been reported in rats exposed to chronic stress, with more pronounced changes occurring in the dentate gyrus.[9]

In response to oxidative stress, the body produces enzymatic and nonenzymatic antioxidants to mitigate its effects. Superoxide dismutase, an antioxidant, transforms superoxide anions into hydrogen peroxide, thereby decreasing the interaction between the superoxide anion and nitric oxide, resulting in the formation of reactive peroxynitrite. Catalase (CAT) is an antioxidant enzyme present in the peroxisomes, and it acts by catalyzing the process of decomposing hydrogen peroxide into nontoxic molecules such as water and oxygen.[10] With its high oxygen demand and lipid-rich composition, the brain is exposed to significant reactive oxygen species (ROS) levels. The rise in ROS and the decrease in antioxidant levels seen in chronic stress render the brain extremely vulnerable to the effects of oxidative stress.[11]

Acetylcholinesterase (AChE) is an enzyme belonging to the serine hydrolase family and is highly involved in transmitting signals throughout the nervous system. It breaks down acetylcholine (ACh), a necessary cholinergic neurotransmitter involved in memory.[12] Prolonged stress causes changes in the levels of the AChE enzyme. This was shown in research conducted on Wistar rats housed in nonstimulating situations.[13] *Centella asiatica* (CA) belongs to the *Apiaceae* family in the plant kingdom and has been traditionally utilized in the Ayurvedic system of medicine for its therapeutic properties in treating a wide range of diseases and enhancing memory.[14] This plant has been widely utilized in traditional herbal treatment in Malaysia and Ayurveda in India and other regions of Asia. CA, sometimes called pegaga in Malaysia and gotu kola or pennywort in the Americas, is commonly consumed as a food and a beverage.[15] Ayurveda has used this herb to treat several chronic ailments, such as anxiety.[5] The extracts derived from pulverized leaves and roots of the CA plant are utilized to manage cognitive impairment, dyspepsia, rheumatism, and leprosy. In China, the CA plant treats scabies, measles, urinary complications, tuberculosis, jaundice, emesis, and dysentery.[15]

Although modern drugs have made a substantial impact on improving the quality of life for those with depression, they still have certain limits. Frequently, the reaction to the treatment is not entirely foreseeable, and occasionally, the reaction is only partial. Most medications require many weeks of use for their therapeutic benefits to become apparent.[16] The issues with current pharmaceutical agents are exacerbated by several drug interactions and the lack of clarity regarding their safety during pregnancy.[4] Therefore, there exists a diverse range of drugs, all of which lack both effectiveness and safety.

Materials and Methods

Plant extract preparation and chemicals

The CA extract, obtained using ethanol as a solvent, is procured from the Universiti Teknologi Mara in Malaysia. The reference number for this is AuRins-MIA-1-0. Using the ethanolic method, the CA extract was derived from the whole plant through dehydration and subsequent extraction into a brown powder.[17] Fluoxetine (Flx) was acquired from Cadila Pharmaceuticals Ltd, located in Bhat, Ahmedabad, India. The AChE ELISA kit was obtained from Elabscience USA.

Apparatus

The experimental apparatuses utilized in the study, consisting of an open field box, an elevated plus maze, a T-maze, and a transparent cylinder, were constructed at the Workshop in the Department of Human Anatomy, Faculty of Medicine and Health Sciences (FMHS), Universiti Putra Malaysia (UPM).

Animals

Thirty-six male albino Wistar rats, 8–10 weeks old and weighing 180 and 220 g, were acquired from Bistari Sdn Bhd, Selangor, Malaysia. They were housed at Animal House in the FMHS at UPM in a controlled laboratory environment, including a 12-h cycle of light and darkness. The lights were illuminated from 0700 to 19.00 h while maintaining a consistent temperature of 25°C ± 2°C. The rats were able to access food and water freely without any restrictions. The animals were acclimatized for 1 week. The Institutional Animal Care and Use Committee (IACUC) at UPM approved the number of rats utilized and the study procedures. The project was assigned the identification code UPM/IACUC/AUP-R078/2018.

Chronic unpredictable mild stress procedure

CUMS was administered to the experimental animals for 8 weeks through the application of psychosocial and environmental stressors, as reported in a previous study.[18] The rats that were not exposed to CUMS

were kept in their home cages except for routine handling and cleaning. The rats exposed to CUMS were exposed to nine different types of mild stressors (S), administering a minimum of two stressors per day for a continuous period of 8 weeks. The study involved several experimental conditions: S1: food deprivation for 24 h, S2: water deprivation for 24, S3: swimming in cold water (temperature of 5°C) for 5 min, S4: change of cage mates for 12 h, S5: 1 min of tail pinch maintained (pinch applied at 1 cm from the tip of the tail), S6: Keep cage tilted at an angle of 45° for 12 h of, S7: Overcrowding for 12 h, S8: Keep the bedding wet for 12 h, and S9: apply physical restraint for 4 h. The stressors were applied randomly during the 1st week, and the same schedule was maintained during the entire experimental period, with no stressor administered in succession to prevent adaptation [Table 1].

Design of the experiment

After acclimatization, the rats were assigned randomly to six groups, each with six rats (n = 6). Group 1 rats were not subjected to stress and were given normal saline and assigned as control. Group 2 rats were administered only CUMS and were given normal saline assigned as a model. Group 3 rats were subjected to CUMS and Flx (10 mg/kg orally). Groups 4, 5, and 6 were administered CUMS and different doses of CA (200 mg/kg, 400 mg/kg, and 800 mg/kg orally), respectively. The dosages were determined using the data from prior research.[19,20] Flx and CA were administered daily, 30 min before the start of CUMS administration, for 8 weeks, commencing from day 0 of the trial. Behavioral assessments were performed at midday, beginning in the 9th week of the investigation. The rats were sacrificed at the end of the experiments, and tissue samples were collected [Figure 1].

Sample collection and preparation

Following euthanization, the rat brains were promptly extracted and then preserved in 10% formalin for 7 days. Subsequently, the specimens underwent mechanized tissue processing and were incorporated into paraffin blocks. The brain tissues were stored at −80°C to facilitate biochemical analysis.

Nissl's staining

The tissue paraffin blocks were used to obtain the coronal sections with a microtome of 5–6 μm thickness. The portions were immersed in a water bath at 38°C to facilitate straightening and transferred onto individual glass slides. The brain tissue sections on the glass slides were subjected to deparaffinization at a temperature of 70°C for 1 h in an oven. Following paraffin removal, the slides were immersed in xylene for 5 min and subsequently underwent rehydration in a series of graded alcohol solutions, starting with 95% alcohol for 3 min, followed by 70% alcohol. The slides were immersed in distilled water for an additional 3 min. The tissues were stored with 0.1% cresyl violet acetate stain for 10 min in an oven at a temperature of 70°C. The slides were extracted and cleansed in distilled water for 3 min, followed by dehydration in ascending alcohol concentrations (70%, 95%, and 100%) for 3 min at each level. Subsequently, the slides were immersed in xylene for 5 min, affixed using mounting material known as dibutyl phthalate xylene, and shielded with a cover slip. The viability of cells in the tissue slides was assessed using the method outlined by Adele. Brain samples were obtained from three rats in each group. Five slices of the hippocampus were produced from each rat brain sample. Scoring was conducted on five sites within each of the hippocampal regions of cornu Ammonis 1 (CA1),

Table 1: Chronic unpredictable mild stress procedure[18]

Stages of stress	Type of stress	Description of the type of stress
S1	Food deprivation	The rats were subjected to 24 h food deprivation. Food was provided following the end of the deprivation period
S2	Water deprivation	The rats were subjected to 24 h water deprivation. Water was provided immediately following the end of the deprivation period
S3	Swimming in cold water	The rats were made to swim for 5 min in cylinders filled with cold water (4±1°C). At the end of this immediately after their swimming, the rats were removed, dried with a towel, and returned to their home cages
S4	Change of cage mates	The cage mates of the rats were changed for 12 h, after which the rats were returned immediately to their respective home cages
S5	Tail pinch	The tails of the rats were clamped at 1 cm from the tips of the tails for 1 min
S6	Cage tilt	The rat cages were kept tilted at 45° for 12 h
S7	Overcrowding of cage	6 rats were packed in a cage for a period of 12 h
S8	Wet bedding	200 mL of water was added to the beddings in the cages where the rats, where they retained for 12 h
S9	Physical restrain	The rats were individually restrained in plastic restrainers (5.5 cm diameter and 12 cm long) with proper ventilation for 4 h

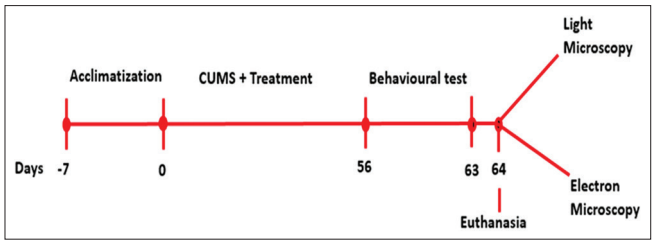

Figure 1: Experimental design

cornu Ammonis 2 (CA2), and cornu Ammonis 3 (CA3). The Olympus microscope, specifically the Olympus BX51TRF-CCD model, examined the tissue slices at a magnification ×400.[21]

The Enzyme-linked immunosorbent test

The AChE activity of the rat brain homogenates was assessed using the quantitative sandwich ELISA technique, following the instructions provided by the manufacturer (Elabscience USA). Subsequently, a Versamax microplate reader was used to determine the optical density of the samples, applying a wavelength of 450 ± 2 nm. The values obtained, which were directly proportionate to AChE quantities, were determined using the standard calibration curves.

Studies on the expression of genes

The RNA was extracted from the rats' brains using the Qiagen RNeasy mini kit, following the manufacturer's instructions manual. The RNA samples were assessed for purity using a Nanodrop spectrophotometer, and their integrity, as indicated by the 28S/18S ribosomal RNA ratio, was verified using agarose gel electrophoresis. The entire RNA sample (100 µg) was subjected to reverse transcription using a qPCRBIO cDNA synthesis kit according to the manufacturer's instructions manual.

The primers for the genes of interest (GOI) for CAT were generated by IDNA, along with one reference gene (RG), while glyceraldehydes-3-phosphate dehydrogenase was utilized to standardize the threshold cycle (CT) values for GOI. The real-time PCR was conducted using the Eppendorf Mastercycler ep realplex 4S instrument and the 2x qPCRBIO SyGreen Blue Mix Seoarate-Rox master mix. The amplification technique employed entailed heat activation at a temperature of 95°C for 2 min, succeeded by 40 cycles consisting of a denaturation phase for 15 s at 95°C, followed by an annealing phase for 30 s at 59°C, and finally an extension phase for 30 s at 72°C. The fluorescence signals were measured at a temperature of 59°C.

The Livak technique was employed to compute the fold change of gene expression based on the CT values acquired.[22] The mean CT values of each gene of interest (CT AVG GOI) were standardized using the mean CT values for the reference genes (ΔCT = CT AVG GOI-CT AVG RG). The ΔΔCT (ΔCT TREATMENT-ΔCT CONTROL) was computed, and each gene's relative change in expression level across the different rat groups was represented as 2-(ΔΔCT). After amplification, the specificity of the primers was determined using a melting curve study.

Quantitative analysis of data using statistical methods

The analysis of the data acquired was done using the one-way ANOVA with the GraphPad Prism version 6 software (ISI, USA). Tukey's *post hoc* comparison was employed, with the value of $P < 0.05$, to determine the statistical significance. The results were reported as the mean value plus or minus the standard deviation (mean ± SD).

Results

Centella asiatica protected the hippocampus Cornu Ammonis 1 pyramidal neurons from neurodegeneration in chronic unpredictable mild stress-induced rats' brains

The neuroprotective effects of CA on the CA1 area of the hippocampus in rats were evaluated by CV staining. Noticeable disparities in the quantity of functional neurons were noted in the hippocampus among the rats. The statistical analysis yielded a test statistic of F (5,444) =62.59, with a $P = 0.0001$. The hippocampus of rats that were administered with CUMS exhibited a significantly lower number of viable neurons (11.25 ± 1.875, $P = 0.0001$) compared to the control group of rats (15.47 ± 2.591). The quantity of functional neurons was significantly greater in rats induced with CUMS and treated with Flx (14.04 ± 1.202, $P = 0.0001$), CA 400 (14.95 ± 2.277, $P = 0.0001$), and CA 800 (14.93 ± 2.559, $P = 0.0001$), compared to the CUMS-induced model group (11.25 ± 1.875). There were no notable differences in the number of functional neurons among the control, Flx, CA 400, and CA 800 groups of rats [Figure 2].

Centella asiatica protected the hippocampus Cornu Ammonis 2 pyramidal neurons from neurodegeneration in chronic unpredictable mild stress-induced rats' brains

The neuroprotective effects of CA on the neurons in the CA2 area of the rats' hippocampus were assessed using CV stain. There were notable variations in the number of functional neurons in the CA2 area of the hippocampus across different groups of rats (F [5,444] = 52.77, $P = 0.0001$). The hippocampus of rats induced with CUMS exhibited a significantly lower number of viable neurons (11.40 ± 1.959, $P = 0.0001$) compared to the control group of rats (15.44 ± 2.688). The rats that were treated with CUMS and also given Flx (15.17 ± 2.286, $P = 0.0001$), CA 400 (14.87 ± 2.418, $P = 0.0001$), or CA 800 (15.00 ± 2.515, $P = 0.0001$) showed a significantly higher number of viable neurons compared to the rats that were only induced with CUMS (15.44 ± 2.688). There were no notable disparities in the number of functional neurons observed across the control, Flx, CA 400, and CA 800 groups of rats [Figure 3].

Centella asiatica protected the hippocampus and Cornu Ammonis 3 pyramidal neurons from neurodegeneration in chronic unpredictable mild stress induced rats' brains

The neuroprotective effects of CA on the neurons of the CA3 area in the rat's hippocampus were assessed using CV stain. A notable disparity was noted in the number of functional neurons in the CA3 area of the hippocampus across the different rats (F [5,444] = 93.98, P = 0.0001). The CUMS-induced model group of rats had a markedly reduced number of viable neurons (14.64 ± 2.769, P = 0.0001) compared to the control group (20.27 ± 3.202). A considerably higher number of viable neurons were found in the rats induced with CUMS and administered with Flx (19.81 ± 2.793, P = 0.0001), CA 400 (19.80 ± 1.366, P = 0.0001), and CA 800 (19.84 ± 1.452, P = 0.0001), compared to the CUMS-only model group (14.64 ± 2.769). There were no significant changes in the number of functional neurons among the control, Flx, CA 400, and CA 800 groups of rats [Figure 4].

The impact of *Centella asiatica* on the concentrations of acetylcholinesterase in rat brain tissues

The levels of AChE in the rats' brains were measured to determine the protective effects of CA on the cholinergic dysfunction caused by CUMS. The results of the one-way ANOVA showed statistically significant variations in the levels of AChE (F [5, 12] = 9.498, P = 0.0007) across the different groups of rats. Tukey's *post hoc* test comparison showed that AChE levels in the CUMS-induced rats (2.426 ± 0.46, P = 0.0013) were significantly higher than in the control group (1.27 ± 0.14). Significant reductions in AChE levels were statistically detected in rats induced with CUMS when supplied with

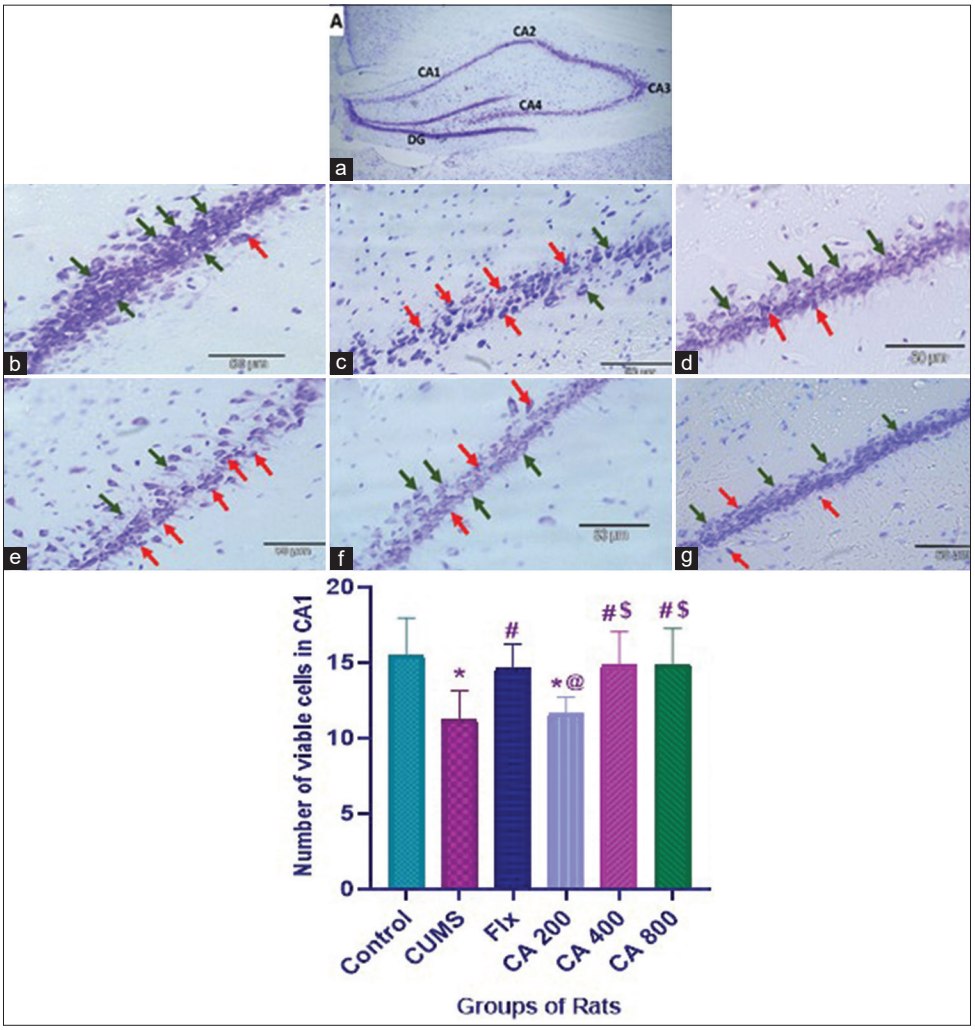

Figure 2: Neuro-protective effects of *Centella asiatica* (CA) on the hippocampal neurons of the CA1 region, as observed by cresyl violet stain of the chronic unpredictable mild stress (CUMS)-induced rats. Images of the cresyl violet staining of the hippocampus showing changes in number of viable cells (shown with green arrow) and degenerated cells (shown with red arrow) after CUMS induction and those co-administered with fluoxetine (Flx) and CA. (a) Hippocampal regions marked, (b) Control group, (c) CUMS-induced group, showing less viable cells (red arrow) (d) Flx group, shows more viable cells (green arrow) (e) CA 200 group shows less number of viable cells and (f and g) CA 400 and 800 groups of rats show more number of viable cells (green arrow). Data presented as mean ± SD, n = 6. *P < 0.05 versus control, #P < 0.05 versus CUMS, @P < 0.05 versus Flx, $$P$ < 0.05 versus 200

Flx (1.353 ± 0.233, P = 0.0024), CA 400 (1.503 ± 0.01, P = 0.0078), and CA 800 (1.38 ± 0.233, P = 0.0030), in comparison to rats exposed to CUMS alone (2.426 ± 0.46). No notable variations in the AChE levels were reported across the rats treated with Flx and CA (400 and 800) [Figure 5].

The impact of *Centella asiatica* on the catalase mRNA levels in brain tissues of chronic unpredictable mild stress-induced rats

The expression of CAT mRNA was done to determine the neuroprotective effects of CA in rats induced with CUMS. The findings revealed notable disparities among the groups of rats. The statistical analysis yielded a result of F (5, 12) = 25.50, with a P = 0.0001. The amount of CAT mRNA in the model group was significantly reduced (fold change of 0.42 ± 0.10, P = 0.0001) compared to the control group (fold change of 1 ± 0). However, in groups of rats induced with CUMS and administered Flx, CA 200, CA 400, or CA 800, there was a significant increase in CAT mRNA levels compared to the model group. The fold change for CAT mRNA levels was as follows: Flx (1.01 ± 0.05, P = 0.0001), CA 200 (0.61 ± 0.10, P = 0.0001), CA 400 (1.11 ± 0.16, P = 0.0001), and CA 800 (1.10 ± 0.10, P = 0.0001). The CAT mRNA levels for rats given CUMS alone were 0.42 ± 0.10. There were no noticeable variations in the levels of CAT mRNA between the Flx and CA (400 and 800) groups of rats, indicating no substantial increase or decrease in fold change [Figure 6].

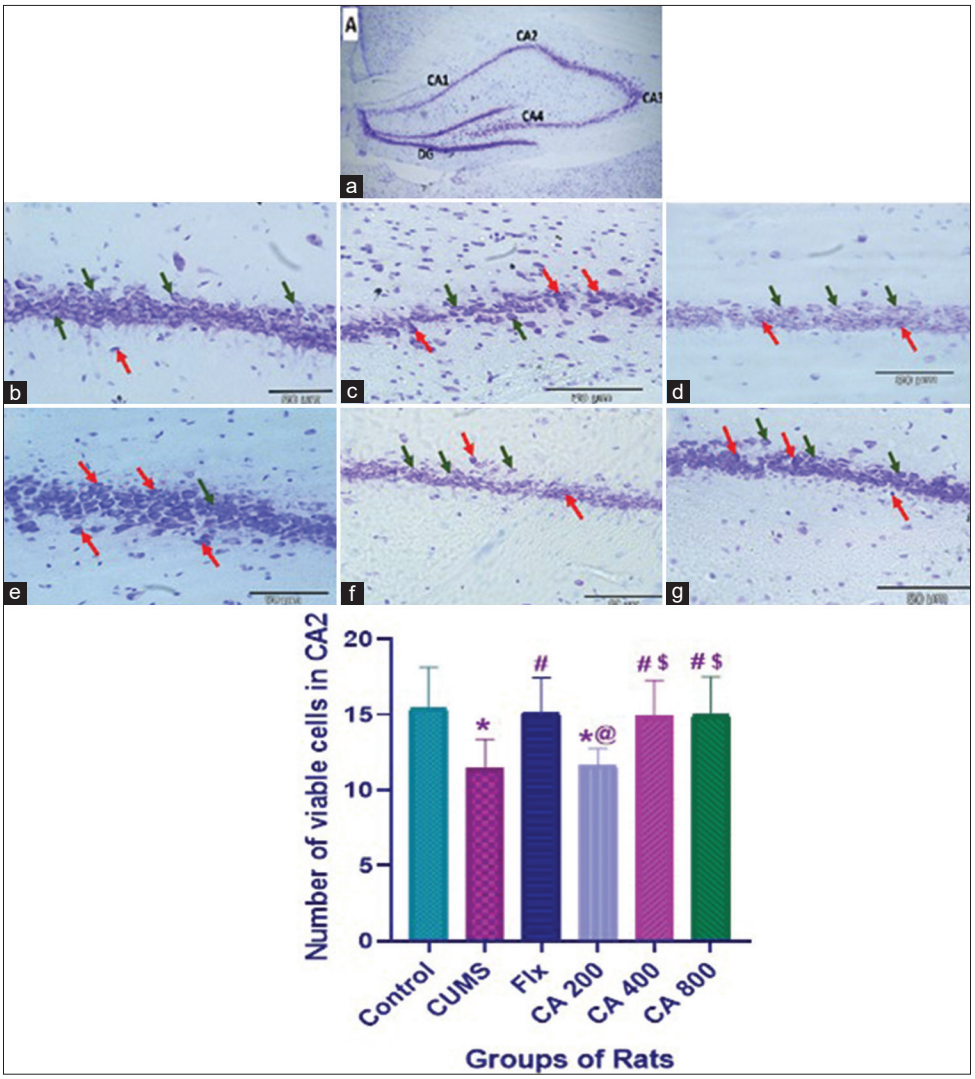

Figure 3: Neuro-protective effects of *Centella asiatica* (CA) on the CA2 region of the hippocampal neurons, observed by cresyl violet stain, on the chronic unpredictable mild stress (CUMS)-induced rats. Images of the cresyl violet staining of the hippocampus showing changes in number of viable cells (shown with green arrow) and degenerated cells (shown with red arrow) after CUMS induction and those co-administered with fluoxetine (Flx) and CA. (a) Hippocampal regions marked, (b) Control group, (c) CUMS-induced group, showing less viable cells (red arrow) (d) Flx group, showed more viable cells (green arrow) (e) CA 200 group shows less number of viable cells and (f and g) CA 400 and 800 groups of rats show a greater number of viable cells (green arrow) Data presented as mean ± SD, *n* = 6. **P* < 0.05 versus control, #*P* < 0.05 versus CUMS, @*P* < 0.05 versus Flx, $*P* < 0.05 versus 200

Discussion

The brain's hippocampus is a component of the limbic system associated with cognitive function and memory. The hippocampus also functions as a regulator of depressive mood, processing information, and can cause behavioral changes in depression.[23] Reduced hippocampus sizes have been seen in humans through postmortem examinations and MRI investigations conducted on individuals with severe depression (MD).[24] Studies have reported changes in the hippocampus brain in stress-induced depression models of rats, which include shrunken dendrites in CA3 and dentate gyrus neurons and loss of spines in CA1 neurons.[25] Multiple studies have reported observing hippocampal shrinkage in various animal models of depression.[26] The results of the present study also revealed structural alterations in the hippocampus of rats caused by CUMS, including reduced number of viable neurons in the pyramidal cell layers. The administration of Flx or CA at 400 and 800 mg/

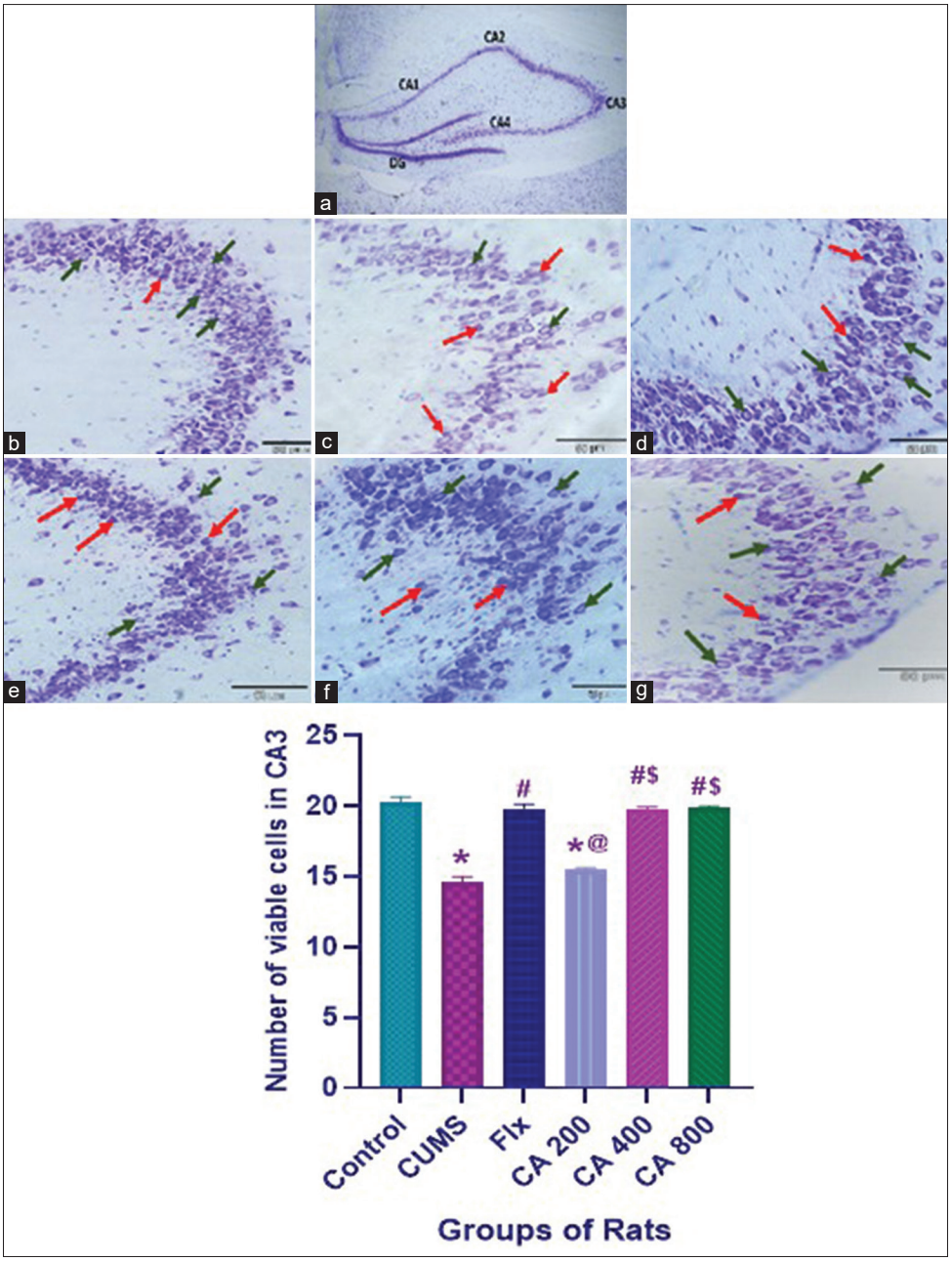

Figure 4: Neuroprotective effects of *Centella asiatica* (CA) on the neurons of the CA3 region of the hippocampus, as observed by cresyl violet stain, on the chronic unpredictable mild stress (CUMS)-induced rats. Images of the cresyl violet staining of the hippocampus showing changes in the number of viable cells (shown with green arrow) and degenerated cells (shown with red arrow) after CUMS induction and those co-administered with fluoxetine (Flx) and CA. (a) Hippocampal regions marked, (b) Control group, (c) CUMS-induced group, showing less viable cells (red arrow) (d) Flx group, showed more viable cells (green arrow) (e) CA 200 group shows less number of viable cells and (f and g) CA 400 and 800 groups of rats show more number of viable cells (green arrow). Data presented as mean ± SD, *n* = 6. **P* < 0.05 versus control, #*P* < 0.05 versus CUMS, @*P* < 0.05 versus Flx, $*P* < 0.05 versus 200

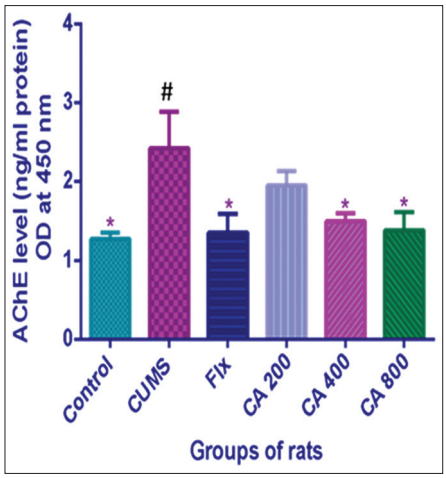

Figure 5: Effect of *Centella asiatica* on acetylcholinesterase levels in the rat's brains. Values are presented as mean ± SD, *n* = 6. #*P* < 0.05 versus control group, **P* < 0.05 versus chronic unpredictable mild stress group

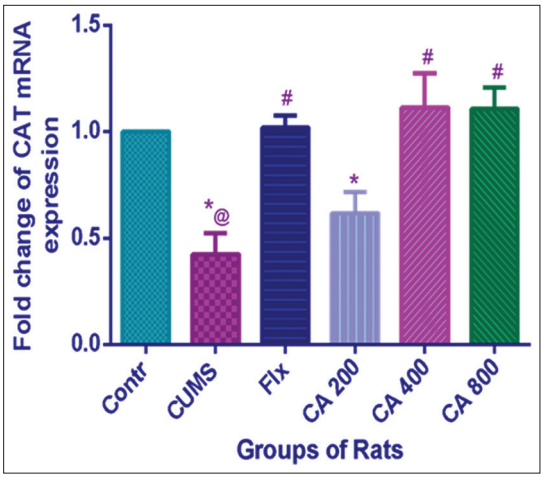

Figure 6: Effect of *Centella asiatica* on the levels of Catalase mRNA in rat's brain. Values are presented as mean ± SD, *n* = 6. @*P* < 0.05 versus control group, **P* < 0.05 versus control group, #*P* < 0.05 versus chronic unpredictable mild stress group

kg doses prevented the above-mentioned alterations. The neuroprotective effects of CA in this study were similar to those of Flx. Significantly, according to the existing literature, this study is the initial documentation of the neuroprotective effects of CA in the rat model of depression generated by CUMS. Prior research has documented the neuroprotective properties of CA in mice subjected to paracetamol toxicity, rats exposed to D-gal/AlCl3 toxicity, and rats with cerebral ischemia perfusion injury.[27-29]

AChE is an essential enzyme that plays a critical role in cholinergic transmission. Its primary function is to break down the neurotransmitter acetylcholine into acetate and choline. This process has a direct impact on memory. This phenomenon has been proven in Wistar rats exposed to long-term noise-induced stress.[30] Previous studies have documented similar findings in rats exposed to long-term stress, showing an elevation in AChE levels and impairments in memory.[31,32] The current investigation revealed that the model group of rats which were exposed only to CUMS had an increase in the levels of AChE in the hippocampus in comparison to the control group of rats. The elevation of AChE levels is believed to have a direct and causal impact on the development of memory impairments. The rat groups that received Flx and CA 400 and 800 also showed reduced AChE levels and enhanced memory performance. Therefore, it can be inferred that CA mitigates the alterations in AChE levels caused by CUMS, thereby improving memory performance. The CA at 400 and 800 mg/kg dosages exhibit nondose-dependent behavior, as they yield comparable benefits in reducing oxidative-antioxidative alterations and AChE levels. On the other hand, the effect of CA varies depending on the dosage. There is a noticeable distinction between CA at 200 mg/kg group and groups receiving CA at 400 and 800 mg/kg.

CAT plays a crucial role as an antioxidant in detoxifying hydrogen peroxide (H2O2).[33] The presence of oxidative stress in Wistar rats reduced the activity of CAT in the brain, leading to oxidative damage.[34] RT-PCR analysis revealed a notable decrease in mRNA expression of CAT in rats exposed to oxidative stress.[35] Rats exposed to long-term, unpredictable stress experienced a noteworthy reduction in their hippocampus's CAT levels.[36] Comparable findings were documented in Wistar rats exposed to stress by prolonged immobilization. The findings of the current investigation align with prior observations.

The current investigation confirms a decrease in mRNA CAT levels in the hippocampus of rats with depression produced by CUMS, compared to a control group of rats. The rats induced with CUMS and treated with Flx and CA at doses of 400 and 800 mg/kg, respectively, exhibited an elevation in mRNA CAT levels. There were no notable variations in mRNA CAT levels between the groups administered Flx and CA (400 and 800 mg/kg), respectively. The findings of this study showed that CA effectively protected against oxidative stress-related harm by elevating the levels of CAT in the brains of rat models induced with CUMS.

Conclusion

When an organism responds both physically and psychologically when exposed to chronic stress, resulting in depression. The changes in the body include alterations in the oxidative stress pathway; this affects its delicate balance by lowering the levels of CAT, which is an antioxidant, and AChE, which is essential for normal synaptic function, thus leading to the loss of hippocampal neurons. The CA, an herb with neuroprotective properties, has been shown to normalize the levels of CAT and AChE and protect the neurons in CUMS-induced rats with depression hence can be concluded that CA has the potential to treat depression.

Financial support and sponsorship

Nil.

Conflicts of interest

There are no conflicts of interest.

References

1. Karrouri R, Hammani Z, Benjelloun R, Otheman Y. Major depressive disorder: Validated treatments and future challenges. World J Clin Cases 2021;9:9350-67.
2. Chodavadia P, Teo I, Poremski D, Fung DS, Finkelstein EA. Prevalence and economic burden of depression and anxiety symptoms among Singaporean adults: Results from a 2022 web panel. BMC Psychiatry 2023;23:104.
3. Cano-López I, Lozano-García A, Catalán-Aguilar J, Hampel KG, Villanueva V, González-Bono E. The relationship between memory and quality of life is mediated by trait anxiety in patients with temporal lobe epilepsy. Qual Life Res 2023;32:739-47.
4. Jagadeesan S, Chiroma SM, Mohd Moklas MA, Hidayat Baharuldin MT, Mat Taib CN, Amom Z, *et al*. *Centella asiatica* L. Urban protects against morphological aberrations induced by chronic unpredictable mild stress in rat's hippocampus via attenuation of oxidative stress. Egypt J Basic Appl Sci 2022;9:324-39.
5. Jagadeesan S, Musa Chiroma S, Baharuldin MT, Taib CN, Amom Z, Adenan MI, *et al. Centella asiatica* prevents chronic unpredictable mild stress-induced behavioral changes in rats. Biomed Res Ther 2019;6:3233-43.
6. Donato F, Alberini CM, Amso D, Dragoi G, Dranovsky A, Newcombe NS. The ontogeny of hippocampus-dependent memories. J Neurosci 2021;41:920-6.
7. MacQueen G, Frodl T. The hippocampus in major depression: Evidence for the convergence of the bench and bedside in psychiatric research? Mol Psychiatry 2011;16:252-64.
8. Lino de Oliveira C, Bolzan JA, Surget A, Belzung C. Do antidepressants promote neurogenesis in adult hippocampus? A systematic review and meta-analysis on naive rodents. Pharmacol Ther 2020;210:107515.
9. VanTieghem M, Korom M, Flannery J, Choy T, Caldera C, Humphreys KL, *et al.* Longitudinal changes in amygdala, hippocampus and cortisol development following early caregiving adversity. Dev Cogn Neurosci 2021;48:100916.
10. Galasso M, Gambino S, Romanelli MG, Donadelli M, Scupoli MT. Browsing the oldest antioxidant enzyme: Catalase and its multiple regulation in cancer. Free Radic Biol Med 2021;172:264-72.
11. Ionescu-Tucker A, Cotman CW. Emerging roles of oxidative stress in brain aging and Alzheimer's disease. Neurobiol Aging 2021;107:86-95.
12. Hasselmo ME. The role of acetylcholine in learning and memory. Curr Opin Neurobiol 2006;16:710-5.
13. Nawaz A, Batool Z, Shazad S, Rafiq S, Afzal A, Haider S. Physical enrichment enhances memory function by regulating stress hormone and brain acetylcholinesterase activity in rats exposed to restraint stress. Life Sci 2018;207:42-9.
14. Thirupathirao V, Gopalakrishna PK, Karikalan B, Jagadeesan S, Baharuldin MT, Thomas W, *et al*. Protective effect of *Centella asiatica* on AlCl3 and D-Galactose induced hepatotoxicity in rats through the alleviation of oxidative stress as demonstrated by histological changes in liver. Int J Anat Res 2023;11:8740-7.
15. Orhan IE. *Centella asiatica* (L.) Urban: From traditional medicine to modern medicine with neuroprotective potential. Evid Based Complement Alternat Med 2012;2012:946259.
16. Ormel J, Hollon SD, Kessler RC, Cuijpers P, Monroe SM. More treatment but no less depression: The treatment-prevalence paradox. Clin Psychol Rev 2022;91:102111.
17. Hafiz ZZ, Amin MM, Johari James RM, Teh LK, Salleh MZ, Adenan MI. Inhibitory effects of raw-extract *Centella asiatica* (RECA) on acetylcholinesterase, inflammations, and oxidative stress activities via *in vitro* and *in vivo*. Molecules 2020;25:892.
18. Tong J, Zhou Z, Qi W, Jiang S, Yang B, Zhong Z, *et al.* Antidepressant effect of helicid in chronic unpredictable mild stress model in rats. Int Immunopharmacol 2019;67:13-21.
19. Chiroma SM, Baharuldin MT, Mat Taib CN, Amom Z, Jagadeesan S, Ilham Adenan M, *et al*. *Centella asiatica* protects d-Galactose/AlCl(3) mediated Alzheimer's disease-like rats via PP2A/GSK-3β signaling pathway in their hippocampus. Int J Mol Sci 2019;20:1871.
20. Gupta GL, Fernandes J. Protective effect of *Convolvulus pluricaulis* against neuroinflammation associated depressive behavior induced by chronic unpredictable mild stress in rat. Biomed Pharmacother 2019;109:1698-708.
21. Adeli S, Zahmatkesh M, Tavoosidana G, Karimian M, Hassanzadeh G. Simvastatin enhances the hippocampal klotho in a rat model of streptozotocin-induced cognitive decline. Prog Neuropsychopharmacol Biol Psychiatry 2017;72:87-94.
22. Livak KJ, Schmittgen TD. Analysis of relative gene expression data using real-time quantitative PCR and the 2(-Delta Delta C(T)) method. Methods 2001;25:402-8.
23. Fournier NM, Duman RS. Illuminating hippocampal control of fear memory and anxiety. Neuron 2013;77:803-6.
24. Dusi N, Barlati S, Vita A, Brambilla P. Brain structural effects of antidepressant treatment in major depression. Curr Neuropharmacol 2015;13:458-65.
25. Chen MC, Hamilton JP, Gotlib IH. Decreased hippocampal volume in healthy girls at risk of depression. Arch Gen Psychiatry 2010;67:270-6.
26. Schoenfeld TJ, McCausland HC, Morris HD, Padmanaban V, Cameron HA. Stress and loss of adult neurogenesis differentially reduce hippocampal volume. Biol Psychiatry 2017;82:914-23.
27. Viswanathan G, Dan VM, Radhakrishnan N, Nair AS, Rajendran Nair AP, Baby S. Protection of mouse brain from paracetamol-induced stress by *Centella asiatica* methanol extract. J Ethnopharmacol 2019;236:474-83.
28. Chiroma SM, Hidayat Baharuldin MT, Mat Taib CN, Amom Z, Jagadeesan S, Adenan MI, *et al.* Protective effect of *Centella asiatica* against (D)-galactose and aluminium chloride induced rats: Behavioral and ultrastructural approaches. Biomed Pharmacother 2019;109:853-64.
29. Luo Y, Yang YP, Liu J, Li WH, Yang J, Sui X, *et al.* Neuroprotective effects of madecassoside against focal cerebral ischemia reperfusion injury in rats. Brain Res 2014;1565:37-47.
30. Malathi S, Vidyashree HM, Rajan R. Restoration of memory and acetylcholinesterase activity by *Michelia champaca* in chronically noise-stressed wistar albino rats. Asian J Pharm Clin Res 2016;9:210-4.
31. Gawali NB, Bulani VD, Gursahani MS, Deshpande PS, Kothavade PS, Juvekar AR. Agmatine attenuates chronic unpredictable mild stress-induced anxiety, depression-like behaviours and cognitive impairment by modulating nitrergic signalling pathway. Brain Res 2017;1663:66-77.
32. Yadav M, Jindal DK, Parle M, Kumar A, Dhingra S. Targeting oxidative stress, acetylcholinesterase, proinflammatory cytokine, dopamine and GABA by eucalyptus oil (*Eucalyptus globulus*) to alleviate ketamine-induced psychosis in rats.

Inflammopharmacology 2019;27:301-11.
33. Baker A, Lin CC, Lett C, Karpinska B, Wright MH, Foyer CH. Catalase: A critical node in the regulation of cell fate. Free Radic Biol Med 2023;199:56-66.
34. Pal G, Mishra HP, Suvvari TK, Tanwar A, Ghosh T, Verma P, *et al.* Oxidative stress in wistar rats under acute restraint stress and its modulation by antioxidants and nitric oxide modulators. Cureus 2023;15:e43333.
35. Matsunami T, Sato Y, Sato T, Ariga S, Shimomura T, Yukawa M. Oxidative stress and gene expression of antioxidant enzymes in the streptozotocin-induced diabetic rats under hyperbaric oxygen exposure. Int J Clin Exp Pathol 2009;3:177-88.
36. Che Y, Zhou Z, Shu Y, Zhai C, Zhu Y, Gong S, *et al.* Chronic unpredictable stress impairs endogenous antioxidant defense in rat brain. Neurosci Lett 2015;584:208-13.

Original Article

Impact of Mild Gestational Diabetes Mellitus on Maternal and Fetal Liver Histopathological Alterations

Sahar Ardalan Khales[1,2], Asghar Mafinezhad[3], Masoud Golalipour[4], Gholamreza Roshandel[1], Soraya Ghafari[2], Mohammad Jafar Golalipour[2]

[1]Golestan Research Center of Gastroenterology and Hepatology, Golestan University of Medical Sciences, [2]Gorgan Congenital Malformations Research Center, Golestan University of Medical Sciences, [4]Medical Cellular and Molecular Research Centre, Golestan University of Medical Sciences, Gorgan, [3]Department of Pathology, Shahid Kamyab Hospital, Mashhad University of Medical Sciences, Mashhad, Iran

Abstract

Background: Gestational diabetes mellitus (GDM) is one of the most common pregnancy complications that can affect the organ systems of the body in both the mother and fetus. This study aimed to determine the impact of mild GDM on maternal and fetal liver histopathological alterations. **Materials and Methods:** In this experimental study, 20 pregnant Wistar rats were randomly allocated in control and diabetic groups. Mild hyperglycemia was induced by intraperitoneal injection of streptozotocin (40 mg/kg body weight) on the 5th day of gestation. The control group received an equal volume of citrate buffer. The diabetic state was confirmed by a blood glucose level of 120–300 mg/dL. Maternal and fetal liver samples were obtained on day 19 of gestation and stained with hematoxylin and eosin for histopathological investigation. **Results:** Liver sections of diabetic dams exhibited edematous hepatocytes and scattered pyknotic and necrotic cells with dilated sinusoids and congested central veins. The portal tracts showed the proliferation of bile ducts with mild chronic inflammatory cells infiltrating together with fibrosis beyond the limited plate which extends to the central vein (porto-central fibrosis). Liver sections of their fetuses revealed edematous hepatocytes with increased necrotic cells, with pyknotic nuclei, dilatation of the hepatic sinusoids, and their central veins. There was also a relative increase in megakaryocytes, which promoted fibrosis and distorted vascular beds of the hepatic tissue. The portal tracts also showed bile duct proliferation. **Conclusion:** This study highlighted the adverse effects of uncontrolled mild GDM on liver structure in rat dams and their fetuses.

Keywords: *Fetus, gestational diabetes mellitus, histopathology, liver, rat*

Introduction

Diabetes mellitus (DM) is one of the top 10 causes of death in the world.[1] Type 1, type 2, and gestational DM (GDM) are three main types of DM.[2]

GDM, one of the most common metabolic disorders in pregnancy, affects approximately one in six pregnancies.[3] It is associated with different adverse pregnancy outcomes, including an increased risk of fetal macrosomia, neonatal hypoglycemia, and large for gestational age,[4,5] as well as maternal hypertension, preeclampsia, and cesarean delivery.[4,6-8]

High blood glucose levels can harm the developing organs of the fetus, causing serious birth defects. Wu *et al*. evaluated the relationships of prepregnancy DM and GDM with 12 subtypes of congenital malformations of the newborn among 29,211,974 live births in the United States. Prepregnancy DM and, to a lesser extent, GDM were associated with several subtypes of congenital malformations of the newborn.[9]

The liver, which plays a central and crucial role in maintaining glucose homeostasis, is one of the organs that is severely damaged in DM.[10-13]

Although numerous studies have shown the effects of type 1 and type 2 DM on liver morphology, architecture, and function, limited data are available on the effects of mild GDM on the liver.

In the present study, the hepatic effects of mild GDM *in vivo* were investigated using streptozotocin (STZ)-induced diabetic rats as an experimental model. This experimental study was designed to assess the effect of mild GDM on maternal and fetal liver histopathological alterations.

Materials and Methods

This experimental study was conducted in the Faculty of Medicine, Golestan University of Medical Sciences, Gorgan, Iran. Ethical

This is an open access journal, and articles are distributed under the terms of the Creative Commons Attribution-NonCommercial-ShareAlike 4.0 License, which allows others to remix, tweak, and build upon the work non-commercially, as long as appropriate credit is given and the new creations are licensed under the identical terms.

For reprints contact: WKHLRPMedknow_reprints@wolterskluwer.com

How to cite this article: Ardalan Khales S, Mafinezhad A, Golalipour M, Roshandel G, Ghafari S, Golalipour MJ. Impact of mild gestational diabetes mellitus on maternal and fetal liver histopathological alterations. J Anat Soc India 2024;73:214-7.

Article Info

Received: 26 September 2023
Revised: 04 April 2024
Accepted: 21 May 2024
Available online: 25 September 2024

Address for correspondence:
Prof. Mohammad Jafar Golalipour, Gorgan Congenital Malformations Research Center, Golestan University of Medical Sciences, Gorgan, Iran.
E-mail: mjgolalipour@yahoo.com

Access this article online

Website: https://journals.lww.com/joai
DOI: 10.4103/jasi.jasi_100_23
Quick Response Code:

© 2024 Journal of the Anatomical Society of India | Published by Wolters Kluwer - Medknow

approval was obtained from the Ethics Committee of Golestan University of Medical Sciences, Gorgan, Iran (ethical code: IR.GOUMS.AEC.1401.007). The experimental procedures were performed according to the Guide for the Care and Use of Laboratory Animals.

Animals

Adult Wistar rats were used for experimentation. Animals were maintained under controlled conditions of temperature and humidity, in a 12:12 h light/dark cycle, with free access to water and standard chow.

Drug

Dry STZ (Sigma, USA) powder was dissolved in citrate buffer (pH 4.5) immediately before use.

Experimental design

Females were paired with male rats overnight. The next morning, mating was confirmed by the presence of sperm in the vaginal smear (gestational day 0 [GD0]). The pregnant rats were randomly allocated into two control and diabetic groups (n = 10).

Induction of diabetes

Mild hyperglycemia in pregnant rats was induced by a single intraperitoneal injection of freshly prepared STZ solution (40 mg/kg body weight [b.w.]) on the 5th day of gestation.[14,15] Control pregnant rats received an equivalent volume of citrate buffer.

Blood glucose measurements

Fasting blood glucose was measured before and 72 h after injection.

The diabetic state was confirmed by a blood glucose level of 120–300 mg/dL[16] through the tail vein using a glucometer (Accu-Chek® Active Glucometer, Roche Diagnostics, Germany). Normal blood glucose level (<120 mg/dL) was also checked in the control group.

Histopathological evaluation

On gestation day 19, six pregnant rats of both control and diabetic groups were anesthetized by an intraperitoneal injection of a mixture of ketamine (90 mg/kg b.w.) and xylazine (10 mg/kg b.w.). Liver tissues of both maternal and fetal rats were removed and subjected to histopathological examination. The specimens were immediately fixed in 10% neutral-buffered formalin, dehydrated in a graded ethanol series, cleared in xylene, embedded in paraffin, sectioned at 4–5 µm thickness, and finally stained with hematoxylin and eosin. Sections were studied at the microscopic level (OLYMPUS BX51 microscope), and an OLYMPUS DP12 camera was applied to take digital photos.

Results

- Histopathological studies
- Light microscopy.

Maternal liver tissue

The normal histological architecture of the liver was observed in the dams of the control group.

The hexagonal lobules of hepatocytes were arranged as cords of cells connecting the portal tracts in the periphery to central veins and intermingled by normal sinusoids [Figure 1].

In contrast, the liver of diabetic dams revealed edematous hepatocytes and scattered pyknotic and necrotic cells with dilated sinusoids and congested central veins. The portal tracts showed the proliferation of bile ducts with mild chronic inflammatory cells infiltrate along with fibrosis beyond the limited plate, extending to the central vein (porto-central fibrosis) [Figure 2].

Fetal liver tissue

The fetal liver consisted of hepatocytes and hematopoietic cells. Fetal hepatocytes and their nuclei were large. Normal cords of hepatocytes were separated by primitive vascular sinusoids containing islets of erythrocytes and hematopoietic cells, including erythroid pools, megakaryocytes, and myeloid series [Figure 3].

Fetal liver sections in the GDM group compared to controls exhibited edematous hepatocytes with moderately increased necrotic cells with pyknotic nuclei, dilated sinusoids, and central veins. There was also a relative increase in megakaryocytes, which induced fibrosis and distorted vascular beds of the hepatic tissue (hemangioma like). The portal tracts also showed a proliferation of bile ducts [Figure 4].

Discussion

Evidence from clinical and animal studies shows that DM in pregnancy negatively affects maternal and fetal health. In the present study, the hepatic effects of mild GDM

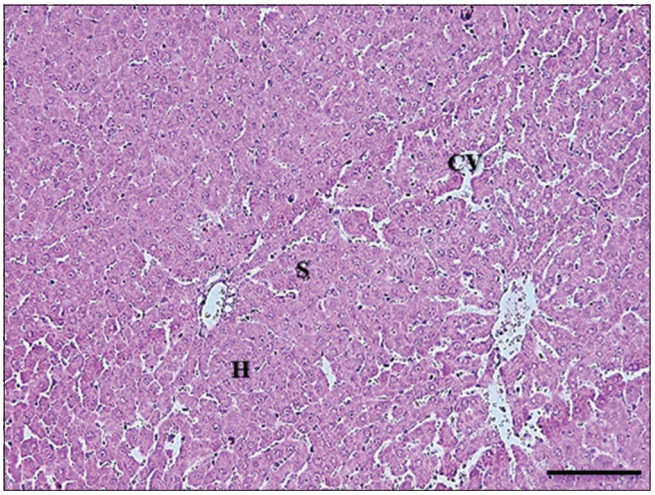

Figure 1: Photomicrograph of hepatic tissue from control dams showing normal histological structure. Hepatocyte, central vein, and blood sinusoid (H and E, ×20, scale bar = 100 µm). H: Hepatocyte, S: Blood sinusoid, CV: Central vein

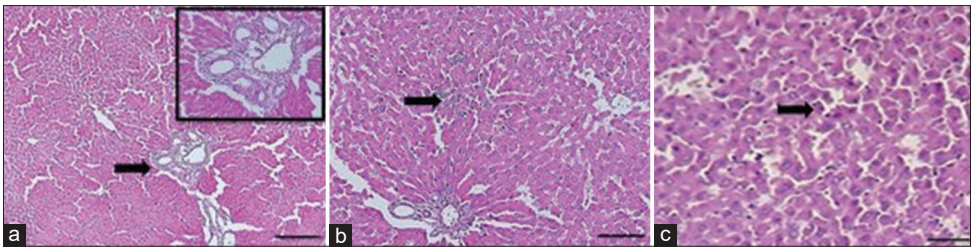

Figure 2: Photomicrographs of hepatic tissue from diabetic dams (H and E). (a) Bile duct proliferation (black arrow) (×10, scale bar = 200 µm, box: ×20), (b) Inflammatory cells (black arrow) (×20, scale bar = 100 µm), (c) Pyknotic nuclei (black arrow) (×40, scale bar = 50 µm)

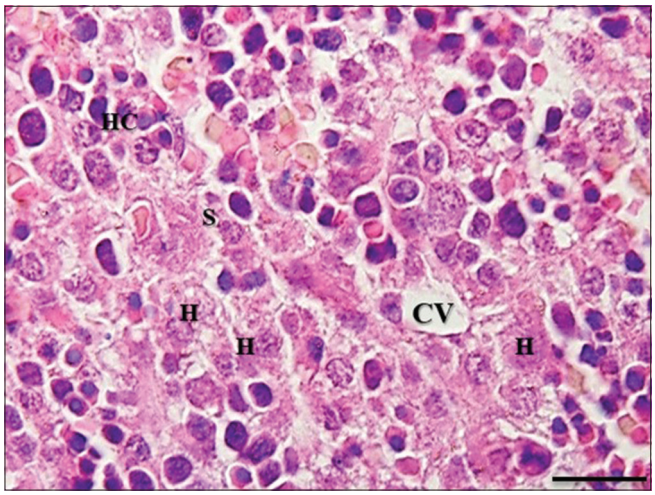

Figure 3: Photomicrograph of the fetal liver section in the control group. Hepatocyte, central vein, blood sinusoid, and hematopoietic cells (H and E, ×100, scale bar = 20 µm). H: Hepatocyte, S: Blood sinusoid, CV: Central vein, HC: Hematopoietic cells

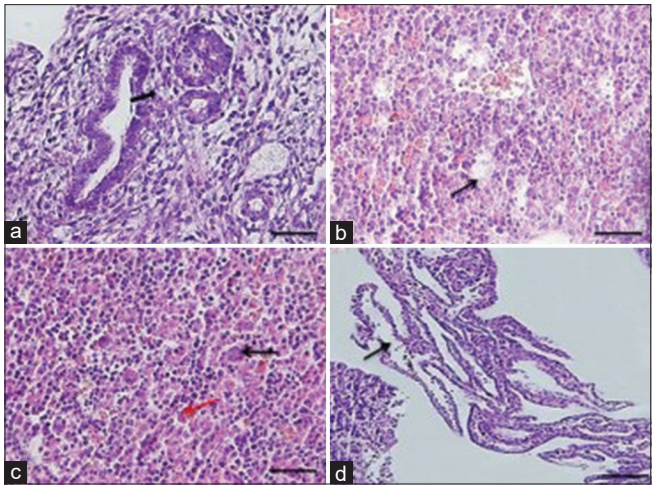

Figure 4: Photomicrographs of fetal liver sections in the diabetic group. (a) Bile duct proliferation (black arrow), (b) Edematous liver tissue (black arrow), (c) Megakaryocytes (black arrow) and pyknotic nuclei (red arrow), (d) Vascular bed tissue proliferation (distorted) (black arrow). (H and E, a,b,c: ×40, scale bar = 50 µm and d: ×20, scale bar = 100 µm)

in vivo were evaluated using STZ-induced diabetic rats as an experimental model. This study highlighted numerous mild-to-moderate histopathological alterations in the liver of rat dams and their fetuses at day 19 of pregnancy following uncontrolled mild GDM.

In line with our findings, previous experimental studies have also shown histological changes in the liver of diabetic rats, their fetuses, and offspring.

Histological changes in the form of an increase in the number of degenerated cells and a significant expansion of the sinusoidal area in the liver of GDM rats (STZ-induced DM in pregnant rats, 40 mg/kg b.w., single intraperitoneal injection) were found in the study of Mahata *et al*.[17]

In examining the effect of maternal DM on fetal liver tissue, the results of the study by El-Sayyad *et al*.,[18] in which DM was induced with two successive intraperitoneal injections of STZ (60 mg/kg b.w.) at days 5 and 6 of gestation and pregnant rats with blood glucose levels above 350 mg/dL were included in the diabetic group, indicated microvesicular and macrovesicular steatosis, moderate fibrotic change, and hepatic necrosis associated with leukocyte infiltration in the liver of mother rats in the diabetic group. Furthermore, edematous blood vessels, increased average of damaged hepatocytes with pyknotic nuclei, and distortion of the hepatic vascular beds were observed in the fetal liver of diabetic mothers.

In another study, the liver of fetuses of diabetic rats (STZ-induced DM before pregnancy, 35 mg/kg b.w., single intraperitoneal injection) on GD20 indicated a loss of cellular boundaries of hepatocytes with dispersed nuclei, hemorrhage with hemosiderin pigments deposition, dilated and congested central veins and sinusoids, vacuolar degenerations, areas of necrosis, abundant lymphocytes, and megakaryocytosis.[19]

In addition, a study by Ahmed *et al*.[20] indicated that maternal DM during pregnancy has also detrimental effects on histological architecture and integrity of the liver in rat offspring. Compared with the normal control group, the liver of offspring of diabetic dams at birth demonstrated abnormal histological architecture. Hepatic strands were less organized, and many hepatocytes had pyknotic nuclei. At the end of the 1st postnatal week, severe widening of the central vein, albuminous material accumulation with focal necrotic areas, and degenerated hepatocytes associated with abnormal distribution of condensed cytoplasm and karyoplasms were reported, whereas at the end of the 2nd postnatal week, the central vein was congested with blood, and the hepatocytes hydropically degenerated, and their nuclei became pyknotic.

In animal models of GDM, hyperglycemia conditions can cause liver injury, which leads to hyperinsulinemia and insulin resistance. Hyperglycemia induces an inflammatory state and oxidative stress, consequently exacerbating the liver injury process by triggering the NF-B activation, which will stimulate the proapoptotic genes activity in liver cells and enhance the reactive oxygen species production.[17,21] Increasing glucose transport from pregnant women with DM to the fetus leads to fetal hyperglycemia and hyperinsulinemia. The fetal liver is directly affected by the fetal glucose levels through excess deposition of glycogen under the action of fetal insulin.[22-24]

Conclusion

Numerous mild-to-moderate histopathological alterations were detected in the liver of rat dams and their fetuses following uncontrolled mild GDM.

Acknowledgments

The authors sincerely appreciate the cooperation of all personnel in the laboratory and Department of the congenital malformations research center and the animal house of Golestan University of Medical Sciences.

Financial support and sponsorship

This work was funded and supported by the Deputy of Research and Technology of Golestan University of Medical Sciences (Grant No. 111755). The results described in this paper were part of the PhD dissertation of S.A.KH

Conflicts of interest

There are no conflicts of interest.

References

1. World Health Organization (WHO). The Top 10 Causes of Death. Available from: https://www.who.int/news-room/fact-sheets/detail/the-top-10-causes-of-death. [Last accessed on 2020 Dec 09].
2. Saeedi P, Petersohn I, Salpea P, Malanda B, Karuranga S, Unwin N, *et al*. Global and regional diabetes prevalence estimates for 2019 and projections for 2030 and 2045: Results from the International Diabetes Federation Diabetes Atlas, 9th edition. Diabetes Res Clin Pract 2019;157:107843. [doi: 10.1016/j.diabres.2019.107843].
3. Cho NH, Shaw JE, Karuranga S, Huang Y, da Rocha Fernandes JD, Ohlrogge AW, *et al.* IDF diabetes atlas: Global estimates of diabetes prevalence for 2017 and projections for 2045. Diabetes Res Clin Pract 2018;138:271-81.
4. HAPO Study Cooperative Research Group, Metzger BE, Lowe LP, Dyer AR, Trimble ER, Chaovarindr U, *et al.* Hyperglycemia and adverse pregnancy outcomes. N Engl J Med 2008;358:1991-2002.
5. Damm P, Houshmand-Oeregaard A, Kelstrup L, Lauenborg J, Mathiesen ER, Clausen TD. Gestational diabetes mellitus and long-term consequences for mother and offspring: A view from Denmark. Diabetologia 2016;59:1396-9.
6. Kim C, Newton KM, Knopp RH. Gestational diabetes and the incidence of type 2 diabetes: A systematic review. Diabetes Care 2002;25:1862-8.
7. Yogev Y, Xenakis EM, Langer O. The association between preeclampsia and the severity of gestational diabetes: The impact of glycemic control. Am J Obstet Gynecol 2004;191:1655-60.
8. Marchetti D, Carrozzino D, Fraticelli F, Fulcheri M, Vitacolonna E. Quality of life in women with gestational diabetes mellitus: A systematic review. J Diabetes Res 2017;2017:12. [doi: 10.1155/2017/7058082].
9. Wu Y, Liu B, Sun Y, Du Y, Santillan MK, Santillan DA, *et al.* Association of maternal prepregnancy diabetes and gestational diabetes mellitus with congenital anomalies of the newborn. Diabetes Care 2020;43:2983-90.
10. Balázs M, Halmos T. Electron microscopic study of liver fibrosis associated with diabetes mellitus. Exp Pathol 1985;27:153-62.
11. Latry P, Bioulac-Sage P, Echinard E, Gin H, Boussarie L, Grimaud JA, *et al.* Perisinusoidal fibrosis and basement membrane-like material in the livers of diabetic patients. Hum Pathol 1987;18:775-80.
12. Tolman KG, Fonseca V, Tan MH, Dalpiaz A. Narrative review: Hepatobiliary disease in type 2 diabetes mellitus. Ann Intern Med 2004;141:946-56.
13. Tolman KG, Fonseca V, Dalpiaz A, Tan MH. Spectrum of liver disease in type 2 diabetes and management of patients with diabetes and liver disease. Diabetes Care 2007;30:734-43.
14. Merzouk H, Madani S, Chabane Sari D, Prost J, Bouchenak M, Belleville J. Time course of changes in serum glucose, insulin, lipids and tissue lipase activities in macrosomic offspring of rats with streptozotocin-induced diabetes. Clin Sci (Lond) 2000;98:21-30.
15. Damasceno DC, Sinzato YK, Bueno A, Netto AO, Dallaqua B, Gallego FQ, *et al.* Mild diabetes models and their maternal-fetal repercussions. J Diabetes Res 2013;2013:473575.
16. Saito FH, Damasceno DC, Kempinas WG, Morceli G, Sinzato YK, Taylor KN, *et al.* Repercussions of mild diabetes on pregnancy in Wistar rats and on the fetal development. Diabetol Metab Syndr 2010;2:26.
17. Mahata LE, Ali H, Murni AW. Effect of streptozotocin on liver histology damage in rats model of gestational diabetes mellitus. Int J Res Rev 2021;8:18-22.
18. El-Sayyad HI, Al-Haggar MM, El-Ghawet HA, Bakr IH. Effect of maternal diabetes and hypercholesterolemia on fetal liver of albino Wistar rats. Nutrition 2014;30:326-36.
19. Mohamed S, Salem N, Hassan H, Abdelrahman G. Role of Vitamin E in modulating the effect of Streptozotocin-induced maternal diabetes on fetal liver development in albino rat. Med Updates 2021;7:25-47.
20. Ahmed OM, Aref AM, Semmler M, Ali LA. Maternal diabetes mellitus disturbs histological architecture and integrity of liver and kidney in rat offspring. Merit Res J Med Med Sci 2015;3:335-46.
21. Ugwu M, Umar I, Utu-Baku A, Dasofunjo K, Ukpanukpong R, Yakubu O, *et al.* Antioxidant status and organ function in streptozotocin-induced diabetic rats treated with aqueous, methanolic and petroleum ether extracts of *Ocimum basilicum* leaf. J Appl Pharm Sci 2013;3:S75.
22. Khoury JC, Dolan LM, Vandyke R, Rosenn B, Feghali M, Miodovnik M. Fetal development in women with diabetes: Imprinting for a life-time? J Matern Fetal Neonatal Med 2012;25:11-4.
23. İlhan G, Gültekin H, Kubat A, Gokmen Karasu AF, Güngör ES, Zebitay GA, *et al.* Preliminary evaluation of foetal liver volume by three-dimensional ultrasound in women with gestational diabetes mellitus. J Obstet Gynaecol 2018;38:922-6.
24. Perovic M, Gojnic M, Arsic B, Pantic I, Stefanovic T, Kovacevic G, *et al.* Relationship between mid-trimester ultrasound fetal liver length measurements and gestational diabetes mellitus. J Diabetes 2015;7:497-505.

Original Article

Hepatoprotective Effects of Curcumin on Liver Injury in Streptozocin-induced Diabetic Rats

Bilge Bal Ozkaptan, Dilek Sagir[1], Fatma Aksoy[2]

Department of Nursing, Faculty of Health Sciences, Sinop University, [1]Department of Occupational Health and Safety, Faculty of Health Sciences, Sinop University, Sinop, [2]Vocational School of Health Services, Tokat Gaziosmanpaşa University, Tokat, Türkiye

Abstract

Introduction: Type 2 diabetes mellitus is characterized by chronically elevated blood sugar levels associated with disruption of the inflammatory and oxidative state and dyslipidemia. Curcumin is a highly pleiotropic molecule with hypoglycemic, hypolipidemic, anti-inflammatory, and antioxidant properties. The aim of this study was to evaluate the effects of curcumin on the liver of streptozotocin-induced diabetic rats. **Materials and Methods:** Thirty-two adult male rats were used in the study. The rats were divided into four groups: Control (C), Diabetes (D), Curcumin (CUR), and Diabetes + Curcumin (D + CUR) (n = 8). The groups given curcumin were given 60 mg/kg curcumin by gavage once a day during the 14-day study period. At the end of the experiment, biochemical, stereological, histological, and immunohistochemical analyses were performed on blood and liver samples taken from rats sacrificed. **Results:** After curcumin treatment in diabetic rats, there was a significant decrease in blood glucose levels, hepatic markers, and levels of thiobarbituric acid reactive substances ($P < 0.01$). Furthermore, a significant increase in enzymatic antioxidants such as superoxide dismutase, catalase, and glutathione peroxidase was observed after treatment ($P < 0.01$). It was determined that curcumin decreased the apoptotic index and the number of dual-nucleated hepatocytes in the liver, and provided support for liver regeneration ($P < 0.01$). **Discussion and Conclusion:** Based on the findings of this study, it can be concluded that curcumin has the potential to protect against hyperglycemia-induced oxidative stress and apoptosis in liver cells, and also induces regeneration in damaged liver.

Keywords: *Apoptosis, curcumin, diabetes, liver, oxidative stress*

Introduction

Diabetes mellitus (DM) is one of the most important chronic noncommunicable diseases in the world and the prevalence of DM is constantly increasing with the continuous increase in the number of patients.[1] Basically, it is a metabolic disease characterized by hyperglycemia resulting from defects in insulin secretion, insulin action, or both.[2] Hyperglycemia promotes oxidative stress, inflammation, and apoptosis in tissues.[3,4] Glucose autoxidation and protein glycosylation[5] are responsible for the production of free radicals[6] that promote inflammation and apoptosis in tissues.[7] Both experimental and clinical studies have shown that oxidative stress plays an important role in the pathophysiology of diabetes.[8] Reactive oxygen species (ROS) are produced disproportionately by various means in diabetes.[9] Changes in oxidative stress biomarkers such as glutathione (GSH), superoxide dismutase (SOD), catalase (CAT), GSH reductase, and glutathione peroxidase (GPx) can be evaluated as a quantitative measure of oxidative damage in diabetes.

The liver is the largest and most complex internal organ in the body. It is involved in many vital functions such as converting toxic substances into useful molecules, secretion, storage and metabolism.[10,11] Diabetes has proven to be the most common cause of liver damage, so the prevalence of liver disease in diabetic patients is high.[12] Oxidative stress and inflammation are diabetes complication parameters that cause hepatic damage.[13]

A definite solution has not yet been found in the treatment of both diabetes and its complications, and studies for the discovery of new active substances for treatment are still continuing intensively. Today, the main clinical treatment of diabetes is insulin given to patients to keep blood sugar under control. In addition, the use of antioxidants

This is an open access journal, and articles are distributed under the terms of the Creative Commons Attribution-NonCommercial-ShareAlike 4.0 License, which allows others to remix, tweak, and build upon the work non-commercially, as long as appropriate credit is given and the new creations are licensed under the identical terms.

For reprints contact: WKHLRPMedknow_reprints@wolterskluwer.com

How to cite this article: Ozkaptan BB, Sagir D, Aksoy F. Hepatoprotective effects of curcumin on liver injury in streptozocin-induced diabetic rats. J Anat Soc India 2024;73:218-26.

Article Info

Received: 05 June 2023
Revised: 11 August 2024
Accepted: 11 August 2024
Available online: 25 September 2024

Address for correspondence:
Dr. Bilge Bal Ozkaptan, Faculty of Health Sciences, Sinop University, Sinop 57000, Turkey.
E-mail: bilgebal57@hotmail.com

Access this article online

Website: https://journals.lww.com/joai
DOI: 10.4103/jasi.jasi_55_23
Quick Response Code:

© 2024 Journal of the Anatomical Society of India | Published by Wolters Kluwer - Medknow

is widely discussed in the literature to prevent secondary complications that may occur due to oxidative stress caused by diabetes, and the use of different antioxidant substances is recommended.[14]

Curcumin is the active ingredient in the dietary spice turmeric (Curcuma longa), which is used as a traditional herbal medicine and is the subject of clinical trials for various diseases such as cancer, diabetes, Alzheimer's disease, and ulcerative colitis.[15] Curcumin is a well-known antioxidant[16] and a highly pleiotropic molecule reported to have a wide variety of pharmacological activities such as antibacterial,[17] anti-inflammatory, anticancer, antioxidant,[18] hypoglycemic,[17] antiatherosclerotic, antimicrobial,[19] and wound healing.[20,21] In addition, curcumin has been found to interact directly with various intracellular signaling molecules.[22] Its healing effects have been shown to be mediated through the modulation of multiple cell signaling molecules such as apoptotic proteins, cyclooxygenase-2, nuclear factor-B,[13] STAT3, IKK, interleukin [IL]-1, IL endothelin-1, C-reactive protein,[23] pro-inflammatory cytokines (tumor necrosis factor,[24] malondialdehyde, GSH,[25] and total cholesterol.[26] Most importantly, it has been reported that curcumin has the capacity to scavenge ROS directly.[22]

As a result of our extensive literature search, we saw that most of the studies focused on the beneficial effects of curcumin on the biochemical parameters of diabetic rats.[22,27,28] We did not find a study in which biochemical data were supported by histopathological and stereological data. Accordingly, in this study, we aimed to investigate how oxidative stress caused by diabetes in the liver of rats with DM by streptozotocin (STZ) would be affected by curcumin, a powerful antioxidant, using biochemical, histochemical, immunohistochemical, and stereological analyses.

Materials and Methods

Animals

This study was carried out with the permission of Ondokuz Mayıs University Animal Experiments Local Ethics Committee. In the study, 32 adult male Wistar albino species (290–330 g) rats raised in Ondokuz Mayıs University Faculty of Medicine Experimental Animals Research and Application Center were used. The rats were housed in a constant temperature (24°C ± 1°C), humidity (50% ± 5%), and 12-h dark/light environment with three rats per cage throughout the study. Tap water and standard laboratory food were available as *ad libitum*.

Experimental plan

Rats were randomly divided into four groups (n = 8); Control (C), Diabetic (D), Diabetic + Curcumin (D + CUR), and Curcumin (CUR). Rats to be treated with curcumin were given 60 mg/kg/day curcumin (Sigma Aldrich, Australia) orally once a day for the 14-day study. No treatment was applied to the control groups. At the end of the 14-day experiment, liver tissues were removed by intracardiac perfusion under ketamine anesthesia in all rats. The removed livers were taken into 10% formaldehyde for fixation for histopathological examination. A portion of the liver was frozen (−80) for biochemical analysis.

Induction of diabetes in rats

To induce diabetes, a single dose of 50 mg/kg STZ (BioShop STR 201.1) was administered intraperitoneally to rats in groups D and D + CUR.[29] Three days later, animals with fasting blood glucose levels of 250 mg/dL and above in the blood samples taken from the tail vein of these rats as measured by a glucometer (Contour TS Bayer) were included in the study.[30]

Measurement of body weight

Body weights of all animals in the study were measured on the 1st day of the study and on the last day of the study before being sacrificed.

Biochemical analysis

At the end of experimentation, whole blood was collected from anesthetized rats through heart puncture. Blood samples were centrifuged at 3000 g, for 15 min at 4°C for the separation of serum.

Assay of hepatic marker enzymes

The estimation of aspartate aminotransferase (AST), alanine aminotransferase (ALT), and alkaline phosphatase (ALP) in serum was estimated using diagnostic kits (Span Diagnostics Ltd, Surat, Gujarat, India).

Estimation of lipid peroxidation and antioxidants

The liver was harvested from all experimental rats, and washed with ice-cold saline. The liver was harvested from all experimental rats, and washed with ice-cold saline. The harvested liver was used for histopathology and estimation of lipid peroxidation and antioxidant status. The level of thiobarbituric acid reactive substance (TBARS), and the activity of SOD, CAT, and GPx enzymes in the liver were measured.[31-34]

Histopathological analysis

Liver tissues were fixed with 10% formaldehyde. After fixation, the tissues were followed by routine histological tissue follow-up procedures and embedded in paraffin. Sections of 5 μm thickness were taken from the tissue blocks and stained with hematoxylin and eosin (H and E) and Periodic Acid–Schiff (PAS) stains for examination under the light microscope. While hydropic degeneration, mononuclear cell infiltration, sinusoidal expansion, necrotic cells, and fibrosis were evaluated in tissues stained with H and E stain,

glycogen content of tissues stained with PAS stain was evaluated. Histopathological evaluations were made with semiquantitative analysis and photomicrographs were taken using Leica DM4000 B and visualization software.

Stereological analysis

In the study, optical dissector (unbiased counting frame) and fractionator methods were used for numerical density estimates of binuclear hepatocytes in liver tissue [Figure 1]. Counting of hepatocytes was done at ×40 and numerical density was estimated using the following formula:[35]

Numerical density (binuclear hepatocytes) = Total markers/ dissector volüme (μm^3) × the number of sampling sites.

Immunohistochemical analysis

Terminal Deoxynucleotidyl Transferase dUTP nick end labeling (TUNEL) assay

The sections were stained in accordance with the recommended standard procedure using the In Situ Cell Death Detection, POD (Roche, Manheim, Germany) apoptosis kit. The 4 µm thick sections were placed on adhesive slides. They were dried in an incubator at 370C for one night. They were deparaffinized in Xylol and dehydrated in serial alcohols. To eliminate the masking effect of formalin on tissue, the sections were boiled in a citrate buffer solution in a microwave oven at 300 W for 5 min. After washing, they were left in 3% H_2O_2 prepared in methanol for 10 min to eliminate endogenous peroxidase activity. After the sections were left in a mixture of terminal deoxynucleotidyl transferase enzyme and marking solution at 37°C for 1 h, they were held in a protein blocking serum for 10 min to prevent their nonspecific antigenic binding. They were incubated with peroxidase-conjugated antifluorescein isothiocyanate antibody at 37°C for 30 min. The sections were washed twice with phosphate-buffered saline for 5 min after all procedures except for the incubation with protein blocking serum. A 3-amino-9-ethylcarbazole (AEC; Zymed RED substrate kit, Paisley, OR, USA) chromogen was used to stain the sections. The staining was performed under a microscope for 10 min. The sections stained with AEC substrate and contrast stained with hematoxylin and sealed using a water-based adhesive (Shandon Immu-mount, Thermo Scientific™- 9990402, Schwerte, Germany).

Apoptotic index measuring

In the tissue sections stained by the TUNEL method, the determination of apoptotic activity was performed under a light microscope (Nikon Eclipse E600W with Nikon DS-5M camera attachment, Tokyo, Japan). In 10 different areas, randomly selected in each section, red-brownstained nuclei were considered positive, and bluestained nuclei were considered negative, regardless of the staining intensity of the cells. At least 100 (positive and negative) nuclei were counted in each area. Then, the apoptotic index was calculated using the following formula:

$$Apoptotic\ Index\ (AI) = \frac{Positive\ apoptotic\ cell\ count}{Total\ positive\ and\ negative\ cell\ count} \text{ X } 100$$

Immunohistochemical stain for Ki67

Liver regeneration analysis was performed against Ki67 antigens by immunohistochemical staining using monoclonal primary anti-Ki67 antibodies (1: 100; Abcam, ab15580). Immunohistochemical analysis was performed using the Ventana BENCHMARK GX automated immunohistochemistry staining device. Regardless of the staining intensity of the cells, nuclei staining brown–black was considered positive and scoring was done in 10 randomly selected areas in each section (scoring; -: none, +: mild, ++: moderate, +++: severe, ++++: very severe).

Statistical analysis

Numerical data obtained from all groups in our study were statistically evaluated using the SPSS program (SPSS version 21.0; SPSS Inc., Chicago, IL, USA). The data used were expressed as mean ± standard deviation. As a result of the normality and homogeneity tests of the data of the groups, the differences between the groups with normal distribution were evaluated with one-way ANOVA and Bonferroni tests, while the groups without normal distribution were examined with the Kruskal–Wallis and Tamhane's T2 tests. In the statistical evaluation, $P < 0.01$ was considered statistically significant.

Results

Body weights and blood glucose values

As a result of the statistical analysis, glucose values of diabetic rats increased significantly compared to the control group ($P < 0.01$), while glucose values of diabetic rats treated with curcumin were higher than the control group and significantly lower than the diabetes group ($P < 0.01$). There was no significant difference in rats in the control and curcumin groups ($P > 0.01$) [Table 1].

When the weighing results before sacrification were compared on the last day of the study, there was no significant change in body weights of rats in the control and curcumin groups, while there was a significant decrease in body weights of diabetic rats ($P < 0.01$). Diabetic rats treated with curcumin did not decrease as much as in diabetic rats ($P < 0.01$) [Table 1].

Biochemical results

Hepatic markers

The hepatic markers AST, ALT, and ALP levels in the serum of rats in the control and experimental groups are shown in Table 2. In diabetic rats, AST, ALT, and ALP levels significantly increased ($P < 0.01$) compared to rats in the control group. Curcumin-treated groups had a

significantly lower level of hepatic markers compared to diabetic control rats. There was no significant difference in the levels of these hepatic markers between rats given curcumin alone and control rats ($P > 0.01$).

Lipid peroxidation

TBARS levels in the liver of rats in the control and experimental groups are shown in Table 2. Diabetic rats were found to have significantly higher TBARS levels ($P < 0.01$) when compared to control rats. Diabetic rats treated with curcumin were found to significantly inhibit high TBARS levels of curcumin when compared to diabetic rats ($P < 0.01$).

Antioxidant enzymes

In the statistical comparison of the activities of antioxidant enzymes such as SOD, CAT, and GPx between the groups [Table 2], it was determined that these enzyme activities were significantly decreased in diabetic rats compared to control rats ($P < 0.01$). Diabetic rats treated with curcumin showed a significant increase in SOD, CAT, and GPx activity in liver tissue compared to control rats ($P < 0.01$).

Histopathological results

No histopathological changes were observed in the liver tissue of the control group rats. In the center of the hepatic lobule, radially arranged hepatocytes separated from each other by the central vein and sinusoids were normal [Figure 2a]. When the PAS staining of the control group was evaluated, it was observed that they had normal glycogen stores [Figure 3a]. Liver sections of rats in the curcumin group were similar to the control group in both staining types [Figures 2b and 3b].

When liver sections of diabetic rats were examined; hydropic degeneration with nonlipid vacuolization in hepatocytes, heterochromatinization in nuclei, and hypertrophy in endothelial and Kupffer cells were clearly seen. Sinusoids showed irregularity, while expanding in some parts of the tissue, there were roundings with narrowing in some parts. There were foci of mononuclear cell infiltration in some parts of the tissue and there was congestion in the veins. Apoptotic hepatocytes, called councilman body, with a low level of pycnotic nuclei and hypereosinophilia cytoplasm were found [Figure 2c and d]. There were more PAS (+) stained cells in this group in direct proportion to the increased amount of glycogen in hepatocytes [Figure 3c].

Diabetic rats treated with curcumin showed improvement in cell arrangement, size of endothelial and Kupffer cells, and morphology of nuclei of hepatocytes when compared to diabetic rats. There were narrowings in the sinusoidal areas around the central vein, as in diabetic rats. In terms of glycogen content, there was a decrease compared to the diabetes group. Hydropic degeneration was found in a small amount in this group. Mononuclear cell infiltration and vein congestion were not observed, and fibrosis was not observed in all groups [Figures 2e and 3d].

Stereological results

The numerical density of binuclear hepatocytes in all groups is shown in Figure 4. When the control group was compared with the diabetes group, an increase in the number of binuclear nuclei was found in the diabetes group ($P < 0.01$). The curcumin group was similar to the control, but there was no statistical difference ($P > 0.01$). In the diabetes group treated with curcumin, there was a tendency toward less binuclear core density compared to diabetes ($P < 0.01$).

Immunohistochemical results

Transferase dUTP nick end labeling staining and apoptotic index results

As a result of the statistical analysis, it was found that the apoptotic index value in the diabetes group was higher than the other groups ($P < 0.01$). The apoptotic index value of the diabetes + curcumin group was also found to be higher than the control and curcumin groups, and less than the diabetes group ($P < 0.01$). There was no significant difference between the control and curcumin groups ($P > 0.01$) [Figure 5 and Table 3].

Ki67 analysis results

Ki67 immunoreactivity was localized in the nucleolus of liver hepatocytes. Cells staining positive as a result of

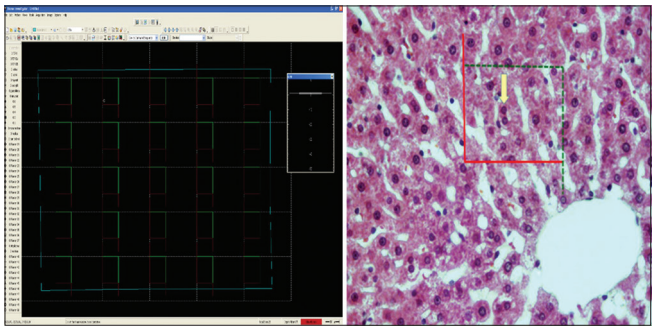

Figure 1: Binuclear hepatocytes were counted using a stereo investigator in a specific area of the confocal microscope image. In the figure, the yellow arrow in the frame shows the binuclear hepatocytes

Table 1: Final body weight and serum glucose concentrations of rats in all groups

Groups	Parameters	
	Body weight±SD	Glucose (mg/dL) ± SD
C	323.13±4.79	101±8.88
D	252.13±6.60*	433.75±34.12*
CUR	312.63±11.46#	104.37±6.41#
D + CUR	290±9.02*,#	190.37±10.95*,#

*Significantly different from C group: $P<0.01$, #Significantly different from D group: $P<0.01$. Data are presented as mean±SD ($n=8$). SD: Standard deviation, CUR: Curcumin, D + CUR: Diabetes + CUR

Ki67 expression are shown in Figure 6a-d. As a result of the semiquantitative evaluation, it was observed that the number of Ki67-positive staining cells in the Curcumin group increased compared to the control, and the number of pale-stained positive cells was higher in the diabetes group compared to the control group. In diabetic rats treated with curcumin, Ki67-stained cell density was found to be lower than in diabetic rats [Table 4].

Discussion

In diabetic rats, oxidative stress increases due to hyperglycemia caused by insulin deficiency and is accompanied by inflammation and apoptosis.[7] Therefore, in our study, we investigated the efficacy of curcumin treatment with STZ on complications related to hyperglycemia in the livers of diabetic rats and found four important findings.

The first of these findings is that curcumin lowers glucose levels in diabetic rats and accordingly treats body weight and liver markers. In our study, a decrease in body weight was observed due to high blood glucose, excessive food consumption, and depletion of insulin-producing pancreatic β-cells in rats in whom we developed diabetes with STZ. We can explain this situation as follows; STZ induces pancreatic β-cell destruction, resulting in decreased insulin synthesis and secretion; this manifests itself as hyperglycemia. It also leads to weight loss due to decreased insulin secretion, and lack of use of carbohydrates as an energy source, thereby increasing the breakdown of protein and fat.[36] Treatment with curcumin significantly lowered blood glucose levels, resulting in an increase in body weight. It has been reported that the antihyperglycemic effects of curcumin and its derivatives are due to lowering plasma levels of free fatty acids in the liver and reducing hepatic glucose production.[37] Therefore, we can say that curcumin reduces hyperglycemia, which can strengthen the anabolic role of carbohydrate metabolism, improves the synthesis of structural proteins, and thus increases body weight. However, hepatic markers such as AST, ALT, and

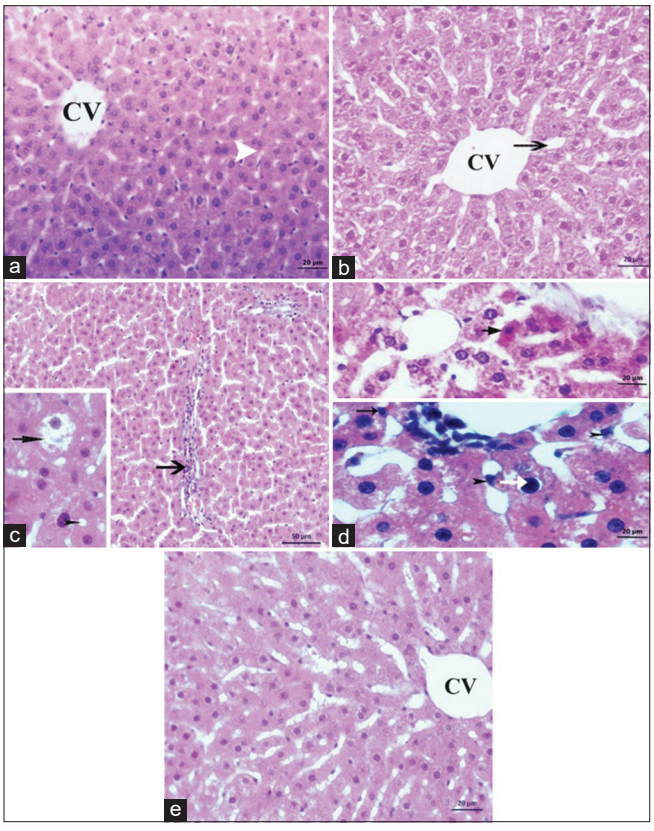

Figure 2: Photomicrographs of rat liver sections stained by H and E. Control group (a): The normal histological appearance of the liver shows the white arrow hepatocytes. Curcumin group (b): Sinusoid (black arrow). Diabetes group (c): Steatosis (white arrow), mononuclear infiltration (black long arrow), hydropic degeneration (black short arrow), sinusoidal narrowing (arrowhead). Diabetes group (d): Councilman body (black short arrow), heterochromatinization in the nucleus (white arrow), hypertrophy in Kupffer cell (arrowhead), hypertrophy in the endothelium (black long arrow), Diabetes+Curcumin group (e). central vein (CV)

Table 2: Hepatic markers, lipid peroxidation markers, enzymatic, and nonenzymatic antioxidant values in the liver of rats in all groups

Parameters	Groups			
	C	D	CUR	D + CUR
AST	73.46±3.00	113.52±7.34*	70.75±2.20#	94.16±5.09*,#
ALT	34.23±2.15	64.85±3.13*	32.50±2.22#	45.27±2.92*,#
ALP	75.39±2.52	140.93±1.75*	74.36±2.68#	103.38±5.53*,#
TBARS	0.88±0.05	3.89±0.14*	0.89±0.08#	2.07±0.17*,#
SOD	8.90±0.30	4.11±0.18*	8.81±0.37#	6.93±0.18*,#
CAT	81.78±2.93	50.06±1.73*	78.98±3.58#	64.09±3.90*,#
GPx	11.07±0.31	4.41±0.37*	10.69±0.47#	8.26±0.40*,#

*Significantly different from C group: $P<0.01$, #Significantly different from D group: $P<0.01$. Data are presented as mean±SD ($n=8$). SD: Standard deviation, CUR: Curcumin, D + CUR: Diabetes + CUR, AST: Aspartate aminotransferase, ALP: Alkaline phosphatase, ALT: Alanine aminotransferase, TBARS: Thiobarbituric acid reactive substances, SOD: Superoxide dismutase, CAT: Catalase, GPx: Glutathione peroxidase

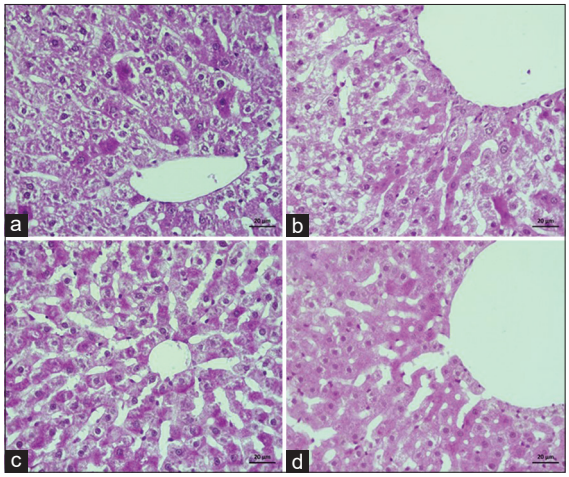

Figure 3: Dark pink stained appearance of glycogen content of all groups with periodic acid–Schiff stain. Control group (a), Curcumin group (b), Diabetes group (c), Diabetes + Curcumin (d)

ALP significantly increased in STZ-induced diabetic rats. This may be due to increased inflammation and necrosis in liver cells due to increased glucose levels in the bloodstream. These enzymes pass from the cytoplasm of hepatocytes into the circulation. Therefore, the increase in the blood levels of these markers indicates the hepatotoxic effect of STZ-induced diabetes.[37] The fact that these hepatic markers in diabetic rats treated with curcumin were lower than those in the diabetes group also showed that curcumin was hepatoprotective.

The second important finding obtained from the study was that curcumin reduces biomarkers of oxidative damage and increases endogenous antioxidant defenses. Increased oxidative stress, lipid peroxide-mediated damages, and impaired antioxidant systems are hallmarks in the pathogenesis of DM.[37-39] The increase of endogenous peroxides in the cell may initiate uncontrolled lipid peroxidation, which may lead to cellular infiltration and cell damage.[40] Increasing lipid peroxidation impairs the functioning of the membrane by reducing membrane fluidity and causes increased membrane stiffness and decreased cellular deformation, which collectively leads to deterioration of the general functioning of the cell by inducing membrane lipid peroxidation induced by free radicals.[41]

TBARS is a widely used lipid peroxidative marker in the STZ-induced diabetic rat model.[42] In this study, it was observed that TBARS levels increased in diabetic rats. This result indicates high levels of oxidative stress in the liver of diabetic rats. Treatment with curcumin significantly reduced the level of TBARS in the liver, indicating that curcumin has antioxidant properties.

SOD, CAT, and GPx are enzymatic antioxidants that block the free radical process. SOD is an important endogenous antioxidant enzyme that acts as a component of the first-line defense system against ROS. It has the ability to reduce the superoxide radical to hydrogen peroxide (H_2O_2). CAT catalyzes the reduction of H_2O_2 and protects tissues against reactive hydroxyl radicals.[43] GPx is an important intracellular enzyme that breaks down H_2O_2 into water and binds lipid peroxides to their corresponding alcohols, mainly in the mitochondria and sometimes in the cytosol.[44]

Table 3: Apoptotic index means and standard deviations of the groups

Groups	Apoptotic index
C	25.60±1.27
D	77.89±2.75*,#
CUR	24.59±1.64
D + CUR	54.41±2.91*,#,!

*Significantly different from C group: $P<0.01$, #Significantly different from D group: $P<0.01$. !Significantly different from CUR group: $P<0.01$. Data are presented as mean±SD ($n=8$). SD: Standard deviation, CUR: Curcumin, D + CUR: Diabetes + CUR

Cells suffer from peroxide overload when there is an increase in SOD levels without a proportional increase in peroxidases (GPx). However, excess peroxide formed can react with transition metals and form the most harmful

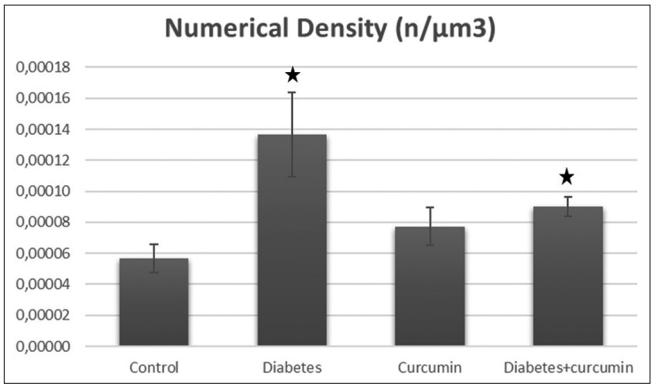

Figure 4: Numerical density data for all groups. *Indicates statistical difference compared to control group ($P < 0.01$)

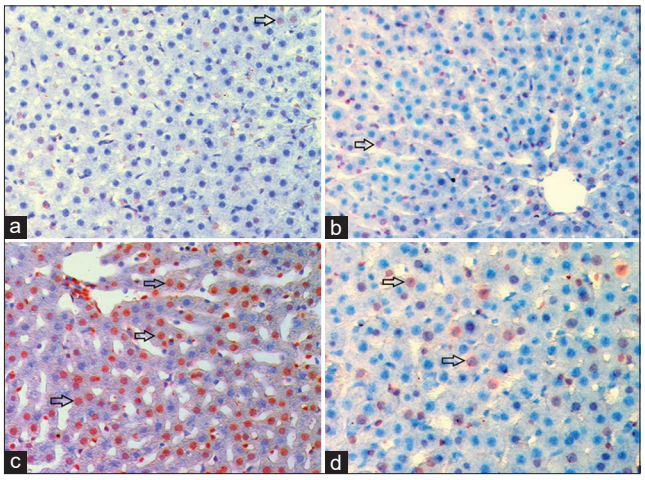

Figure 5: Apoptotic nuclei in liver tissues of rats in all groups. Arrows: Positive nuclei. Control group (a), Curcumin group (b), Diabetes group (c), Diabetes + Curcumin (d). Transferase dUTP nick end labeling ×200

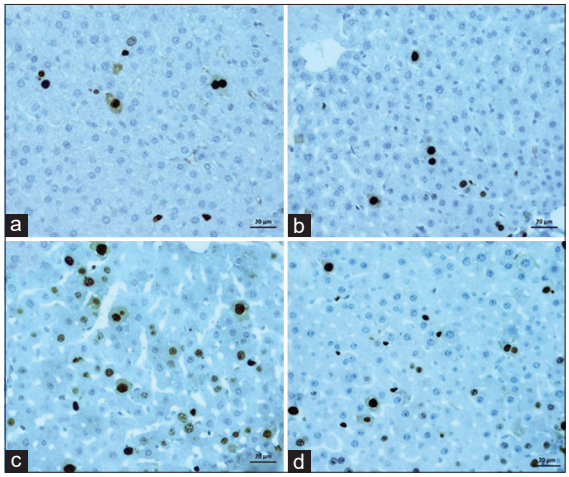

Figure 6: Photomicrographs of liver sections stained with Ki67 in the different groups. Control group (a), Curcumin group (b), Diabetes group (c), Diabetes + Curcumin (d)

Table 4: Density of cells staining Ki67 positive in the livers of rats in all groups

	C	D	CUR	D + CUR
Density of cells staining Ki67 positive	+	+++	++	++++

−: None, +: Mild, ++: Moderate, +++: Severe, ++++: Very severe. CUR: Curcumin, D+CUR: Diabetes+CUR

hydroxyl radicals.[45] The increase in glucose level caused by DM can inactivate antioxidant enzymes such as SOD, CAT, and GPx by glycating these proteins and thus initiating oxidative stress that causes lipid peroxidation.[46] Several previous studies have reported that curcumin can improve CAT, SOD, and GPx activity levels in diabetic rats.[47,48] In the current study, we believe that curcumin has a strong effect on reducing oxidative stress in diabetic rats since curcumin brought CAT, SOD, and GPx activities to similar levels to the rats in the control group.

The third important finding in the study was that curcumin reduced the apoptotic index in hepatocytes, which increased with DM in the liver. The first cellular response to the challenge of elevated glucose in diabetes is the production of ROS, which rapidly induces apoptotic cell death.[49] ROS has been described as an autocatalytic mechanism that can lead to programmed cell death.[50] It has been suggested that reactive oxygen radicals play a role in the apoptotic cell death of hepatocytes and endothelial cells in the liver.[51] In the histopathological evaluation of the livers of diabetic rats in this study, the presence of a large number of hepatocytes with vacuolar degeneration, pycnotic nuclei, and hypereosinophilic cytoplasm indicates that the cells are undergoing apoptosis. In addition, according to the apoptotic index findings we calculated as a result of immunohistochemical (TUNEL) staining, the reason for the higher apoptotic index in hepatocytes in the liver of diabetic rats compared to other groups; we can say that increased insulin causes oxidative stress and this leads hepatocytes to apoptosis.

However, in the study, we showed that in the livers of diabetic rats treated with curcumin, apoptotic changes in hepatocytes improved and the apoptotic index value decreased compared to diabetic rats. In our biochemical analysis, we reported that curcumin improves the levels of antioxidant enzymes and is a powerful antioxidant. In line with these data, we can say that curcumin prevents apoptosis in hepatocytes by reducing the oxidative stress caused by diabetes with its antioxidant properties.

The fourth finding from the study was that curcumin increased regeneration in the liver. The most widely used proliferation-associated marker is Ki-67, a nuclear antigen found only in proliferating cells.[52] In this study, it was observed that the density of Ki67-stained cells in diabetic rats increased compared to the control group, and it was less in the group treated with curcumin than in the diabetes group. In addition, in the stereological analysis, it was determined that the number of dual-core hepatocytes increased statistically significantly in the diabetes group compared to the control group, and it was lower in the curcumin-treated group compared to the diabetes group. Liver cells are very long-lived cells, with a life span of approximately 150 days. Therefore, mitotic cells are very rare.[53] The liver cell population is fairly stable and mitosis is very rare in normal liver. When liver tissue is damaged in rats, parenchymal cells appear larger than normal and binuclear cells proliferate. Regeneration is provided by the mitosis and growth of the remaining intact cells.[54] Mitosis in the liver is controlled by a mitosis inhibitor called Chalon circulating in the blood. In case of tissue damage or partial removal of the tissue, rapid mitosis begins in the tissue because the amount of Chalon decreases. As the regeneration event progresses, the amount of Chalon increases and decreases mitotic activity.[55]

Conclusion

Based on the findings of the study, we can say that curcumin has the potential to protect against oxidative stress and apoptosis caused by hyperglycemia in hepatic cells, and it also induces regeneration in the damaged liver, and therefore, it can be used as a curative and prophylactic drug for the treatment of DM.

Financial support and sponsorship

This research was supported by the Sinop University Scientific Research Projects Coordinatorship (Project number: SYO-1901-18-38).

Conflicts of interest

There are no conflicts of interest.

References

1. Srinivasan M. Effect of curcumin on blood sugar as seen in a diabetic subject. Indian J Med Sci 1972;26:269-70.
2. Ghosh J, Das J, Manna P, Sil PC. The protective role of arjunolic acid against doxorubicin induced intracellular ROS dependent JNK-p38 and p53-mediated cardiac apoptosis. Biomaterials 2011;32:4857-66.
3. Babu PV, Liu D, Gilbert ER. Recent advances in understanding the anti-diabetic actions of dietary flavonoids. J Nutr Biochem 2013;24:1777-89.
4. Yin W, Li B, Li X, Yu F, Cai Q, Zhang Z, *et al*. Anti-inflammatory effects of grape seed procyanidin B2 on a diabetic pancreas. Food Funct 2015;6:3065-71.
5. Elosta A, Ghous T, Ahmed N. Natural products as anti-glycation agents: Possible therapeutic potential for diabetic complications. Curr Diabetes Rev 2012;8:92-108.
6. Coskun O, Kanter M, Korkmaz A, Oter S. Quercetin, a flavonoid antioxidant, prevents and protects streptozotocin-induced oxidative stress and beta-cell damage in rat pancreas. Pharmacol Res 2005;51:117-23.
7. Rashid K, Sil PC. Curcumin enhances recovery of pancreatic islets from cellular stress induced inflammation and apoptosis in diabetic rats. Toxicol Appl Pharmacol 2015;282:297-310.
8. Das J, Sil PC. Taurine ameliorates alloxan-induced diabetic renal

injury, oxidative stress-related signaling pathways and apoptosis in rats. Amino Acids 2012;43:1509-23.
9. Maritim AC, Sanders RA, Watkins JB 3rd. Diabetes, oxidative stress, and antioxidants: A review. J Biochem Mol Toxicol 2003;17:24-38.
10. Uthandi A, Ramasamy K. Hepatoprotective activity of sesame meal on high fat fed wistar rats. Int J Pharm Sci Res 2011;2:205-11.
11. Bisht S, Khan MA, Bekhit M, Bai H, Cornish T, Mizuma M, *et al*. A polymeric nanoparticle formulation of curcumin (NanoCurc™) ameliorates CCl4-induced hepatic injury and fibrosis through reduction of pro-inflammatory cytokines and stellate cell activation. Lab Invest 2011;91:1383-95.
12. Tolman KG, Fonseca V, Dalpiaz A, Tan MH. Spectrum of liver disease in type 2 diabetes and management of patients with diabetes and liver disease. Diabetes Care 2007;30:734-43.
13. Nahvinejad M, Pourrajab F, Hekmatimoghaddam S. Extract of dorema aucheri induces PPAR-γ for activating reactive oxygen species metabolism. J Herb Med 2016;6:171-9.
14. Lima TF, Costa MC, Figueiredo ID, Inácio MD, Rodrigues MR, Assis RP, *et al*. Curcumin, alone or in combination with aminoguanidine, increases antioxidant defenses and glycation product detoxification in streptozotocin-diabetic rats: A therapeutic strategy to mitigate glycoxidative stress. Oxid Med Cell Longev 2020;1:1036360.
15. Hatcher H, Planalp R, Cho J, Torti FM, Torti SV. Curcumin: From ancient medicine to current clinical trials. Cell Mol Life Sci 2008;65:1631-52.
16. Lin J, Zheng S, Chen A. Curcumin attenuates the effects of insulin on stimulating hepatic stellate cell activation by interrupting insulin signaling and attenuating oxidative stress. Lab Invest 2009;89:1397-409.
17. Schraufstatter E, Bernt H. Antibacterial action of curcumin and related compounds. Nature 1949;164:456.
18. Sharma OP. Antioxidant activity of curcumin and related compounds. Biochem Pharmacol 1976;25:1811-2.
19. Nishiyama T, Mae T, Kishida H, Tsukagawa M, Mimaki Y, Kuroda M, *et al*. Curcuminoids and sesquiterpenoids in turmeric (*Curcuma longa* L.) suppress an increase in blood glucose level in type 2 diabetic KK-Ay mice. J Agric Food Chem 2005;53:959-63.
20. Aggarwal BB, Sung B. Pharmacological basis for the role of curcumin in chronic diseases: An age-old spice with modern targets. Trends Pharmacol Sci 2009;30:85-94.
21. Sharma S, Kulkarni SK, Chopra K. Curcumin, the active principle of turmeric (*Curcuma longa*), ameliorates diabetic nephropathy in rats. Clin Exp Pharmacol Physiol 2006;33:940-5.
22. Gupta SC, Patchva S, Aggarwal BB. Therapeutic roles of curcumin: Lessons learned from clinical trials. AAPS J 2013;15:195-218.
23. Holt PR, Katz S, Kirshoff R. Curcumin therapy in inflammatory bowel disease: A pilot study. Dig Dis Sci 2005;50:2191-3.
24. He ZY, Shi CB, Wen H, Li FL, Wang BL, Wang J. Upregulation of p53 expression in patients with colorectal cancer by administration of curcumin. Cancer Invest 2011;29:208-13.
25. Kalpravidh RW, Siritanaratkul N, Insain P, Charoensakdi R, Panichkul N, Hatairaktham S, *et al*. Improvement in oxidative stress and antioxidant parameters in beta-thalassemia/Hb E patients treated with curcuminoids. Clin Biochem 2010;43:424-9.
26. Kim SG, Veena MS, Basak SK, Han E, Tajima T, Gjertson DW, *et al*. Curcumin treatment suppresses IKKβ kinase activity of salivary cells of patients with head and neck cancer: A pilot study. Clin Cancer Res 2011;17:5953-61.
27. Palma HE, Wolkmer P, Gallio M, Corrêa MM, Schmatz R, Thomé GR, *et al*. Oxidative stress parameters in blood, liver, and kidney of diabetic rats treated with curcumin and/or insulin. Mol Cell Biochem 2014;386:199-210.
28. Sun C, Zhang Y, Kong T, Li Y, Feng R, Wang G. Effects of curcumin intake on kidney and liver pathological changes in T2DM rats. Wei Sheng Yan Jiu 2013;42:6-9.
29. Malcangio M, Tomlinson DR. A pharmacologic analysis of mechanical hyperalgesia in streptozotocin/diabetic rats. Pain 1998;76:151-7.
30. Kuhad A, Sethi R, Chopra K. Lycopene attenuates diabetes-associated cognitive decline in rats. Life Sci 2008;83:128-34.
31. Sinha AK. Colorimetric assay of catalase. Anal Biochem 1972;47:389-94.
32. Rotruck JT, Pope AL, Ganther HE, Swanson AB, Hafeman DG, Hoekstra WG. Selenium: Biochemical role as a component of glutathione peroxidase. Science 1973;179:588-90.
33. Ohkawa H, Ohishi N, Yagi K. Assay for lipid peroxides in animal tissues by thiobarbituric acid reaction. Anal Biochem 1979;95:351-8.
34. Kakkar P, Das B, Viswanathan PN. A modified spectrophotometric assay of superoxide dismutase. Indian J Biochem Biophys 1984;21:130-2.
35. Karaduman D, Eren B, Keles ON. The protective effect of beta-1,3-D-glucan on taxol-induced hepatotoxicity: A histopathological and stereological study. Drug Chem Toxicol 2010;33:8-16.
36. Chatterjea MN, Shinde R. Textbook of Medical Biochemistry. 8th edn. India: Jaypee Brothers Medical Publishers; 2012.
37. Pongchaidecha A, Lailerd N, Boonprasert W, Chattipakorn N. Effects of curcuminoid supplement on cardiac autonomic status in high-fat-induced obese rats. Nutrition 2009;25:870-8.
38. Brownlee M. The pathobiology of diabetic complications: A unifying mechanism. Diabetes 2005;54:1615-25.
39. Giacco F, Brownlee M. Oxidative stress and diabetic complications. Circ Res 2010;107:1058-70.
40. Pasupathi P, Chandrasekar V, Kumar US. Evaluation of oxidative stress, enzymatic and non-enzymatic antioxidants and metabolic thyroid hormone status in patients with diabetes mellitus. Diabetes Metab Syndr Clin Res Rev 2009;3:160-5.
41. Bandeira Sde M, Guedes Gda S, da Fonseca LJ, Pires AS, Gelain DP, Moreira JC, *et al.* Characterization of blood oxidative stress in type 2 diabetes mellitus patients: increase in lipid peroxidation and SOD activity. Oxid Med Cell Longev 2012;2012:819310.
42. Kakkar R, Kalra J, Mantha SV, Prasad K. Lipid peroxidation and activity of antioxidant enzymes in diabetic rats. Mol Cell Biochem 1995;151:113-9.
43. Eliza J, Daisy P, Ignacimuthu S. Antioxidant activity of costunolide and eremanthin isolated from costus speciosus (Koen ex. Retz) Sm. Chem Biol Interact 2010;188:467-72.
44. Góth L, Rass P, Páy A. Catalase enzyme mutations and their association with diseases. Mol Diagn 2004;8:141-9.
45. Vonk Noordegraaf A, Groeneveldt JA, Bogaard HJ. Pulmonary hypertension. Eur Respir Rev 2016;25:4-11.
46. Kennedy AL, Lyons TJ. Glycation, oxidation, and lipoxidation in the development of diabetic complications. Metabolism 1997;46:14-21.
47. Xie Z, Wu B, Shen G, Li X, Wu Q. Curcumin alleviates liver oxidative stress in type 1 diabetic rats. Mol Med Rep 2018;17:103-8.
48. Lu X, Wu F, Jiang M, Sun X, Tian G. Curcumin ameliorates gestational diabetes in mice partly through activating AMPK.

Pharm Biol 2019;57:250-4.

49. Park KS, Kim JH, Kim MS, Kim JM, Kim SK, Choi JY, *et al*. Effects of insulin and antioxidant on plasma 8-hydroxyguanine and tissue 8-hydroxydeoxyguanosine in streptozotocin-induced diabetic rats. Diabetes 2001;50:2837-41.
50. Jones BE, Lo CR, Liu H, Pradhan Z, Garcia L, Srinivasan A, *et al.* Role of caspases and NF-kappaB signaling in hydrogen peroxide- and superoxide-induced hepatocyte apoptosis. Am J Physiol Gastrointest Liver Physiol 2000;278:G693-9.
51. Jaeschke H. Reactive oxygen and mechanisms of inflammatory liver injury. J Gastroenterol Hepatol 2000;15:718-24.
52. Lebe B, Pabuççuoğlu U, Ozer E. The significance of Ki-67 proliferative index and cyclin D1 expression of dysplastic nevi in the biologic spectrum of melanocytic lesions. Appl Immunohistochem Mol Morphol 2007;15:160-4.
53. Gartner LP. Textbook of Histology. 4th ed. Philadelphia, PA: Elsevier Health Sciences; 2017.
54. Ross MH, Pawlina W. Histology: A Text and Atlas: With Correlated Cell and Molecular Biology. 6th ed. Philadelphia, PA: Wolters Kluwer/Lippincott Williams & Wilkins Health; 2011.
55. Mescher AL. Junqueira's Basic Histology: Text & Atlas. 15th ed. New York: McGraw Hill Medical Books; 2018.

Original Article

Anthropometric Study of Nasal Indices among the Akan People in the Assin Districts of Central Region, Ghana

Gordon Kyei, Daniel Lawer Egbenya[1], Ato Ampomah Brown, Eric Aidoo

Departments of Anatomy and Cell Biology and [1]Physiology, School of Medical Sciences, College of Health and Allied Sciences, University of Cape Coast, Cape Coast, Ghana

Abstract

Introduction: Nasal index (NI) may establish racial and ethnic identity and serves as a useful tool in forensic medicine and reconstructive surgery. Previous studies on nasal indices in many races and ethnicities serve as baseline and reference points for forensic and surgical purposes in those populations. However, there is scanty or no data on NI in Ghana including the Akan ethnicity. The study was conducted to provide baseline data on NI among the Akan people in the Assin Districts of the central region of Ghana. **Materials and Methods:** Four hundred adults between the ages of 20 and 58 years were used. Nasal height (NH) and nasal width (NW) were measured using Vernier caliper. NI computation and statistical analyses such as *z*-test and Pearson correlation were performed. **Results:** Mean NI of 91.32 ± 8.66 and 89.39 ± 10.16 were recorded in males and females, respectively, indicating that the predominant nose type in the study population is platyrrhine. There was a strong positive correlation between NH and NW, but there was no sexual dimorphism in NI among the Akan population. **Discussion and Conclusion:** This study provides a baseline data on NI anthropometry of the Akan people of the Assin Districts and will be a reference point for nasal anthropometry for clinical practice, rhinoplasty, and forensic science.

Keywords: *Akan people, anthropometry, nasal breadth, nasal height, nasal index, platyrrhine*

Introduction

Due to its central positioning, the nose plays an important role in defining the beauty of an individual. It is also part of the upper respiratory tract. Different individuals have different nose types, shapes, lengths, and sizes that are affected by sex, climate, ethnicity, and region. Race, ethnicity, and sex can, therefore, be predicted from the parameters of nasal anthropometry. The shape of the external nose is varied and is determined by the ethmoid bone and nasal septum, which is made of cartilage and separates the nasal openings.[1]

Variation in physical body parts of humans has been an area of interest for scientists, and as a result, anthropometry as a subdiscipline in biological anthropology was developed. Anthropometry is a standard scientific tool for measuring living and fossil human body dimensions.[2] Such measurements are very useful in the analysis, classification, and identification of living populations as well as fossil remains.[3] There are several anthropometric techniques including nasal anthropometry that are used by anthropologists. Nasal anthropometry involves the study of the proportion, size, and shape of the human nose.[4]

Nasal index (NI) is one of the most commonly used measurements in nasal anthropometry.[2] It is the ratio of nasal width (NW) to nasal height (NH) multiplied by hundred percent, i.e., NI = (NW/NH) × 100%.

The NI measurement is one of the methods anthropologists use to differentiate sex, race, ethnicity, and subspecies of humans.[5] It is also important in rhinoplasty surgery and forensic analysis. Rhinoplasty is the surgical procedure done on the nose to alter its shape and size for cosmetic purposes or to improve breathing. In rhinoplasty surgery, information on nasal anthropometry such as NW, NH, and NI is very useful in choosing the appropriate procedure.[6]

On the basis of NH and width, Martin and Saller[7] categorized noses into five different types [Table 1]. As shown in Figure 1, various types of noses are presented.[8] NI has been found to relate to regional and

This is an open access journal, and articles are distributed under the terms of the Creative Commons Attribution-NonCommercial-ShareAlike 4.0 License, which allows others to remix, tweak, and build upon the work non-commercially, as long as appropriate credit is given and the new creations are licensed under the identical terms.

For reprints contact: WKHLRPMedknow_reprints@wolterskluwer.com

How to cite this article: Kyei G, Egbenya DL, Brown AA, Aidoo E. Anthropometric study of nasal indices among the Akan people in the Assin districts of central region, Ghana. J Anat Soc India 2024;73:227-32.

Article Info

Received: 26 May 2023
Accepted: 11 August 2024
Available online: 25 September 2024

Address for correspondence:
Dr. Gordon Kyei, Department of Anatomy and Cell Biology, School of Medical Sciences, College of Health and Allied Sciences, University of Cape Coast, Cape Coast, Ghana.
E-mail: gordon.kyei@ucc.edu.gh

Access this article online

Website: https://journals.lww.com/joai

DOI: 10.4103/jasi.jasi_50_23

Quick Response Code:

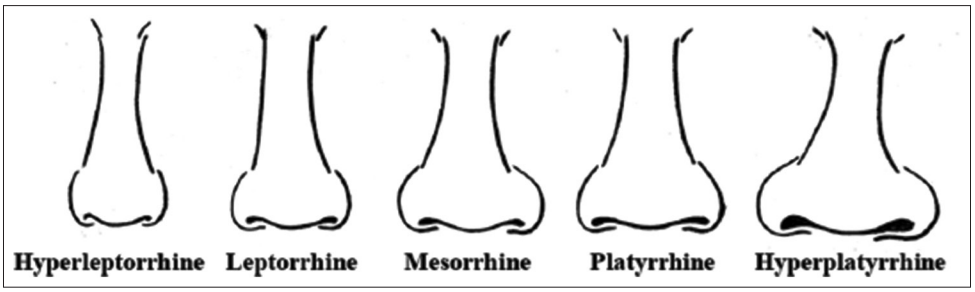

Figure 1: Nose types based on nasal index computation (Rohith *et al*., 2020)

climatic differences.[9-11] The narrower noses are observed in persons who live in cold and dry climates, whereas broader noses are common in persons who live in warmer and moister climates, thus being a consequence of natural selection in human evolution.[12]

Akan is the largest ethnic group in Ghana, making up about 47.3% of the total population of Ghana. It comprises Bono, Asante, Fante, Assin, Adanse, Twifo, Fante, Nzema, Akyem, Sehwi, Kwahu, Akwamu, Akuapem, and Ahanta people.[13] Most scholars agree that the Akan people may have originated from some parts of Sudan, the old Mali Empire, Burkina Faso, and even from ancient Mesopotamia and lived in the southern part of the West African forest region where ethnogenesis of the various Akan groups took place.[14,15]

Various studies have indicated racial and ethnic differences in NI among different populations.[11,16,17] However, as far as we know, there is no such data on the Akan ethnic group of Ghana. This study, therefore, aims to determine the NI and classify or specify the nose types of the Akan people living in the Assin districts of the central region of Ghana.

Materials and Methods

A total of 400 (200 males and 200 females) adults between the ages of 20 and 58 years (mean age of 29.7 for males and 30.7 for females) were recruited for the study. The volunteers, who were randomly selected, were all inhabitants of the Assin districts (North, Central, and South). Data collection was carried out at the premises of Obiri Yeboah SHS, Assin Fosu. To be included in the study, a prospective participant was verified, by interrogation, to be an Akan. Participants who had congenital nasal anomalies, previous surgery, or trauma of the nose or cleft lips were excluded from the study.

In this study, the procedure for taking measurements was adopted from Hegazy.[18] In summary, NH and NW were measured for each subject following standard methods. Anatomical landmarks used in measuring the NH were the nasion (the midpoint of the nasofrontal suture) and the subnasale in the midline (a point on the living body where the nasal septum and the upper lip meet in the midsagittal plane). NH was measured with a sliding Vernier caliper, from the nasion to the subnasale. NW, which is the maximum breadth of the nose, was measured at a right angle to the NH; from ala to ala [Figure 2]. Before the commencement of data collection, participants were informed of what the study was about and their informed consent was verbally obtained. Any prospective participant who did not understand anything about the study was given the opportunity to ask and was answered in the participant's preferred means or language of communication. They were also informed that they could withdraw from participation in the study, at any time, if they so wished. In addition, prospective participants were assured of confidentiality of any data obtained from them. The procedure of measurement used in the study was noninvasive and did not provoke any pain. All measurements were taken with the participant in a seated, relaxed mood, the head in anatomical position, and relaxed facial muscles. To reduce technical error in the measurements, each measurement was taken thrice and the average was computed. All measurements were taken to the nearest 1.0 mm. The NI was computed using the formula below:

$$NI = \left(\frac{NW}{NH}\right) X\ 100$$

Table 1: Types of nose based on nasal index (Martin and Saller, 1957)

Category of nose	Description of the nose	NI	
		On living head	On skull
Hyperleptorrhine	Long narrow nose	40–54.9	–
Leptorrhine	Moderately narrow nose	55–69.5	<47
Mesorrhine	Medium nose	70–84.9	47–50.9
Platyrrhine	Wide nose	85–99.9	51–57.9
hyperleptorrhine	Very wide nose	≥100	≥58

NI: Nasal index

Statistical analysis

The data obtained were analyzed using Statistical Package for Social Sciences version 22 (IBM. NY, USA) and Microsoft Excels 2016 (Microsoft Corporation, Washington USA). Basic descriptive statistics, *z*-test, and Pearson correlation test were performed at a 95% confidence interval ($P < 0.05$ was considered statistically significant).

Results

Basic statistics of NH and NW are shown in Tables 2 and 3. The mean NH and NW in males were 4.72 ± 0.44 cm and

Table 2: Basic descriptive statistic of nasal height

Gender	*n*	Mean±SD (cm)	SEM	Range	95% CI	CV (%)	*Z*/*P*
Male	200	4.72±0.44	0.062	3.86–5.70	4.59–4.84	9.32	*Z*=5.47
Female	200	4.26±0.41	0.058	3.40–4.96	4.14–4.37	9.62	*P*<0.0001
Total	400	4.49±0.48	0.048	3.40–5.70	4.39–4.58	10.69	

SD: Standard deviation, SEM: Standard error of mean, CI: Confidence interval

Table 3: Basic descriptive statistic of nasal width

Gender	*n*	Mean±SD (cm)	SEM	Range	95% CI	CV (%)	*Z*/*P*
Male	200	4.30±0.53	0.080	3.10–5.54	4.15–4.45	12.32.	*Z*=5.29
Female	200	3.79±0.44	0.062	3.00–4.90	3.66–3.91	11.61	*P*<0.0001
Total	400	4.07±0.58	0.058	3.00–5.82	3.95–4.18	14.25	

SD: Standard deviation, SEM: Standard error of mean, CI: Confidence interval

Table 4: Basic descriptive statistic of nasal index

Gender	*n*	Mean±SD (cm)	SEM	Range	95% CI	CV (%)	*Z*/*P*
Male	200	91.32±8.66	1.225	70.78–108.63	88.87–93.79	9.48	*Z*=1.03
Female	200	89.39±10.16	1.436	72.00–108.04	85.50–92.27	11.37	*P*=0.1531
Total	400	90.36±9.44	0.944	70.78–108.63	88.42–92.23	10.45	

SD: Standard deviation, SEM: Standard error of mean, CI: Confidence interval

Table 5: Pearson correlation of nasal height and nasal width

Variables	NH	
	r	*P*
NW	0.648	<0.001

NH: Nasal height, NW: Nasal width

4.30 ± 0.53 cm, respectively, whereas those in females were 4.26 ± 0.41 cm and 3.79 ± 0.44 cm, respectively. There was a significant difference in both mean NH and width between male and female subjects ($P < 0.0001$).

Table 4 shows a mean NI of 91.32 ± 8.66 cm and 89.39 ± 10.16 cm for males and females, respectively; however, the difference is statistically not significant ($P = 0.1531$).

NH and NW were analyzed for correlation using the Pearson correlation test. There was a strong positive correlation between these two parameters as displayed in Table 5.

Table 6 and Figure 3 show that the dominant type of nose found among the Akan people in the Assin districts of Ghana is platyrrhine, which is an average of 55% (males 56% and females 54%). In addition, mesorrhine nose type was, on average, 29% (males 28% and females 30%). The least nose type was hyperleptorrhine with both male and female subjects having equal distribution of 16%.

Discussion

NI and its determinants are influenced by racial, ethnic, regional, and climatic differences.[19] The present study revealed that the mean NH and NW in males were 4.72 cm and 4.30 cm, respectively, whereas in females, NH and NW were 4.26 cm and 3.79 cm, respectively. There was a significant difference in mean NH and NW in both male and female subjects. Comparative studies have shown that significant differences exist between males and females in mean NH and NW.[20-23] Therefore, our finding is in agreement with previous reports in the literature.

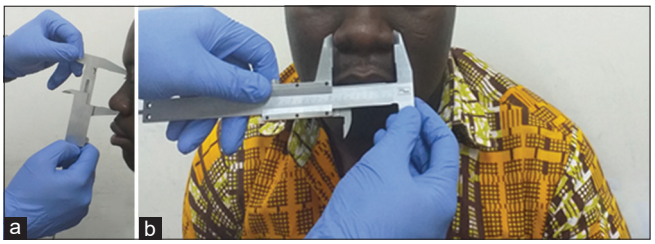

Figure 2: Measurement of parameters of nasal index using Vernier caliper. (a) Nasal height. (b) Nasal width

In addition, our results indicate a strong positive correlation between NH and NW. This implies that among the study population, nose height is proportional to nose width. Gaurav *et al*.[24] and Gulsen *et al*.[25] have reported similar findings.

The mean NI of males and females in the present study are 91.32 and 89.39, respectively, with no significant difference between the two genders. Importantly, these mean nasal indices are of the platyrrhine type of nose.[7] In addition, these values show that there is no sexual dimorphism of NI among the Akan people in the Assin districts of Ghana. Other authors have reported similar values of NI among males and females. For instance, Pandey[26] reported NI of 87.43 and 90.07 for males and females, respectively, among Onges people of the Andaman islands. Furthermore, among the Yoruba people of Nigeria, Oladipo *et al*.[17] reported NI

of 90.0 and 88.8 for males and females, respectively. The Okrika people of Nigeria also had NI of 86.23 and 86.46, for males and females, respectively.[27] Furthermore, among Caucasians, Farkas *et al*.,[2] found NI of 65.5 and 64.2 for males and females, respectively. Moreover, our result conforms with that of Eboh.[28] Nevertheless, differences in NI between males and females have been reported in many populations. In a south Indian population, Patil *et al*.[29] reported NI of 84.99 and 67.75 for males and females, respectively. Furthermore, in Egypt's East Delta population, NI of 71.46 and 64.56 for males and females, respectively, was reported.[18]

Table 6: Frequency (percentage) of nose types among the Akan population in Assin districts

Category of nose	Male, *n* (%)	Female, *n* (%)	Total, *n* (%)
Hyperleptorrhine	–	–	–
Leptorrhine	–	–	–
Mesorrhine	56 (28)	60 (30)	116 (29)
Platyrrhine	112 (56)	108 (54)	220 (55)
hyperleptorrhine	32 (16)	32 (16)	64 (16)

The reason for the absence of significant sexual dimorphism in the NI as shown in the present study is not clearly understood but may be due to the possibility of a lack

Table 7: Comparative references for predominant nasal indices from various populations

Population	Author(s)	NI	Nose type
Onges (Andaman Islands) male	Pandey (2006)	87.43	Platyrrhine
Onges (Andaman Islands) female	Pandey (2006)	90.07	Platyrrhine
Ahiwars (M.P) male	Singh and Purkait (2006)	81.00	Mesorrhine
Ahiwars (M.P) female	Singh and Purkait (2006)	82.00	Mesorrhine
Bhil Meena (Rajasthan) male	Gangrade and Babel (2012)	83.00	Mesorrhine
Bhil Meena (Rajasthan) female	Gangrade and Babel (2012)	79.73	Mesorrhine
Hindu - male	Sharma *et al*. (2014)	80.59	Mesorrhine
Hindu - female	Sharma *et al*. (2014)	77.72	Mesorrhine
Brahmins - male	Kaushal *et al*. (2013)	70.02	Mesorrhine
Brahmins - female	Kaushal *et al*. (2013)	69.89	Leptorrhine
East Delta (Egypt) - male	Hegazy (2014)	71.46	Mesorrhine
East Delta (Egypt) - female	Hegazy (2014)	64.56	Leptorrhine
Serbia - male	Jovanović *et al*. (2014)	67.56	Leptorrhine
Serbia - male	Jovanović *et al*. (2014)	66.01	Leptorrhine
Caucasian - male	Farkas *et al*. (1986)	65.50	Leptorrhine
Caucasian - female	Farkas *et al*. (1986)	64.20	Leptorrhine
Kosovo Albania - male	Staka *et al*. (2012)	67.07	Leptorrhine
Kosovo Albania - female	Staka *et al*. (2012)	63.87	Leptorrhine
Hausa (Nigeria) - male	Anas and Saleh (2014)	70.70	Mesorrhine
Hausa (Nigeria) - female	Anas and Saleh (2014)	67.20	Leptorrhine
South Indian - male	Patil *et al*. (2014)	84.99	Mesorrhine
South Indian - female	Patil *et al*. (2014)	67.75	Leptorrhine
Yoruba (Nigeria) - male	Oladipo *et al*. (2006)	88.10	Platyrrhine
Yoruba (Nigeria) - female	Oladipo *et al*. (2006)	90.80	Platyrrhine
Turkis (male)	Gulsen *et al*. (2006)	59.40	Leptorrhine
Sistan (Iran) - female	Heidari *et al*. (2009)	69.70	Leptorrhine
Okrika - male	Oladipo *et al*. (2009)	86.23	Platyrrhine
Okrika - female	Oladipo *et al*. (2009)	86.46	Platyrrhine
Arabic	Daniel (2000)	68.49	Leptorrhine
Western Europeans	Mulchand (2004)	69.90	Leptorrhine
German	Nichani and Willatt (2004)	71.00	Mesorrhine
Lebanon	Daniel (2000)	63.30	Leptorrhine
Qazvin Residents	Zolbin *et al*. (2015)	90.7	Platyrrhine
African American	Porter and Olson (2003)	79.70	Mesorrhine
Greek	Daniel (2000)	68.49	Leptorrhine
Africans	Risely (1969)	90–100	Platyrrhine
Yoruba (Nigerians)	Oladipo *et al*. (2006)	89.20	Platyrrhine
Igbo (Nigeria)	Akpa *et al*. (2003)	116.70	Platyrrhine
Akan (Ghana) - male	Present study	91.32	Platyrrhine
Akan (Ghana) - female	Present study	89.39	Platyrrhine

NI: Nasal index

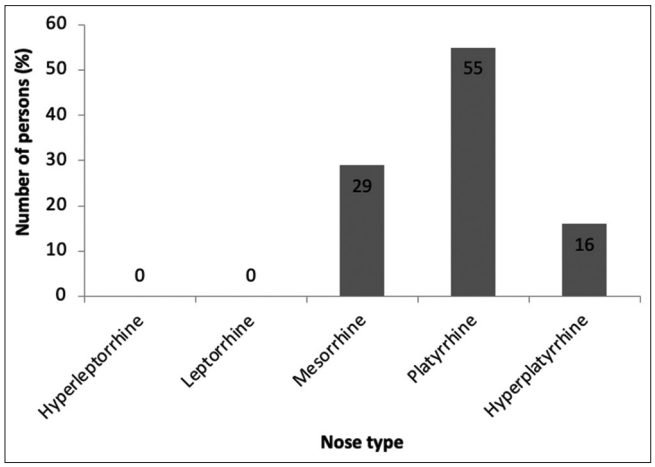

Figure 3: Nose type distribution among Akan people in Assin districts, Ghana. The predominant nose type found among the Akan people in the Assin districts is the platyrrhine nose type

of gender differences in the effect of growth and thyroid hormones. Furthermore, the nasal dimensions of both males and females may have evolved in a similar way among the Akan population. Another possible reason may be due to variation in sample size and techniques of measurements used by different authors.

The present study has also revealed that the mean NI in the study population is 90.36. Various studies have indicated racial and ethnic differences in NI among different populations.[30] Most Caucasians are leptorrhine, having a long and narrow nose with a NI of 69.9 or less. Indo-Aryans have a nose type similar to that of Europeans, possession of long nose.[31] The Jingpo people in China are mesorrhine,[32] whereas Indo-Africans[31] and Afro-Americans have platyrrhine nose type.[33]

The results of the present study conform to earlier reports on the African population with a NI of 90–100.[16,17,30] Surprisingly, the NI of the Akan people reported in the current study (90.36) is close to the result of an earlier study by Zolbin *et al*.,[34] who recorded an NI of 90.7 among males of Qazvin residents (Caucasians by race) in Iran. Table 7 gives a summary of NI of various populations as reported by various authors.

The present study has revealed that the predominant nose type among the Akan population in the North, Central, and South Assin districts of the Central Region of Ghana is platyrrhine (55%), followed by hyperleptorrhine (29%). Few subjects (8%) possess mesorrhine type of nose. The Akan people are believed to have lived in the coastal part of West Africa since the 11th century.[35] This area is characterized by moist and hot climatic conditions. The predominant nose types of platyrrhine and hyperleptorrhine among the Akan people might be an evolutional adaptation to living in such an environment. This suggests that the platyrrhine type of nose is typically African and is associated with living in a hot and moist climatic area.[12]

Conclusion

The NI of the Akan people living in the Assin districts of the Central Region of Ghana has been determined in the present study. The results showed that the principal nose type in this population is platyrrhine, and there is no sexual dimorphism among them. The result of this study will be useful in anthropometry for clinical practice, rhinoplasty, and forensic science. It will also serve as a baseline for estimating other craniofacial variables in the same population. Since this study is the first of its kind among the Akan people of Ghana, it is recommended that more studies should be conducted on other Akan populations living elsewhere in Ghana as well as on other ethnicities in the country.

Financial support and sponsorship

Nil.

Conflicts of interest

There are no conflicts of interest.

References

1. Standring S. Gray's Anatomy: The Anatomical Basic of Clinical Practice. 40th ed. London: Elsevier; 2008.
2. Farkas LG, Katic MJ, Forrest CR, Alt KW, Bagic I, Baltadjiev G, *et al.* International anthropometric study of facial morphology in various ethnic groups/races. J Craniofac Surg 2005;16:615-46.
3. Alex FR, Stevan B, Timothy GL. Human Body Composition. 4th ed. Champaign, Illinois, USA: Human Kinetics Publishers; 1996.
4. Eliakim-Ikechukwu C, Bassey T, Ihentuge C. Study of the nasal indices and bialar angle of the Ibo and Yoruba ethnic groups of Nigeria. J Biol Agric Healthc 2012;2:149-52.
5. Risely HH. The People of India. 2nd ed. Delhi: Oriental Books; 1969.
6. Pawar R, Thorat S. Study of nasal index. J Forensic Res 2021;12:472-6.
7. Martin R, Saller K. Textbook of Anthropology. Stuttgart: Gustav Fisher Verlag; 1957.
8. Rohith M, Roy J, Johnson A. Morphometric variations of nasal parameters in Gujarati population: An anatomical study. J Anat Soc India 2020;69:127.
9. Anas IY, Saleh MS. Anthropometric comparison of nasal indices between Hausa and Yoruba ethnic groups in Nigeria. J Sci Res Rep 2014;3:437-44.
10. Last RJ. Anatomy Applied and Regional. 6th ed. London, UK: Churchill Livingston; 1981.
11. Porter JP, Olson KL. Analysis of the African American female nose. Plast Reconstr Surg 2003;111:620-6.
12. Hall RL, Hall DA. Geographic variation of native people along the pacific coast. Hum Biol 1995;67:407-26.
13. Buah FK. A History of Ghana. Oxford: Macmillan; 1998.
14. Forde D. African worlds: Studies in the cosmological ideas and social values of African peoples. LIT Verlag Münster; 1999.
15. Cockerill GL. The New International Commentary on the New Testament: The Epistle to the Hebrews. Grand Rapids, MI: William B. Eerdmans Publishing Company; 2012.
16. Franciscus RG, Long JC. Variation in human nasal height and breadth. Am J Phys Anthropol 1991;85:419-27.
17. Oladipo GS, Olabiyi AO, Oremosu AA, Noronlu CC. Nasal indices among major ethnic groups in Southern Nigeria. Sci Res

Essay 2007;2:20-2.
18. Hegazy AA. Anthropometric study of nasal index of Egyptians. Int J Anat Res 2014;2:761-7.
19. Farkas LG, Kolar JC, Munro IR. Geography of the nose: A morphometric study. Aesthetic Plast Surg 1986;10:191-223.
20. Fatemeh T, Maryam K, Soheila M, Gholamreza H. Anthropometric study of nasal parameters in Iranian University students. Anatomical Sci J 2015;12:167-70.
21. Mohammed I, Mokhtari T, Ijaz S, Omotosho DA, Abubakar Ngaski A, Milanifard M, *et al.* Anthropometric study of nasal index in Hausa ethnic population of Northwestern Nigeria. J Contemp Med Sci 2018;4:26-9.
22. Rahimi Jaberi K, Kavakebian F, Mojaverrostami S, Najibi A, Safari M, Hassanzadeh G, *et al.* Nasofacial anthropometric study among students of Shiraz University of medical sciences, Iran: A population based study. Indian J Otolaryngol Head Neck Surg 2019;71:206-11.
23. Sharma SK, Jehan M, Sharma RL, Saxena S, Trivedi A, Bhadkaria V. Anthropometric comparison of nasal parameters between male and female of Gwalior Region. IOSR J Dent Med Sci 2014;13:57-62.
24. Gaurav T, Anil S, Jaj HS, Vivek M, Priyanka N, Ashish J. To evaluate relationship between craniofacial structures and nose in Himachali ethnic population. Indian J Dent Sci 2016;8:193-8.
25. Gulsen A, Okay C, Aslan BI, Uner O, Yavuzer R. The relationship between craniofacial structures and the nose in Anatolian Turkish adults: A cephalometric evaluation. Am J Orthod Dentofacial Orthop 2006;130:131.e15-25.
26. Pandey AK. Cephalo-facial variation among Onges. Anthropologist 2006;8:245-9.
27. Oladipo GS, Eroje MA, Fahwehinmi HB. Anthropometric comparison of nasal indices between Andoni and Okrika tribes of Rivers State, Nigeria. Int J Med Med Sci 2009;1:135-7.
28. Eboh DE. Nasal indices among Bini adolescents in Edo State, Nigeria. Int J Morphol 2011;29:1231-4.
29. Patil G, Kumar S, Apoorva D, Thejeswari SJ, Sheshgiri C, Sushanth N. Study on nasal index in South Indian population. Int J Curr Res 2014;6:8163-4.
30. Oladipo GS, Gwunireama IU, Asawo OD. Anthropometric comparison of nasal indices between the Igbos and Yorubas in Nigeria. Glob J Med Sci 2006;5:37-40.
31. Sparks CS, Jantz RL. A reassessment of human cranial plasticity: Boas revisited. Proc Natl Acad Sci U S A 2002;99:14636-9.
32. Xu B, Wang Y, Ma J, Li M, Xu L. A computer-aid study on the craniofacial features of Archang race in Yunnan province of China. Hua Xi Kou Qiang Yi Xue Za Zhi 2001;19:394-6.
33. Ofodile FA, Bokhari F. The African-American nose: Part II. Ann Plast Surg 1995;34:123-9.
34. Zolbin MM, Hassanzadeh G, Mokhtari T, Arabkheradmand A, Hassanzadeh S. Anthropometric studies of nasal parameters of qazvin residents, Iran. MOJ Anat Physiol 2015;1:00002.
35. Effah-Gyamfi K. Bono Manso: An Archaeological Investigation into Early Akan Urbanism (African Occasional Papers, No. 2). Calgary: University of Calgary Press; 1985.

Original Article

Estimation of Formaldehyde Levels in Indoor Air of Gross Anatomy Laboratory

Abstract

Introduction: Medical students spend majority of their times in Anatomy lab during their first year MBBS. Formalin has attracted attention as a health hazard for students and instructors as formalin concentrations in air of gross anatomy laboratories are often higher than permissible limits. Despite the known toxicity of formaldehyde and its potential health effects, laboratory workers and others have little enthusiasm for reducing or replacing the formaldehyde working solution **Materials and Methods:** The FA concentration (in ppm) of indoor air in Anatomy laboratory was measured using a SMILEDRIVE Portable air quality pollution meter. The mean FA concentration was measured after 1 hour after the cadavers were shifted to dissection table at three different levels a. At the level of floor b. At the level of roof c. 2 feets above the table (Breathing Zone of medical students) Three air samples from the breathing zones were tested and mean concentration of FA was taken with exhaust fan on at the level of roof and recorded as a. S1R- First immediately before the dissection (Zero hour), b. S2R- Second sample was collected after one hour after first sample was taken (First hour) and c. S3R- Third sample after two hours after first sample was taken (Second hour). Three air samples from the breathing zones were tested and mean concentration of FA was taken with exhaust fan on at the level of floor and recorded as a. S1F- First immediately before the dissection (Zero hour), b. S2F- Second sample was collected after one hour after first sample was taken (First hour) and c. S3F- Third sample after two hours after first sample was taken (Second hour). **Results:** The vertical distribution of FA was measured by taking the mean air samples at the level of floor, at roof level and about 2 feet above dissection table immediately after the cadavers were shifted to tables. It was found to be about 0.54ppm at the level of floor, 0.52 at the breathing zone and 0.51 ppm at roof level. The FA concentration was highest at the level of floor and least at the level of roof. On comparing S2F and S2R the p value was 1.335. Thus, it was not statistically significant. On comparing S3F and S3R the p value was 0.411. Thus, it was not statistically significant. **Conclusion:** The mean FA at the level of floor was 0.54 ppm. At the breathing zone the mean FA concentration was 0.51 ppm before the dissection was started. Exhaust fans at the level of roof were switched on and the second sample was taken after 1 hour. The FA concentration was 0.23 ppm. Third sample was taken at 2nd hour and FA concentration was 0.11 ppm. The exhaust fans at the level of floor were switched on. The air samples were measured at 0, 1st and 2nd hour at breathing zones. It was 0.51, 0.31 and 0,15 ppm respectively.

Keywords: *Air pollution monitor, anatomy laboratory, formaldehyde, indoor air*

Vinay Kumar Veeranna Shetty, Sathvik Singla[1], D. M. Sangeetha[2]

Department of Anatomy, A. J. Institute of Medical Sciences, [1]K. S. Hegde Medical Academy, NITTE (Deemed to be University), [2]Department of Civil Engineering, A. J. Institute of Engineering and Technology, Mangalore, Karnataka, India

Article Info

Received: 17 February 2024
Accepted: 11 August 2024
Available online: 25 September 2024

Address for correspondence:
Dr. Vinay Kumar Veeranna Shetty,
Department of Anatomy, A. J. Institute of Medical Sciences, Mangalore, Karnataka, India.
E-mail: drshettyvinay@gmail.com

Access this article online

Website: https://journals.lww.com/joai
DOI: 10.4103/jasi.jasi_24_24
Quick Response Code:

Introduction

Cadaveric dissection is one of the essential tools for gross anatomy teaching in most of the medical colleges; cadavers are embalmed and preserved in formaldehyde (FA) for long-term use. Vapors of FA emitted during the dissection sessions elevate the indoor FA concentration that results in increased level of exposure for medical students and instructors.[1] Medical students, thus during their dissection course, are exposed to FA and reported to suffer from various physical symptoms such as burning eyes, lacrimation, irritation of airways, and dermatitis.[2]

The only way out of all these problems is to reduce the amount of FA in the indoor air. Despite the known toxicity of FA and its potential health effects, laboratory workers and others have little enthusiasm for reducing or replacing the FA working solution. It is the responsibility of the laboratory workers to understand and adopt good laboratory practices to achieve a healthy environment.[3]

There is very little scientific literature on indoor FA concentration in medical colleges

This is an open access journal, and articles are distributed under the terms of the Creative Commons Attribution-NonCommercial-ShareAlike 4.0 License, which allows others to remix, tweak, and build upon the work non-commercially, as long as appropriate credit is given and the new creations are licensed under the identical terms.

For reprints contact: WKHLRPMedknow_reprints@wolterskluwer.com

How to cite this article: Shetty VK, Singla S, Sangeetha DM. Estimation of formaldehyde levels in indoor air of gross anatomy laboratory. J Anat Soc India 2024;73:233-6.

of a large country like India, and so the potential health risk to FA in medical colleges in India is relatively unknown. In 2011, India had the highest number of medical colleges in the world. Therefore, the medical student population under likely FA exposure risk is going to increase significantly. The WHO indoor air quality guideline proposed <0.08 ppm for indoor concentration of FA. The American Conference of Governmental Industrial Hygienists has set a ceiling limit for FA at 0.3 ppm. The International Agency for Research on Cancer and the U.S. Environmental Protection Agency classified FA as a human carcinogen during high or prolonged exposure. The participants of gross anatomy laboratory are exposed to a higher concentration of FA than the general population.

The permissible levels of FA in work environment time-weighted average concentration are 1.0 ppm (parts per million) and short-term exposure limits (15 min.) are 2 ppm as mentioned in the permissible levels of certain chemical substances in work environment – the second schedule. Concentrations of 100 parts FA per million parts air are immediately dangerous to health. At the embalming room, the laboratory staffs are exposed to FA concentration up to 9 ppm. Short-term exposure of FA at levels up to 5 ppm cause irritation of the eye, nose, and throat and exposure at levels from 10 to 20 ppm causes irregularities in heartbeat, tightness on the chest, and cough. Even if the individual is exposed to low levels of FA for longer duration, it may cause sensitization and eczema. Exposures from 50 to 100 ppm of FA may cause collection of fluid around the lungs, which later may cause death.[4]

The Japan Ministry of Health, Labour and Welfare has prescribed 0.08 and 0.25 ppm FA as the upper limits in domestic and specified workplaces, respectively.[5,6] Despite having very good ventilation, the levels of FA may reach unsafe levels in anatomy laboratories.

If a person is close to the cadavers during the gross anatomy laboratory, his/her personal exposure level is possibly 2–3-fold higher than the mean indoor FA concentration.[7]

A study completed by Kim *et al*. sampled a group of Korean medical students to determine FA exposure levels during cadaver dissections in an anatomy laboratory as well as the prevalence rates of FA-specific immunoglobulin (Ig) E or IgG antibodies and comparing them to symptoms associated with FA exposure. The group of 167 medical students who had previous exposure to FA was studied along with 67 medical students who had no previous exposure. National Institute for Occupational Safety and Health (NIOSH) method 3500 was used to collect area samples at 48 locations within the laboratory. Air sampling pumps were calibrated to a rate of 1.1–1.2 L/min for sample times of either 60 or 120 min. The students were also given a questionnaire with listed responses about any symptoms that they experienced during the dissection as well as a health questionnaire about their medical histories. Results showed that FA concentrations within the laboratory ranged from 0.16 to 9.16 ppm. The questionnaire revealed that 92.8% of the students complained of eye soreness, 51.5% headaches, 26.3% sore throat, and 25.1% shortness of breath. These results showed that the students sampled were being exposed to FA concentrations higher than the university's recommended limits during dissection practices. Majority of the medical students experienced symptoms of irritation while dissecting in the laboratory.[8] If a person is close to the cadavers during the gross anatomy laboratory, his/her personal exposure level is possibly 2–3-fold higher than the mean indoor FA concentration.

Figure 1: Smile drive pollution meter which is used to measure formaldehyde levels

The research question of the present study:

1. FA concentration is higher in air samples near to floor than air near to the roof
2. Exhaust fans are better when they are placed near to the floor than that those near the roof.

The objectives of the present study are:

1. To measure the FA concentration of indoor air at the level of floor, at the level of roof and in between roof and floor
2. To measure the FA concentration at above three levels at 0 h, 1st h, and 2nd h
3. To compare all the above parameters with the exhaust fan switched on at roof level and fan switched on at the level of floor.

Materials and Methods

This cross-sectional study was done at the anatomy dissection laboratory.

The FA concentration (in ppm) of indoor air in the anatomy laboratory was measured using a SMILEDRIVE Portable air quality pollution meter [Figure 1].

The mean FA concentration was measured after 1 h after the cadavers were shifted to the dissection table at three different levels.

a. At the level of floor
b. At the level of roof

c. Two feet above the table (breathing zone of medical students).

Three air samples from the breathing zones were tested and mean concentration of FA was taken with exhaust fan on at the level of the roof and recorded as:

a. S1R - First immediately before the dissection (0 h)
b. S2R - Second sample was collected after 1 h after the first sample was taken (1st h) and
c. S3R - Third sample after 2 h after the first sample was taken (2nd h).

Three air samples from the breathing zones were tested and mean concentration of FA was taken with exhaust fan on at the level of the floor and recorded as:

a. S1F - First immediately before the dissection (0 h)
b. S2F - Second sample was collected after 1 h after the first sample was taken (1st h) and
c. S3F - Third sample after 2 h after first sample was taken (2nd h).

Results

The vertical distribution of FA was measured by taking the mean air samples at the level of floor, at roof level, and about 2 feet above dissection table immediately after the cadavers were shifted to tables. It was found to be about 0.54 ppm at the level of floor, 0.52 at the breathing zone, and 0.51 ppm at roof level. The FA concentration was highest at the level of floor and least at the level of roof.

On comparing S2F and S2R, the *P* value was 1.335. Thus, it was not statistically significant. On comparing S3F and S3R, the *P* value was 0.411. Thus, it was not statistically significant.

Discussion

Recently, the issue of FA exposure is becoming a matter of concern among the participants of cadaveric dissection sessions in the gross anatomy laboratories. To prevent significant sensory irritation in the general population, the WHO recommends an air quality guideline value of 0.1 mg/m^3 (0.08 ppm) as a 30-min average for FA. Previous studies have demonstrated that indoor FA levels in gross anatomy laboratory exceeding the limits set by the WHO. The critical health effect of FA exposure at low concentrations is sensory irritation. In volunteers, eye irritation is observed first at levels of 1 ppm and higher (reviewed by Paustenbach *et al*., 1997; Arts *et al*., 2006a).[10] Furthermore, in the study by Lang *et al*. (2008),[9] it was shown that peaks of 1 ppm were most likely responsible for the induction of eye irritation, as minimal objective eye irritation was observed only at a level of 0.5 ppm with peaks of 1 ppm. Eye irritation was not seen at a level of 0.5 ppm without peaks. Nose and/or throat irritation was seen at levels of 2 ppm and higher (reviewed by Paustenbach *et al*., 1997; Arts *et al*., 2006a).[10] These levels of 1 and 2 ppm were based on controlled human volunteer studies including objective measurements, rather than on studies in workers or the general population. Hence, the associated uncertainties in estimating the exact exposure-effect concentration and the potential variability in exposure concentrations, as well as other confounding factors were minimized. The value of 1 ppm should, therefore, be the starting point for establishing an indoor air exposure limit. Although volunteers were exposed only during short periods (minute–hour) whereas workers and the general population may be exposed daily for life-time.

Based on an extensive review of available literature, including carcinogenicity data, the Federal Institute of Risk Assessment (body under public law) in Germany proposed a concentration of 0.1 ppm as a safe level. It was also based on an additional analysis of human cancer data that showed that 0.1 ppm FA would not result in an increased cancer risk. Since the level of 0.1 ppm is 10 times lower than the threshold for eye irritation and 20 times lower than the threshold for nose/throat irritation.

The present study also suggests that the personal exposure level for a person close to the dissecting table is always greater than the average indoor FA concentration because vaporization from cadavers and their containers is the main pathway of FA exposure in the gross anatomy laboratories. It is suggested that personal exposure level of a person is directly proportional to the time spent in an area of relatively higher FA concentration [Tables 1 and 2]. However, it is not possible to measure the FA exposure level of all the subjects. However, its concentration can be reduced. This can be achieved by providing the local ventilation system or/and the indoor air may immediately be exhausted before it spreads in the laboratory.

Overall, it has been concluded that an indoor air exposure limit of 0.1 ppm, would be a safe, realistic and meaningful level, while still taking into account the carcinogenicity

Table 1: Formaldehyde concentration in the breathing zone with exhaust fans switched on at the level of floor

	Mean FA concentration (ppm)	SD
Sample 1 (0 h) S1F	0.52 (0.51–0.54)	0.01
Sample 2 (after 1 h) S2F	0.23 (0.21–0.26)	0.02
Sample 3 (after 2 h) S3F	0.11 (0.09–0.14)	0.15

FA: Formaldehyde, SD: Standard deviation

Table 2: Formaldehyde concentration in the breathing zone with exhaust fans switched on at the level of roof

	Mean FA concentration (ppm)	SD
Sample 1 (0 h) S1R	0.51 (0.48–0.54)	0.019
Sample 2 (after 1 h) S2R	0.32 (0.3–0.35)	0.18
Sample 3 (after 2 h) S3R	0.15 (0.14–0.17)	0.009

FA: Formaldehyde, SD: Standard deviation

of FA. This level is (much) higher than indoor air or rural levels in general.

It is suggested that further studies are needed to protect the medical students and the teaching staff from harmful effect of FA.

Conclusion

The mean FA at the level of the floor was 0.54 ppm. At the breathing zone, the mean FA concentration was 0.51 ppm before the dissection was started. Exhaust fans at the level of the roof were switched on and the second sample was taken after 1 h. The FA concentration was 0.23 ppm. The third sample was taken at 2nd h and FA concentration was 0.11 ppm.

The exhaust fans at the level of the floor were switched on. The air samples were measured at 0, 1st, and 2nd h at breathing zones. It was 0.51, 0.31, and 0, 15 ppm, respectively.

On comparing three samples, it was found that there was a significant decrease in FA concentrations when the exhaust fans at the level of floor were used.

Very few scientific studies done on indoor FA concentration in the Anatomy laboratory of Indian medical colleges and so the potential health risk to FA in Indian medical colleges is relatively unknown.

Since is FA considered an industrial air pollutant, it has numerous effects on the health of the individual. Due to lack of information on actual FA levels in the anatomy laboratory, precautionary measures may not be even contemplated, and hence, health impacts could be substantial. Routinely checks should be done on levels of FA in the indoor air of anatomy laboratories and measure to reduce their exposure should be done. The FA concentration if found, to be significantly less on the usage of exhaust fans that are near to floor which helps in bringing down the amount of FA exposure to students.

Financial support and sponsorship

Nil.

Conflicts of interest

There are no conflicts of interest.

References

1. Shiraishi N. Levels of formaldehyde, phenol and ethanol in dissection room air and measures for reduction. Jpn J Occup Med Traumatol 2006;54:1-10.
2. Mirabelli MC, Holt SM, Cope JM. Anatomy laboratory instruction and occupational exposure to formaldehyde. Occup Environ Med 2011;68:375-8.
3. Jayalakshmi K, Ravikumar H, Naidu J, Raghavendra R. A silent killer in the laboratory – Formaldehyde: Review of effects and management. Int J Oral Maxillofac Pathol 2011;2:13-9.
4. Bedino JH. Formaldehyde exposure hazards and health effects: A comprehensive review for embalmers. The Champion Expanding Encyclopedia of Mortuary Practices; The Champion Company, Springfield: Geneseo, IL, USA. 2004;650.
5. Ministry of Health and Welfare. A Sectional Meeting of Healthy-House Related Standard. A Report of Subcommittee of Chemical Substance. Japan: Department of Living and Sanitary, Ministry of Health and Welfare; 1997.
6. Ministry of Health and Welfare. A Guideline for Indoor Level and Standard Determination of a Chemical Substance in Room Air No: 1093. Japan: Department of Living and Sanitary, Ministry of Health and Welfare; 2000.
7. Ohmichi K, Komiyama M, Matsuno Y, Takanashi Y, Miyamoto H, Kadota T, *et al*. Formaldehyde exposure in a gross anatomy laboratory – Personal exposure level is higher than indoor concentration. Environ Sci Pollut Res Int 2006;13:120-4.
8. Kim H, Kim YD, Cho SH. Formaldehyde exposure levels and serum antibodies to formaldehyde-human serum albumin of Korean medical students. Arch Environ Health 1999;54:115-8.
9. Lang I, Bruckner T, Triebig G. Formaldehyde and chemosensory irritation in humans: A controlled human exposure study. Regul Toxicol Pharmacol 2008;50:23-36.
10. Paustenbach D, Alarie Y, Kulle T, Schachter N, Smith R, Swenberg J, *et al*. A recommended occupational exposure limit for formaldehyde based on irritation. J Toxicol Environ Health 1997;50:217-63.

Original Article

Gender-wise Description of Morphometric Measures of Knee Joint Based on Magnetic Resonance Imaging Scan: A Descriptive Cross-sectional Study

Sonika Sharma, Rakesh Gupta, Sanjeev Kumar Jain[1], Rajul Rastogi[2]

Department of Anatomy, RMCH, Bareilly, Departments of [1]Anatomy and [2]Radio Diagnosis, TMMC and RC, Moradabad, Uttar Pradesh, India

Abstract

Background: Customization of Total Knee Replacement (TKR) and the design of knee prostheses are paramount. Conventionally, surgeons select from a spectrum of pre-fabricated implants, assessing their fit based on the patient's knee morphology via magnetic resonance imaging. **Aim and Objective:** This research endeavours to identify and quantify gender-related variations in knee morphometry by examining the distal femur and proximal tibia of the population of North India. **Materials and Methods:** A Descriptive cross-sectional study included 59 males and 59 females' knees. A 1.5 TESLA MRI unit (Avanto Magnetomtim + dot system, Siemens, Erlangen, Germany) was utilized for imaging. The morphological features of proximal Tibia and distal femur were taken. Correlation between morphometric parameters were calculated using Karl Pearson's correlation coefficient. P-value <0.05 was set statistically significant. **Results:** All the FEMUR parameters were significantly higher in males than females. The mean FML in males was 8.04±0.50SD and in females was 6.97±0.33SD (P<0.05). Mean FMAP in males was 5.98±0.46SD and in females it was 5.36±0.35SD (P<0.05). All the TIBIA parameters were significantly higher in males than females. The mean TML in males was 7.56±0.37SD and in females was 6.49±0.28SD (P<0.05). Mean TAP in males was 4.64±0.41SD and in females it was 4.13±0.25 (P<0.05). **Conclusion:** Variations in bone dimensions were attributed to a complex interplay of genetic, ethnic, and environmental factors. In conclusion, this study makes a substantial contribution to the understanding of knee joint morphology.

Keywords: *Knee arthroplasty, knee joint, magnetic resonance imaging, osteoarthritis, prosthesis design*

Introduction

The knee's composition is characterized by the union of the femur with the tibia, constituting the tibiofemoral joint, and the association between the femur and the patella, forming the patellofemoral joint.[1]

The integrity of the knee, from the skeletal foundation to the resilience of the menisci, depends on a concerted physiological mechanism to preserve the articular surfaces from the degradative effects associated with osteoarthritic conditions.[2]

Knee osteoarthritis (OA) is a widespread condition, recognized as a leading contributor to disability and an encumbrance on the daily lives of those affected, thereby amplifying health-care expenditures on a global scale.[3] With the advance of population aging, the incidence and impact of OA are projected to intensify. Magnetic resonance imaging (MRI) has become the preferred noninvasive imaging modality for the diagnosis of OA, acclaimed for its exceptional delineation of soft tissues and precise morphological evaluation of joints.[4,5]

The occurrence rates of OA demonstrate a broad international spectrum, with percentages ranging from 3.8% to 70%, a variance influenced by the diversity of diagnostic criteria and population demographics under study.[6,7]

Total knee arthroplasty (TKA), also known as total knee replacement (TKR), is a pivotal orthopedic intervention targeting the knee's articulating surfaces, specifically the femoral condyles and tibial plateau. This procedure emerges as the definitive solution for alleviating pain and restoring mobility in knees afflicted by severe arthritis, particularly when conservative treatments have proven ineffective.[8]

This is an open access journal, and articles are distributed under the terms of the Creative Commons Attribution-NonCommercial-ShareAlike 4.0 License, which allows others to remix, tweak, and build upon the work non-commercially, as long as appropriate credit is given and the new creations are licensed under the identical terms.

For reprints contact: WKHLRPMedknow_reprints@wolterskluwer.com

How to cite this article: Sharma S, Gupta R, Jain SK, Rastogi R. Gender-wise description of morphometric measures of knee joint based on magnetic resonance imaging scan: A descriptive cross-sectional study. J Anat Soc India 2024;73:237-48.

Article Info

Received: 26 May 2024
Accepted: 10 July 2024
Available online: 25 September 2024

Address for correspondence:
Dr. Sonika Sharma, Faculty Block, TMU Campus, Moradabad, Uttar Pradesh, India.
E-mail: soniyasharma.mbd@gmail.com

Access this article online

Website: https://journals.lww.com/joai

DOI: 10.4103/jasi.jasi_69_24

Quick Response Code:

Optimizing the outcome of TKA hinges on the precise tailoring of the prosthetic components to mirror the patient's knee anatomy.[9] Recognizing the nuances in femoral morphology across genders has steered advancements toward the development of prosthesis designs that cater to the narrower femoral condyles and modified trochlear geometries typically found in female anatomy.[10,11] Furthermore, disparities in femoral dimensions between Asian and Western populations have been observed, which presents a challenge as current prosthesis models are predominantly based on Caucasian anatomical data, potentially resulting in suboptimal fits for Asian patients.[12]

The success of TKA is significantly influenced by the meticulous matching of the prosthetic to the patient's distal femur and proximal tibia, ensuring the preservation of bone integrity and optimal load distribution.[13] Incorrect sizing of components can lead to issues such as early prosthesis loosening with a smaller tibial component or soft-tissue irritation and pain with an oversized component.[14]

The primary goals of TKR are to alleviate pain and to rejuvenate knee function and mobility. Regarded as a highly effective modality for treating terminal knee degenerative diseases, TKR boasts a commendable clinical success rate of about 95% at a 10-year follow-up.[15,16] Prosthesis design must conform to stringent anatomical, biological, mechanical, and manufacturing standards to facilitate these successful patient outcomes.[17,18]

MRI technology employs a potent magnetic field and radiofrequency pulses to generate detailed imagery of knee joint structures, aiding in the diagnosis and assessment of joint conditions. It is a critical tool for evaluating pain, weakness, swelling, or internal derangement of the knee without the use of ionizing radiation, often informing the decision on whether surgery is necessary. While radiography is the initial standard in imaging for knee diagnosis, MRI provides a more comprehensive evaluation of both osseous and soft-tissue structures.[19,20]

Recent research within Caucasian populations has uncovered notable variations in knee shape, with distinct sex-based differences observed in the femoral midshaft, distal femur, and patella. Automated three-dimensional (3D) morphologic analysis has highlighted these differences, revealing that females typically have narrower distal femurs with a smaller mediolateral to anteroposterior (AP) ratio.[21,22] In various Asian countries, studies on implant mismatching have raised concerns about the indiscriminate selection of TKA implants, which are often based on a limited demographic and fail to account for regional morphological diversity.[23] This highlights the necessity of acknowledging ethnic differences in the distal femur and proximal tibia dimensions when assessing the clinical impact of current TKA designs.

It is crucial to measure and quantify these morphological discrepancies by comparing the resected knees of specific populations with existing Western implants. This comparison will facilitate improvements in the performance of TKA. The present study seeks to examine the knee morphology of the Indian population using 3D models, juxtaposing these findings with global research to ensure a judicious selection of TKA implants available commercially.

Materials and Methods

Study design

A descriptive cross-sectional study conducted at Rohillkhand Medical College with the collaboration of Teerthanker Mahaveer Medical College after approval from the College Research Committee and Institutional Ethical Committee (IEC No. BIU/REG/PhD/551).

Sample size

Sample size was 59 males and 59 females (total 118 individuals). The knee joint data included 59 males and 59 females' knees.

Study period

This study was conducted for approximately 1 year after the approval from the Central Research Committee.

Inclusion criteria

1. Age group of 22–60 years of age[24]
2. Healthy knee joints
3. Only complete and fully ossified bones were included.

The study received ethical approval from the Institutional Review Board.

Exclusion criteria

Patients with previous knee joint surgeries or had a knee trauma, fracture, dislocation, or a ruptured or torn anterior cruciate ligament of any sprained ligament (sprain II and above) will not be included in the study.[7]

Magnetic resonance imaging technique

A 1.5 TESLA MRI unit (Avanto Magnetomtim + dot system, Siemens, Erlangen, Germany) was utilized for imaging. Images were obtained at a thickness of 3 mm with a 0.3 mm interval. Subjects were positioned supine with their knee joints at a 0° angle, and patella facing forward to capture axial images parallel to the knee joints. The NUMARIS/4 syngo MR D13 system was employed to measure morphometric parameters in the axial images of the proximal tibia and distal femur.

In this study, about 13 morphological features will be measured.

The parameters of distal femur

1. Femur epicondylar width (fEW): "It is defined as the transverse distance across the femur at the level of the epicondyles, which are the rounded bony prominences

at the distal end of the femur where ligaments and tendons attach. This measurement is taken as the straight line distance between the most lateral point of the lateral epicondyle and the most medial point of the medial epicondyle" [Figure 1]

2. Femur medial condyle anterioposterior length (fMAP) defined as the distance from the most anterior point on the femur medial condyle to the posterior condylar line [Figure 2]
3. Femur lateral condyle anterioposterior length (fLAP) distance from the most anterior point on the femur lateral condyle [Figure 2]
4. Femur medial-lateral length (fML) referenced by the femoral epicondyle axis, defined as the most salient point between the medial and lateral attachment on the femoral condyle [Figure 2]
5. Femur medial condyle width (fMW): The transverse distance across the medial condyle of the femur, which is the innermost of the two rounded prominences at the end of the thigh bone, where it meets the knee [Figure 3]
6. Femur lateral condyle width (fLW): The measurement of the transverse distance across the lateral condyle of the femur, the outermost of the two prominences [Figure 3]
7. Intercondylar fossa width (ICW): The measurement of the distance across the intercondylar fossa, the groove between the medial and lateral femoral condyles [Figure 4]
8. Intercondylar fossa height (ICH): Vertical measurement from the deepest part of the intercondylar fossa to the top of the 'fossa's ridge [Figure 4]
9. Femoral aspect ratio (FAR) (ratio of femoral medial-lateral [ML]/AP): The data extraction will be done along the three different view planes such as transverse plane, sagittal plane, and coronal plane of the scan [Figure 5].[7]

The parameters of proximal tibia

1. Tibia anterioposterior (tAP) width: Distance between two tangents parallel to transepicondylar axis and passing

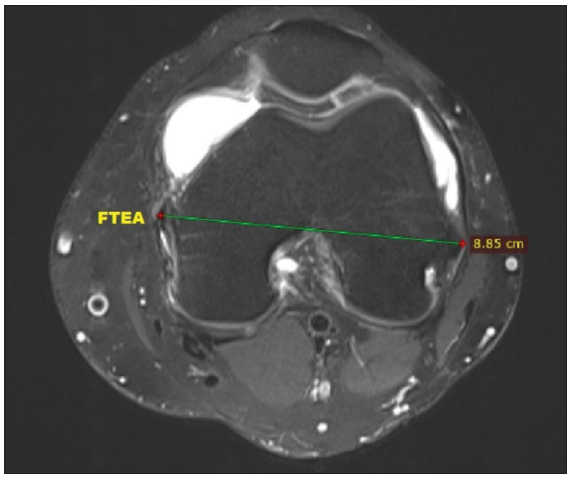

Figure 1: Trans epicondylar axis of the femur. FTEA: Femoral trans epicondylar axis

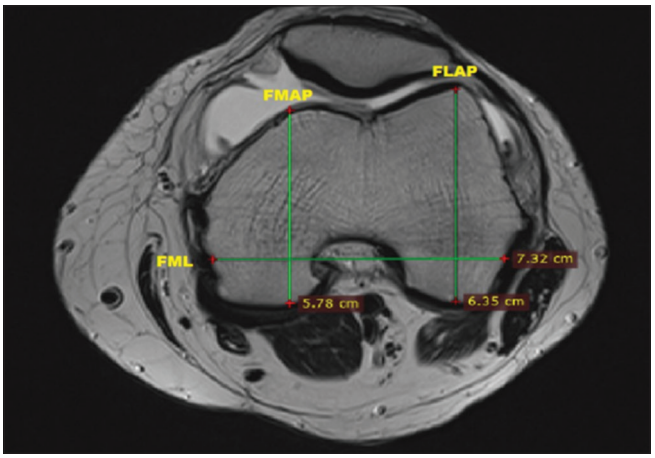

Figure 2: Femur medial-lateral length, femur medial condyle anterioposterior length, femur lateral condyle anterioposterior length. FLAP: Femur lateral condyle anteroposterior length, FMAP: Femur medial condyle anteroposterior length, FML: Femur medial-lateral length

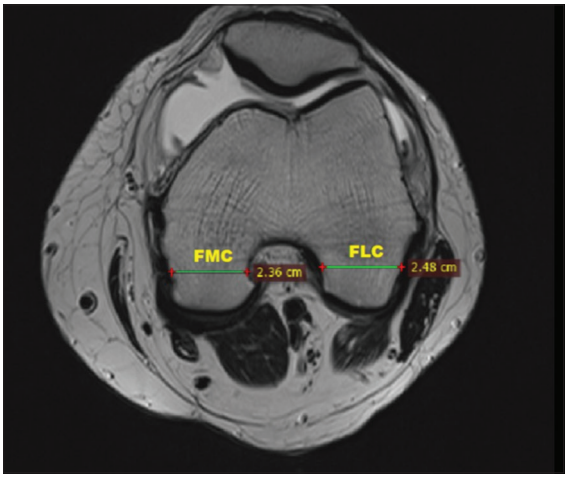

Figure 3: Femur medial and lateral condyles. FMC: Femur medial condyle, FLC: Femur lateral condyle

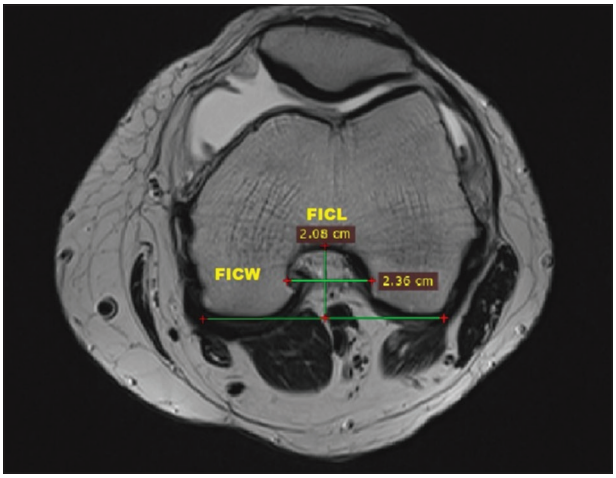

Figure 4: Intercondylar fossa width and height

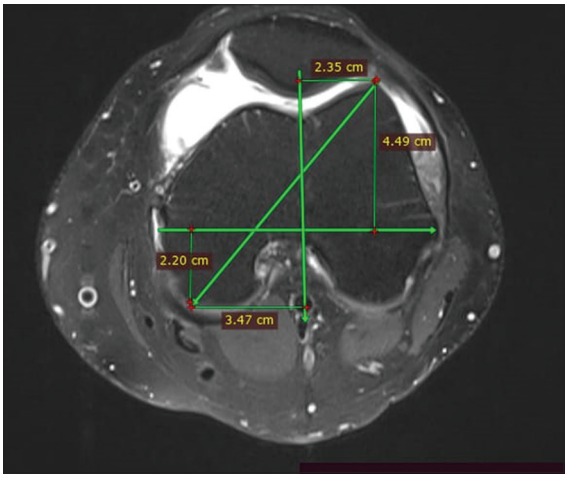

Figure 5: Aspect ratio of distal femur

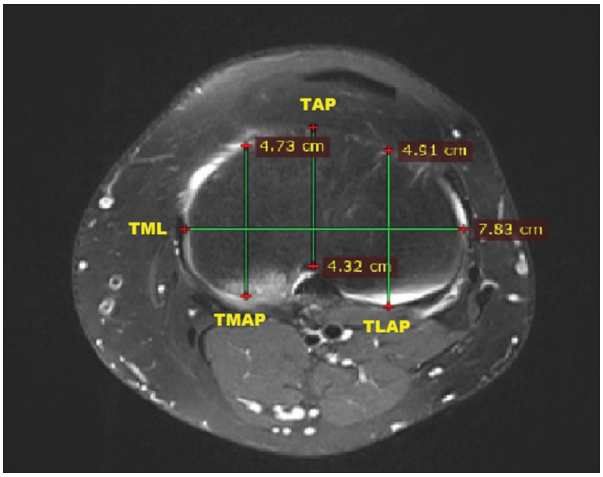

Figure 6: Axial plane of tibia. TAP: Tibia Anteroposterior, TML: Tibial mediolateral, TMAP: Tibia medial condyle anteroposterior, TLAP: Tibia lateral condyle anteroposterior

through anterior and posterior extremities [Figure 6]
Trans epicondylar axis (TEA) – distance between the lateral and medial epicondyles

2. Tibia medial condyle anterioposterior length (tMAP): The tibia medial condyle anteroposterior length (tMAP) is the length from the anterior medial tibia plateau to the posterior plateau [Figure 6]
3. The tibia lateral condyle anteroposterior length (tLAP): The length from the anterior lateral tibia plateau to the posterior plateau [Figure 6]
4. Tibial mediolateral width (tML): The distance between medial and lateral extremities in the resected plane measured parallel to the mediolateral axis was defined as tibial mediolateral width (tML) [Figure 6].[17] Figure 7 shows the Sagittal MRI of Knee Showing Femur, Tibia, and Patellar Regions.

Statistical analysis

Data were entered in Excel and analyzed using SPSS (IBM SPSS Statistics 20.0. IBM Corp., Armonk, N.Y., USA). Matirx data were expressed in mean ± standard deviation, and categorical data were expressed in frequencies/percentages. Morphometric measures between the genders were compared using an independent sample *t*-test. The correlation between morphometric parameters was calculated using Karl Pearson's correlation coefficient. Receiver operating characteristics (ROCs) analysis was performed to determine cutoff values for each parameter to differentiate males from females. $P < 0.05$ was set as statistically significant.

Results

There were 59 male and 59 female participants with a total of 118 included in the study [Table 1].

The mean age of all participants was 22.20 ± 5.03. Mean height and weight were 164 ± 8.46 (cm) and 61.53 ± 11.28 (kg), respectively [Table 2 and Figure 8].

The mean values (TIBIA) of TML, TAP, TMAP, and TLAP, respectively, were 7.02 ± 0.63, 4.39 ± 0.42, 4.49 ± 0.48, and 4.22 ± 0.46. The mean values (FEMUR) of FML, FMAP, FLAP, FEW, FMW, FLW, ICW, ICL, and FAR, respectively, were 7.50 ± 0.68, 5.67 ± 0.51, 6.00 ± 0.51, 7.58 ± 0.86, 2.43 ± 0.28, 2.31 ± 0.26, 2.39 ± 0.29, 2.36 ± 0.35, and 0.92 ± 0.10 [Figures 9 and 10]. Table 3 shows the Morphometric measures of knee joint.

Table 1: Sex distribution of study participants

Sex	Frequency, *n* (%)
Male	59 (50.0)
Female	59 (50.0)
Total	118 (100.0)

It was observed that there were significant mean differences in age, height, and weight between males and females ($P < 0.01$) [Table 4 and Figure 11].

There was a significant mean difference in all morphometric parameters observed between males and females ($P < 0.01$). Mean values were significantly less in females as compared to males. Mean TML in males was 7.56 ± 0.37, and in females, it was 6.49 ± 0.28. Mean TMAP in males was 4.84 ± 0.33, whereas in females, it was 4.13 ± 0.31 [Figure 12].

Mean FML, FEW, and FLW in males was 8.04 ± 0.50, 8.24 ± 0.63, and 2.49 ± 0.16, respectively, while in females, it was 6.97 ± 0.33, 6.92 ± 0.46, and 2.13 ± 0.19 [Table 5 and Figure 13].

There was a very high correlation observed between TML and TAP, TMAP, TLAP, FML, FMAP, FLAP, and FEW. Furthermore, there was a high correlation between FML and FMAP, FLAP, and FEW. FEW had a moderate correlation with FMW, FLW, ICW, and ICL [Table 6].

In females, there was a strong correlation observed between TML and FML and moderate correlation with

Table 2: Age and anthropometric measures of all participants

Variables	Mean±SD	Minimum	Maximum
Age	22.20±5.03	18.00	44.00
Height (cm)	164.66±8.46	144.00	186.00
Weight (kg)	61.53±11.28	38.00	90.00

SD: Standard deviation

Table 3: Morphometric measures of knee joint

Variables	Mean±SD	Minimum	Maximum
Tibia			
TML	7.02±0.63	5.87	8.45
TAP	4.39±0.42	3.47	5.70
TMAP	4.49±0.48	3.32	5.81
TLAP	4.22±0.46	3.38	5.32
Femur			
FML	7.50±0.68	5.98	9.16
FMAP	5.67±0.51	4.14	7.34
FLAP	6.00±0.51	4.90	7.29
FEW	7.58±0.86	5.98	9.32
FMW	2.43±0.28	2.06	3.06
FLW	2.31±0.26	1.85	2.90
ICW	2.39±0.29	1.73	2.90
ICL	2.36±0.35	1.73	3.08
FAR	0.92±0.10	0.67	1.24

TML: Tibial mediolateral width, TAP: Tibia anterioposterior width, TMAP: Tibia medial condyle anteroposterior length, TLAP: Tibia lateral condyle anteroposterior length, FML: Femur medial-lateral length, FMAP: Femur medial condyle anterioposterior length, FLAP: Femur lateral condyle anterioposterior length, FEW: Femur epicondylar width, FMW: Femur medial condyle width, ICW: Intercondylar fossa width, ICL: Intercondylar fossa length, FAR: Femoral aspect ratio

TMAP, FMAP, and FLAP. Moderate correlation was observed between TMAP and TLAP, FML, FMAP, and FLAP ($P < 0.01$) [Table 6 and Figures 14, 15].

Discussion

Based on the findings, it is evident that when examining various parameters of both the tibia and femur, distinct gender-based differences emerge. Specifically, in the case of the tibia, including measurements such as tAP, tibia medial anteroposterior (tMAP), tibia lateral anteroposterior (tLAP), and tibia mediolateral (tML), it is apparent that these parameters exhibit larger dimensions in males compared to females. This trend holds true consistently across all these tibial measurements.

A detailed comparison of morphometric measures between genders, specifically focusing on male and female subjects was done. Males had a significantly longer average tibia length (7.56 cm ± 0.37) compared to females (6.49 cm ± 0.28). Once again, males exhibited a significantly greater AP measurement (4.64 cm ± 0.41) compared to females (4.13 cm ± 0.25). Tibia medial condyle anteroposterior (TMAP) and tibia lateral condyle anteroposterior (TLAP) also showed significant differences, with males having larger values.

Table 4: Comparison of anthropometric measures between gender

Sex	Male	Female	*t*	*P**
Age	23.51±5.82	20.90±3.71	2.905	0.004
Height (cm)	170.66±6.21	158.66±5.72	10.925	<0.001
Weight (kg)	66.14±10.22	56.92±10.43	4.850	<0.001

*Based on independent sample *t*-test

Table 5: Comparison of morphometric measures between gender

Sex	Male	Female	*t*	*P**
Tibia				
TML	7.56±0.37	6.49±0.28	17.865	<0.001
TAP	4.64±0.41	4.13±0.25	8.096	<0.001
TMAP	4.84±0.33	4.13±0.31	12.060	<0.001
TLAP	4.56±0.34	3.88±0.27	12.008	<0.001
Femur				
FML	8.04±0.50	6.97±0.33	13.810	<0.001
FMAP	5.98±0.46	5.36±0.35	8.074	<0.001
FLAP	6.34±0.40	5.66±0.34	9.933	<0.001
FEW	8.24±0.63	6.92±0.46	13.041	<0.001
FMW	2.61±0.19	2.25±0.24	9.227	<0.001
FLW	2.49±0.16	2.13±0.19	11.205	<0.001
ICW	2.52±0.15	2.25±0.32	5.919	<0.001
ICL	2.57±0.21	2.15±0.33	8.190	<0.001
FAR	0.97±0.10	0.88±0.09	5.220	<0.001

*Based on independent sample *t*-test. TML: Tibial mediolateral width, TAP: Tibia anterioposterior width, TMAP: Tibia medial condyle anteroposterior length, TLAP: Tibia lateral condyle anteroposterior length, FML: Femur medial-lateral length, FMAP: Femur medial condyle anterioposterior length, FLAP: Femur lateral condyle anterioposterior length, FEW: Femur epicondylar width, FMW: Femur medial condyle width, ICW: Intercondylar fossa width, ICL: Intercondylar fossa length, FAR: Femoral aspect ratio

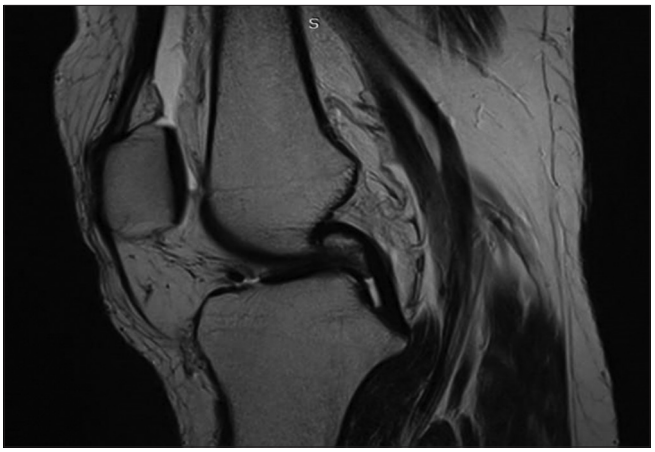

Figure 7: Sagittal magnetic resonance imaging of knee showing femur, tibia, and patellar regions

Table 6: Correlation between Morphometric measures

Correlation between morphometric measures (male)												
	TML	**TAP**	**TMAP**	**TLAP**	**FML**	**FMAP**	**FLAP**	**FEW**	**FMW**	**FLW**	**ICW**	**ICL**
TAP	0.36**	1.00										
TMAP	0.59**	0.40**	1.00									
TLAP	0.40**	0.53**	0.28*	1.00								
FML	0.49**	0.35**	0.46**	0.132	1.00							
FMAP	0.53**	0.32*	0.40**	0.09	0.72**	1.00						
FLAP	0.69**	0.49**	0.50**	0.31*	0.55**	0.61**	1.00					
FEW	0.52**	0.19	0.24	0.17	0.34**	0.39**	0.59**	1.00				
FMW	0.26*	0.10	0.15	−0.09	0.14	0.32*	0.30*	0.33**	1.00			
FLW	0.19	−0.11	−0.07	−0.24	0.28*	0.12	0.17	0.42**	0.26*	1.00		
ICW	0.14	0.26*	0.30*	0.20	0.19	0.09	0.33*	0.53**	0.05	0.23	1.00	
ICL	0.23	−0.00	0.21	0.13	0.22	0.22	0.15	0.38**	0.26*	0.33*	0.13	1.00
FAR	0.23	−0.07	0.02	0.03	−0.14	−0.02	0.25	0.29*	0.15	0.15	0.14	−0.02
Correlation between morphometric measures (female)												
	TML	**TAP**	**TMAP**	**TLAP**	**FML**	**FMAP**	**FLAP**	**FEW**	**FMW**	**FLW**	**ICW**	**ICL**
TAP	−0.03	1.00										
TMAP	0.41**	0.29*	1.00									
TLAP	0.29*	0.48**	0.39**	1.00								
FML	0.67**	0.27*	0.46**	0.22	1.00							
FMAP	0.41**	0.25	0.40**	0.41**	0.26*	1.00						
FLAP	0.39**	0.39**	0.50**	0.51**	0.44**	0.53**	1.00					
FEW	0.10	−0.19	0.26	0.06	0.07	0.05	0.01	1.00				
FMW	−0.12	−0.01	−0.13	−0.03	−0.18	−0.11	−0.07	0.13	1.00			
FLW	0.271*	−0.03	0.11	0.19	0.18	0.12	0.12	−0.07	0.08	1.00		
ICW	−0.10	−0.23	−0.10	−0.22	0.15	−0.03	−0.09	−0.01	−0.17	−0.10	1.00	
ICL	−0.15	−0.307*	−0.11	−0.18	−0.13	0.05	−0.05	0.12	0.04	−0.19	0.37**	1.00
FAR	0.22	0.07	0.21	0.18	0.14	0.14	0.13	0.38**	0.07	0.12	0.02	0.03

*Correlation is significant at the 0.05 level, **Correlation is significant at the 0.01 level. TAP: Tibia anterioposterior width, TMAP: Tibia medial condyle anteroposterior length, TLAP: Tibia lateral condyle anteroposterior length, FML: Femur medial-lateral length, FMAP: Femur medial condyle anterioposterior length, FLAP: Femur lateral condyle anterioposterior length, FEW: Femur epicondylar width, FMW: Femur medial condyle width, ICW: Intercondylar fossa width, ICL: Intercondylar fossa length, FAR: Femoral aspect ratio, TML: Tibial mediolateral width

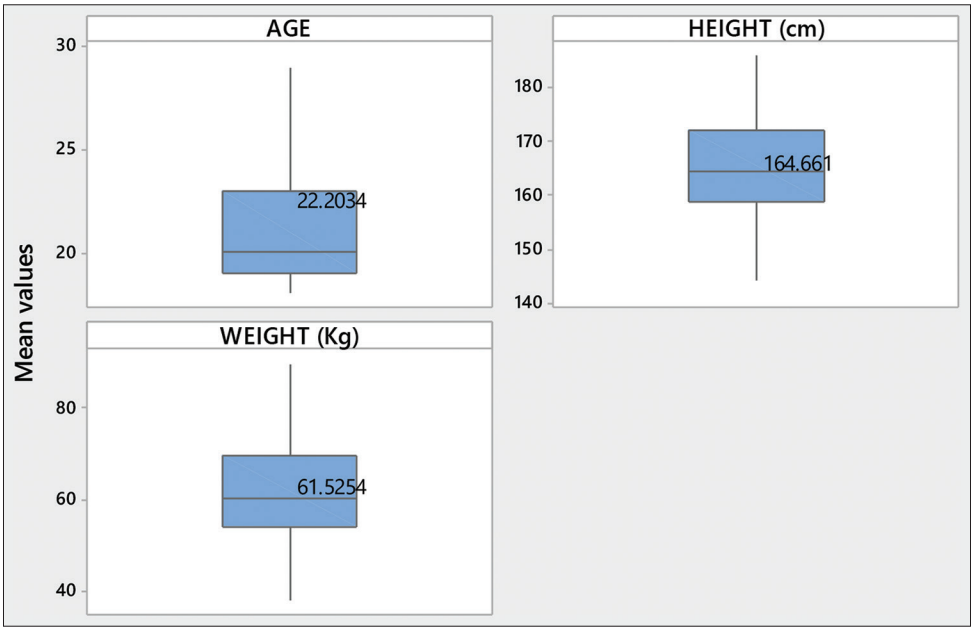

Figure 8: Age and anthropometric measures of all participants

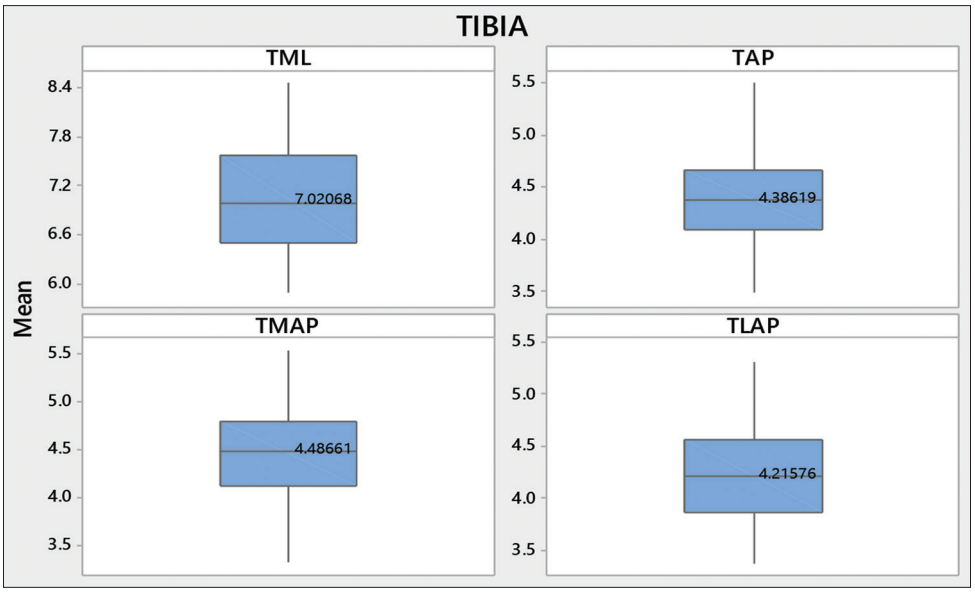

Figure 9: Morphometric measures of the knee joint (TIBIA). TAP: Tibia anterioposterior, TML: Tibial mediolateral, TMAP: Tibia medial condyle anteroposterior, TLAP: Tibia lateral condyle anteroposterior

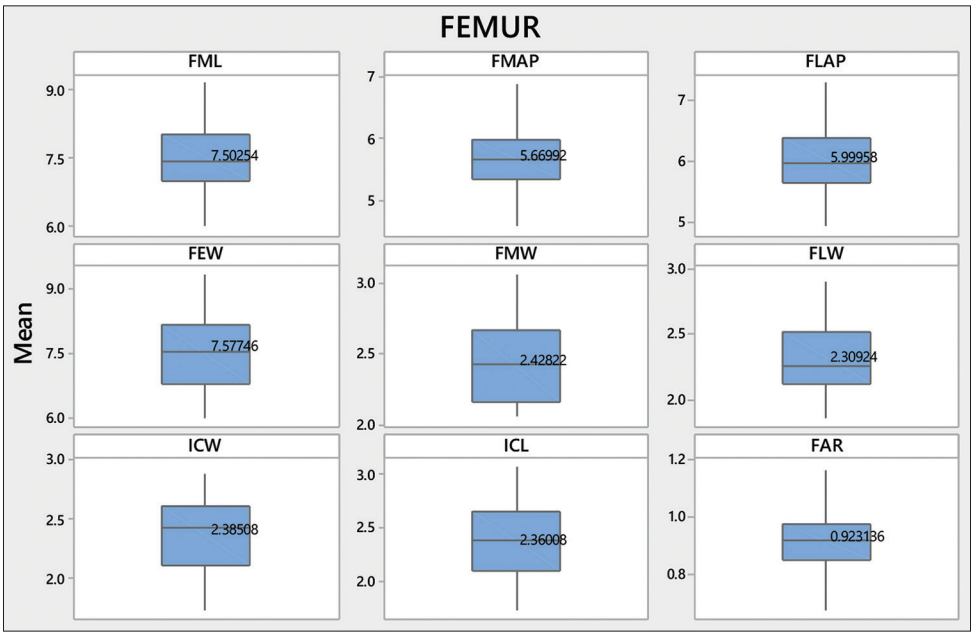

Figure 10: Morphometric measures of the knee joint (FEMUR). FAR: Femoral aspect ratio, FML: Femur medial-lateral length, FMAP: Femur medial condyle anteroposterior length, FLAP: Femur lateral condyle anteroposterior length, FEW: Femur epicondylar width, FMW: Femur medial condyle width, FLW: Femur lateral condyle width, ICW: Intercondylar fossa width, ICL: Intercondylar fossa length

The findings of this research are in concordance with similar studies focusing on the morphometrics of knee joints. Research by Tummala *et al*. has highlighted differences in knee joint structures such as condylar alignment (CA) and congruity index (CI) between genders, particularly within medial tibiofemoral joints. Their research suggests that female knees often have a higher CA and a lower CI, which could reflect the gender-specific variations in tibial dimensions that our study also identifies.[25,26] Similarly, Park *et al*. have reported significant differences in knee dimensions between genders, specifically in measurements such as notch width, bicondylar width, and medial condylar width. Such findings give additional support to the gender-related differences noted in the present study.[27]

In the comparison of morphometric parameters of knee joints related to the femur, males have substantially longer femurs, with an average of 8.04 cm (±0.50) compared to females with 6.97 cm (±0.33). Femur medial condyle anteroposterior length (FMAP) and femur lateromedial anteroposterior (FLAP): both measurements indicate that males have larger dimensions compared to females. Males

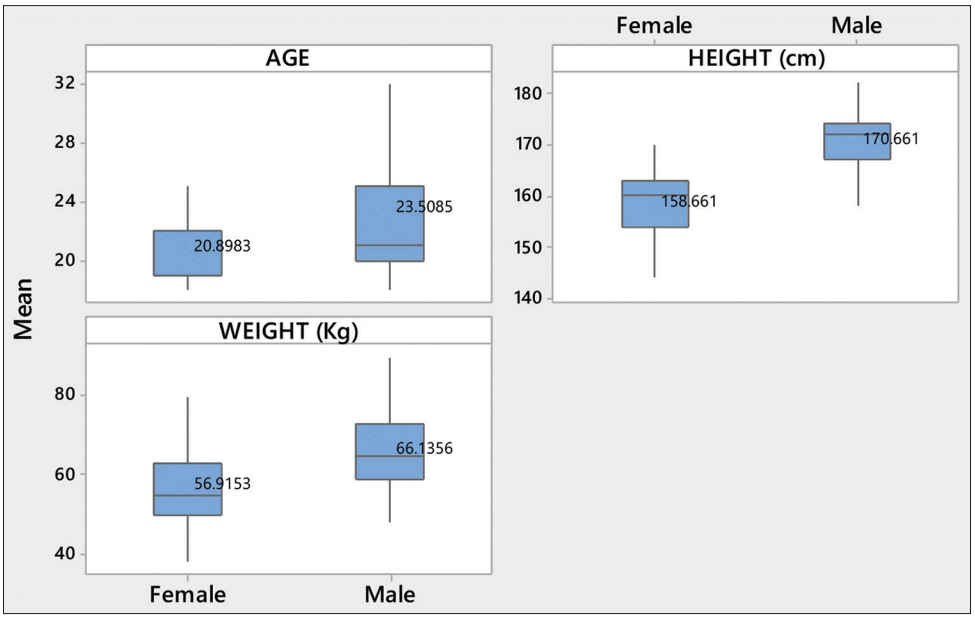

Figure 11: Comparison of anthropometric measures between gender

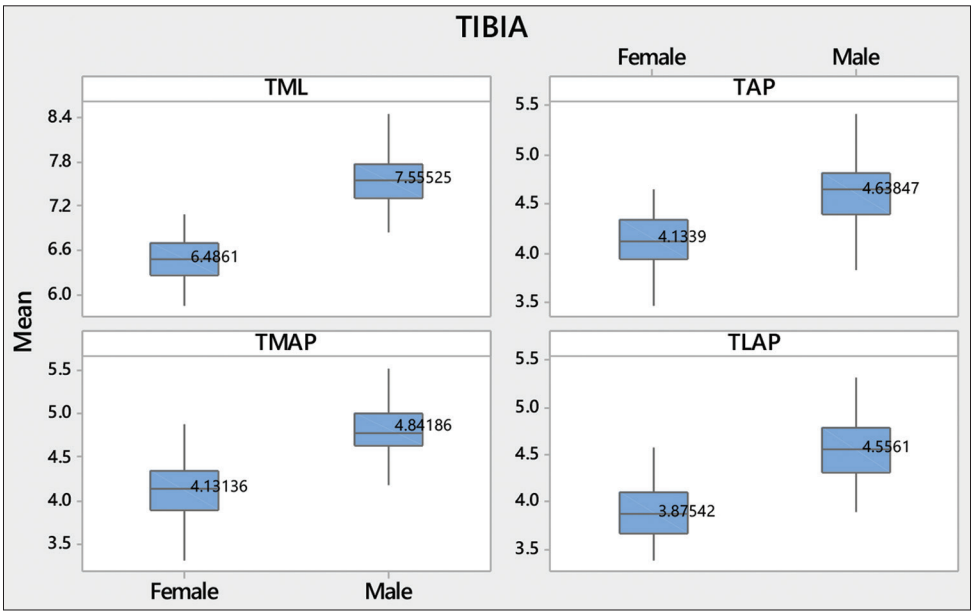

Figure 12: Comparison of morphometric measures between gender (TIBIA). TAP: Tibia anterioposterior, TML: Tibial mediolateral, TMAP: Tibia medial condyle anteroposterior, TLAP: Tibia lateral condyle anteroposterior

have a wider femur endocortical width (8.24 cm ± 0.63) compared to females (6.92 cm ± 0.46). Femur medial condyle width (FMW) and femur lateral condyle width (FLW): Once again, males exhibit greater values in both measurements. The comparison of anthropometric measures between genders in the context of knee joint morphometrics is a critical area of study, especially considering the objectives of understanding the variations in the Indian population and comparing them with global data. In contrast, Cheng *et al*. proposed that morphological data could be valuable for prosthesis design, emphasizing the suitability of sex-specific designs.[9,14] Guy *et al*. discovered significant disparities in the distal femoral morphology between men and women, particularly noting that many female cases exhibited femoral component overhang in standard prostheses.[20]

Loures *et al.*'s study, which examines the correlation between knee anthropometrics and prosthetic implant sizing, also confirms the presence of gender-specific variations in the dimensions of the distal femur.[28] These studies collectively highlight the importance of recognizing and understanding the differences in knee joint morphology along gender lines, particularly within the Indian demographic. Such insights are crucial for orthopedic

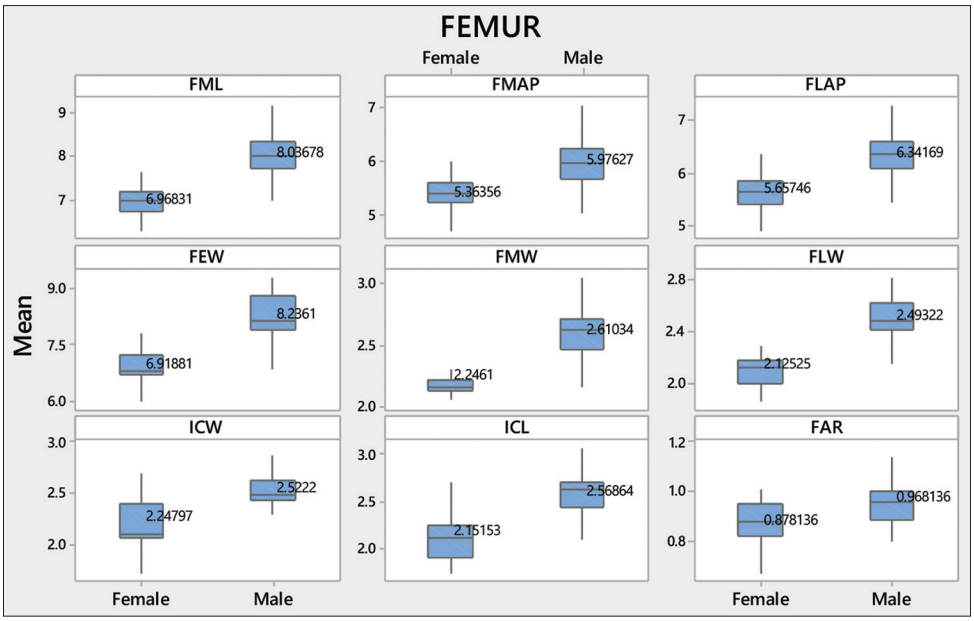

Figure 13: Comparison of morphometric measures between gender (FEMUR). FAR: Femoral aspect ratio, FML: Femur medial-lateral length, FMAP: Femur medial condyle anteroposterior length, FLAP: Femur lateral condyle anteroposterior length, FEW: Femur epicondylar width, FMW: Femur medial condyle width, FLW: Femur lateral condyle width, ICW: Intercondylar fossa width, ICL: Intercondylar fossa length

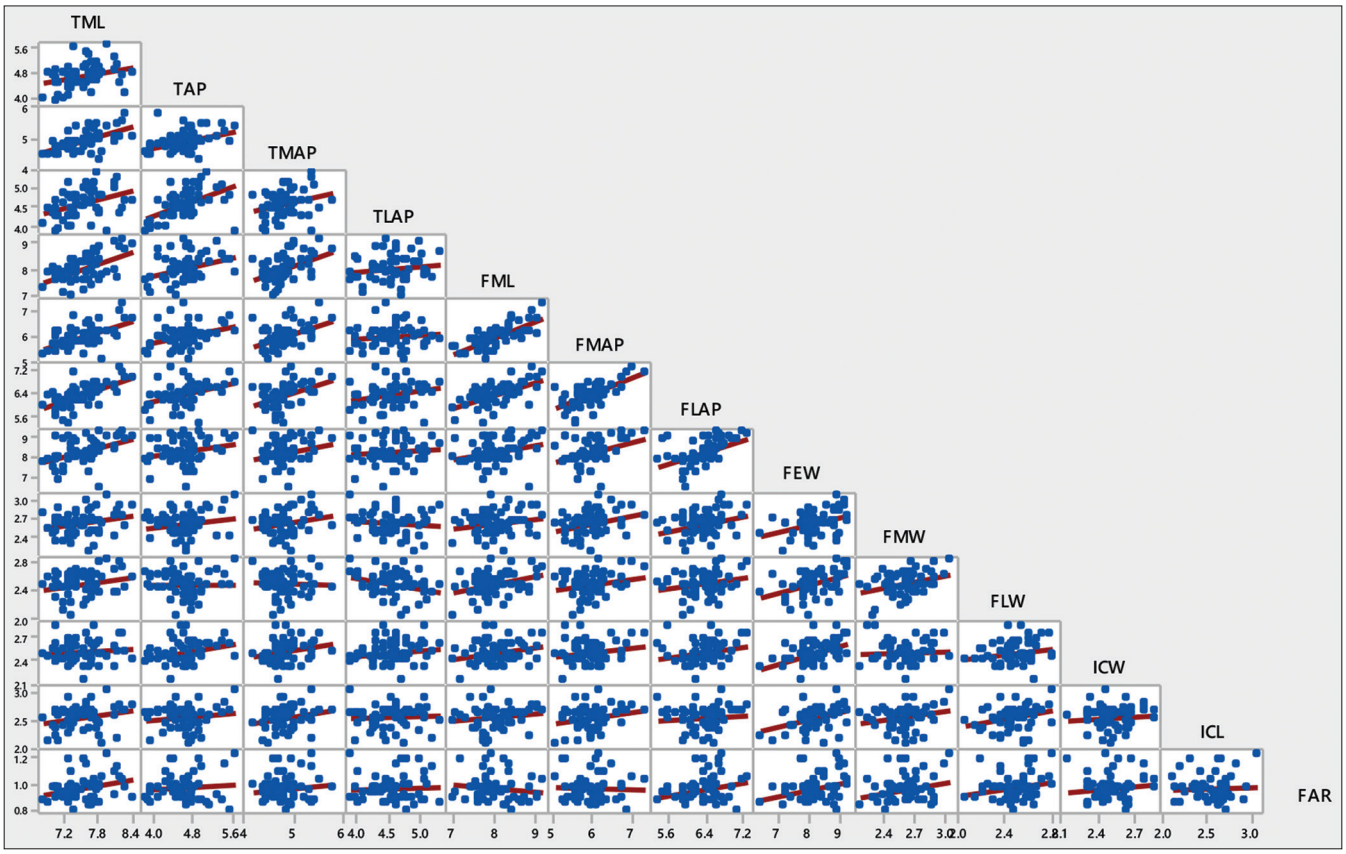

Figure 14: Correlation between morphometric measures (male). TAP: Tibia anterioposterior, FAR: Femoral aspect ratio, FML: Femur medial-lateral length, FMAP: Femur medial condyle anteroposterior length, FLAP: Femur lateral condyle anteroposterior length, FEW: Femur epicondylar width, FMW: Femur medial condyle width, FLW: Femur lateral condyle width, ICW: Intercondylar fossa width, ICL: Intercondylar fossa length, TML: Tibial mediolateral, TMAP: Tibia medial condyle anteroposterior, TLAP: Tibia lateral condyle anteroposterior

surgical planning and provide a useful point of reference for global comparative studies.

In the morphometric analysis conducted by Lim *et al.*,[29] which utilized MRI for precision, the ML width for the

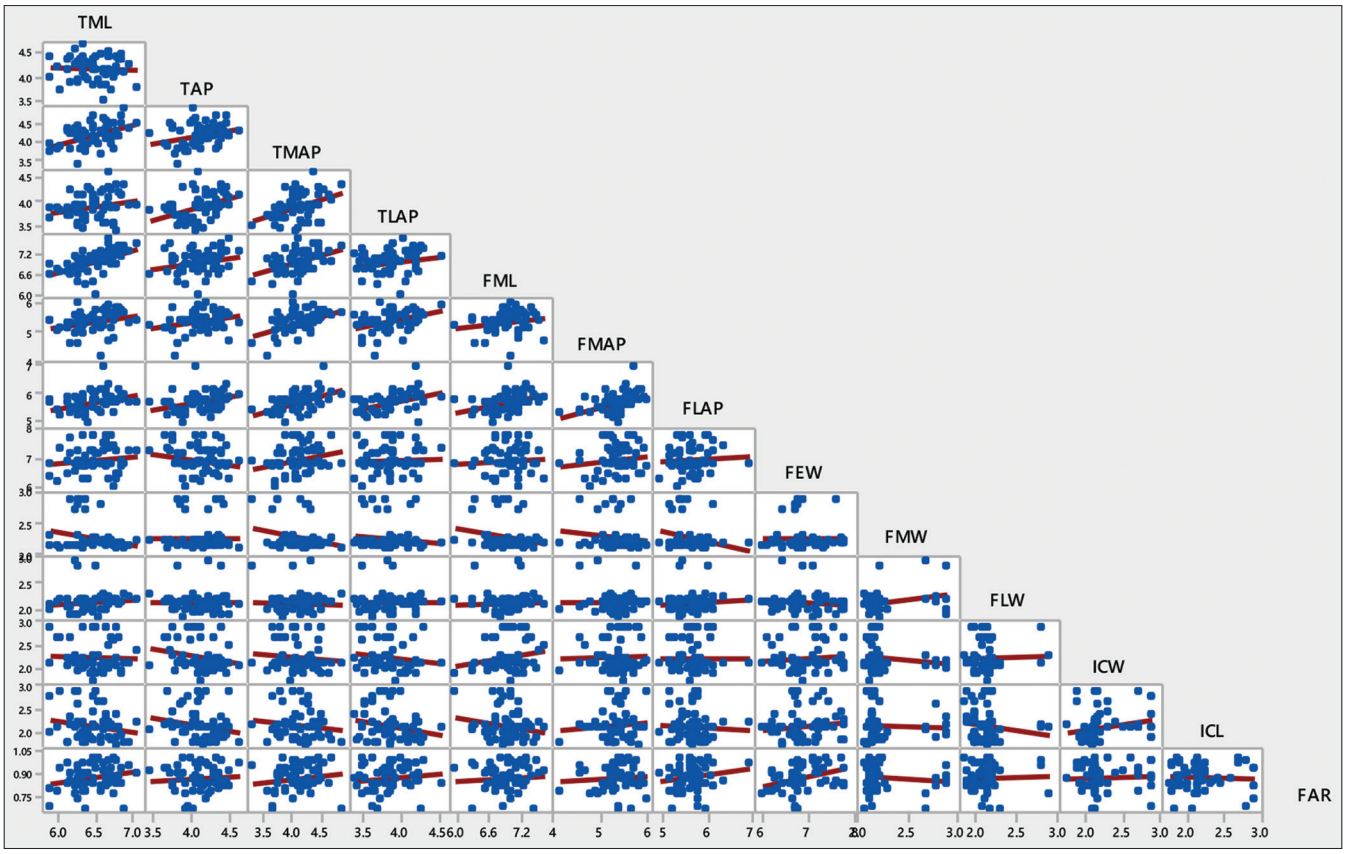

Figure 15: Correlation between morphometric measures (female). TAP: Tibia anterioposterior, FAR: Femoral aspect ratio, FML: Femur medial-lateral length, FMAP: Femur medial condyle anteroposterior length, FLAP: Femur lateral condyle anteroposterior length, FEW: Femur epicondylar width, FMW: Femur medial condyle width, FLW: Femur lateral condyle width, ICW: Intercondylar fossa width, ICL: Intercondylar fossa length, TML: Tibial mediolateral, TMAP: Tibia medial condyle anteroposterior, TLAP: Tibia lateral condyle anteroposterior

studied cohort averaged 81.5 mm in males and 76.7 mm in females. The study further revealed that the AP width of the medial compartment measured 62.7 mm in males and 56.8 mm in females, and for the lateral compartment, the dimensions were 59.0 mm in males compared to 58.4 mm in females.[29] Other parameters, including the intercondylar fossa width (ICW), intercondylar fossa length (ICL), and FAR, also presented significant variations between the sexes. Statistical analysis indicated a highly significant difference in these morphometric parameters between male and female subjects ($P < 0.001$). There was a moderate correlation between TML and TAP, with $r = 0.603$**, suggesting a moderate connection between the tibia ML length and Tibia AP length. A strong correlation with $r = 0.822$** was observed between TML and tibia medial condyle anterior-posterior (TMAP), indicating a robust relationship between these measures. In addition, TML shows a strong positive correlation of 0.754** with tibia lateral condyle anteroposterior (TLAP), signifying a substantial connection. Furthermore, there was a very strong correlation of 0.858** between TML and femur medial-lateral length (FML), highlighting a highly significant association. TML also exhibits strong positive correlations with femur medial condyle anteroposterior (FMAP) at 0.706**, femur lateral condyle anteroposterior (FLAP) at 0.785**, and femur epicondylar width (FEW) at 0.775**, suggesting significant relationships. Moreover, TML shows moderate correlations with femur medial condyle width (FMW) at 0.564**, femur lateral condyle width (FLW) at 0.674**, intercondylar fossa width (ICW) at 0.413**, intercondylar fossa length (ICL) at 0.514**, and FAR at 0.485**, indicating noticeable connections with these parameters. The study reveals notable variations in bone dimensions between India and other countries such as China, Saudi Arabia, Caucasians, Korea, and Turkey. These differences can be attributed to genetic, ethnic, and environmental factors, highlighting the significance of considering population-specific data in medical and anthropological studies.[30-32]

Conclusion

This extensive research focused on investigating gender-based disparities in knee joint morphometry using MRI among Indian adults stands as a significant contribution to the realms of orthopedics and anthropometry. The study offered valuable insights into knee joint anatomy and its implications for medical practice.

The study outcomes emphasized noticeable gender-related distinctions in critical tibia and femur parameters, consistently revealing larger dimensions in males. These findings hold relevance for knee health, orthopedic evaluations, and prosthetic design considerations. Moreover, the research employed ROC analysis to demonstrate the discriminatory power of various anatomical parameters linked to bone dimensions. These analytical approaches served as indispensable tools for both clinicians and researchers, aiding in establishing cutoff values for specific morphometric measurements. Furthermore, the study's comparative examination across various populations, including India and other nations, accentuated the need to account for population-specific data in orthopedic and anthropological investigations. Variations in bone dimensions were attributed to a complex interplay of genetic, ethnic, and environmental factors. In conclusion, this study makes a substantial contribution to the understanding of knee joint morphology. Its implications extend to orthopedic surgery, prosthetic design, and medical interventions in the context of knee joints.

Acknowledgments

I would like to acknowledge the teaching, technical, and nontechnical staff.

Financial support and sponsorship

Nil.

Conflicts of interest

There are no conflicts of interest.

References

1. Chhajer B. Anatomy of knee. In: Knee Pain. Knee Pain Fusion Books. New Delhi: Diamond Pocket Books; 2006. p. 10-1.
2. How to Measure Joint Congruency. Available from: https://www.stratovan.com/blog/how-measure-joint-congruency. [Last accessed on 2023 Dec 29].
3. Yelin E, Weinstein S, King T. The burden of musculoskeletal diseases in the United States. Semin Arthritis Rheum 2016;46:259-60.
4. Guermazi A, Roemer FW, Burstein D, Hayashi D. Why radiography should no longer be considered a surrogate outcome measure for longitudinal assessment of cartilage in knee osteoarthritis. Arthritis Res Ther 2011;13:247.
5. Recht MP, Goodwin DW, Winalski CS, White LM. MRI of articular cartilage: Revisiting current status and future directions. AJR Am J Roentgenol 2005;185:899-914.
6. Palazzo C, Nguyen C, Lefevre-Colau MM, Rannou F, Poiraudeau S. Risk factors and burden of osteoarthritis. Ann Phys Rehabil Med 2016;59:134-8.
7. Singer SP, Dammerer D, Krismer M, Liebensteiner MC. Maximum lifetime body mass index is the appropriate predictor of knee and hip osteoarthritis. Arch Orthop Trauma Surg 2018;138:99-103.
8. Total Knee Arthroplasty (TKA); 2023. Available from: https://www.emedicine.medscape.com/article/1250275-overview?form=fpf. [Last accessed on 2023 Dec 29].
9. Cheng FB, Ji XF, Lai Y, Feng JC, Zheng WX, Sun YF, *et al.* Three dimensional morphometry of the knee to design the total knee arthroplasty for Chinese population. Knee 2009;16:341-7.
10. Conley S, Rosenberg A, Crowninshield R. The female knee: Anatomic variations. J Am Acad Orthop Surg 2007;15 Suppl 1:S31-6.
11. Lonner JH, Jasko JG, Thomas BS. Anthropomorphic differences between the distal femora of men and women. Clin Orthop Relat Res 2008;466:2724-9.
12. Yue B, Varadarajan KM, Ai S, Tang T, Rubash HE, Li G. Differences of knee anthropometry between Chinese and white men and women. J Arthroplasty 2011;26:124-30.
13. Berend ME, Small SR, Ritter MA, Buckley CA. The effects of bone resection depth and malalignment on strain in the proximal tibia after total knee arthroplasty. J Arthroplasty 2010;25:314-8.
14. Cheng FB, Ji XF, Zheng WX, Lai Y, Cheng KL, Feng JC, *et al.* Use of anthropometric data from the medial tibial and femoral condyles to design unicondylar knee prostheses in the Chinese population. Knee Surg Sports Traumatol Arthrosc 2010;18:352-8.
15. Song Y, Zhu F, Lin F, Zhang F, Zhang S. Bone quality, and the combination and penetration of cement-bone interface: A comparative micro-CT study of osteoarthritis and rheumatoid arthritis. Medicine (Baltimore) 2018;97:e11987.
16. Metcalfe AJ, Ahearn N, Hassaballa MA, Parsons N, Ackroyd CE, Murray JR, *et al.* The Avon patellofemoral joint arthroplasty: Two-to 18-year results of a large single-centre cohort. Bone Joint J 2018;100-B: 1162-7.
17. Ethgen O, Bruyère O, Richy F, Dardennes C, Reginster JY. Health-related quality of life in total hip and total knee arthroplasty. A qualitative and systematic review of the literature. J Bone Joint Surg Am 2004;86:963-74.
18. Gillespie RJ, Levine A, Fitzgerald SJ, Kolaczko J, DeMaio M, Marcus RE, *et al.* Gender differences in the anatomy of the distal femur. J Bone Joint Surg Br 2011;93:357-63.
19. Desrochers J, Amrein MW, Matyas JR. Viscoelasticity of the articular cartilage surface in early osteoarthritis. Osteoarthritis Cartilage 2012;20:413-21.
20. Guy SP, Farndon MA, Sidhom S, Al-Lami M, Bennett C, London NJ. Gender differences in distal femoral morphology and the role of gender specific implants in total knee replacement: A prospective clinical study. Knee 2012;19:28-31.
21. Ho WP, Cheng CK, Liau JJ. Morphometrical measurements of resected surface of femurs in Chinese knees: Correlation to the sizing of current femoral implants. Knee 2006;13:12-4.
22. Hosaka K, Saito S, Ishii T, Mori S, Sumino T, Tokuhashi Y. Asian-specific total knee system: 5-14 year follow-up study. BMC Musculoskelet Disord 2011;12:251.
23. Westrich GH, Haas SB, Insall JN, Frachie A. Resection specimen analysis of proximal tibial anatomy based on 100 total knee arthroplasty specimens. J Arthroplasty 1995;10:47-51.
24. Alrowaili MG. Magnetic resonance evaluation of knee osteoarthritis among the Saudi population. Pak J Med Sci 2019;35:1575-81.
25. Tummala S, Schiphof D, Byrjalsen I, Dam EB. Gender differences in knee joint congruity quantified from MRI: A validation study with data from center for clinical and basic research and osteoarthritis initiative. Cartilage 2018;9:38-45.
26. Vrooijink SH, Wolters F, Van Eck CF, Fu FH. Measurements of knee morphometrics using MRI and arthroscopy: A comparative study between ACL-injured and non-injured subjects. Knee Surg Sports Traumatol Arthrosc 2011;19 Suppl 1:S12-6.
27. Park JS, Nam DC, Kim DH, Kim HK, Hwang SC. Measurement of knee morphometrics using MRI: A comparative study between ACL-

injured and non-injured knees. Knee Surg Relat Res 2012;24:180-5.
28. Loures FB, de Araújo Góes RF, da Palma IM, Labronici PJ, Granjeiro JM, Olej B. Anthropometric study of the knee and its correlation with the size of three implants available for arthroplasty. Rev Bras Ortop 2016;51:282-9.
29. Lim HC, Bae JH, Yoon JY, Kim SJ, Kim JG, Lee JM. Gender differences of the morphology of the distal femur and proximal tibia in a Korean population. Knee 2013;20:26-30.
30. Ma QL, Lipman JD, Cheng CK, Wang XN, Zhang YY, You B. A comparison between Chinese and Caucasian 3-dimensional bony morphometry in presimulated and postsimulated osteotomy for total knee arthroplasty. J Arthroplasty 2017;32:2878-86.
31. Nishikawa M, Owaki H, Kaneshiro S, Fuji T. Preoperative morphometric differences in the distal femur are based on skeletal size in Japanese patients undergoing total knee arthroplasty. Knee Surg Sports Traumatol Arthrosc 2014;22:2962-8.
32. Cho HJ, Kwak DS, Kim IB. Morphometric evaluation of Korean femurs by geometric computation: Comparisons of the sex and the population. Biomed Res Int 2015;2015:730538.

Original Article

Radiological Characteristics of the Interlaminar Foramen in Patients with Herniated Lumbar Disc: Implications for Interlaminar Lumbar Endoscopic Discectomy

Abstract

Background and Objectives: While interlaminar endoscopic discectomy has gained prominence as an effective treatment for lumbar disc herniation, there remains a paucity of research investigating the correlation between the radiological features of the interlaminar window and the intra-operative indications and techniques. This study aims to delineate several indices of a patient's radiological characteristics of the interlaminar window and their corresponding relationships. **Subjects and Methods:** We measured parameters of interlaminar foramen using optimized coronal oblique projection computed tomography images. Measurements were conducted at the L2, L3, L4, and L5 levels. **Results:** As we descended from the L2-3 to the L5-S1 levels, we observed that the transverse interlaminar diameter increased from 14.04 ± 2.24 mm to 24.82 ± 3.41 mm. The superior angles of the interlaminar windows increased from 46.96° ± 11.30° to 97.53° ± 17.94°. The interlaminar height declined from 9.43 ± 1.95 mm to 8.79 ± 2.38 mm, while the interpedicular distance expanded from 18.30 ± 3.18 mm to 29.36 ± 3.22 mm. **Conclusions:** The morphology of the interlaminar windows transitions from a vertically elongated shape to a horizontally flattened form as we move downward along the spine. This transformation should be taken into consideration during the intraoperative planning and execution of interlaminar endoscopic discectomy procedures.

Keywords: *Endoscopic interlaminar surgery, interlaminar foramen, interlaminar foramen height, interlaminar foramen morphology, lumbar disc herniation*

Vo Van Thanh[1,2], Nguyen Le Bao Tien[1,3], Dao Xuan Thanh[2,4], Ngo Thanh Tu[1], Nguyen Viet Luc[1], Pham Hong Phong[3], Nguyen Vu Cong Bao Long[2,3], Le Thanh Dung[5], Dinh Ngoc Son[1,2], Nguyen Hoang Long[1], Vu Van Cuong[1], Do Manh Hung[1], Nguyen Van Thach[1], Nguyen Duc Nghia[6], Le Manh Thuong[6], Tran Quang Loc[5]

[1]Department of Spine Surgery, Institute of Orthopedics and Trauma Surgery, Viet Duc University Hospital, Departments of [2]Surgery and [6]Anatomy, Hanoi Medical University, [4]Department of Orthopedic Surgery and Sports Medicine, Hanoi Medical University Hospital, [3]Department of Spine Surgery, University of Medicine and Pharmacy, Vietnam National University, [5]Department of Radiology, Viet Duc University Hospital, Hanoi, Vietnam

Article Info

Received: 16 May 2024
Revised: 20 July 2024
Accepted: 11 August 2024
Available online: 25 September 2024

Address for correspondence:
Dr. Dao Xuan Thanh, Hanoi Medical University Hospital, No. 1 Ton That Tung Street, Dong Da District, Hanoi 100000, Vietnam.
E-mail: daoxuanthanh@gmail.com

Access this article online

Website: https://journals.lww.com/joai
DOI: 10.4103/jasi.jasi_64_24
Quick Response Code:

Introduction

Lumbar disc herniations (LDH) are among the leading causes of lower back pain, affecting around 1%–3% of the population each year.[1] A recent systematic review found disc bulges in 30% of individuals in their 20s and 84% among those in their eighties.[2] LDH resulted in an annual healthcare expenditure of over $100 billion in the United States.[1]

LDH was more common in L4-5 and L5-S1. Based on disc degeneration, is often caused by the rupture of the fibrous ring, due to acute and chronic injury, resulting in disc herniation. This is also an important cause of lateral recess stenosis. Most of the herniation of the intervertebral disc is combined with spinal stenosis.[3] LDH commonly leads to radiculopathy.[4] The fundamental surgical objective is to relieve this compression resulting from the herniation.[4] It is crucial to comprehend the most suitable surgical method for decompressing the nerve root and removing the disc fragment. Nevertheless, the available treatment choices differ and are primarily influenced by the surgeon's preference.

In recent years, lumbar endoscopic discectomy has gained significant popularity. Technological advancements and improved surgical skills have led to enhanced surgical outcomes,[5-7] thus motivating surgeons to broaden the scope of lumbar endoscopic discectomy applications.[8,9] The utilization of magnification and illumination systems through microscopes and endoscopes has revolutionized minimally invasive procedures. Existing literature indicates that various approaches yield similar high-quality clinical results.[4]

Nevertheless, challenges persist in certain cases, such as L5-S1 herniations, downward migrated herniations, and herniations situated medial to the lumbar pedicle.[10,11] To overcome these

This is an open access journal, and articles are distributed under the terms of the Creative Commons Attribution-NonCommercial-ShareAlike 4.0 License, which allows others to remix, tweak, and build upon the work non-commercially, as long as appropriate credit is given and the new creations are licensed under the identical terms.

For reprints contact: WKHLRPMedknow_reprints@wolterskluwer.com

How to cite this article: Thanh VV, Tien NL, Thanh DX, Tu NT, Luc NV, Phong PH, *et al*. Radiological characteristics of the interlaminar foramen in patients with herniated lumbar disc: Implications for interlaminar lumbar endoscopic discectomy. J Anat Soc India 2024;73:249-58.

hurdles, the surgical approach was adjusted to utilize the interlaminar foramen of the spine.[12] Initially, this method was primarily applied at the L5S1 level before being expanded to the L4-5 level, and potentially to higher levels. Based on practical surgical experience, we believe that performing endoscopic herniated disc surgery through a larger lumbar interlaminar window is easier for the surgeon during the operation. Previous studies reported the morphology of the lumbar canal in various populations,[13-15] but there was no study conducted on the Vietnamese population. Besides, no study figured out related factors to the anatomical characteristics of the interlaminar foramen, including sex, age, and body mass index (BMI) status. Therefore, we conducted this study to measure the indices of the interlaminar foramen at the L2-3, L3-4, L4-5, and L5-S1 levels.

Subjects and Methods

Study design and participants

This cross-sectional, descriptive study was conducted between August 2022 and February 2023 at the Spine Surgery Department of Viet Duc Hospital. The participants were selected using a convenience sampling method, with a total of 76 patients' computed tomography (CT) scans included in the study.

Inclusion criteria

The inclusion criteria for the study participants were as follows:

- Age above 18 years
- Diagnosis of LDH with clinical signs of nerve root compression
- Central or lateral herniated disc visible on magnetic resonance imaging (MRI)
- Disc herniation at a lumbar spine level causing root pain, corroborated with MRI findings
- A minimum of 6 weeks of conservative treatment without symptomatic improvement.
- Availability of complete lumbar spine CT scans
- Undergoing endoscopic surgery for disc herniation via the interlaminar approach
- Consent to participate in the study.

Data collection

Radiological measurements were performed using a 32-slice GE Optima CT660 SE system (GE Healthcare, Chicago, Illinois, USA), stored as DICOM files, and analyzed on a computer using Horos version 3.3.6 software.

Measurements

Radiographic measurements were conducted to determine the indices of the interlaminar foramina in adults at the L2-3, L3-4, L4-5, and L5-S1 levels.

For each level, 12 distinct indices were assessed on CT scanners, following the protocols delineated in the preceding research.[9] In an independent assessment, two experienced radiologists conducted measurements of indices derived from CT scans. The final result presented is the arithmetic mean of these independently obtained values.

- Transverse Interlaminar Diameter: This is quantified as the maximum diameter on the horizontal plane of the interlaminar foramen [Figure 1]
- Distance Between Transverse Interlaminar Diameter and Upper Endplate of the Lower Vertebra: This metric measures the space from the transverse interlaminar diameter to the upper endplate of the lower vertebra [Figure 1]
- Distance Between Transverse Interlaminar Diameter and Lower Endplate of the Upper Vertebra: This index quantifies the distance from the transverse interlaminar diameter to the lower endplate of the upper vertebra [Figure 2]
- Superior Interlaminar Foramen Angle: This angle is formed by the lower borders of the left and right laminar of the superior vertebra [Figure 3]
- Angle Between Lamina and Horizontal Line: This angle is assessed on both the left and right sides [Figure 3]
- Interlaminar Foramen Height: This measurement represents the distance between the transverse interlaminar diameter line and the superior interlaminar foramen angle [Figure 3]
- Interpedicular Distance: Defined as the distance between the most medial border of right and left pedicles [Figure 4].

Data analysis

Descriptive analysis was used to summarize demographic data and the dimensions of the interlaminar foramen. The Student's *t*-test was utilized for comparing the interlaminar foramen dimensions across different groups (such as by sex, age, height, and BMI) when the data followed a normal distribution. In cases of non-normal distribution, the Mann–Whitney *U*-test was employed. A $P < 0.05$ determined statistical significance. All statistical analyses were conducted using STATA software (version 16.0, Stata Corp. LLC, College Station, TX, USA).

Results

Transverse interlaminar diameter

There was an increase in the transverse interlaminar diameter from 14.04 ± 2.24 mm at L2-3 to 24.82 ± 3.41 mm at L5-S1 [Table 1].

Our study demonstrated a progressive decrease in the transverse interlaminar diameter when ascending from the L5-S1 to the L2-3 levels. The diameter decreased substantially from 24.82 ± 3.41 mm at L5-S1 to 14.04 ± 2.24 mm at L2-3. This tapering transverse dimension at the higher lumbar levels poses potential constraints for interlaminar endoscopic access and instrumentation. The study found that at the L2-3 level, the transverse interlaminar diameter was influenced by a

person's sex. At the L4-5 level, age seemed to affect this diameter measurement. However, across all levels, there was no clear relationship between transverse diameter and a person's BMI status.

Distance between transverse interlaminar diameter and upper endplate of lower vertebra

The distance between transverse interlaminar diameter and upper endplate of lower vertebra exhibited a decreasing trend from L2-3 to L5-S1 levels, both at midline and bilaterally. Negative values at L4-5 and L5-S1 indicate that the transverse interlaminar diameter was positioned below the upper endplate of the lower vertebra.

At L2-3, this distance parameter is significantly associated with sex but not with age or BMI status. Conversely, at L4-5, the association was significant with age but not with sex or BMI. Across levels L3-4 and L5-S1, no statistically significant relationships were observed with age, sex, or BMI for this measurement [Table 2].

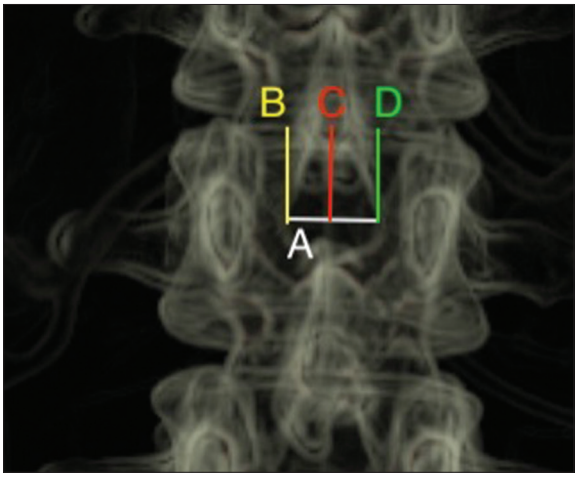

Figure 1: (A) Transverse Interlaminar Diameter; (B) Distance Between Transverse Interlaminar Diameter and Upper Endplate of the Lower Vertebra on the left; (C) Distance Between Transverse Interlaminar Diameter and Upper Endplate of the Lower Vertebra in the midline; (D) Distance Between Transverse Interlaminar Diameter and Upper Endplate of the Lower Vertebra on the right

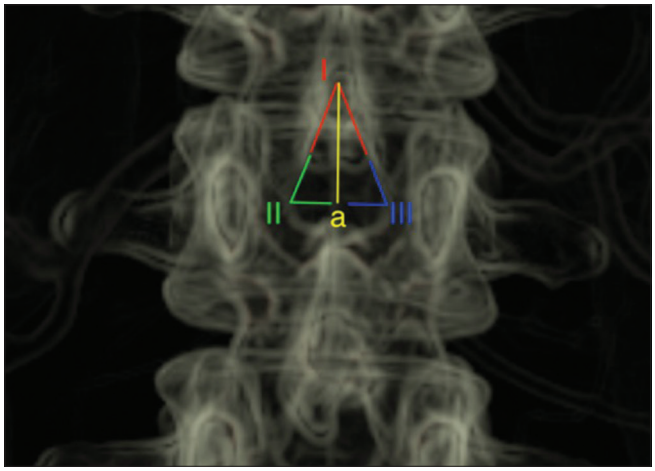

Figure 3: (I) Superior Interlaminar Foramen Angle; (II) Angle Between Lamina and Horizontal Line on the left; (III) Angle Between Lamina and Horizontal Line on the right; (a) Interlaminar foramen height

Distance between transverse interlaminar diameter and lower endplate of upper vertebra

The distance between transverse interlaminar diameter and upper endplate of the Lower vertebra exhibited a decreasing trend from L2-3 to L5-S1 levels, both at midline and bilaterally. Negative values at L4-5 and L5-S1 indicate that the transverse inter-laminar diameter was positioned below the upper endplate of the lower vertebra.

At L2-3, this distance parameter is significantly associated with sex but not with age or BMI status. Conversely, at L4-5, the association was significant with age but not with sex or BMI. Across levels L3-4 and L5-S1, no statistically significant relationships were observed with age, sex, or BMI for this measurement [Table 3].

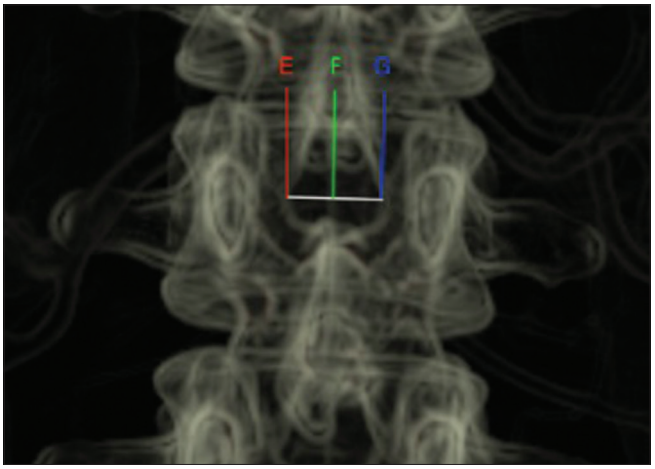

Figure 2: (E) Distance Between Transverse Interlaminar Diameter and Lower Endplate of the Upper Vertebra on the left; (F) Distance Between Transverse Interlaminar Diameter and Lower Endplate of the Upper Vertebra in the midline; (G) Distance Between Transverse Interlaminar Diameter and Lower Endplate of the Upper Vertebra on the right

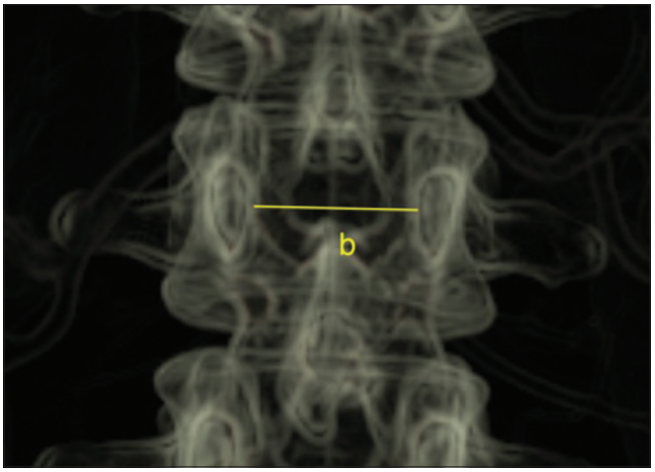

Figure 4: Interpedicular distance (b)

Table 1: The transverse interlaminar diameter (mm) and associated factors (*n*=76)

	n (%)	L23		L34		L45		L5S1	
		Mean±SD	*P*	Mean±SD	*P*	Mean±SD	*P*	Mean±SD	*P*
Total	76 (100)	14.043±2.24		16.509±2.75		20.32±3.39		24.82±3.41	
Sex									
Male	44 (57.89)	14.22±2.33	0.4	16.64±2.63	0.4	21.18±3.55	0.01	25.44±3.31	0.1
Female	32 (42.11)	13.80±2.12		16.32±2.95		19.14±2.79		23.96±3.42	
Age									
<40	21 (27.63)	13.47±2.43	0.4	16.58±2.77	0.6	20.16±3.43	0.9	24.61±3.85	0.6
40–49	24 (31.58)	14.62±1.82		17.10±2.86		20.72±3.47		24.35±3.49	
50–59	25 (32.89)	13.95±2.10		16.03±2.80		20.09±3.26		25.06±3.02	
≥60	6 (7.89)	14.05±3.48		15.88±2.07		20.23±4.19		26.37±3.32	
Height (cm)									
<155	8 (10.53)	14.19±2.31	0.6	17.18±4.53	0.1	19.25±3.09	0.1	23.54±1.78	0.1
155–159	22 (28.95)	14.04±2.20		16.19±2.32		19.52±2.79		24.75±3.88	
160–164	14 (18.42)	13.99±2.26		15.98±1.82		19.66±2.48		23.16±2.99	
165–169	19 (25.00)	14.30±2.58		17.45±2.78		22.49±4.40		26.60±3.71	
170–174	10 (13.16)	13.11±1.97		14.95±2.34		19.29±2.21		24.96±1.92	
≥175	3 (3.95)	15.33±0.83		18.80±2.51		21.83±3.35		24.63±3.64	
BMI group									
<18.5	3 (3.95)	13.46±2.33	0.1	14.20±3.86	0.4	18.73±1.36	0.8	24.37±2.51	0.1
18.5–22.9	39 (51.32)	14.61±2.48		16.67±2.29		20.55±3.67		25.65±3.73	
23.0–24.9	22 (28.95)	13.56±1.90		16.60±3.41		20.11±3.34		23.54±2.42	
≥25	12 (15.79)	13.20±1.61		16.38±2.66		20.37±3.01		24.57±3.62	

SD: Standard deviation, BMI: Body mass index

Superior interlaminar foramen angle

The superior interlaminar foramen angle exhibited a progressive increase from 46.96° at the L2-3 level to 97.53° at the L5-S1 level, indicating a more laterally expanded interlaminar foramen at the lower lumbar levels.

At the L2-3 level, this angle demonstrated a significant association with age but not with sex or BMI status. The angle at the L4-5 level exhibited a significant relationship with both age and BMI, but not sex. Across the remaining levels of L3-4 and L5-S1, no statistically significant associations were found between the superior interlaminar foramen angle and age, sex, or BMI factors [Table 4].

Angle between laminar and horizontal line

The angle between the lower border of the lamina and the horizontal line demonstrated a decreasing trend along the lumbar spine from the L2-3 to the L5-S1 level, suggesting a more horizontally oriented laminar morphology at the lower lumbar levels.

At the L2-3 level, this angle exhibited a significant association with age but not with sex or BMI status. Conversely, at the L4-5 level, the relationship was significant with both sex and BMI, but not with age. For the L3-4 and L5-S1 levels, no statistically significant correlations were observed between the angle between the lamina and the horizontal line, and age, sex, or BMI [Table 5].

Interlaminar foramen height

A progressive decrease in the interlaminar foramen height was noted from the L2-3 to the L5-S1 level, indicating a reduction in the vertical dimension of the interlaminar window at the lower lumbar levels.

At the L2-3 level, the interlaminar foramen height demonstrated a significant relationship with sex but not with age or BMI status. However, at the L4-5 level, this parameter was significantly associated with both age and BMI, while no such correlation was observed with sex. Across the L3-4 and L5-S1 levels, no statistically significant associations were found between the interlaminar foramen height and age, sex, or BMI factors [Table 6].

Interpedicular distance

The interpedicular distance, representing the horizontal diameter of the spinal canal, exhibited a progressive increase from the L2-3 to the L5-S1 level, suggesting a widening of the spinal canal in the lower lumbar regions.

At the L2-3 level, the interpedicular distance is significantly associated with age but not with sex or BMI status. However, at the L4-5 level, this parameter was significantly related to both sex and BMI, while no such correlation was observed with age. Across the L3-4 and L5-S1 levels, no statistically significant relationships were found between the interpedicular distance and age, sex, or BMI factors [Table 7].

Discussion

The transverse interlaminar line is representative of the horizontal dimension of the interlaminar foramen. Our findings indicate a gradual increase in this dimension from the L2-3 to the L5-S1 level. The average transverse

Table 2: Distance between transverse interlaminar diameter and upper endplate of lower vertebra (mm) and associated factors (*n*=76)

	L23			L34			L45			L5S1		
	Left	Center	Right	Left	Center	Right	Left	Center	Right	Left	Center	Right
Total	5.33±1.85	5.04±1.95	5.41±1.66	4.03±1.54	3.71±1.57	4.23±1.56	1.57±2.34	0.81±2.32	1.68±2.47	−5.26±2.41	−6.50±2.55	−5.07±2.88
Sex												
Male	5.48±1.82	5.27±2.00	5.51±1.68	4.06±1.38	3.78±1.55	4.19±1.27	2.15±1.74*	1.48±1.80†	2.30±1.71*	−4.98±2.37	−6.27±2.36	−4.62±3.09
Female	5.13±1.89	4.73±1.87	5.28±1.63	4.00±1.76	3.62±1.60	4.28±1.92	0.76±2.80	−0.10±2.65	0.83±3.06	−5.65±2.45	−6.81±2.79	−5.69±2.48
Age												
<40	5.36±1.72	5.08±1.76	5.52±1.48	4.09±1.32	3.80±1.25	4.24±1.09	1.81±1.91	1.18±1.88	2.04±2.04	−5.07±1.94	−6.16±2.15	−5.08±1.80
40–49	5.70±1.81	5.53±2.01	5.68±1.46	4.56±1.71	4.23±1.77	4.75±1.70	2.13±2.08	1.15±1.76	2.23±2.06	−4.86±2.13	−6.21±2.17	−4.95±2.35
50–59	4.95±2.10	4.62±2.16	5.10±2.06	5.52±1.57	3.21±1.64	3.80±1.77	0.84±2.96	0.20±3.15	0.87±3.20	−5.92±2.98	−7.03±3.09	−5.14±4.07
≥60	5.38±1.27	4.70±1.17	5.27±1.18	3.83±0.92	3.42±0.79	3.82±1.02	1.45±0.83	0.77±1.39	1.58±0.95	−4.82±2.30	−6.62±3.00	−5.22±2.54
Height (cm)												
<155	5.94±2.16	5.56±2.00	6.01±1.59	4.31±2.47	4.23±2.12	5.28±2.69	1.34±3.67	0.24±3.14	1.19±4.02	−6.46±3.25	−7.10±3.79	−6.30±3.58
155–159	5.00±1.68	4.61±1.70	5.19±1.52	3.95±1.53	3.53±1.38	3.98±1.53	1.08±2.01	0.40±2.00	1.32±2.19	−4.92±2.16	−6.38±2.63	−5.10±2.16
160–164	4.98±2.38	4.66±2.57	4.91±2.34	4.41±1.29	3.76±1.26	4.56±1.19	1.06±3.25	0.23±3.33	1.13±3.55	−5.21±2.46	−6.41±2.36	−3.81±4.14
165–169	5.77±1.46	5.61±1.85	5.87±1.22	3.49±1.49	3.35±1.89	3.76±1.41	1.88±1.64	1.08±1.59	2.01±1.39	−5.58±2.46	−6.89±2.35	−5.72±2.60
170–174	4.83±1.45	4.71±1.60	4.94±1.41	4.24±1.15	3.93±1.22	4.13±1.06	2.58±1.23	2.27±1.65	2.69±1.33	−4.76±2.19	−5.76±2.35	−4.62±2.07
≥175	6.70±2.62	6.07±1.89	6.47±1.82	5.00±0.46	5.03±1.31	4.93±0.87	2.63±1.67	1.57±0.74	2.80±1.41	−4.47±2.57	−6.17±1.85	−4.87±2.07
BMI group												
<18.5	5.43±3.69	4.77±2.64	5.30±2.91	4.70±0.57	3.60±0.92	3.73±0.72	4.13±0.64*	3.60±1.59	4.23±0.50	−3.10±3.38	−4.80±4.11	−3.17±3.25
18.5–22.9	4.59±1.30	4.35±1.50	4.78±1.21	3.93±1.54	3.53±1.48	4.09±1.38	1.34±2.12	0.63±2.21	1.54±2.33	−5.29±2.21	−6.55±2.38	−5.34±2.06
23.0–24.9	6.52±1.91*	6.10±1.96†	6.42±1.74	4.23±1.31	4.24±1.65	4.57±1.74	1.75±2.55	0.94±2.37	1.69±2.69	−5.24±2.32	−6.37±2.39	−4.31±3.59
≥25	5.56±1.77	5.43±2.32	5.66±1.66	3.91±2.09	3.38±1.74	4.17±1.94	1.31±2.66	0.49±2.53	1.49±2.67	−5.77±2.97	−7.00±3.10	−6.08±3.47

*P<0.05, †P<0.01. BMI: Body mass index

Table 3: Distance between transverse interlaminar diameter and lower endplate of upper vertebra (mm)

	L23			L34			L45			L5S1		
	Left	Center	Right	Left	Center	Right	Left	Center	Right	Left	Center	Right
Total	11.64±2.25	12.22±2.35	11.68±2.15	9.58±2.47	10.51±2.54	9.82±2.51	5.91±2.32	7.16±2.62	6.06±2.40	−2.64±2.16	−2.21±2.49	−2.77±2.12
Sex												
Male	11.84±1.99	12.57±1.99	11.93±1.90	9.78±2.51	10.94±2.45	10.05±2.56	6.53±2.00†	7.85±2.30†	6.75±2.06†	−2.00±1.89	−1.57±2.01	−2.13±1.86
Female	11.36±2.57	11.73±2.72	11.32±2.44	9.30±2.42	9.93±2.59	9.51±2.44	5.05±2.49	6.20±2.75	5.10±2.53	−3.51±2.22†	−3.10±2.82*	−3.65±2.17†
Age												
<40	10.90±2.24	11.42±2.32	10.97±2.10	9.22±2.49	9.78±2.38	9.26±2.45	5.56±2.38	6.68±2.59	5.72±2.31	−3.10±1.49	−2.57±1.83	−3.21±1.39
40–49	12.55±2.26	13.09±2.03*	12.53±2.04*	10.27±2.44	11.42±2.45	10.61±2.52	6.40±1.90	7.91±2.29	6.51±1.99	−1.92±1.96	−1.60±2.11	−1.97±1.94
50–59	11.59±2.24	12.14±2.57	11.61±2.26	9.05±2.65	10.24±2.83	9.42±2.72	5.73±2.84	6.88±3.10	5.87±3.03	−3.00±2.77	−2.54±3.13	−3.18±2.68
≥60	10.83±1.06	11.82±1.98	11.03±1.30	10.32±0.85	10.63±1.21	10.30±0.69	5.90±1.09	6.97±1.24	6.18±1.01	−2.40±1.56	−2.07±3.00	−2.73±1.80
Height (cm)												
<155	13.01±3.21	12.78±3.72	12.55±2.94	9.84±3.15	10.43±3.73	10.46±3.03	4.98±3.33	6.70±3.82	4.91±3.35	−4.22±3.41	−3.54±4.19	−4.25±3.24
155–159	10.93±1.96	11.51±2.11	11.07±1.96	9.20±2.17	9.96±2.20	9.31±2.21	5.57±2.13	6.48±2.31	5.65±2.16	−2.91±1.75	−2.43±2.51	−3.08±1.79
160–164	11.07±2.64	11.67±2.32	11.17±2.62	10.19±2.31	11.23±2.13	10.36±2.35	6.06±2.50	7.40±2.81	6.07±2.49	−2.57±2.25	−2.13±2.28	−2.75±2.19
165–169	11.93±11.78	12.52±2.18	12.05±1.79	9.43±2.52	10.47±2.73	9.80±2.67	6.42±2.46	7.65±2.88	6.64±2.63	−2.52±1.57	−2.03±1.72	−2.54±1.50
170–174	12.11±1.50	13.17±1.24	12.13±1.51	9.49±3.20	10.59±2.68	9.51±3.01	6.15±1.42	7.61±1.20	6.68±1.38	−1.44±2.34	−1.33±2.65	−1.64±2.48
≥175	12.47±3.37	13.37±3.21	12.27±2.58	10.13±1.32	11.50±2.26	10.47±2.06	6.07±1.99	7.60±2.60	6.33±1.96	−1.47±1.27	−1.63±0.40	−1.90±1.23
BMI group												
<18.5	12.80±2.59*	13.83±2.68	12.57±2.05	8.60±1.56	10.03±2.94	9.03±2.05	7.60±0.82	8.87±1.46	8.13±1.00	0.03±3.45	−0.37±4.61	−0.2±3.56
18.5–22.9	10.95±2.34	11.59±2.68	11.11±2.41	8.92±2.27	9.95±2.70	9.26±2.46	5.79±2.45	6.94±2.60	5.93±2.51	−2.76±1.54	−2.15±2.22	−2.94±1.57
23.0–24.9	12.75±1.85	13.06±1.45	12.65±1.37	10.75±2.10*	11.44±1.79	10.98±1.97	5.82±2.37	7.40±2.66	5.85±2.39	−3.10±2.12	−2.45±2.27	−3.17±2.03
≥25	11.58±1.83	12.28±1.95	11.53±1.93	9.85±3.20	10.78±2.86	9.72±3.16	6.03±2.10	7.00±2.87	6.33±2.23	−2.08±3.17	−2.45±3.24	−2.15±3.06

*P<0.05, †P<0.01. BMI: Body mass index

Table 4: Superior interlaminar foramen angle and associated factors (*n*=76)

	L23		L34		L45		L5S1	
	Mean±SD	*P*	Mean±SD	*P*	Mean±SD	*P*	Mean±SD	*P*
Total	46.96±11.30		55.40±14.82		73.92±14.22		97.53±17.94	
Sex								
Male	46.26±10.77	0.5	53.80±11.90	0.6	74.17±15.12	1	97.98±20.83	0.6
Female	47.93±12.10		57.62±18.05		73.57±13.11		96.91±13.29	
Age								
<40	47.10±9.31	0.3	58.27±17.69	0.1	74.94±13.76	0.6	102.93±15.10	0.3
40–49	49.56±11.90		57.13±15.32		76.99±17.10		93.50±22.50	
50–59	45.06±11.64		54.07±12.01		71.25±12.48		98.15±15.84	
≥60	44.05±14.34		44.00±7.48		69.15±8.46		92.12±12.13	
Height (cm)								
<155	50.70±15.47	0.7	61.85±14.22	0.4	78.11±12.49	0.3	90.47±10.31	0.3
155–159	46.14±10.98		57.25±19.70		72.56±13.67		98.00±22.28	
160–164	49.19±10.43		53.16±9.51		68.52±9.23		94.57±18.07	
165–169	45.69±10.44		54.85±14.51		78.55±16.63		103.24±17.22	
170–174	43.84±11.04		48.87±9.17		69.01±14.52		94.46±14.45	
≥175	51.13±16.14		60.43±9.87		84.90±16.86		100.80±11.15	
BMI group								
<18.5	49.03±17.32	0.9	55.00±14.58	0.4	68.90±18.70	0.6	84.63±15.66	0.2
18.5–22.9	47.75±11.96		57.84±16.28		75.62±14.93		100.26±21.80	
23.0–24.9	45.07±8.21		52.22±11.51		70.51±11.75		95.56±12.73	
≥25	47.34±13.50		53.43±15.64		75.89±15.40		95.48±10.74	

SD: Standard deviation, BMI: Body mass index

Table 5: Angle between lamina and horizontal line (°) and associated factors (*n*=76)

	L23		L34		L45		L5S1	
	Left	Right	Left	Right	Left	Right	Left	Right
Total	65.03±9.20	65.25±9.69	60.21±10.73	60.84±8.30	57.39±39.11	52.23±8.44	43.44±10.20	42.42±10.13
Sex								
Male	65.34±8.08	65.66±8.70	57.98±11.83	59.65±8.16	52.65±8.76	51.96±8.42	43.08±10.56	41.35±10.75
Female	64.61±10.68	64.69±11.02	63.28±8.23*	62.46±8.35	63.91±59.31	52.61±8.58	43.92±9.84	43.86±9.20
Age								
<40	64.07±5.91	65.20±2.27	60.69±7.08	60.76±7.00	51.83±6.78	50.53±6.45	39.37±9.91	38.80±9.56
40–49	65.99±8.69	66.93±9.81	57.53±15.69	61.48±9.93	66.75±68.76	52.16±10.56	43.71±10.66	42.55±11.11
50–59	65.02±12.24	63.74±11.47	60.87±7.26	59.08±7.87	54.04±7.78	53.30±7.48	44.79±9.00	44.10±8.94
≥60	64.63±7.50	65.02±9.85	66.50±7.53	65.87±6.29	53.43±9.75	54.05±10.34	50.93±10.54	48.52±10.95
Height (cm)								
<155	61.99±16.52	60.45±14.10	59.47±7.70	57.50±8.59	51.80±8.69	51.03±7.84	52.04±8.54*	49.71±10.57
155–159	65.50±8.23	66.95±9.63	64.46±8.48	64.29±8.03	69.26±71.23	53.14±9.63	40.41±8.51	41.05±7.51
160–164	60.67±9.84	59.96±10.06	59.30±6.60	59.09±7.51	53.94±7.17	53.78±6.37	42.54±9.11	42.59±9.25
165–169	66.82±6.56	67.61±7.37	57.56±15.92	60.92±8.11	51.42±9.87	50.82±9.43	41.46±12.12	40.11±13.02
170–174	69.15±6.24	69.15±7.07	59.60±8.87	59.62±8.75	52.99±9.10	51.00±8.90	49.40±8.10	45.63±7.97
≥175	65.03±5.59	62.40±4.00	54.10±10.28	56.07±10.35	53.83±3.61	54.27±2.72	39.53±9.49	37.13±10.27
BMI group								
<18.5	68.97±10.02	66.97±8.91	59.67±7.60	58.37±5.79	57.20±0.69	55.47±1.40	49.07±5.69	47.17±5.42
18.5–22.9	64.98±10.47	65.21±10.68	61.34±8.01	61.10±9.41	60.83±54.26	52.44±8.93	42.13±10.70	41.48±10.52
23.0–24.9	63.68±7.36	64.21±8.29	61.65±8.19	61.54±6.86	55.14±6.19	53.50±7.06	43.82±10.47	43.16±10.90
≥25	66.70±8.14	66.88±9.73	54.06±19.36	59.29±7.92	50.39±8.82	48.11±9.66	45.58±8.90	42.95±8.71

*P<0.05. BMI: Body mass index

dimension of the interlaminar foramen at the L3-4 level exceeded 15 mm, and it surpassed 20 mm at the L4-5 and L5-S1 levels. The L2-3 level was the only exception with a dimension <15 mm, consistent with the findings of Zakir Sakci.[14] A larger horizontal diameter of the interlaminar foramen facilitates the insertion of the endoscope system's working tube and reduces the need for foramen expansion using a drill. This is especially

Table 6: Interlaminar foramen height (mm) and associated factors (*n*=76)

	L23		L34		L45		L5S1	
	Mean±SD	*P*	Mean±SD	*P*	Mean±SD	*P*	Mean±SD	*P*
Total	9.43±1.95		9.16±1.72		9.05±1.87		8.79±2.38	
Sex								
Male	9.57±1.86	0.3	9.17±1.78	0.9	9.04±2.03	1	8.66±1.98	0.7
Female	9.24±2.08		9.13±1.67		9.06±1.65		8.97±2.85	
Age								
<40	9.47±2.81	0.1	8.82±1.78	0.6	8.74±2.12	0.8	8.50±3.39	0.2
40–49	9.89±1.42		9.50±1.85		9.27±1.85		9.11±1.96	
50–59	9.16±1.44		9.11±1.45		9.17±1.67		9.00±1.66	
≥60	8.62±1.98		9.12±2.23		8.78±2.08		7.76±1.09	
Height (cm)								
<155	10.28±2.35	0.4	9.19±1.64	0.3	9.74±1.41	0.1	10.11±2.07	0.02
155–159	8.97±1.97		9.07±1.67		8.78±1.52		8.38±2.94	
160–164	9.48±1.11		9.31±1.29		9.56±2.28		9.42±1.96	
165–169	9.25±1.52		9.07±2.25		8.62±2.11		8.09±2.03	
170–174	9.12±0.98		8.61±1.01		8.58±1.32		8.26±1.83	
≥175	12.60±5.29		11.33±1.58		11.17±1.95		10.67±2.30	
BMI group								
<18.5	9.10±1.55	1	10.00±2.46	0.6	9.00±1.68	1	10.10±0.00	0.4
18.5–22.9	9.14±1.54		8.93±1.53		9.01±1.72		8.45±2.52	
23.0–24.9	9.93±2.66		9.50±2.04		9.20±2.08		9.45±2.36	
≥25	9.54±1.69		9.04±1.56		8.93±2.18		8.67±1.79	

SD: Standard deviation, BMI: Body mass index

Table 7: Interpedicular distance (mm) and associated factors (*n*=76)

	L23		L34		L45		L5S1	
	Mean±SD	*P*	Mean±SD	*P*	Mean±SD	*P*	Mean±SD	*P*
Total	18.30±3.18		20.63±3.09		24.41±3.46		29.36±3.22	
Sex								
Male	18.38±3.24	0.8	20.85±2.91	0.3	25.42±3.51	0.0023	30.07±2.72	0.02
Female	18.20±3.14		20.33±3.35		23.02±2.91		28.39±3.61	
Age								
<40	17.82±3.49	0.5	20.54±3.01	0.8	24.31±3.33	1	28.95±3.41	0.7
40–49	19.10±3.32		20.97±3.46		24.56±3.14		29.18±2.73	
50–59	18.09±2.59		20.63±2.99		24.31±3.59		29.57±3.13	
≥60	17.67±3.89		19.58±2.68		24.58±5.22		30.63±4.93	
Height (cm)								
<155	19.26±4.87	0.4	21.23±5.32	0.03	23.04±1.72	0.0028	28.23±2.19	0.05
155–159	18.23±2.37		20.22±2.48		23.51±3.18		29.29±3.72	
160–164	17.84±2.42		20.18±2.54		23.53±2.55		27.88±3.56	
165–169	19.22±3.03		21.64±2.07		27.08±3.93		31.10±2.51	
170–174	16.65±1.97		18.50±2.65		23.19±2.84		28.66±2.38	
≥175	18.13±8.42		24.80±4.36		25.93±3.71		31.13±2.28	
BMI group								
<18.5	19.23±5.55	0.6	20.60±7.13	0.9	23.37±2.11	0.9	30.53±2.59	0.3
18.5–22.9	18.65±2.42		20.62±2.49		24.50±3.46		29.89±3.51	
23.0–24.9	18.04±4.32		20.74±3.71		24.15±3.91		28.44±2.82	
≥25	17.43±2.39		20.45±2.84		24.86±3.09		29.04±2.92	

SD: Standard deviation, BMI: Body mass index

significant when compared to the average outer diameter of the second-generation endoscope system, reported as 7.9 mm.[16]

Simultaneously, the position of the transverse interlaminar line relative to the disc varied across levels. At the L4-5 and L5-S1 levels, the line was located below the disc,

whereas at the L2-3 and L3-4 levels, it was above the disc. This relationship was further elucidated by measuring the distance between this line and the inferior endplate of the superior vertebra and the superior endplate of the inferior vertebra.[17] Notably, as the lumbar spine descends to the lower levels, this distance decreases, reaching a negative value at the L4-5 and L5-S1 levels (indicating that the transverse interlaminar line is below the disc), which aligns with the findings of Sakci.[14] Given that most LDHs occur at the nerve root's shoulder, the herniated discs will be positioned on the outer upper side of the corresponding nerve root. Consequently, a transverse interlaminar line positioned lower relative to the disc facilitates access to the herniated mass via the upward expansion of the interlaminar foramen.[18]

In addition to the horizontal diameter, the vertical diameter, denoted by the height of the interlaminar foramen in our study, is paramount in endoscopic surgery. The height of the interlaminar foramen increases as we ascend along the spinal column. However, at lower levels such as L4-5 and L5-S1, adjustments to the patient's posture can influence the vertical diameter of the interlaminar window, with a bent-back posture increasing and an arched-back posture decreasing the vertical diameter.[19] This is a significant consideration when undertaking endoscopic surgery at the lower L4-5 and L5-S1 levels, especially in cases of axillary position herniated discs, where the herniated mass is below the transverse interlaminar line.

To describe the morphology of the interlaminar foramen, we measured and analyzed the angles of the interlaminar foramen. The findings reveal that, as we descend, the interlaminar foramen tends to widen laterally, as indicated by the increasing superior interlaminar angle and decreasing bilateral interlaminar angle.[20] This implies that at lower levels, including L4-5 and L5-S1, the interlaminar foramen expands laterally, thereby facilitating easier access to the lateral recess compared to the upper levels.[21] This observation is critically important during the planning and execution of endoscopic surgery.

The interpedicular distance represents the horizontal diameter of the spinal canal, which progressively increases from L2-3 to L5-S1. A larger interpedicular distance enhances the mobility of the nerve roots. When juxtaposed with the corresponding interlaminar foramen's horizontal diameter, it is observed that the interlaminar foramen is relatively wider than the spinal canal at lower levels. This factor underscores the ability to approach the lateral recess during endoscopic surgery at the L4-5 and L5-S1 levels compared to the upper levels.

The results derived from the aforementioned indices reveal a notable trend along the lumbar spine: as we descend, the interlaminar foramen tends to broaden and expand bilaterally, and its positioning becomes lower relative to the intervertebral disc.

Conclusions

The morphology of the interlaminar foramen undergoes a transformation from a vertically elongated shape to a laterally expanded form as one descends along the lumbar spine. This transformation is characterized by an increase in the transverse diameter, a decrease in the vertical height, and a progressive lateral expansion of the interlaminar window at lower lumbar levels. These morphological changes should be considered during the planning and execution of interlaminar endoscopic discectomy procedures to facilitate optimal access and instrumentation.

Acknowledgment

The authors would like to thank the patients involved in this study.

Financial support and sponsorship

Nil.

Conflicts of interest

There are no conflicts of interest.

References

1. Zhang AS, Xu A, Ansari K, Hardacker K, Anderson G, Alsoof D, *et al.* Lumbar disc herniation: Diagnosis and management. Am J Med 2023;136:645-51.
2. Brinjikji W, Luetmer PH, Comstock B, Bresnahan BW, Chen LE, Deyo RA, *et al.* Systematic literature review of imaging features of spinal degeneration in asymptomatic populations. AJNR Am J Neuroradiol 2015;36:811-6.
3. Li G, Niu W. Challenges toward musculoskeletal injuries and diseases. In: Nanoengineering in Musculoskeletal Regeneration. Amsterdam: Elsevier; 2020. p. 1-41.
4. Alvarado AM, Kalfas IH, Arnold PM. Disc herniation (primary, recurrent, residual). In: Revision Lumbar Spine Surgery. Amsterdam: Elsevier; 2021. p. 63-72.
5. Smith N, Masters J, Jensen C, Khan A, Sprowson A. Systematic review of microendoscopic discectomy for lumbar disc herniation. Eur Spine J 2013;22:2458-65.
6. Corniola MV, Stienen MN, Tessitore E, Schaller K, Gautschi OP. Minimally invasive spine surgery: Past and present. Rev Med Suisse 2015;11:2186-9.
7. Alvi MA, Kerezoudis P, Wahood W, Goyal A, Bydon M. Operative approaches for lumbar disc herniation: A systematic review and multiple treatment meta-analysis of conventional and minimally invasive surgeries. World Neurosurg 2018;114:391-407.e2.
8. Lee CW, Yoon KJ, Kim SW. Percutaneous endoscopic decompression in lumbar canal and lateral recess stenosis – The surgical learning curve. Neurospine 2019;16:63-71.
9. Kim M, Kim HS, Oh SW, Adsul NM, Singh R, Kashlan ON, *et al.* Evolution of spinal endoscopic surgery. Neurospine 2019;16:6-14.
10. Lewandrowski KU, Telfeian AE, Hellinger S, Jorge Felipe Ramírez León, Paulo Sérgio Teixeira de Carvalho, Ramos MR, *et al.* Difficulties, challenges, and the learning curve of avoiding complications in lumbar endoscopic spine surgery. Int J Spine Surg 2021;15:S21-37.

11. Ju CI, Lee SM. Complications and management of endoscopic spinal surgery. Neurospine 2023;20:56-77.
12. Sebben AL, Kulcheski ÁL, Graells XS, Benato ML, Santoro PG. Comparison of two endoscopic spine surgical techniques. Rev Assoc Med Bras (1992) 2021;67:243-7.
13. Trinh A, Hashmi SS, Massoud TF. Imaging anatomy of the vertebral canal for trans-sacral hiatus puncture of the lumbar cistern. Clin Anat 2021;34:348-56.
14. Sakçı Z, Önen MR, Fidan E, Yaşar Y, Uluğ H, Naderi S. Radiologic anatomy of the lumbar interlaminar window and surgical considerations for lumbar interlaminar endoscopic and microsurgical disc surgery. World Neurosurg 2018;115:e22-6.
15. Demondion X, Lefebvre G, Fisch O, Vandenbussche L, Cepparo J, Balbi V. Radiographic anatomy of the intervertebral cervical and lumbar foramina (vessels and variants). Diagn Interv Imaging 2012;93:690-7.
16. Telfeian AE, Veeravagu A, Oyelese AA, Gokaslan ZL. A brief history of endoscopic spine surgery. Neurosurg Focus 2016;40:E2.
17. Piera V, Rodriguez A, Cobos A, Hernández R, Cobos P. Morphology of the lumbar vertebral canal. Acta Anat (Basel) 1988;131:35-40.
18. Gouzien P, Cazalbou C, Boyer B, Darodes de Tailly P, Guenec Y, Sénécail B. Measurements of the normal lumbar spinal canal by computed tomography. Segmental study of L3-L4 and L4-L5 related to the height of the subject. Surg Radiol Anat 1990;12:143-8.
19. Wilmink JT, Korte JH, Penning L. Dimensions of the spinal canal in individuals symptomatic and non-symptomatic for sciatica: A CT study. Neuroradiology 1988;30:547-50.
20. Ullrich CG, Binet EF, Sanecki MG, Kieffer SA. Quantitative assessment of the lumbar spinal canal by computed tomography. Radiology 1980;134:137-43.
21. Andreisek G, Deyo RA, Jarvik JG, Porchet F, Winklhofer SF, Steurer J, *et al.* Consensus conference on core radiological parameters to describe lumbar stenosis – An initiative for structured reporting. Eur Radiol 2014;24:3224-32.

Original Article

Study of Left Coronary Artery and Its Variations: A Cadaveric Study from Gujarat Region

Jyoti Bhardwaj, Paras Sanjay Shrimankar, Dipali Jayesh Trivedi, Devanshi Jagdishbhai Vaishnav[1]

Department of Anatomy, B. J. Medical College, Ahmedabad, [1]Department of Anatomy, Government Medical College, Bhavnagar, Gujarat, India

Abstract

Background: A lot of variations have been analyzed in the case of the left coronary artery (LCA) which makes it a leading cause of death globally. Therefore, awareness of normal and variant anatomy of this artery in relation to its main trunk and branches is the key to physicians, cardiologists, and radiologists in the management of various cardiac pathologies. **Materials and Methods:** Eighty embalmed and formalin-fixed adult human cadaveric hearts of both genders with no history or signs of pathology were dissected meticulously during educational hours. **Results and Conclusion:** Among 80 hearts studied, 71 hearts left coronary ostia were located below the sinotubular junction. The mean distance of left coronary ostia from the supravalvular ridge lying above and below was 2.93 ± 0.39 mm and 2.72 ± 0.92 mm, respectively. The mean diameter of the left coronary ostium was 3.67 ± 0.94 mm. The mean length and diameter of the LCA main trunk (LCAMT) were 13.06 ± 2.42 mm and 4.93 ± 0.60 mm, respectively. The most common branching pattern of LCAMT was bifurcation. The most frequent range of length of left anterior descending (LAD) and circumflex (Cx) artery was 10–12 cm and 6.5–8 cm, respectively. The most common termination point of LAD was at the anterior one-third part of posterior interventricular sulcus and for Cx artery was between the crux and obtuse border of the heart. Right coronary dominance was the most common.

Keywords: *Circumflex artery, left anterior descending artery, left coronary artery, sinotubular junction, supravalvular ridge*

Introduction

The two coronary arteries arising from the ascending aorta supply to the heart in humans. They are the ones where blood flows in diastole. The left coronary artery (LCA), larger in caliber provides blood flow to the major portion of the heart.[1] The origin, number, location, and size of the ostium are very prime in the successful execution of cardiac interventional procedures.[2] The length of the LCA main trunk (LCAMT) may affect the placement of atherosclerotic stenosis. Short LCAMT may cause atherosclerosis at the initial parts of the left anterior descending (LAD) artery and circumflex (Cx) artery. These atherosclerotic lesions appear earlier, progress faster, and lead more frequently to myocardial infarction than in cases with a long LCAMT.[3] The most frequent branching pattern of LCA is bifurcation. Variations in branching patterns may cause technical complexity during coronary catheterization and stenting.[3] The artery contributing posterior interventricular artery determines cardiac dominance. Most frequently right dominance is found. The probability of generating collaterals may be lower in patients with left coronary dominance.[3] Transthoracic echocardiography is the most commonly used imaging method[4] and can also identify anomalous coronary arteries in young individuals. The understanding of the morphological and anatomical variations of LCA allows physicians and cardiologists to diagnose and treat congenital and acquired heart disease. For thoracic surgeons, it is important to keep the variations of LCA in mind while executing surgical procedures.

Materials and Methods

Materials

The study comprised 80 properly embalmed and formalin-fixed adult human cadaveric hearts of both genders with no history of pathology or signs of trauma. These hearts were obtained from the

This is an open access journal, and articles are distributed under the terms of the Creative Commons Attribution-NonCommercial-ShareAlike 4.0 License, which allows others to remix, tweak, and build upon the work non-commercially, as long as appropriate credit is given and the new creations are licensed under the identical terms.

For reprints contact: WKHLRPMedknow_reprints@wolterskluwer.com

How to cite this article: Bhardwaj J, Shrimankar PS, Trivedi DJ, Vaishnav DJ. Study of left coronary artery and its variations: A cadaveric study from Gujarat region. J Anat Soc India 2024;73:259-64.

Article Info

Received: 12 June 2022
Accepted: 11 August 2024
Available online: 25 September 2024

Address for correspondence:
Dr. Devanshi Jagdishbhai Vaishnav,
Government Medical College, Bhavnagar - 364 001, Gujarat, India.
E-mail: djv20695@gmail.com

Access this article online

Website: https://journals.lww.com/joai

DOI: 10.4103/jasi.jasi_88_22

Quick Response Code:

Anatomy Department of B. J. Medical College and also from anatomy departments of various medical colleges of Ahmedabad, Gujarat. These colleges receive human body donations from different regions of Gujarat. The present work was conducted with the aim to study LCA and its variations. Ethical clearance from the institutional ethical committee was obtained with Registration No.ECR/72/Inst/GJ/2013/RR-2019. The study was done with the help of the following materials: scalpel with blade, forceps (pointed forceps, tooth forceps, and blunt forceps), scissors, digital vernier caliper, scale and thread, and high-resolution mobile camera.

Methods

The dissection was done step by step during educational dissection hours according to Cunningham's manual.[5] The heart was exposed and removed from the thoracic cavity. The parietal pericardium was stripped off from the surface of the heart, and the fat was removed. Each specimen was thoroughly washed with tap water to remove the blood clots. The course of the LCA and its branches were analyzed grossly by cleaning and dissection method from origin to its termination for any variation. The observations of LCA were made in reference to its origin, number, location of ostium, and distance of ostium with respect to the supravalvular ridge. The right coronary artery was dissected and traced along its course. On the diaphragmatic surface, the arteries lying in the posterior interventricular sulcus (PIS) were finely dissected and noted. Photographs of specimens showing normal and variant anatomy of LCA were taken with a high-resolution mobile camera. At the end, the data were collected, analyzed, and compared with the available data.

Results

The LCA originated from the left posterior aortic sinus in all cases from a single ostium. Although the presence of two ostia was an occasional finding seen in one heart for LAD and Cx artery [Figure 1]. The most common location of the left coronary ostium (LCO) in aortic sinus was below the sinotubular junction (STJ). Out of 80 hearts studied, in 71 hearts (88.75%) LCO was located below STJ, in 5 hearts (6.25%) at the STJ [Figure 2], and 4 hearts (5%) above the STJ. The mean distance of LCO from the supravalvular ridge lying above and below was 2.93 ± 0.39 mm and 2.72 ± 0.92 mm, respectively. The mean diameter of LCO was 3.67 ± 0.94 mm. The most common branching pattern of LCA was bifurcation in 45 hearts (56.25%). LCA with trifurcation and quadrifurcation in 24 (30%) and 10 (12.5%) hearts, respectively. The least common branching pattern was pentafurcation in 1 heart (1.25%) [Figure 3].

The mean length and diameter of LCAMT were 13.06 ± 2.42 mm and 4.93 ± 0.60 mm, respectively. The most frequent range of length of the LAD artery was 10–12 cm in 47 hearts (58.75%), followed by the range of 12–14 cm in 24 hearts (30%). Only 9 hearts (11.25%) were having a range of length between 8 and 10 cm. The most frequent range of length of the Cx artery was 6.5–8 cm in 57 hearts (71.25%), followed by the range of 5–6.5 cm in 13 hearts (16.25%). Only 10 hearts (12.5%) were having the range varying from 8 to 9.5 cm. The point of termination of the LAD artery was at anterior to apex in 20 hearts (25%); at apex in none of the hearts (0%), at anterior one-third part of PIS in 44 hearts (55%); at middle one-third part of PIS in 12 hearts (15%), and at posterior one-third part of PIS in only 4 hearts (5%) [Figure 4]. None of the heart was noted with hyperdominant LAD artery. The point of termination of the Cx artery was at obtuse border in 21 hearts (26.25%); between the crux and obtuse border in 50 hearts (62.5%); at PIS in 9 hearts (11.25%) [Figure 5]. None of the heart was noted with the termination point of the Cx artery either before the obtuse border or at the crux of the heart. The most common coronary dominance pattern was right dominance in 71 hearts (88.75%), followed by left dominance noted in 9 hearts (11.25%).

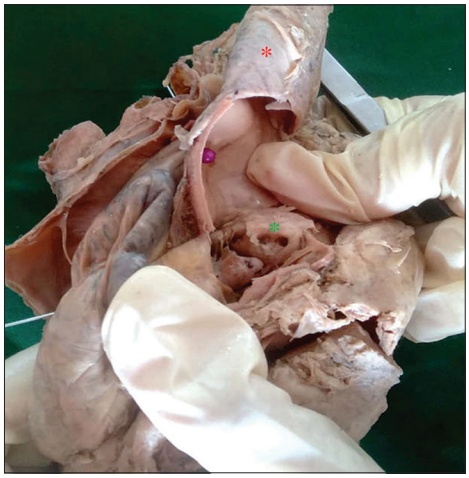

Figure 1: Double left coronary ostia. *Aorta. *Double ostia

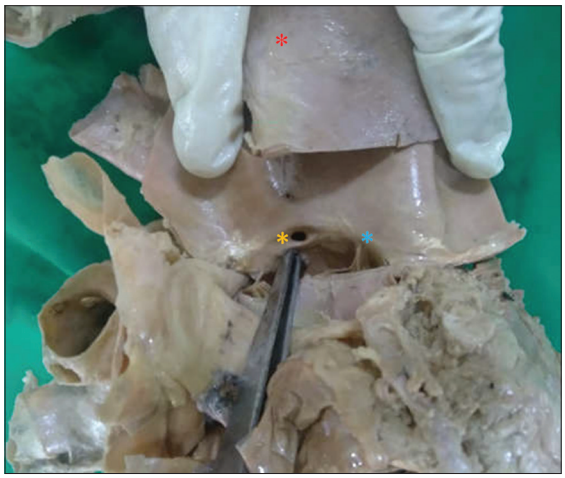

Figure 2: Left coronary ostium at supravalvular ridge (SVR). *Aorta. *SVR. *left coronary ostium

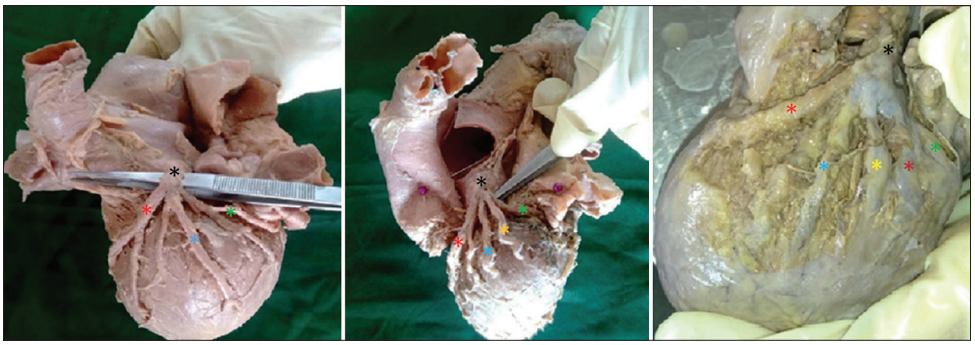

Figure 3: Branching pattern of left coronary artery main trunk (*). Left - trifurcation, middle - quadrifurcation, right - pentafurcation. Left anterior descending (*), Circumflex (*), Diagonal artery. DA 1-*, DA 2-*, DA 3-*

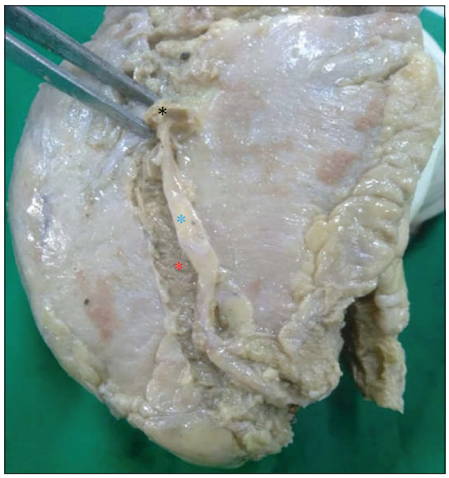

Figure 4: Left anterior descending artery termination point at posterior 1/3rd part of posterior interventricular sulcus on diaphragmatic surface. *Left anterior descending artery, *Termination point, *Posterior interventricular sulcus

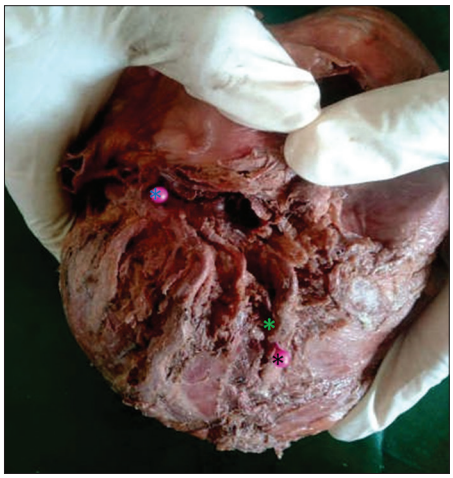

Figure 5: Circumflex (*) artery termination at posterior interventricular sulcus (*) as posterior interventricular artery (*) on diaphragmatic surface

Discussion

The origin of coronaries shows great variability.[5] An accessory origin of the coronary opening may derail in making an aortotomy incision for aortic exposure, in root replacement surgery, or direct delivery of cardioplegic solution through the coronary orifices.[6] In the current study, no variation was seen in relation to the origin of LCA. The presence of two ostia seen in one heart (1.25%) was an occasional finding. The tubular location of the ostium may put disturbance in cardiac catheterization for angiographic procedures.[7] In the present study, the most common LCO location was below the STJ. Dhobale *et al*.[3] and Kulkarni and Paranjpe[7] observed LCO most commonly placed at the STJ in 75.33% and 52.2% of cases, respectively. Whereas Cavalcanti *et al*.,[8] Pejković *et al*.,[9] Sirikonda and Sreelatha,[6] and Roy *et al*.[10] found hearts with LCO located above the STJ in 40%, 60%, 36%, and 34% of cases, respectively. The observations suggest that positioning of the ostium within the sinus is functionally advantageous.[11] The possible clinical drawback of the high origin of the coronary openings lying above the supravalvular ridge is myocardial ischemia and sudden death [Table 1].[12]

Size of the coronary ostia plays remarkable role in the ease of cannulation in various cardiac procedures.[13] The mean diameter of LCO in the present study was very similar to the result of Ballesteros and Ramirez [Table 2].[14]

The LCAMT <5 mm is considered short and when it is more than 15 mm, it is regarded as long.[15] Variation in the length of LCAMT is very important during coronary angiography and for the cannulae used in myocardial perfusion during aortic valve surgery. The shortest length was 5.64 mm, which is more than the minimum lengths observed in the study of Kalpana,[16] Fiss,[17] Dombe *et al*.,[18] Bhele *et al*.,[15] and Dhobale *et al*.[3] The maximum length of LCAMT in this study was 21.24 mm which coincides with the study of Roy *et al*.[10] The diameter of LCAMT is significant in assessing the scope and severity of dilatation in cases of coronary aneurysm, calcification, and stenosis.[7] The mean diameter of LCAMT in the present study coincides with the study of Dombe *et al*. [Table 3].[18]

There is a great difference in the branching pattern of LCAMT in the normal population.[7] As per many studies, the most common branching pattern of LCA was bifurcation into LAD and Cx arteries, followed by trifurcation and quadrifurcation. The least common branching pattern was

Table 1: Comparison of range of distance and mean distance of ostia from supravalvular ridge lying above and below among various studies

Author	Year	Range of distance of Ostia from supravalvular ridge lying above and below (mm)		Mean distance from supravalvular ridge (mm)
		Above	Below	
Pejković *et al*.[9]	2008	0.2–10	0.5–2	-
Dakhane Prafulla and Patil Tushar[13]	2018	-	-	1.4
Present study	2020	2.54–3.42	1.24–4.24	2.72

Table 2: Comparison of diameter of ostia of left coronary artery among various studies

Authors	Year	Mean diameter of left coronary Ostia (mm)
Cavalcanti *et al*.[8]	2003	4.25±0.24
Ballesteros and Ramirez[14]	2008	3.77±0.61
Dombe *et al*.[18]	2012	3.3±0.57
Kulkarni and Paranjpe[7]	2015	2.8±1
Dakhane Prafulla and Patil Tushar[13]	2018	3.31±0.52
Present study	2020	3.67±0.94

Table 3: Comparison of length and diameter of left coronary artery main trunk reported in different studies

Author	Year	Range of length of LCAMT (mm)	Mean length of LCAMT (mm)	Range of diameter of LCAMT (mm)	Mean diameter of LCAMT (mm)
Ballesteros and Ramirez[14]	2008	-	6.48±2.57	-	3.58±0.59
Dombe *et al*.[18]	2012	4–20	11.2±3.6	3–6.8	4.64±1.03
Roy *et al*.[10]	2014	5–21.5	11.42±4.98	-	-
Reddy and Pusala[24]	2016	15–25	-	2–6	-
Dhobale *et al*.[3]	2018	4–22	11.66±3.52	-	5.02±1.03
Present study	2020	5.64–21.24	13.06±2.42	2.5–8.5	4.93±0.60

LCAMT: Left coronary artery main trunk

Table 4: Comparison of length of left anterior descending artery and circumflex artery in various studies

Author	Year	Range of length of LAD artery (cm)	Range of length of Cx artery (cm)
Waller and Schlant[25]	1995	10–13	6–8
Bhele *et al*.[15]	2015	-	3–11
Reddy and Pusala[24]	2016	12–14.5	6–8
Present study	2020	8–14	5–9.5

LAD: Left anterior descending, Cx: Circumflex

pentafurcation. A thorough knowledge of the trifurcation pattern is vital while doing stenting as it is a challenging and tedious percutaneous procedure.[19]

In the present study, the range of length LAD and Cx artery concurs with the observations of the past studies [Table 4]. In left coronary dominance, the LAD artery is usually long wrapping around the apex of the heart giving a major portion of the myocardium, and angiographic procedures in such cases have great clinical significance.[20] The number of posterior branches of the Cx artery is variable which depends on the length of the Cx artery.[14] Most of the authors analyzed that the LAD artery terminated at the PIS. In PIS, the LAD artery most commonly ended at anterior one-third part of the sulcus. Mallashetty and Bhosale[21] and Alam[2] have reported the incidence of the termination point of LAD at apex in 50% and 68% of hearts, respectively. The results of the current study match with the majority of authors [Table 5]. For the proper clarification of coronary angiographies and surgical myocardial revascularization, the disparity in the termination of the LAD artery is significant.[17] The variation in the termination of the Cx artery is very frequent.[22] Among most of the studies done, the Cx artery terminated between the crux and obtuse border. The data of present study are very close to Kalpana *et al*.,[16] Mallashetty and Itagi,[23] and Lakshmiprabha *et al*.[22] for the termination of the Cx artery between the crux and obtuse border of the heart seen in 67%, 60%, and 60% of specimens, respectively. Termination of the Cx artery before the obtuse border of the heart was observed only by Mallashetty and Itagi[23] in 6.6% of specimens. The termination of the Cx artery either before the obtuse border or at the crux of the heart was not seen in any case [Table 6]. In the present study, right dominant circulation was the most common which matches with the majority of previous studies. No case of codominance was observed in the present study. In left coronary dominant individuals, obstruction of LCA may produce a massive infarct with output failure of the heart.[3]

Table 5: Comparison of point of termination of left anterior descending artery among various studies

Author	Anterior to apex (%)	Apex (%)	Posterior intervetricular sulcus		
			Anterior 1/3rd part (%)	Middle 1/3rd part (%)	Posterior 1/3rd part (%)
Kalpana[16]	8	12	80	-	-
Ballesteros and Ramirez[14]	1.3	27.3	63.6	4	3.3
Present study	25	-	55	15	5

Table 6: Comparison of point of termination of circumflex artery in various studies

Author	Before obtuse border (%)	At obtuse border (%)	Between crux and obtuse border of heart (%)	At crux (%)	At PIS (%)
Kalpana[16]	-	13	67	6	-
Ballesteros and Ramirez[14]	-	25.3	58.4	9.1	5.2
Mallashetty and Itagi[23]	6.6	-	60	26.6	-
Lakshmiprabha *et al*.[22]	-	4	60	-	29
Present study	-	26.25	62.5	-	11.25

PIS: Posterior interventricular sulcus

Conclusion

The results of the current study may be used as a reference guide for future studies about LCA and its branches as well as for surgical and radiological interventions. When the LCO was located above the supravalvular ridge, its distance from the ridge was found more than the distance of the ostium lying below the ridge. Large ostium diameter was associated with a large diameter of LCAMT. Although the most common branching pattern of LCA was bifurcation, LCA with trifurcation, quadrifurcation, and pentafurcation are common. The length of the LCAMT was found to be shorter than normal in the right dominance of the heart. The length of the LCAMT did not show any correlation with the diameter of LCA or the lengths of its two terminal branches. The length of the LAD artery was more than the length of the Cx artery in all cases. The length of the LAD artery terminating earlier anterior to apex could be longer in length. Similarly, the LAD artery after running a long course terminating into posterior one-third part of the PIS could be shorter in length. The length of the Cx artery was more than its normal range in hearts with left dominance. The left dominance pattern was frequently associated with a bifurcation pattern.

Acknowledgments

We are thankful to Dr. Sucheta Chaudhary, Professor and Head of the Anatomy Department of B. J. Medical College, and Heads of the Anatomy Department of various medical colleges of Ahmedabad. We appreciate the nonacademic staff for their assistance.

Financial support and sponsorship

Nil.

Conflicts of interest

There are no conflicts of interest.

References

1. Standring S. Chestwall. In: Gray's Anatomy. The Anatomical Basis of Clinical Practice. 39th ed. London: Elsevier; 2008. p. 931-4.
2. Alam SR. Variations in the left coronary artery. Chattagram Maa O Shishu Hosp Med Coll J 2017;16:42-7.
3. Dhobale MR, Mudiraj NR, Puranik MG. Clinically relevant morphometric study of left coronary artery in adult human cadavers. Int J Anat Res 2018;6:5605-12.
4. Saikrishna C, Talwar S, Gulati G, Kumar AS. Normal coronary artery dimensions in Indians. Indian J Thorac Cardiovasc Surg 2006;22:159-64.
5. Diwan D, Diwan Y, Chauhan RS, Negi PC. Main Trunk of Left Coronary Artery: Anatomy and Clinical Implications. J Med Sci Clin Res 2017;05:15658-63.
6. Sirikonda P, Sreelatha S. Measurements and location of coronary Ostia. Int J Biol Med Res 2012;3:2489-96.
7. Kulkarni JP, Paranjpe V. Topography, morphology and morphometry of coronary Ostia: A cadaveric study. Eur J Anat 2015;19:165-70.
8. Cavalcanti JS, de Melo NC, de Vasconcelos RS. Morphometric and topographic study of coronary Ostia. Arq Bras Cardiol 2003; 81:359-62.
9. Pejković B, Krajnc I, Anderhuber F. Anatomical variations of coronary Ostia, aortocoronary angles and angles of division of the left coronary artery of the human heart. J Int Med Res 2008;36:914-22.
10. Roy S, Gupta A, Nanrah BK, Verma M, Saha R. Morphometric study of left coronary artery trunk in adult human cadavers: A study on the Eastern region population. J Clin Diagn Res 2014;8:7-9.
11. Joshi SD, Joshi SS, Athavale SA. Origins of the coronary arteries and their significance. Clinics (Sao Paulo) 2010;65:79-84.
12. Luckrajh JS, Satyapal KS, Lazarus L. An anatomical investigation of the coronary Ostia and its relationship to the sinotubular junction within a select South African population. Eur J Anat 2019;23:159-65.
13. Dakhane Prafulla S, Patil Tushar R. Study of coronary Ostia in preserved human cadaveric heart specimens in Western Maharashtra by dissection method. Int J Anat Res 2018;6:5400-4.
14. Ballesteros LE, Ramirez LM. Morphological expression of the left coronary artery: A direct anatomical study. Folia

Morphol (Warsz) 2008;67:135-42.
15. Bhele AV, Ughade HM, Shaikh S, Joge US. A study of course, branches and variations of the coronary arteries in the human cadaveric heart. Int J Contemp Med Res 2017;4:1533-7.
16. Kalpana R. A study of principal branches of coronary arteries in human. J Anat Soc India 2003;52:2:137-47.
17. Fiss DM. Normal coronary anatomy and anatomic variations. Appl Radiol 2007:36:14-26.
18. Dombe DD, Anitha T, Giri PA, Dombe SD, Ambiye MV. Clinically relevant morphometric analysis of left coronary artery. Int J Biol Med Res 2012;3:1327-30.
19. Agnihotri G, Kaur M, Kalyan GS. Branching patterns of left coronary artery among North Indians. Anat J Africa 2013;2:145-50.
20. Vinitha G, Sarala HS, Priya R. A cadaveric study on coronary preponderance. Int J Anat Res 2015;3:1289-92.
21. Mallashetty N, Bhosale S. The study of number of Ostia, inner and outer diameters of coronary arteries at their origin in human heart: A cadeveric study. Int J Sci Res 2014;3:1628-30.
22. Lakshmiprabha S, Afroze KH, Ramesh P, Asha KR, Shivaleela C, Anupama D. Variations in the anatomical and branching pattern of the left coronary artery: A cadaveric study. Int J Res Med Sci 2018;6:1235-40.
23. Mallashetty N, Itagi V. The study of branching pattern and variations in the left coronary artery in human heart with a unique case of crossing of coronary arteries-a cadaveric study. Indian J Clin Anat Physiol 2017;4:48-50.
24. Reddy MV, Pusala B. Anatomical variations in branching pattern and dimensions of coronary arteries: A cadaveric study from South India. IOSR J Dent Med Sci 2016;15:21-8.
25. Waller B, Schlant R. Anatomy of heart. In: Husst's The Heart. 13th ed. New York, United States: The McGra-Hill Companies. Inc.:2011:2500.

Original Article

Morphometric Investigation of Nasal Structure with Nasal Septum Deviation in Young Adults and Correlation with 2:4 Digit Ratio

Kadir Desdicioglu, Buket Oguz, Vahide Tutuk

Department of Anatomy, Faculty of Medicine, Ankara Yıldırım Beyazıt University, Ankara, Turkiye

Abstract

Aim: The nose, both anatomically and esthetically, is a central feature of the human face. This study aims to morphometrically investigate the nasal structure with septal deviation in young adults and examine its correlation with 2:4 digit ratio. **Materials and Methods:** The study was conducted on 194 volunteers (female: 100 and male: 94), aged 18–25 years, studying at Yıldırım Beyazıt University Faculty of Medicine, Ankara. Volunteers with nasal septum deviation were included in the study. Initially, participants' height and weight measurements were taken, followed by morphometric measurements of the nasal and hand regions by the same researcher. Body mass index (BMI) was also calculated. Subsequently, the volunteers were divided into eight age groups for age and four for BMI. The data were analyzed using the Student's *t*-test for normally distributed continuous variables and the Mann–Whitney *U*-test for ordinal or nonnormally distributed continuous variables. $P < 0.05$ was considered statistically significant. **Results:** Initially, the averages and standard deviations of parametric data taken from the nose and hand according to gender, age, and BMI were calculated. Then, the nasal and hand parameters were statistically evaluated according to gender, age, and BMI. The correlation between nasal parameters and the 2:4 digit ratio was also examined. The evaluation revealed statistically significant differences and correlation relationships between the parameters ($P < 0.05$). **Conclusion:** The data obtained from our study will assist clinicians involved in evaluating nasal development, determining gender in forensic medicine, diagnosing and treating pathologies related to the nose, describing anatomical points in surgical procedures applied to this region, and planning these surgical procedures.

Keywords: *2:4 digit ratio, hand, morphometry, nasal septum deviation, nose*

Introduction

Facial development begins at the end of the 4th week of the embryonic period. In humans, testosterone levels affect both the hand and face, leading to broader and more pronounced structures such as cheeks, nose, and chin due to testosterone.[1] Developmentally, one of the structures contributing to the formation of the palate is the nasal septum.[2] The nasal cavity, or cavitas nasi, consists of two similar cavities separated by the nasal septum, septum nasi, which has four walls: superior, inferior, inner, and outer. The inner wall is formed by the septum nasi, composed of bony part, cartilaginous part, and membranous part. The bony part at the back is formed by the vomer and the perpendicular plate of the ethmoid bone. The cartilaginous part in front is made up of septal nasal cartilage. The membranous part is the mucosa covering the bones and cartilages of the nasal cavity.[3] It is noted that the position and structural features of the nasal septum influence and regulate airflow in the nose. It is even suggested that the nasal septum, due to its influence on nasal physiology akin to that of the inferior concha, is referred to as the septal concha. In addition, in patients with nasal septal deviation, hypertrophy on the opposite side of the deviation in the inferior concha is noted.[4]

The nose, anatomically and esthetically, is a central feature of the human face. Diseases related to the nose can arise from congenital, developmental, and acquired causes. Moreover, malformations related to the nose are emphasized as significantly impactful on an individual's future well-being. Nasal septum deviation is mentioned to occur due to developmental reasons during the embryonic period, infections during pregnancy affecting the

This is an open access journal, and articles are distributed under the terms of the Creative Commons Attribution-NonCommercial-ShareAlike 4.0 License, which allows others to remix, tweak, and build upon the work non-commercially, as long as appropriate credit is given and the new creations are licensed under the identical terms.

For reprints contact: WKHLRPMedknow_reprints@wolterskluwer.com

How to cite this article: Desdicioglu K, Oguz B, Tutuk V. Morphometric investigation of nasal structure with nasal septum deviation in young adults and correlation with 2:4 digit ratio. J Anat Soc India 2024;73:265-76.

Article Info

Received: 28 June 2024
Revised: 26 July 2024
Accepted: 11 August 2024
Available online: 25 September 2024

Address for correspondence:
Dr. Kadir Desdicioglu, Department of Anatomy, Faculty of Medicine, Ankara Yıldırım Beyazıt University, Ankara, Turkiye.
E-mail: kdesdici@yahoo.com

Access this article online

Website: https://journals.lww.com/joai

DOI: 10.4103/jasi.jasi_96_24

Quick Response Code:

mother, or traumas during birth affecting the elastic septum or developmental anomalies in skeletal growth. It is also highlighted that deviations can occur in either the bony or cartilaginous part of the nasal septum.[5] Hartman *et al*.'s[6] study indicates that during development, the nose and nasal septum cartilage exert a morphogenetic effect on the facial skeleton, serving as a growth center for the face. The mechanical forces produced by the nasal septum are thought to facilitate the separation of facial sutures. It is also stated that the nasal septum acts like a growth plate due to expansion resulting from endochondral ossification along the perpendicular plate of the ethmoid bone. The same study mentions that skeletal and dental asymmetries could potentially be significant consequences of deviated growth of the nasal septum.[6] Nasal septum deviation is suggested to exert pressure on the maxilla, leading to elevation in the floor of the nasal cavity and flawed development of the palate.[5] Furthermore, the nasal septum plays a crucial role in the normal and abnormal growth of the human face and in the morphological variations of the face.[6]

During the intrauterine period around weeks 21–24, hand development occurs. Previous studies have demonstrated a relationship between bone development and hormones, with evidence suggesting that in males, the fourth digit is longer than the second, whereas in females, the second digit tends to be longer than the fourth. This difference is primarily attributed to higher prenatal testosterone concentrations in males.[7]

Past study results indicate a relationship between the 2:4 digit ratio and other body regions, with a significant correlation between the 2:4 digit ratio and facial and nasal regions.[1,8] While the nose structure is one of the facial organs proven to be linked with the 2:4 digit ratio, information on the correlation between nasal parameters and the 2:4 digit ratio remains limited.[8] In previous studies, it is stated that some parameters are determined for measurement objectivity while examining nasal anthropometry, and the distances forming the nasal morphology are measured using these parameters. It has been suggested that an increased 2:4 digit ratio corresponds to a narrower, smaller, and more "feminine" nose structure, whereas a decreased ratio is associated with a more "masculine" nose structure.[9]

There is a significant relationship between genes and transcription factors involved in the development of the face and hands. The growth of frontonasal, maxillary, and mandibular prominences in facial shaping, like the development of limb buds, depends on mesenchymal–ectodermal interaction. HOX gene family, coding for transcription factors with crucial roles in developmental processes, plays significant roles in both hand and nasal embryology.[10]

Upon reviewing previous studies, we did not encounter any research that morphometrically investigates the nasal septum deviation in the nasal structure of adolescents and compares it with the 2:4 digit ratio. Our study aimed to morphometrically investigate the nasal structure with septum deviation in young adults and explore its correlation with the 2:4 digit ratio.

Materials and Methods

The study was conducted between June 1, 2023, and July 31, 2023, on 194 volunteers (female: 100 and male: 94) aged between 18 and 25 years (mean: 20.96 ± 1.69) studying at Ankara Yıldırım Beyazıt University Faculty of Medicine. The condition for nasal septum deviation was identified as the nasal septum or columella structure not being exactly in the midline when viewed from the outside [Figure 1]. Based on this criterion, only volunteers with nasal septum deviation were included in the study. Those with normal nasal septum structure, those who had undergone surgery on their nose or hand, or those with any anomalies in their hand or nose were excluded from the study. Initially, volunteers' height and weight measurements were taken, followed by morphometric measurements of the nasal and hand regions by the same researcher. Body mass index (BMI) was also calculated. The volunteers were then divided into eight age groups for age and four for BMI. Ethical approval for the study was obtained from the Ankara Yıldırım Beyazıt University Health Sciences Ethics Committee on May 16, 2023, with decision number 244/05.

For measuring nasal-related parameters, anatomical points used in previous studies were identified, and measurements were taken accordingly.[11,12] The designated points are glabella (g), nasion (n), maxillofrontale (mf), alare (al'), alare medial (al), pronasale (prn), columella (c), the lowest point of the nostrils (nb), the highest point of the nostrils (c'), subnasale (sn), labiale superius (ls), and gnathion (gn) [Figure 2]. Furthermore, morphometric measurements related to the nose were conducted with the head in the Frankfurt horizontal position.[13]

The parameters used in nasal morphometric measurements include:

- Facial height: Distance between nasion (n) and gnathion (gn)

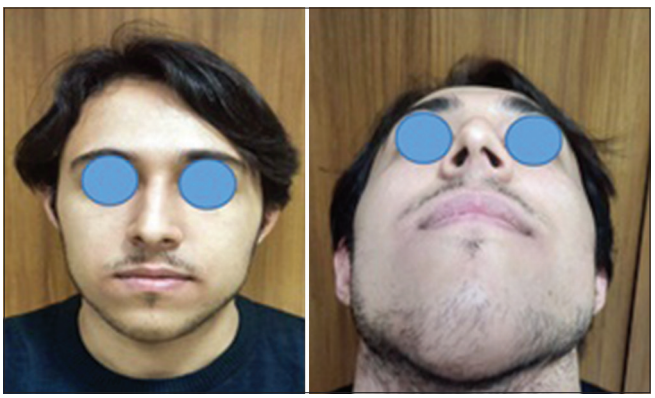

Figure 1: Image of nasal septum deviation

- Nasal length: Distance between nasion (n) and pronasale (prn)
- Nasal height: Distance between nasion (n) and subnasale (sn)
- Nasal width: Distance between both alares (al)
- Nasal depth: Distance between pronasale (prn) and subnasale (sn)
- Nasal root width: Distance between both maxillofrontales (mf)
- Right-left nostril width: The widest mediolateral distance of the nostril
- Right-left nostril length: The longest distance of the nostril
- Columella length: The longest distance of the columella
- Lower columella width: Distance between the lowest points of the nostrils (nb)
- Upper columella width: Distance between the highest points of the nostrils (c')
- Philtrum length: Distance between subnasale (sn) and labiale superius (ls)
- Alar thickness: Transverse width of the ala of the nose
- Nasofrontal angle: Angle between glabella (g), nasion (n), and pronasale (prn)
- Alar slope angle: Angle between right alare (al), pronasale (prn), and left alare (al)
- Nostril medial longitudinal angle: Angle between the upper point of the nostril (c), the lower point of the nostril (nb), and the lower point of the opposite nostril (nb)
- Nasal tip angle: Angle between nasion (n), pronasale (prn), and subnasale (sn)
- Nasolabial angle: Angle between pronasale (prn), subnasale (sn), and labiale superius (ls).

Subsequently, measurements of hand parameters were taken. Parameters measured from both hands included the length of the second finger, the length of the fourth finger, hand width, and hand length. Based on these data, the 2:4 digit ratio for both the right and left hand was calculated.[14]

Statistical analyses were performed using IBM SPSS Statistics (IBM Corp. version 26, 2019, New York USA). Mean and standard deviations for parameters were calculated. The Student's *t*-test was used to test the difference between two groups for normally distributed continuous variables. The Mann–Whitney *U*-test was used for ordinal or nonnormally distributed continuous variables. $P < 0.05$ was considered statistically significant.

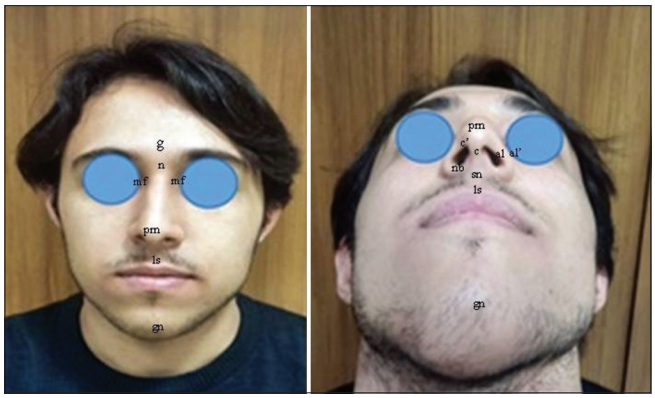

Figure 2: Image of nasal parameter measurement points

Results

Our study included 194 volunteers aged between 18 and 25 (mean: 20.96 ± 1.69) consisting of 100 females and 94 males. Initially, the height and weight information of the participants were collected, followed by the measurement of morphometric parameters related to the nose and hand. Subsequently, the averages and standard deviations of the parametric data obtained from the nose and hand were calculated according to gender, age, and BMI [Tables 1-6]. The correlation between parameters was also examined [Table 7].

When evaluating nasal parameters by gender, it was found that excluding nasal root width, nasal tip angle, nasolabial angle, and nostril medial longitudinal angle parameters, there was a significant relationship between other nasal parameters and gender [$P < 0.05$, Table 1]. In addition, there was a significant difference between the right and left nostril widths within the same gender [$P < 0.05$, Table 1]. It

Table 1: Nasal parameter averages and standard deviations by gender (mm)

Parameters	Gender (*n*)		
	Female (100)	Male (94)	Total (194)
Facial height	108.67±15.30	119.60±7.15	113.97±13.21
Nasal length	48.02±5.13	51.54±5.74	49.72±5.70
Nasal height	53.14±4.23	56.07±5.53	54.56±5.10
Nasal width	32.35±2.97	36.11±2.87	34.17±3.47
Nasal depth	31.58±3.58	35.53±3.77	33.49±4.16
Nasal root width	15.20±3.24	15.34±2.31	15.27±2.82
Right nostril width	9.09±1.88	9.64±1.81	9.35±1.87
Right nostril length	12.39±2.12	14.31±2.15	13.32±2.33
Right nostril width	8.54±1.69	9.55±1.99	9.03±1.90
Right left nostril length	12.79±4.50	14.53±2.27	13.63±3.69
Columella length	10.32±1.87	10.93±1.98	10.62±1.94
Lower columella width	13.36±1.72	14.93±2.18	14.10±2.10
Upper columella width	8.16±1.38	8.82±1.42	8.48±1.44
Philtrum length	12.69±2.07	13.47±2.41	13.07±2.27
Alar thickness	5.92±1.20	6.38±1.27	6.15±1.25
Nasofrontal angle (°)	137.33±8.78	132.84±9.77	135.16±9.52
Alar slope angle (°)	79.33±12.88	84.43±10.38	81.80±11.98
Nostril medial longitudinal angle (°)	53.98±8.04	52.74±8.24	53.38±8.14
Nasal tip angle (°)	69.63±9.32	68.65±7.25	69.15±8.38
Nasolabial angle (°)	93.57±14.42	96.75±14.85	95.11±14.67

$P<0.05$: Significant differences exist between parameters, excluding nasal root width ($P=0.718$), nostril medial longitudinal angle ($P=0.293$), nasal tip angle ($P=0.418$), and nasolabial angle ($P=0.132$)

Table 2: Hand parameter averages and standard deviations by gender (mm)

Parameters	Gender (*n*)		
	Female (100)	Male (94)	Total (194)
Length of the right second finger	67.15±3.37	71.79±3.84	69.40±4.28
Length of the right fourth finger	65.85±4.02	73.49±3.90	69.55±5.50
Length of the right hands	175.43±7.25	192.14±9.74	183.53±11.95
Width of the right hand	72.26±4.48	80.55±5.32	76.28±6.42
Length of the left second finger	66.71±3.48	71.65±3.98	69.10±4.47
Length of the left fourth finger	65.72±3.97	73.14±4.22	69.32±5.52
Length of the left hands	176.62±7.71	193.84±9.46	184.96±12.17
Width of the left hand	71.57±5.15	79.64±4.84	75.48±6.42
Right 2:4 digit ratio	1.02±0.03	0.97±0.03	0.99±0.04
Left 2:4 digit ratio	1.01±0.02	0.98±0.03	0.99±0.03

$P<0.05$: Significant differences exist among all parameters

Table 3: Nasal parameter averages and standard deviations by age (mm)

Age	*n*	Parameters									
		Facial height	Nasal length	Nasal height	Nasal width	Nasal depth	Nasal root width	Right nostril width	Right nostril length	Left nostril width	Left nostril length
18	8	110.97±14.53	51.76±3.62	57.31±3.72	32.99±2.58	33.29±2.35	18.12±8.36	9.65±1.64	15.17±1.64	9.52±1.21	14.62±1.69
19	36	113.49±18.54	50.65±6.18	56.64±4.82	35.43±3.31	33.15±4.08	15.38±2.36	9.74±1.53	14.29±2.34	9.49±1.49	14.35±2.49
20	38	114.27±9.56	49.37±6.32	54.32±5.46	33.78±3.51	34.50±3.77	15.79±2.33	9.56±1.80	13.52±2.33	9.12±2.41	14.89±6.87
21	42	115.33±8.37	49.90±5.25	53.44±4.23	34.44±3.89	32.81±4.87	14.32±1.69	9.27±2.32	12.71±2.29	8.91±1.82	12.39±2.26
22	36	112.57±18.78	49.15±5.85	53.89±5.92	34.02±2.66	33.71±4.29	15.66±2.20	9.29±1.64	13.04±2.30	8.71±2.03	13.01±2.25
23	18	114.35±6.07	49.23±3.80	56.11±4.06	33.67±4.37	34.01±3.98	15.50±2.98	9.97±1.71	13.75±2.00	9.82±1.69	14.33±1.56
24	9	114.31±8.12	47.81±6.55	52.70±4.40	32.87±3.07	33.93±3.20	13.39±2.30	7.18±1.31	11.45±1.71	7.43±1.12	12.38±1.15
25	7	115.75±5.82	50.17±7.27	50.57±4.97	33.28±3.28	31.13±4.50	14.10±1.11	7.99±0.75	11.53±1.06	7.94±0.54	12.51±1.32
Total	194	113.97±13.21	49.72±5.70	54.56±5.10	34.17±3.47	33.49±4.16	15.27±2.82	9.35±1.87	13.32±2.33	9.03±1.90	13.6±3.69

Age	Parameters									
	Columella length	Lower columella width	Upper columella width	Philtrum length	Alar thickness	Nasofrontal angle	Alar slope angle	Nostril medial longitudinal angle	Nasal tip angle	Nasolabial angle
18	10.12±1.45	12.68±1.81	9.47±1.81	12.59±1.30	5.96±0.96	141.11±8.30	86.24±7.99	53.13±4.50	68.08±7.71	93.48±10.20
19	10.67±1.98	14.49±1.80	9.08±1.20	13.20±1.75	6.38±1.15	134.85±8.40	89.38±8.08	53.01±7.53	66.47±7.50	96.51±13.21
20	10.68±2.09	14.89±2.35	8.19±1.39	12.69±2.96	5.95±1.15	135.62±9.70	77.43±9.50	55.54±7.81	70.29±6.82	98.24±10.81
21	10.67±2.02	14.16±2.46	8.34±1.66	13.93±2.30	6.21±1.52	135.49±10.14	81.58±12.06	50.76±9.81	69.39±10.85	93.20±12.56
22	10.39±2.00	13.82±1.97	8.36±1.33	12.82±2.24	6.64±1.19	134.48±10.07	83.55±10.52	56.15±6.29	73.08±6.21	96.23±17.74
23	10.83±1.79	13.48±1.56	8.87±1.10	12.42±1.87	5.84±1.13	138.80±8.16	81.96±8.81	55.12±7.75	67.70±6.59	97.83±23.61
24	10.22±1.25	13.95±1.33	7.57±1.05	13.15±1.89	5.30±0.77	133.61±5.21	79.84±7.52	51.56±5.95	62.95±11.49	86.26±8.94
25	11.38±2.29	12.81±0.98	7.46±1.07	12.66±1.88	5.17±0.70	134.35±5.42	78.45±8.29	50.94±5.36	68.05±5.67	82.92±6.64
Total	10.62±1.94	14.12±2.10	8.48±1.44	13.07±2.27	6.15±1.25	135.16±9.52	82.61±10.47	53.38±8.14	69.15±8.38	95.11±14.67

$P>0.05$: No significant differences between parameters, excluding nasal root width (18–21 years: $P=0.011$, 18–24 years: $P=0.012$); right nostril width (19–24 years=P: 0.005, 20–24 years: $P=0.013$, 23–24 years: $P=0.006$); right nostril length (18–24 years: $P=0.019$, 19–24 years: $P=0.020$), alar slope angle (19–20 years: $P=0.000$, 19–21 years: $P=0.017$); nasofrontal angle (18–24 years: $P=0.004$, 19–24 years: $P=0.035$, 20–24 and 21–24 years: $P=0.015$, 23–24 years: $P=0.002$); nasal tip angle (19–22 years: $P=0.019$, 22–24 years: $P=0.028$)

was determined that there was no correlation between nasal root width, nostril medial longitudinal angle, nasal tip angle, nasolabial angle parameters, and gender [$P > 0.05$, Table 7], a negative correlation with the nasofrontal angle [$P < 0.01$, Table 7], and a significant correlation between other nasal parameters and gender [$P < 0.01$, Table 7]. Subsequently, hand parameters were evaluated by gender. The evaluation found a significant relationship between hand parameters and gender [$P < 0.05$, Table 2], and a strong correlation between gender and hand parameters was determined [$P < 0.01$, Table 7].

The statistical evaluation of nasal parameters by age is shown in Table 3. In addition, a negative correlation between age and nasal parameters was identified [$P < 0.01$, Table 7]. Hand parameters were then evaluated by age. The evaluation found no significant relationship between

Table 4: Hand parameter averages and standard deviations by age (mm)

Age	*n*	Parameters									
		Length of the right second finger	Length of the right fourth finger	Length of the right hands	Width of the right hand	Length of the left second finger	Length of the left fourth finger	Length of the left hands	Width of the left hand	Right 2:4 digit ratio	Left 2:4 digit ratio
18	8	68.58±5.08	68.19±6.31	180.00±15.07	74.50±5.93	67.63±5.10	68.55±5.36	182.87±16.19	73.92±5.13	1.00±0.03	0.98±0.02
19	36	70.84±3.92	71.34±5.31	186.27±12.24	76.84±5.57	70.95±4.52	70.95±5.35	186.94±10.75	75.48±6.25	0.99±0.04	1.00±0.03
20	38	70.30±4.62	69.92±5.33	185.05±12.24	75.67±7.22	69.44±4.33	69.66±5.79	187.21±13.39	74.39±6.99	1.00±0.03	0.99±0.03
21	42	68.99±3.82	69.67±5.61	184.14±11.46	78.74±7.19	69.02±4.34	69.36±5.60	185.21±11.43	78.45±7.01	0.99±0.04	0.99±0.03
22	36	68.19±4.04	69.15±5.27	181.86±11.34	75.30±5.22	67.97±4.37	68.53±5.42	182.97±12.25	74.41±5.16	0.98±0.03	0.99±0.03
23	18	69.33±4.96	68.47±5.42	180.44±11.19	73.30±6.51	68.78±4.72	68.81±5.58	183.16±12.06	73.48±6.06	1.01±0.04	1.00±0.03
24	9	69.32±4.78	68.51±6.75	184.88±14.25	77.42±5.73	68.67±4.64	67.90±6.41	185.55±13.44	76.86±5.84	1.01±0.03	1.01±0.04
25	7	66.94±2.65	65.38±4.15	176.28±8.36	75.16±4.27	67.13±2.80	66.87±3.51	177.57±9.81	74.16±5.39	1.02±0.03	1.00±0.01
Total	194	69.40±4.28	69.55±5.50	183.53±11.95	76.28±6.42	69.10±4.47	69.32±5.52	184.96±12.17	75.48±6.42	0.99±0.04	0.99±0.03

P>0.05: No significant differences among all parameters

Table 5: Nasal parameter averages and standard deviations by body mass index (mm)

Parameters	Gender (*n*)				
	Group 1 (48)	Group 2 (102)	Group 3 (37)	Group 4 (7)	Total (194)
Facial height	107.82±15.18	114.19±13.01	119.07±6.84	125.91±7.15	113.97±13.21
Nasal length	48.51±6.08	49.82±5.71	50.13±4.66	54.46±5.98	49.72±5.70
Nasal height	53.06±4.13	54.85±5.43	54.77±5.01	59.47±3.10	54.56±5.10
Nasal width	31.87±3.25	34.37±2.93	36.27±3.61	35.94±2.62	34.17±3.47
Nasal depth	32.10±4.03	33.81±3.67	33.78±5.15	37.00±3.61	33.49±4.16
Nasal root width	14.38±1.81	15.38±3.12	15.80±2.81	16.89±2.71	15.27±2.82
Right nostril width	8.72±1.86	9.37±1.57	10.10±2.33	9.53±1.97	9.35±1.87
Right nostril length	12.30±1.73	13.59±2.27	13.75±2.67	14.18±3.20	13.32±2.33
Right nostril width	8.26±1.70	9.19±1.82	9.48±2.01	9.61±2.61	9.03±1.90
Right left nostril length	13.29±6.15	13.62±2.38	13.78±2.48	15.34±2.21	13.63±3.69
Columella length	10.01±1.86	10.52±1.85	11.45±2.02	11.82±1.76	10.62±1.94
Lower columella width	13.14±1.76	14.35±2.67	14.59±2.38	14.89±1.26	14.12±2.10
Upper columella width	8.13±1.34	8.49±1.49	8.84±1.19	8.77±2.16	8.48±1.44
Philtrum length	11.83±2.01	13.20±2.07	14.33±2.50	13.08±1.67	13.07±2.27
Alar thickness	5.55±0.95	6.26±1.18	6.56±1.53	6.43±1.40	6.15±1.25
Nasofrontal angle (°)	135.44±9.15	134.64±10.29	135.32±8.29	139.83±5.71	135.16±9.52
Alar slope angle (°)	76.96±14.56	83.34±10.50	84.80±10.60	76.83±10.55	81.80±11.98
Nostril medial longitudinal angle (°)	52.96±8.70	53.81±8.10	52.64±7.67	53.84±8.54	53.38±8.14
Nasal tip angle (°)	69.11±8.61	69.44±7.74	68.51±10.07	68.69±7.36	69.15±8.38
Nasolabial angle (°)	93.28±11.10	96.90±14.58	92.02±17.83	98.13±18.06	95.11±14.67

P>0.05: No significant differences between parameters, excluding facial height (Group 1–Group 2: *P*=0.025, Group 1–Group 3: *P*=0.000, Group 1–Group 4: *P*=0.003), nasal height (Group 1–Group 4: *P*=0.011), nasal width (Group 1–Group 2: *P*=0.000, Group 1–Group 3: *P*=0.000, Group 1–Group 4: *P*=0.010, Group 2–Group 3: *P*=0.012), nasal depth (Group 1–Group 4: *P*=0.020), right nostril width (Group 1–Group 3: *P*=0.004), right nostril length (Group 1–Group 2: *P*=0.008, Group 1–Group 3: *P*=0.024), left nostril width (Group 1–Group 2: *P*=0.030, Group 1–Group 3: *P*=0.019), philtrum length (Group 1–Group 2: *P*=0.002, Group 1–Group 3: *P*=0.000, Group 2–Group 3: *P*=0.038), columella length (Group 1–Group 3: *P*=0.004), lower columella width (Group 1–Group 2: *P*=0.005, Group 1–Group 3: *P*=0.008), alar thickness (Group 1–Group 2: *P*=0.005, Group 1–Group 3: *P*=0.001)

all hand parameters and age [$P > 0.05$, Table 4], but a negative correlation between age and hand parameters was observed [$P < 0.01$, Table 7].

The statistical evaluation of nasal parameters by BMI is shown in Table 5. It was found that except for the nasofrontal angle, alar slope angle, nostril medial longitudinal angle, nasal tip angle, and nasolabial angle parameters, there was a significant correlation between other nasal parameters and BMI [$P < 0.01$, Table 7]. The statistical evaluation of hand parameters by BMI is presented in Table 6. It was determined that except for specific parameters such as the lengths of the second and fourth fingers, hand length and width for both hands, and the 2:4 digit ratios, there was no significant relationship between other parameters and BMI [$P > 0.05$, Table 6]. However, a significant correlation was observed between BMI and hand parameters [$P < 0.01$, Table 7].

Table 6: Hand parameter averages and standard deviations by body mass index

BMI	*n*	Parameters									
		Length of the right second finger	Length of the right fourth finger	Length of the right hands	Width of the right hand	Length of the left second finger	Length of the left fourth finger	Length of the left hands	Width of the left hand	Right 2:4 digit ratio	Left 2:4 digit ratio
Group 1	48	67.64±3.88	66.20±4.30	176.50±9.15	71.86±4.68	67.01±3.79	66.03±4.67	177.43±10.05	71.10±5.02	1.02±0.03	1.01±0.02
Group 2	102	69.44±4.41	70.11±5.64	185.30±12.49	76.32±5.78	69.36±4.72	69.90±5.64	186.59±12.09	75.36±5.76	0.99±0.04	0.99±0.03
Group 3	37	71.15±3.86	72.01±4.65	187.13±10.69	81.20±6.27	70.72±3.80	71.58±4.49	189.29±11.40	80.63±5.68	0.98±0.03	0.98±0.03
Group 4	7	71.50±2.42	71.37±5.19	186.85±9.13	79.98±5.83	71.10±3.26	71.37±4.82	189.85±9.51	79.99±5.94	1.00±0.04	0.99±0.03
Total	194	69.40±4.28	69.55±5.50	183.53±11.95	76.28±6.42	69.10±4.47	69.32±5.52	184.96±12.17	75.48±6.42	0.99±0.04	0.99±0.03

P>0.05: No significant differences between parameters, except for right 2nd finger length (Group 1–Group 3: *P*=0.001); right 4th finger length (Group 1–Group 2: *P*=0.000, Group 1–Group 3: *P*=0.000); right hand Length (Group 1–Group 2: *P*=0.000, Group 1–Group 3: *P*=0.000); right hand width (Group 1–Group 2: *P*=0.000, Group 1–Group 3: *P*=0.000, Group 1–Group 4: *P*=0.003); left 2nd finger length (Group 1–Group 2: *P*=0.012, Group 1–Group 3: *P*=0.011); left 4th finger length (Group 1–Group 2: *P*=0.000, Group 1–Group 3: *P*=0.000); left hand length (Group 1–Group 2: *P*=0.000, Group 1–Group 3: *P*=0.000, Group 1–Group 4: *P*=0.047); left hand width (Group 1–Group 2: *P*=0.000, Group 1–Group 3: *P*=0.000, Group 1–Group 4: *P*=0.001, Group 2–Group 3: *P*=0.000); right 2:4 digit ratio (Group 1–Group 2: *P*=0.000, Group 1–Group 3: *P*=0.001); left 2:4 digit ratio (Group 1–Group 2: *P*=0.001, Group 1–Group 3: *P*=0.001)

Discussion

The nose, both anatomically and esthetically, is a central feature of the human face. Diseases related to the nose can arise from congenital, developmental, and acquired causes. The 2:4 digit ratio is indicated as a significant marker accompanying the diagnosis of many diseases and, in addition to its association with diseases, there is a relationship between the 2:4 digit ratio and the lengths of body organs, including certain facial organs.[15] However, information on the correlation between the 2:4 digit ratio and nasal parameters is limited.[8] We did not find any previous studies comparing nasal structure with septum deviation in young adults and the 2:4 digit ratio. Therefore, we explored the morphometrically nasal structure with septum deviation in adolescents and its correlation with the 2:4 digit ratio.

Our study first evaluated nasal parameters according to gender. Except for the nasofrontal angle, nostril medial longitudinal angle, nasal tip angle, and nasolabial angle, other nasal parameter values were larger in males compared to females, and there was a significant difference between genders for these parameters, excluding nasal root width, nasal tip angle, nasolabial angle, and nostril medial longitudinal angle [Table 1]. Similar findings were reported by He *et al*.[16] and Sforza *et al*.,[17] who found significant differences in nasal parameters between genders.[18] Our study and others indicate that the nasal angular values between males and females show similarities [Table 8].

When evaluating hand parameters according to gender, except for the 2:4 digit ratios, other hand parameter values were larger in males, and a significant difference was observed for all parameters between genders [Table 2]. Fink *et al*.[1] investigated the relationship between the 2:4 finger ratio and facial shape in 106 volunteers and found that the 2:4 finger ratio was lower in males than females, and this result was statistically significant. Manning *et al*.[23] investigated the relationship between hand and foot finger ratios and HOX genes in 680 subjects and reported that the 2:4 finger ratio was lower in males than females and this result was statistically significant.

In this study, we evaluated nasal parameters according to the age. We found that there was no significant correlation between age and all parameters except nasal root width, right nostril width, right nostril length, alar tilt angle, nasofrontal angle, and nasal tip angle [$P > 0.05$, Table 3]. We also observed a negative correlation between age and nasal parameters [$P < 0.01$, Table 7]. Sforza *et al*.,[17] in their study of 519 males and 340 females between the ages of 4–73 years, which examined the changes in the nose depending on age and gender, reported that most nasal linear values, except nasal angular values, were significant with age. They also stated that nasal width, nasal height, nasal root width, philtrum length, nostril length, and width increased with age.

We then evaluated the hand parameters according to the age. As a result of the evaluation, we observed that there was no significant correlation between age and all hand parameters [$P > 0.05$, Table 4], and there was a negative correlation between age and hand parameters [$P < 0.01$, Table 7]. In a study conducted by Fink *et al*.[1] in 106 volunteers aged 18–38 years, no significant correlation was found between age and 2:4 finger ratio.

We analyze the nasal parameters according to the BMI. We found that there was no significant relationship between BMI and other parameters except for some groups in the parameters of facial height, nasal height, nasal depth, right nostril width, right nostril length, left nostril width, philtrum length, columella length, columella subwidth, and alar thickness [$P > 0.05$, Table 5]. In addition, it was determined that there was a significant correlation between BMI and other nasal parameters except nasofrontal angle, alar slope angle, nostril medial longitudinal angle, nasal tip

Table 7: Correlation table between parameters

	Gender	Age	BMI	Facial height	Nasal length	Nasal height	Nasal width	Nasal depth	Nasal root width	Right nostril width	Right nostril length
Gender	1	−0.113	0.368**	0.414**	0.309**	0.287**	0.542**	0.474**	0.026	0.147*	0.412**
Age	−0.113	1	−0.067	0.027	−0.096	−0.202**	−0.116	−0.027	−0.170*	−0.195**	−0.284**
BMI	0.368**	−0.067	1	0.334**	0.166*	0.197**	0.415**	0.206**	0.204**	0.220**	0.223**
Facial height	0.414**	0.027	0.334**	1	0.271**	0.235**	0.307**	0.320**	−0.013	0.029	0.253**
Nasal length	0.309**	−0.096	0.166*	0.271**	1	0.653**	0.257**	0.393**	0.099	0.116	0.316**
Nasal height	0.287**	−0.202**	0.197**	0.235**	0.653**	1	0.283**	0.398**	0.260**	0.126	0.367**
Nasal width	0.542**	−0.116	0.415**	0.307**	0.257**	0.283**	1	0.458**	0.238**	0.518**	0.315**
Nasal depth	0.474**	−0.027	0.206**	0.320**	0.393**	0.398**	0.458**	1	0.156*	0.086	0.331**
Nasal root width	0.026	−0.170*	0.204**	−0.013	0.099	0.260**	0.238**	0.156*	1	0.237**	0.084
Right nostril width	0.147*	−0.195**	0.220**	0.029	0.116	0.126	0.518**	0.086	0.237**	1	0.418**
Right nostril length	0.412**	−0.284**	0.223**	0.253**	0.316**	0.367**	0.315**	0.331**	0.084	0.418**	1
Left nostril width	0.265**	−0.169*	0.219**	0.126	0.162*	0.230**	0.468**	0.202**	0.198**	0.680**	0.422**
Left nostril length	0.235**	−0.154*	0.084	0.128	0.181*	0.167*	0.162*	0.257**	0.050	0.210**	0.359**
Columella length	0.158*	0.025	0.268**	0.251**	0.213**	0.226**	0.180*	0.267**	0.008	0.048	0.253**
Lower columella width	0.372**	−0.141	0.242**	0.269**	0.216**	0.294**	0.444**	0.515**	0.106	0.173*	0.370**
Upper columella width	0.229**	−0.211**	0.159**	−0.041	0.097	0.196**	0.309**	0.128	0.117	0.264**	0.138
Philtrum length	0.172*	−0.033	0.316**	0.248**	−0.040	−0.036	0.285**	0.122	0.117	0.110	0.097
Alar thickness	0.182*	−0.116	0.257**	0.131	0.252**	0.277**	0.380**	0.174*	0.199**	0.249**	0.169*
Nasofrontal angle	−0.236**	−0.118	0.041	−0.198**	−0.063	0.033	−0.043	−0.201**	0.242**	0.160*	−0.007
Alar slope angle	0.207**	−0.163*	0.131	0.031	−0.016	0.027	0.417**	0.051	0.164*	0.366**	0.072
Nostril medial longitudinal angle	−0.113	0.000	−0.048	−0.063	−0.026	−0.026	−0.220**	−0.091	0.100	−0.061	0.019
Nasal tip angle	−0.059	0.024	−0.023	−0.069	0.033	0.049	−0.110	−0.011	0.231**	−0.126	−0.112
Nasolabial angle	0.109	−0.130	0.007	−0.016	−0.067	0.020	0.098	0.148*	0.105	0.085	0.155*
Length of the right second finger	0.542**	−0.168*	0.282**	0.296**	0.275**	0.266**	0.538**	0.442**	0.058	0.194**	0.281**
Length of the right fourth finger	0.695**	−0.171*	0.341**	0.328**	0.319**	0.268**	0.572**	0.466**	0.034	0.271**	0.347**
Length of the right hands	0.701**	−0.130	0.293**	0.391**	0.406**	0.331**	0.519**	0.506**	0.039	0.083	0.279**
Width of the right hand	0.647**	−0.056	0.470**	0.414**	0.307**	0.234**	0.581**	0.494**	0.030	0.203**	0.297**
Length of the left second finger	0.554**	−0.157*	0.285**	0.293**	0.338**	0.269**	0.546**	0.475**	0.000	0.211**	0.293**
Length of the left fourth finger	0.673**	−0.147*	0.332**	0.362**	0.356**	0.292**	0.557**	0.467**	0.007	0.238**	0.377**
Length of the left hands	0.709**	−0.127	0.328**	0.422**	0.395**	0.312**	0.551**	0.569**	0.008	0.134	0.312**
Width of the left hand	0.629**	−0.015	0.489**	0.417**	0.335**	0.231**	0.555**	0.472**	−0.020	0.235**	0.313**
Right 2:4 digit ratio	−0.519**	0.079	−0.232**	−0.180*	−0.189*	−0.105	−0.287**	−0.230**	0.027	−0.225**	−0.247**
Left 2:4 digit ratio	−0.521**	0.050	−0.236**	−0.288**	−0.188**	−0.171*	−0.270**	−0.193**	−0.013	−0.162*	−0.322**

Contd...

Table 7: Contd...

	Left nostril width	Left nostril length	Columella length	Lower columella width	Upper columella width	Philtrum length	Alar thickness	Nasofrontal angle	Alar slope angle	Nostril medial longitudinal angle	Nasal tip angle
Gender	0.265**	0.235**	0.158*	0.372**	0.229**	0.172*	0.182*	−0.236**	0.207*	−0.113	−0.059
Age	−0.169*	−0.154*	0.025	−0.141	−0.211**	−0.033	−0.116	−0.118	−0.163*	0.000	0.024
BMI	0.219**	0.084	0.268**	0.242**	0.159*	0.316**	0.257**	0.041	0.131	−0.048	−0.023
Facial height	0.126	0.128	0.251**	0.269**	−0.041	0.248**	0.131	−0.198**	0.031	−0.063	−0.069
Nasal length	0.162*	0.181*	0.213**	0.216**	0.097	−0.040	0.252**	−0.063	−0.016	−0.026	0.033
Nasal height	0.230*	0.167*	0.226**	0.294**	0.196**	−0.036	0.277**	0.033	0.027	−0.026	0.049
Nasal width	0.468*	0.162*	0.180*	0.444**	0.309**	0.285**	0.380**	−0.043	0.417**	−0.220**	−0.110
Nasal depth	0.202**	0.257**	0.267**	0.515**	0.128	0.122	0.174*	−0.201**	0.051	−0.091	−0.011
Nasal root width	0.198*	0.050	0.008	0.106	0.117	0.117	0.199**	0.242**	0.164*	0.100	0.231**
Right nostril width	0.680**	0.210**	0.048	0.173*	0.264**	0.110	0.249**	0.160*	0.366**	−0.061	−0.126
Right nostril length	0.422**	0.359**	0.253**	0.370**	0.138	0.097	0.169*	−0.007	0.072	0.019	−0.112
Left nostril width	1	0.326**	0.062	0.233**	0.250**	0.173*	0.169*	0.073	0.430**	−0.211**	−0.091
Left nostril length	0.326**	1	0.133	0.329**	0.039	−0.075	0.041	−0.056	0.000	−0.019	−0.050
Columella length	0.062	0.133	1	0.366**	0.032	0.202**	0.103	−0.032	−0.081	−0.006	0.016
Lower columella width	0.233**	329**	366**	1	0.144*	0.250**	0.266**	−0.142*	0.011	−0.108	−0.091
Upper columella width	0.250**	0.039	0.032	0.144*	1	0.079	0.301**	0.003	0.320**	0.032	−0.205**
Philtrum length	0.173*	−0.075	0.202**	0.250**	0.079	1	0.124	0.062	0.129	−0.108	0.025
Alar thickness	0.169*	0.041	0.103	0.266**	0.301**	0.124	1	0.061	0.166*	0.103	0.077
Nasofrontal angle	0.073	−0.056	−0.032	−0.142*	0.003	0.062	0.061	1	0.075	−0.044	0.028
Alar slope angle	0.430**	0.000	−0.081	0.011	0.320**	0.129	0.166*	0.075	1	−0.139	−0.066
Nostril medial longitudinal angle	−0.211**	−0.019	−0.006	−0.108	0.032	−0.108	0.103	−0.044	−0.139	1	0.225**
Nasal tip angle	−0.091	−0.050	0.016	−0.091	−0.205**	0.025	0.077	0.028	−0.066	0.225**	1
Nasolabial angle	0.055	0.110	0.104	0.210**	0.−031	0.085	0.162*	0.054	0.084	0.230**	0.220**
Length of the right second finger	0.253**	0.119	0.161*	0.327**	0.338**	0.183*	0.172*	−0.191**	0.165*	−0.029	−0.066
Length of the right fourth finger	0.303**	0.201**	0.200**	0.389**	0.275**	0.232**	0.228**	−0.241**	0.178*	−0.043	−0.004
Length of the right hands	0.200**	0.191**	0.190**	0.476**	0.195**	0.180**	0.213**	−0.319**	0.094	−0.091	0.014
Width of the right hand	0.202**	0.099	0.347**	0.500**	0.155*	0.356**	0.153*	−0.184*	0.062	−0.210**	−0.067
Length of the left second finger	0.244**	0.119	0.211**	0.392**	0.269**	0.217**	0.184*	−0.217**	0.169*	−0.013	−0.046
Length of the left fourth finger	0.274**	0.180*	0.246**	0.392**	0.279**	0.239**	0.208**	−0.258**	0.167*	−0.038	−0.056
Length of the left hands	0.247**	0.244**	0.247**	0.505**	0.234**	0.184	0.207**	−0.315	0.097	−0.109	−0.016
Width of the left hand	0.220**	0.136	0.311**	0.439**	0.165**	0.270**	0.205**	−0.209**	0.071	−0.161*	−0.099
Right 2:4 digit ratio	−0.192**	−0.211**	−0.140	−0.256**	−0.023	−0.170*	−0.164*	0.173*	−0.096	0.041	−0.086
Left 2:4 digit ratio	−0.175*	−0.193**	−0.171*	−0.165*	−0.144*	−0.141*	−0.140	0.185**	−0.081	0.074	0.051

Contd...

Table 7: Contd...

	Nasolabial angle	Length of the right second finger	Length of the right fourth finger	Length of the right hands	Width of the right hand	Length of the left second finger	Length of the left fourth finger	Length of the left hands	Width of the left hand	Right 2:4 digit ratio	Left 2:4 digit ratio
Gender	0.109	0.542**	0.695**	0.701**	0.647**	0.554**	0.673**	0.709**	0.629**	−0.519**	−0.521**
Age	−0.130	−0.168	−0.171*	0.079	−0.056	−0.157*	−0.147*	−0.127	−0.015	0.079	0.050
BMI	0.007	0.282**	0.341**	0.293**	0.470**	0.285**	0.332**	0.328**	0.489**	−0.232**	−0.238**
Facial height	−0.016	0.296**	0.328**	0.391**	0.414**	0.293**	0.362**	0.422**	0.417**	−0.180*	−0.288**
Nasal length	−0.067	0.275**	0.319**	0.406**	0.307**	0.338**	0.356**	0.395**	0.335**	−0.189**	−0.188**
Nasal height	0.020	0.266**	0.268**	0.331**	0.234**	0.269**	0.292**	0.312**	0.231**	−0.105	−0.171*
Nasal width	0.098	0.538**	0.572**	0.519**	0.581**	0.546**	0.557**	0.551**	0.555**	−0.287**	−0.270**
Nasal depth	0.148*	0.442**	0.466**	0.506**	0.494**	0.475**	0.467**	0.569**	0.472**	−0.230**	−0.193**
Nasal root width	0.105	0.058	0.034	0.039	0.030	0.000	0.007	0.008	−0.020	0.027	−0.013
Right nostril width	0.085	0.194**	0.271**	0.083	0.203**	0.211**	0.238**	0.134	0.235**	−0.225**	−0.162*
Right nostril length	0.155*	0.281**	0.347**	0.279**	0.297**	0.293**	0.377**	0.312**	0.313**	−0.247**	−0.322**
Left nostril width	0.055	0.253**	0.303**	0.200**	0.202**	0.244**	0.274**	0.247**	0.220**	−0.192**	−0.175*
Left nostril length	0.110	0.119	0.201**	0.191**	0.099	0.119	0.180*	0.244**	0.136	−0.211**	−0.193**
Columella length	0.104	0.161*	0.200**	0.190**	0.347**	0.211**	0.246**	0.247**	0.311**	−0.140	−0.171*
Lower columella width	0.210**	0.327**	0.389**	0.476**	0.500**	0.392**	0.392**	0.505**	0.439**	−0.256**	−0.165*
Upper columella width	−0.031	0.338**	0.275**	0.195**	0.155*	0.269**	0.279**	0.234**	0.165*	−0.023	−0.144*
Philtrum length	0.085	0.183*	0.232**	0.180*	0.356**	0.217**	0.239**	0.184*	0.270**	−0.170*	−0.141*
Alar thickness	0.162*	0.172*	0.228**	0.213**	0.153*	0.184*	0.208**	0.207**	0.205**	−0.164*	−0.140
Nasofrontal angle	0.054	−0.191**	0.−0.241**	−0.319**	−0.184*	−0.217**	−0.258**	−0.315**	−0.209**	0.173**	0.185**
Alar slope angle	0.084	0.165*	0.178*	0.094	0.062	0.169*	0.167*	0.097	0.071	−0.096	−0.081
Nostril medial longitudinal angle	0.230**	−0.029	−0.043	−0.091	−0.210**	−0.013	−0.038	−0.109	−0.161*	0.041	0.074
Nasal tip angle	0.220*	−0.066	−0.004	0.014	−0.067	−0.046	−0.056	−0.016	−0.099	−0.086	0.051
Nasolabial angle	1	0.122	0.144*	0.071	0.018	0.115	0.100	0.049	−0.009	−0.093	−0.013
Length of the right second finger	0.122	1	0.847**	0.750**	0.666**	0.904**	0.860**	0.788**	0.612**	−0.132	−0.295**
Length of the right fourth finger	0.144*	0.847**	1	0.806**	0.732**	0.857**	0.928**	0.828**	0.716**	−0.637**	−0.542**
Length of the right hands	0.071	0.750**	0.806**	1	0.713**	0.775**	0.814**	0.945**	0.666**	−0.419**	−0.427**
Width of the right hand	0.018	666**	0.732**	0.713**	1	0.702**	0.735**	0.748**	0.912**	−0.407**	−0.387**
Length of the left second finger	0.115	0.904**	0.857**	0.775**	0.702**	1	0.907**	0.811**	0.640**	−0.292**	−0.228**
Length of the left fourth finger	0.100	0.860**	0.928**	814**	735**	0.907**	1	0.856**	0.711**	−0.489**	−0.615**
Length of the left hands	0.049	0.788**	0.828**	0.945**	0.748**	0.811**	0.856**	1	0.704**	−0.409**	−0.458**
Width of the left hand	−0.009	0.612**	0.716**	0.666**	0.912**	0.640**	0.711**	704**	1	−0.452**	−0.450**
Right 2:4 digit ratio	−0.093	−0.132	−0.637**	−0.419**	−0.407**	−0.292**	−0.489**	−0.409**	−0.452**	1	590**
Left 2:4 digit ratio	−0.013	−0.295**	−0.542**	−0.427**	−0.387**	−0.228**	−0.615**	−0.458**	−0.450**	590**	1

*P<0.05, **P<0.01

Table 8: Comparison of nasal angular parameters between our study and other studies

Author	*n*	Parameters							
		Nasofrontal angle		Alar slope angle		Nasal tip angle		Nasolabial angle	
		Female	Male	Female	Male	Female	Male	Female	Male
Uzun and Ozdemir[12]	115	133.16	123.85	80.89	85.98	77.91	82.16	98.91	97.91
Sforza *et al*.[17]	192			75.43	74.45	93.84	94.99		
Husein *et al*.[19]	200	134.30		59.40		67.40		104.20	
Choe *et al*.[20]	72	136.80		81.90		78.50		92.10	
Aung *et al*.[21]	90	139.09	137.43	90.89	89.07	83.87	82.55	9791	99.91
Dong *et al*.[22]	289	144.04	138.19			96.16	94.16	103.42	104.30
Our study	194	137.33	132.84	79.33	84.43	69.63	68.65	93.57	96.75

angle, and nasolabial angle [$P < 0.01$, Table 7]. In a study conducted by Ozsoy and Bikem Süzen[18] on 40 subjects aged 19–26 years, it was emphasized that there was no correlation between BMI and nasal parameters.

Upon assessing hand parameters according to BMI, we found that there was no significant correlation between BMI and hand parameters except for right second finger length, right fourth finger length, right-hand length, right-hand width, left second finger length, left fourth finger length, left-hand length, left-hand width, right 2:4 finger ratio, and left 2:4 finger ratio [$P > 0.05$, Table 6]. We also observed a significant correlation between BMI and hand parameters [$P < 0.01$, Table 7]. A study conducted in Turkey in 2021 reported a negative correlation between BMI and the right 2:4 finger ratio.[24] In our study, we found a negative correlation between the 2:4 finger ratio of both hands and BMI [$P < 0.01$, Table 7].

After investigated the relationship between the 2:4 finger ratio and nasal parameters, we found that the right 2:4 finger ratio was significantly negatively correlated with all nasal parameters except nasal height, nasal root width, alar tilt angle, nostril medial longitudinal angle, nasal tip angle, and nasolabial angle [$P < 0.01$, Table 7]. We determined that the left 2:4 finger ratio was significantly negatively correlated with the other nasal parameters except alar thickness, nasal root width, alar slope angle, nostril medial longitudinal angle, nasal tip angle, and nasolabial angle [$P < 0.01$, Table 7]. In our study, we observed that as the 2:4 finger ratio increased in both hands, the other linear parameters except the facial height parameter decreased or remained constant, whereas the nasolabial angle increased, nasofrontal angle, alar slope angle, and nostril medial longitudinal angle decreased [Tables 3 and 4]. In studies, it has been reported that there is a curvilinear relationship between the 2:4 finger ratio and facial asymmetry and that asymmetry is higher on the side with very high and very low 2:4 finger ratio.[25] In addition, in a study conducted by Weinberg *et al*.[8] on facial photographs of 151 male volunteers in 2015, it was emphasized that there was an inverse relationship between the 2:4 finger ratio and facial features and that the philtrum became shorter as the 2:4 finger ratio increased.

It is stated that factors such as race, genetic factors, and climatic conditions are important in nasal typing. It is also stated that there is a relationship between nostril medial longitudinal angle and nostril flatness. In our study, we performed nostril typing according to the nostril medial longitudinal angle range and the classification made by Farkas *et al*.[26] Type 3 nostril type was observed most frequently according to the nostril medial longitudinal angle result [Figure 3 and Table 9]. Farkas *et al*.[26] reported that Type 3 nostril type was observed most frequently in their study. Garandawa *et al*.[27] reported that Type 6 nostril type was the most common type in their study on 1010 adults. In the studies, it was emphasized that the Type 3 nostril type showed Caucasian, and Type 6 and Type 7 nostril types showed black nostril characteristics.[1,26]

The nasal index was also calculated to determine the nasal type (nasal index = nasal width/nasal height × 100). In studies, nasal index has been reported as a parameter used in nasal typing and associated with narrow or wide nasal type.[28,29] In our study, we classified the general nasal shape according to the classification made by Martin and Sallar based on nasal index.[28] According to the results of our classification, leptin (moderately narrow nose) type nose was observed most frequently in our study [Table 10]. Kılıc Safak *et al*.[28] reported that the most common type of nose in adults was mesorrhine type as a result of their study in 874 healthy individuals. In studies, it has been reported that Caucasians and Orientals have leptorrhine type nose, Africans have platyrrhine type nose, and Indians have mesorrhine type nose on average.[2] In addition, it has been emphasized that platyrrhinetype nose is observed in Nigeria, Egypt, and Iran, and leptin-type nose is observed in Albania.[28,29]

Since hormones in the prenatal period may determine which disease a person will be prone to in future, there is a link between these diseases and the 2:4 finger ratio.[14] Congenital adrenal hyperplasia (CAH), age at myocardial infarction (MI), autism, migraine, and some cancers are associated with 2:4 finger ratio. Studies have shown that people with a high 2:4 finger ratio have a higher risk of breast cancer, a lower age of MI, and a higher likelihood of

migraine in men. In addition, in previous studies, a lower 2:4 finger ratio was observed in some diseases such as CAD, autism, and migraine in women.[30]

The anthropometry of the face has always been an interesting subject for many artists and plastic surgeons, and it is emphasized that different rules have been proposed for an ideal face since ancient times.[13] In previous studies, it has been stated that the middle part of the face is esthetically important and the nasal structure is the most important part of this region.[16] It is also stated that the size, shape, and proportions of the nose reflect the character of the person.[16] The nose, which is the starting point of inspiration, is an important anatomical structure that can provide information about gender, age, and race. External features of the nose are important for surgeons to obtain the best results after rhinoplasty or traumatic nasal deformity operations. After all, the face is a whole and the ideal nose should be in harmony with the rest of the face. To maintain this harmony, the angular relationship should be accurately evaluated in soft-tissue profiling.

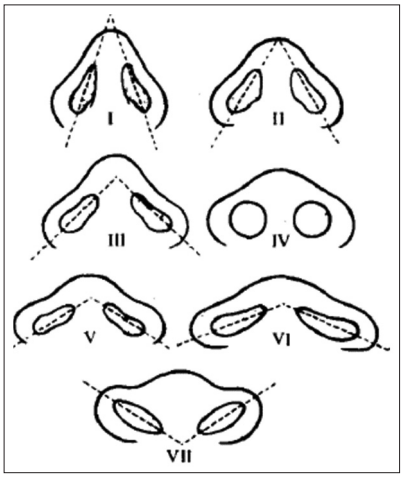

Figure 3: Nostril types according to Farkas *et al*.[26]

Table 9: Nostril typology data table from our study

Nostril types	Nostril medial longitudinal angle range	Number and percentage of participants (%)
Tip 1	70–90	3 (1.55)
Tip 2	55–69	84 (43.3)
Tip 3	40–54	100 (51.55)
Tip 4	0	0
Tip 5	25–39	7 (3.60)
Tip 6	10–24	0
Tip 7	−50–−20	0

Although the measurement values we obtained as a result of our study are different from the measurement values obtained in previous studies, our study results and the results of other studies show similar characteristics. We think that the differences in measurement values between our study and other studies are due to the different number of cases and age ranges used in the study, the researcher who performed the measurement, the methods used, and racial reasons. As is known, nasal morphometric measurements may vary according to gender, age, race, and ethnicity. We consider our study as a preliminary study in a young population aged 18–25 years. We think that the use of direct anthropometric methods for the measurement of linear and angular parameters in our study is an important factor that makes our study important. In addition, we consider the fact that our study was conducted only in a young population aged 18–25 years and that radiologic images were not used in the determination of nasal septum deviation as factors limiting our study. Therefore, to morphometrically evaluate the developmental process in the nose with deviated nasal septum, we believe that it would be useful to support our study with studies that will include pediatric, adolescent, and adult periods, where the number of participants is higher and radiologic images are also used.

Conclusion

The data we obtained in this study will contribute to the evaluation of nasal development, gender, age, and race determination in forensic medicine and the formation of a data bank about our population. In addition, we think that our study results will help clinicians who are interested in this region in the diagnosis and treatment of pathologies related to the nose, in the description of anatomical points in surgical procedures to be applied to the nasal region, in the planning of surgical procedures, and in the pre- and postoperative evaluation of the procedure to be performed.

Author contributions

All authors contributed to the study's conception and design. Desdicioğlu K. Project development and manuscript writing, Oğuz B. Data collection and manuscript writing, Tutuk V. Data collection and data analysis.

Table 10: Nasal types data table from our study

Category	Nasal size	Nasal index (on the living head)	Number and percentage of participants (%)
Hyperleptorrhine	Long narrow nose	40–54.9	24 (12.37)
Leptorrhine	Moderately narrow nose	<70	138 (71.13)
Mesorrhine	Medium nose	70–84.9	27 (13.92)
Platyrrhine	Moderately wide nose	85–99.9	3 (1.55)
Hyperplatyrrhine	Very wide nose	>100	2 (1.03)

Ethics approval

Ethical approval for the study was obtained from the Ankara Yıldırım Beyazıt University Health Sciences Ethics Committee on May 16, 2023, with decision number 244/05.

Financial support and sponsorship

Nil.

Conflicts of interest

There are no conflicts of interest.

References

1. Fink B, Grammer K, Mitteroecker P, Gunz P, Schaefer K, Bookstein FL, *et al*. Second to fourth digit ratio and face shape. Proc Biol Sci 2005;272:1995-2001.
2. Standring S. Gray's Anatomy: The Anatomical Basis of Clinical Practice. London: Churchill Livingstone Elsevier; 2016.
3. Cellina M, Gibelli D, Cappella A, Martinenghi C, Belloni E, Oliva G. Nasal cavities and the nasal septum: Anatomical variants and assessment of features with computed tomography. Neuroradiol J 2020;33:340-7.
4. Setlur J, Goyal P. Relationship between septal body size and septal deviation. Am J Rhinol Allergy 2011;25:397-400.
5. Teul I, Slawinski G, Lewandowski J, Dzieciolowska-Baran E, Gawlikowska-Sroka A, Czerwinski F. Nasal septum morphology in human fetuses in computed tomography images. Eur J Med Res 2010;15 Suppl 2:202-5.
6. Hartman C, Holton N, Miller S, Yokley T, Marshall S, Srinivasan S, *et al*. Nasal septal deviation and facial skeletal asymmetries. Anat Rec (Hoboken) 2016;299:295-306.
7. Manning JT. Resolving the role of prenatal sex steroids in the development of digit ratio. Proc Natl Acad Sci U S A 2011;108:16143-4.
8. Weinberg SM, Parsons TE, Raffensperger ZD, Marazita ML. Prenatal sex hormones, digit ratio, and face shape in adult males. Orthod Craniofac Res 2015;18:21-6.
9. Burriss RP, Little AC, Nelson EC. 2D: 4D and sexually dimorphic facial characteristics. Arch Sex Behav 2007;36:377-84.
10. Carlson BM. Human Embryology and Developmental Biology. Philadelphia: Elsevier; 2014.
11. Etöz BC, Etöz A, Ercan I. Nasal shapes and related differences in nostril forms: A morphometric analysis in young adults. J Craniofac Surg 2008;19:1402-8.
12. Uzun A, Ozdemir F. Morphometric analysis of nasal shapes and angles in young adults. Braz J Otorhinolaryngol 2014;80:397-402.
13. Borman H, Ozgür F, Gürsu G. Evaluation of soft-tissue morphology of the face in 1,050 young adults. Ann Plast Surg 1999;42:280-8.
14. Malas MA, Dogan S, Evcil EH, Desdicioglu K. Fetal development of the hand, digits and digit ratio (2D: 4D). Early Hum Dev 2006;82:469-75.
15. Geschwind N, Galaburda AM. Cerebral lateralization. Biological mechanisms, associations, and pathology: I. A hypothesis and a program for research. Arch Neurol 1985;42:428-59.
16. He ZJ, Jian XC, Wu XS, Gao X, Zhou SH, Zhong XH. Anthropometric measurement and analysis of the external nasal soft tissue in 119 young Han Chinese adults. J Craniofac Surg 2009;20:1347-51.
17. Sforza C, Grandi G, De Menezes M, Tartaglia GM, Ferrario VF. Age- and sex-related changes in the normal human external nose. Forensic Sci Int 2011;204:9.e1.
18. Ozsoy U, Bikem Süzen L. Nose asymmetry correlates with external nose volume and area: 3D analysis of nasal dimensions in a young Turkish population. Anatomy 2018;12:7-12.
19. Husein OF, Sepehr A, Garg R, Sina-Khadiv M, Gattu S, Waltzman J, *et al*. Anthropometric and aesthetic analysis of the Indian American woman's face. J Plast Reconstr Aesthet Surg 2010;63:1825-31.
20. Choe KS, Yalamanchili HR, Litner JA, Sclafani AP, Quatela VC. The Korean American woman's nose: An in-depth nasal photogrammatic analysis. Arch Facial Plast Surg 2006;8:319-23.
21. Aung SC, Foo CL, Lee ST. Three dimensional laser scan assessment of the oriental nose with a new classification of oriental nasal types. Br J Plast Surg 2000;53:109-16.
22. Dong Y, Zhao Y, Bai S, Wu G, Wang B. Three-dimensional anthropometric analysis of the Chinese nose. J Plast Reconstr Aesthet Surg 2010;63:1832-9.
23. Manning JT, Callow M, Bundred PE. Finger and toe ratios in humans and mice: Implications for the aetiology of diseases influenced by HOX genes. Med Hypotheses 2003;60:340-3.
24. Acar G, Digilli B, Saglam A, Cicekcibası A. The relationship of the digit ratio (2D: 4D) with body fat distribution and handgrip strength in medical students. Cukurova Med J 2021;46:555-65.
25. Teatero ML, Netley C. A critical review of the research on the extreme male brain theory and digit ratio (2D: 4D). J Autism Dev Disord 2013;43:2664-76.
26. Farkas LG, Hreczko TA, Deutsch CK. Objective assessment of standard nostril types – A morphometric study. Ann Plast Surg 1983;11:381-9.
27. Garandawa H, Nwaorgu O, Oluwatosin O. Morphometric nose parameters in adult Nigerians. Internet J Otorhinolaryngol 2009;10:1-6.
28. Kılıc Safak N, Durgun B, Yucel AH, Oguz O. Anthropometric measurements of the nose and nose types. J Harran Univ Med Fac 2023;20:248-55.
29. Mehta N, Srivastava RK. The Indian nose: An anthropometric analysis. J Plast Reconstr Aesthet Surg 2017;70:1472-82.
30. Lee SH, Aziz SA, Hamid M, Lim YC, Koh D, Chaw LL. 2D: 4D ratio and autism spectrum disorder in Brunei Darussalam. J Autism Dev Disord 2021;51:4577-86.

Original Article

The Relationship between Basal Ganglia Volume and Audiovisual Reaction Time in Turkish Elite Athletes

Selim Karabekir, Funda Aksu[1], Erkan Gunay[2], Nuket Gocmen Karabekir[1]

Departments of Anatomy and [1]Neurosurgery, School of Medicine, Dokuz Eylül University, Izmir, [2]Department of Coaching Education, Faculty of Sport Sciences, Manisa Celal Bayar University, Manisa, Turkey

Abstract

Background: In this study involving young adult elite athletes and healthy sedentary individuals, volumetric analyses were performed on basal ganglia (BG) involved in the coordination of motor movements. **Aims and Objectives:** In a group of athletes with high coordination speed, potential relationship between BG volumes and audiovisual reaction time of acquired-trained hand movements was explored by examining whether these individuals had significant differences in terms of BG volumes. **Materials and Methods:** Nineteen elite athletes aged between 19 and 25 years (9 male and 10 female) and 20 sedentary subjects (10 male, 10 female) were included. Gender, age, height, weight, and body-mass index (BMI) were recorded. In each group, audiovisual reaction time and stereological basal ganglia volumes were assessed and statistically analyzed. **Results:** Elite athletes react more rapidly to auditory stimuli than visual stimuli. As compared to sedentary individuals, elite athletes exhibited significantly shorter visual reaction time and only numerically shorter (statistically insignificant) visual reaction time. Left BG volume was higher in both groups, compared to right side). **Conclusion:** Our data may contribute to the construction of a database of normal BG morphology and provide useful information for clinicians and athletes.

Keywords: *Basal ganglia, elite athletes, nuclei basales, reaction time, stereology, volume*

Introduction

Classically, nuclei basales which are called basal ganglia (BG) have been intriguing anatomical structures due to their concealed location in between brain convolutions. BG or basal nuclei consist of five pairs of nuclei located deep in cranial hemispheres and are referred to as *nucleus caudatus, putamen, globus pallidus, substantia nigra*, and *nucleus subthalamicus*. Nucleus caudatus, putamen, and globus pallidus are collectively termed as "corpus striatum."[1,2]

BG has been shown to be involved in the coordination of motor movements as well as in mental and emotional functions. Their main functions include utilization of input coming from the sensory cortex, thalamus, and brainstem; conveyance of information from multiple nonspecific areas to somatomotor areas; regulation of impulses associated with muscle tone, posture, and movement; and regulation of muscular movements through effects on the activity of motor centers within the brainstem.[2] In addition, BG is known to be associated with mental and emotional functions such as comprehension and appraisal.[2-5]

The harmonious activity of the motor and sensory cortices to regulate movements during physical activity is referred to as sensory-motor integration. The primary motor cortex utilizes the sensory afferent input very efficiently to ensure a concerted activity between muscle groups.[6] An examination of the association between the sensory-motor system and BG in athletes indicates that this system has important roles in the integration of motor, sensory, and central systems as well as in the processes involved. Visual and auditory reaction input as well as the information obtained from muscles, skin, tendons, and joints are processed within this system. Therefore, the sensory-motor system has significant roles in the perception, planning, execution, and regulation of the movements during physical activity in athletes. Furthermore, it has an important role in the protection against injury and the level of sportive performance due to its complex structure and intricate connections.

Until now, although many studies have been published regarding the functional, volumetric, or pathological changes

This is an open access journal, and articles are distributed under the terms of the Creative Commons Attribution-NonCommercial-ShareAlike 4.0 License, which allows others to remix, tweak, and build upon the work non-commercially, as long as appropriate credit is given and the new creations are licensed under the identical terms.

For reprints contact: WKHLRPMedknow_reprints@wolterskluwer.com

How to cite this article: Karabekir S, Aksu F, Gunay E, Karabekir NG. The relationship between basal ganglia volume and audiovisual reaction time in Turkish elite athletes. J Anat Soc India 2024;73:277-83.

Article Info

Received: 18 February 2024
Revised: 11 August 2024
Accepted: 05 September 2024
Available online: 25 September 2024

Address for correspondence:
Prof. Funda Aksu, Department of Anatomy, Dokuz Eylül University Medical Faculty, Inciralti, Izmir 35340, Turkey.
E-mail: funda.aksu@deu.edu.tr

Access this article online

Website: https://journals.lww.com/joai
DOI: 10.4103/jasi.jasi_25_24
Quick Response Code:

according to age and gender in disease processes involving BG, none have specifically looked at the association of BG volume with reaction times and gender in normal healthy individuals and elite athletes, and only scarce data have been made available recently, regarding the age-related effect of exercise on BG.[7,8] Similarly, gender-based comparisons among young adult elite athletes using different methodologies are few.[4,5] In addition, our literature search for BG volume studies using stereological methods did not yield any published data that assessed the association of BG volume with acquired-trained repetitive movements and audiovisual reaction time.[8-13]

In the present study involving young adult elite athletes and healthy sedentary individuals, volumetric analyses were performed in BG areas involved in the coordination of motor movements. For this purpose, significant volume differences in a group of sportsmen with high coordination speed were explored, in an effort to identify potential links between BG volumes and audiovisual reaction time in acquired-trained hand movements.

Materials and Methods

The study is a prospective comparative experimental study. Following approval from the Ethics Committee for Non-Interventional Studies of Dokuz Eylul University Medical Faculty, audiovisual reaction time and morphological (height, weight, and body mass index [BMI]) measurements of elite athletes and sedentary individuals were performed at the Department of Anatomy and Sport Academy. Then, each participant underwent a cranial magnetic resonance imaging (MRI) examination at the radiology department of Dokuz Eylul University Medical Faculty Hospital. Data were statistically assessed.

A total of 19 right-handed elite athletes (9 male and 10 female) aged between 19 and 25 years with no audiovisual impairment and 20 otherwise healthy sedentary individuals (10 male and 10 female) aged between 18 and 28 years were included in the study. Audiovisual reaction tests and MRI examinations could not be performed in some cases due to poor adherence. The number of cases (*n*) who underwent assessment for each parameter was indicated in tables.

Elite athletes included those who achieved a good performance level or a ranking in a team or individual sports activity at the national level, Olympic Games, or World Championships and who followed a consistent training program for at least 10 years.[14] Ten of the elite athletes were involved in a team sport such as basketball or volleyball, and 9 were involved in an individual sport activity, namely swimming. A total of 20 age- and sex-matched, right-handed, healthy, and sedentary individuals (10 male and 10 female) with no regular physical activity served as controls.

Radiological examination

BG measurements in both study groups were performed using T1–T2 weighed three-dimensional gradient echo images 3-Dimensional T1-Weighted Turbo Field Echo acquired with an MRI device 1.5-T unit (Integra, Philips, the Netherlands). Sedentary group images were obtained from healthy at the discretion of the radiologist right-handed individuals. Specifically, conventional spin echo (SE) T1A cross-sections (Repetition time [TR]: 500–700 ms; Echo time [TE]: 10–30 ms) were obtained in sagittal and axial planes, and T1-weighed sagittal images were recorded. No sedation or IV contrast enhancement was used. The image acquisition and recording of measurements were performed by the same operator to minimize the risk of error.

In both groups, manual stereological measurements were performed in sagittal 0.3 mm cross-sections in T1-weighed MRI images to determine BG (caudate and lentiform nuclei) volumes according to side (left vs. right) and gender. All BG structures other than the corpus striatum were excluded from measurements, due to their small size and technical inability to acquire image sections <0.3 cm in thickness.

Stereological volumetric method

Stereological assessment with a point counting method involves the use of a marked scale in randomly selected positions to assess cross sections. The counted points are summed and multiplied by the thickness of the cross-section to yield the volume. The following formula was used for the point counting method, $V = t \times ([(SU) \times d]/SL)\ 2\times \Sigma P$, where *t*, SU, *d*, SL, and p correspond to cross-section thickness, MRI scale unit, distance between two points in the grid, scale length, and the number of points counted, respectively.[4,15-19] In volumetric assessments, the sagittal and axial MRI cross-sections were measured to allow that the optimal plane corresponded to the smallest diameter of the anisotropic structure.

A stable and consecutive cross-section thickness of 0.3 cm was maintained to reduce the error of margin. For each participant, all cross-sections were separately evaluated for the left and right hemispheres, and the point counts were performed manually [Figure 1]. These mathematical processes are known as Cavalieri's principle.[4,5,15,17,20]

Audiovisual reaction time measurement method

Visual reaction time

A Lafayette Multi-Operational Apparatus for Reaction Time (MOART) Reaction Device (Lafayette, USA) was used. This device can record auditory and visual reaction time with 1/1000 s units. For visual reaction recording, the lights on the right and left buttons randomly flash without any visual stimuli to detect the visual reaction time. Before recording, each participant performed five repetitions of a practice test.

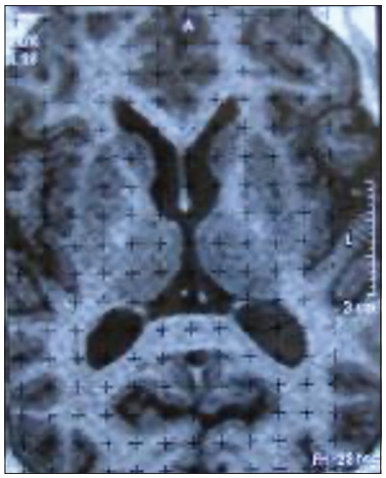

Figure 1: Stereological nucleus lentiformis and nucleus caudatus measurement on axial T1-weighted magnetic resonance imaging section

Auditory reaction time

A Lafayette MOART Reaction Device (Lafayette, USA) was used. This device can record auditory and visual reaction time with 1/1000 s units. During the test, the participant is asked to press a button in the middle of the device using his/her dominant hand upon being exposed to auditory stimuli given at random intervals. Before recording, each participant performed five repetitions of a practice test. Measurements were repeated at least 10 times in all participants, and the average value was recorded.

Subjects were excluded from the study if they had osteoarthritis, structural deformity, history of head or body trauma, active infection, or any health problem during the study period. Also excluded were the subjects with disability precluding MRI examination and those with claustrophobia and/or anxiety.

Statistical methods

The normality of the distribution of the continuous variables was checked with Shapiro–Wilk test, whereas Box's M statistics were performed for the homogeneity of the variance-covariance matrices. Since the assumptions of the parametric tests were met, dependent variables were used in a "variance analysis on repeated measures" with 3 factors with repetition of one factor to reduce the error. For variables without repeated measurements, a 2-factor variance analysis and independent two-group *t*-test were performed for variables meeting the assumptions of the parametric tests.

Mann–Whitney *U*-test was used for variables not meeting the parametric test assumptions. Association between variables was evaluated with Pearson and Spearman rho correlation coefficients. Results were expressed as mean ± standard deviation, median, and correlation coefficients. A $P < 0.05$ was considered statistically significant. SPSS 22.0 statistical software pack was used for analyses (SPSS Ver. 22.0, SSPS Inc., Chicago, IL, USA).

Results

Physical data for elite athletes and sedentary individuals

Age, gender, weight, height, and BMI data were recorded and compared between the two age- and gender-matched groups. In females, there were significant height and weight differences between athletes and sedentary subjects ($P = 0.05$, $P = 0.033$, respectively). In males, a significant BMI difference was found between athletes and sedentary subjects ($P = 0.041$) [Table 1].

Data for audiovisual reaction time

Audiovisual reaction time data were obtained from right-handed athletes and sedentary individuals for statistical analysis. Table 2 shows the reaction times in millisecond units in both groups. A significant difference was noted in auditory and visual reaction times between the two groups ($P_1 = 0.001$). This difference was found to vary according to the groups tested (P_2 interaction [auditory and visual × Group] = 0.001). The mean visual reaction time among athletes was higher as compared to the mean auditory reaction times, with no gender difference (P_3 interaction [visual and auditory × Gender] = 0.825, P_4 interaction [visual and auditory × Group × Gender] = 0.618). Thus, as compared to sedentary subjects, athletes have a shorter reaction time to auditory stimuli than visual stimuli.

In right-handed athletes with higher right BG volume, auditory reaction times were shorter, i.e., more rapid, than visual reaction times. As compared to sedentary individuals, athletes were significantly more rapid in terms of auditory reaction time. Although athletes had more rapid reactions to visual stimuli than sedentary individuals, the difference was not statistically significant. It was assumed that a larger sample size could have yielded more significant results. Although these data were recorded independent of gender, female and male athletes had more rapid reaction times to auditory stimuli than sedentary males and females, although the differences were not significant.

Stereological volume analysis data for basal ganglia

Caudate nucleus volume

Right and left caudate nucleus volumes were recorded in cubic centimeters in the two age- and gender-matched groups for statistical analysis [Table 3]. In general, there was a significant difference between right and left caudate nucleus volumes in athletes and sedentary subjects ($P < 0.05$), with higher left-sided volume measurements ($P_1 = 0.045$).

However, these differences between athletes and sedentary subjects ($P_2 = 0.925$) and differences regarding gender ($P_3 = 0.074$) were not significant. Thus, the right and left caudate nucleus volume did not differ significantly

Table 1: Physical data for athletes and sedentary individuals

	Female			Male		
	Athlete, *n* Mean±SD Median	**Sedentary, *n* Mean±SD Median**	***P***	**Athlete, *n* Mean±SD Median**	**Sedentary, *n* Mean±SD Median**	***P***
Age	10	10	0.104	9	10	0.776
	20.900±1.286	22.700±3.093		22.555±1.943	22.200±3.190	
	20.000	21.500		22.000	21.000	
Height (cm)	9	9	0.050*	9	10	0.869
	1.718±0.064	1.660±0.030		1.767±0.065	1.762±0.082	
	1.7750	1.650		1.770	1.750	
Weight (kg)	9	9	0.033*	9	10	0.07*
	60.222±3.763	56.222±3.492		70.222±7.870	80.100±13.370	
	60.000	56.000		69.000	82.000	
BMI	9	9	0.873	9	10	0.041*
	20.388±1.060	20.481±1.333		22.500±2.330	25.843±4.223	
	20.500	20.569		23.000	26.524	

*$P \leq 0.05$. SD: Standard deviation, BMI: Body mass index

Table 2: Audiovisual reaction time data for athletes and sedentary individuals

Group	**Gender**	**Reaction time - auditory (ms), *n* Mean±SD Median**	**Reaction time - visual (ms), *n* Mean±SD Median**	***P***
Athlete	Female	9	9	P_1=0.001*
		471.333±59.902	224.777±15.417	P_2=0.001*
		464.000	223.000	P_3=0.825
	Male	9	9	P_4=0.618
		422.777±51.664	192.555±12.640	
		413.000	199.000	
Sedentary	Female	9	9	
		432.122±46.115	281.222±36.591	
		430.000	275.000	
	Male	10	10	
		446.000±60.929	288.800±63.308	
		457.500	262.000	

*$P \leq 0.05$. SD: Standard deviation

according to group and gender ($P_4 = 0.578$). Interestingly, left and right caudate nucleus volumes were smaller among athletes than sedentary individuals, although the difference was not significant.

Lentiform nucleus volume

Left and right nucleus lentiform volume data in the two age- and gender-matched groups were recorded in cubic centimeters and statistically analyzed [Table 4]. In both groups and genders, lentiform nucleus volume was higher on the left, although the difference was not significantly different ($P_1 = 0.903$). This result was independent of the group (i.e., athlete or sedentary) ($P_2 = 0.338$) and gender ($P_3 = 0.477$). Statistically, the left and right lentiform nucleus volumes did not differ according to group and gender ($P_4 = 0.863$).

Overall, left caudate nucleus and left lentiform nucleus volumes were higher as compared to the right in both elite athletes and sedentary individuals.

Discussion

Reaction time is a natural response reflecting the duration of time between a stimulus and the first moment of muscular response or movement and corresponds to the sum of time from the reception of an immediate and unpreceded signal and the response to that signal. Previous literature has reported higher auditory and visual reaction speed among elite athletes compared to lay individuals. Audiovisual reaction time is a significant and determining factor in many branches of sports and is known to be feasible to improve with regular training. Furthermore, shorter reactions to visual stimuli have been reported among well-trained athletes as compared to athletes with poorer training status. Furthermore, responses to auditory stimuli have been generally more rapid as compared to responses to visual stimuli,[21] similar to our observations where athletes responded to auditory stimuli faster than visual stimuli. Furthermore, in our study, athletes exhibited significantly more rapid auditory reactions than sedentary subjects. In contrast, elite athletes participating in our study also had shorter visual reaction times as compared to sedentary individuals, but the difference was insignificant. However, a larger sample size could have yielded significant differences. Similarly, these response times were shorter in male athletes as compared to sedentary males, although there were no significant differences. Interestingly, among female athletes, auditory reaction times were longer than their visual reaction times. Although the visual reaction time among female athletes was shorter than that of the

Table 3: Nucleus caudatus volume data in cm³ for athletes and sedentary individuals

Group	Gender	Right nucleus caudatus, *n* Mean±SD Median	Left nucleus caudatus, *n* Mean±SD Median	*P*
Athlete	Female	10	10	P_1=0.045*
		3.548±0.734	3.588±0.522	P_2=0.925
		3.539	3.731	P_3=0.074
	Male	9	9	P_4=0.578
		3.365±0.556	3.551±0.409	
		3.380	3.635	
Sedentary	Female	10	10	
		3.754±0.606	3.741±0.602	
		3.641	3.881	
	Male	10	10	
		3.526±0.394	3.787±0.411	
		3.571	3.922	

*$P \leq 0.05$. SD: Standard deviation

Table 4: Nucleus lentiformis volume data in cm³ for athletes and sedentary individuals

Group	Gender	Right nucleus lentiformis, *n* Mean±SD Median	Left nucleus lentiformis, *n* Mean±SD Median	*P*
Athlete	Female	10	10	P_1=0.903
		4.684±0.662	4.498±0.510	P_2=0.338
		4.751	4.337	P_3=0.477
	Male	9	9	P_4=0.863
		5.303±1.148	5.308±1.375	
		5.56640600	4.980	
Sedentary	Female	10	10	
		5.476±0.666	5.535±0.448	
		5.485	5.612	
	Male	10	10	
		5.021±0.741	5.197±0.812	
		4.974	5.134	

$P \leq 0.05$. SD: Standard deviation

sedentary female subjects, the difference was insignificant. Based on gender, female and male athletes had shorter auditory response times than sedentary female and male subjects, again with no significant differences.

The motor performance among athletes is determined by several skills such as endurance, strength, and speed. Previous experimental studies showed that motor speed is coded in the BG, sensory-motor cortex, and cerebellum. Again, a previous study of motor speed difference between strength and endurance athletes showed neurofunctional and structural differences specific to motor speed in the peripheral and central nervous systems.[6] This has led to the question whether "strength athletes" had a unique structural attribute that allowed them to perform simple foot movements much more rapidly as compared to "endurance athletes."

Several studies have assessed the correlation between BG volume, gender, and age among healthy individuals.[4,15] In our study involving right-handed elite athletes and sedentary individuals, left BG volumes were larger than right BG volumes independent of age, gender, and physical activity status. Athletes with larger right BG were found to respond more rapidly to auditory stimuli than visual stimuli. However, the volume measurements were not associated with the reaction times in sedentary individuals.

It has been previously shown that automatic motor movements are modulated by BG, and regular exercise has beneficial effects on cortical activities responsible for attention and cognition through effects that facilitate neuronal transmisyon.[22-24] Human studies also showed that putamen and the caudate nucleus play fundamental roles in performance-related processes that involve cognitive control, motor integration, and motor reaction.[7]

In the study by Chaddock *et al*.,[24] no associations were observed between putamen and caudate nucleus volumes and sports performance in children participating in aerobic fitness activities, whereas a link was observed between globus pallidus volume and physical performance, which was explained in the basis of the association between globus pallidus and efferent stimuli conveying motor instructions. Our study bears some similarity to that study in assessing the lentiform and caudate nucleus volumes. In our study, the volume of the right and left caudate nucleus was smaller among athletes than in sedentary subjects, although the difference was insignificant. On the other hand, right-handed elite athletes with larger BG volumes had shorter auditory reaction times than visual reaction times, irrespective of gender. However, our study did not aim to assess the performance among athletes. In sportive activities where hearing is a contributory factor to performance, this attribute may have positive implications.

When BG was separately evaluated, significant differences in the volume of right and left caudate nuclei were found in both groups, with significantly higher left-sided volume measurements. Again, the volume of the lentiform nucleus was higher on the left side in both groups and genders. In both groups of participants, left-sided caudate nucleus and lentiform nucleus volumes were higher as compared to right-sided volumes.

Corpus striatum is involved in the acquisition and maintenance of motor skills. Several studies have shown that motor learning induces neuronal changes in striatum.[25,26] In Park *et al*.'s study,[25] examining basketball players and healthy controls using three-dimensional MRI volumetry, morphological volume expansion was found in the striatum of basketball players as compared to

healthy controls.[25] According to the authors of that study, persistent repetition and execution of motor skills relevant to basketball as well as repeated motor performances may lead to plastic structural alterations in the human striatum. In sports such as basketball requiring double-handed coordination and visuomotor activity skills, it has been purported that putamen is responsible for the execution of complex movements such as ball driving, ball chasing, and ball throwing.[25] In the same line of thinking, we decided to compare MRI-based BG volume measurements in athletes and sedentary individuals due to their role in motor control of learned-acquired movements.

Previously, ballerinas have been reported to have lower left putamen volumes,[6] in addition to data indicating lower left caudate nucleus volumes in professional divers.[27] Furthermore, male javelin throwers and male long jumpers had higher ventral striatum volumes bilaterally as compared to controls.[28] In our study, we found statistically significant differences between right and left caudate nucleus volumes, with the latter exhibiting larger volumes. However, this difference was not statistically significant between sedentary individuals and athletes and between genders. A larger sample size could have yielded more meaningful results. The volumes of the right and left caudate nuclei were lower among athletes than in sedentary subjects, similar to the data reported in ballerinas and professional divers.

Hänggi *et al*.[26] measured age-corrected intracranial volume, right and left total gray matter volume, right and left total mid-sagittal cortical surface area, and mean cortical thickness in professional handball players versus controls and found higher BG volumes among handball players, although the difference could not reach statistical significance.[26] Furthermore, in another study assessing the association between BG volume, age, and professional training duration, no significant differences between athletes and controls could be detected for either variable. In contrast with that study, we were unable to evaluate the relation between training duration and performance, since all the elite athletes participating in our study were required to have a minimum regular training duration of 10 years. In that study, there was no information on the dominant hand. Although subjects had to use both of their hands during handball matches, information on the dominant hemisphere would have provided further insights into their findings. Due to such considerations, only elite athletes and controls with right-hand dominance were included in our study, which showed larger BG volumes on the left than on the right in both athletes and sedentary individuals, probably due to the fact that the left brain comprised the dominant hemisphere in our participants. However, there was no difference when compared with the sedentary group. In addition, the BG sizes of athletes were higher than sedentary individuals in our study, although the difference was not statistically significant. It is possible that similar studies with larger sample size may allow more meaningful conclusions on that matter.

Our results showed significantly shorter auditory reaction time than visual reaction time in athletes, suggesting a more rapid responsiveness to auditory stimuli in these individuals. Therefore, athletes might have developed concentration habits mainly for responding to auditory stimuli rather than visual stimuli during sportive activities.

Our study has several limitations. Our sample size was relatively limited due to a number of factors such as the low number of volunteering young adult elite athletes as well as the claustrophobic subjects who were unable to undergo MRI examination. Furthermore, several BG structures such as the subthalamic nucleus, nucleus accumbens, and substantia nigra were excluded from analyses due to their small size and poor image quality on MRI. Since the putamen and globus pallidus could not be readily discerned, they were collectively measured under the umbrella term of "lentiform nucleus." Furthermore, subjects who refused to perform 5 repetitions of preparatory tests and 10 consecutive repetitions of formal measurements were excluded.

Conclusion

Identification of differences between professional elite athletes and sedentary subjects is important using the volumetric evaluation technique through stereological analysis. The technique is unbiased, easy, and simple.[15,17,29-31] Assessment of the effect of motor coordination and motor movement control on BG volume changes may provide valuable information, not only for elite athletes but also for improving motor coordination in diseases affecting the neuromuscular system.[27,28] Establishing reference ranges for BG volumes and audiovisual reaction time among elite athletes may allow researchers to develop selection criteria in different fields of sports for the early identification of potential elite athletes. To the best of our knowledge, our study is the first of its kind in assessing the effect of exercise on BG volume as well as the correlation between BG volume and audiovisual reaction time.

Further cross-sectional, multidisciplinary studies comparing athletes from different branches of sports that also include volume measurements in other relevant brain structures affecting motor control (e.g., cerebellum) may shed further light on this subject. We believe that our results represent a valuable contribution to the knowledge on BG morphology in athletes and sedentary individuals and may prove to be important for sportspeople and clinicians alike.

Financial support and sponsorship

Nil.

Conflicts of interest

There are no conflicts of interest.

References

1. Saunders A, Huang KW, Sabatini BL. Globus pallidus externus neurons expressing parvalbumin interconnect the subthalamic nucleus and striatal interneurons. PLoS One 2016;11:e0149798.
2. Standring S, editor. Gray's Anatomy: The Anatomical Basis of Clinical Practice. Spain: Thirty-Ninth Edition Elsevier Ltd 2005. p. 241-74.
3. Andreasen NC, Rajarethinam R, Cizadlo T, Arndt S, Swayze VW 2nd, Flashman LA, *et al*. Automatic atlas-based volume estimation of human brain regions from MR images. J Comput Assist Tomogr 1996;20:98-106.
4. Gocmen-Mas N, Pelin C, Canan S, Yazici AC, Zagyapan R, Senan S, *et al*. Stereological evaluation of volumetric asymmetry in healthy human cerebellum. Surg Radiol Anat 2009;31:177-81.
5. Mas N, Senan S, Firat M, Tuncel M, Basar R. Evaluation of human brain volume by the tracing technique. Neurosciences (Riyadh) 2009;14:96-7.
6. Hänggi J, Koeneke S, Bezzola L, Jäncke L. Structural neuroplasticity in the sensorimotor network of professional female ballet dancers. Hum Brain Mapp 2010;31:1196-206.
7. Aron AR, Poldrack RA, Wise SP, editors. Cognition: Basal ganglia role. In: Encyclopedia of Neuroscience. Vol 2. Oxford: Academic Press; 2009. p. 1069-77.
8. Bonelli RM, Kapfhammer HP, Pillay SS, Yurgelun-Todd DA. Basal ganglia volumetric studies in affective disorder: What did we learn in the last 15 years? J Neural Transm (Vienna) 2006;113:255-68.
9. Barber R, McKeith I, Ballard C, O'Brien J. Volumetric MRI study of the caudate nucleus in patients with dementia with Lewy bodies, Alzheimer's disease, and vascular dementia. J Neurol Neurosurg Psychiatry 2002;72:406-7.
10. Booij J, Tissingh G, Boer GJ, Speelman JD, Stoof JC, Janssen AG, *et al*. [123I]FP-CIT SPECT shows a pronounced decline of striatal dopamine transporter labelling in early and advanced Parkinson's disease. J Neurol Neurosurg Psychiatry 1997;62:133-40.
11. Caslake R, Moore JN, Gordon JC, Harris CE, Counsell C. Changes in diagnosis with follow-up in an incident cohort of patients with parkinsonism. J Neurol Neurosurg Psychiatry 2008;79:1202-7.
12. Crossman AR. Primate models of dyskinesia: The experimental approach to the study of basal ganglia-related involuntary movement disorders. Neuroscience 1987;21:1-40.
13. Geng DY, Li YX, Zee CS. Magnetic resonance imaging-based volumetric analysis of basal ganglia nuclei and substantia nigra in patients with Parkinson's disease. Neurosurgery 2006;58:256-62.
14. Swann C, Moran A, Piggott D. Defining elite athletes: Issues in the study of expert performance in sport psychology. Psychol Sport Exerc 2015;16:3-14.
15. Acer N, Sahin B, Usanmaz M, Tatoğlu H, Irmak Z. Comparison of point counting and planimetry methods for the assessment of cerebellar volume in human using magnetic resonance imaging: A stereological study. Surg Radiol Anat 2008;30:335-9.
16. Mas N. Evaluation of Cerebrum-Diencephalon and Cerebellum Volumes and Total Intracranial Volume In Healthy Individuals By Magnetic Resonance Imaging Method. Hacettepe University Institute of Health Sciences Doctoral Thesis, Turkey; 2005.
17. Roberts N, Puddephat MJ, McNulty V. The benefit of stereology for quantitative radiology. Br J Radiol 2000;73:679-97.
18. Sahin B, Ergur H. Assessment of the optimum section thickness for the estimation of liver volume using magnetic resonance images: A stereological gold standard study. Eur J Radiol 2006;57:96-101.
19. Sahin B, Acer N, Sonmez OF, Emirzeoglu M, Basaloglu H, Uzun A, *et al*. Comparison of four methods for the estimation of intracranial volume: A gold standard study. Clin Anat 2007;20:766-73.
20. Ekinci N, Acer N, Akkaya A, Sankur S, Kabadayi T, Sahin B. Volumetric evaluation of the relations among the cerebrum, cerebellum and brain stem in young subjects: A combination of stereology and magnetic resonance imaging. Surg Radiol Anat 2008;30:489-94.
21. Bompa TO, editor. Theory and Methodology of Training. 2nd ed. Dubuque, Lowa: Kendall Hunt Publishing Co; 1990. p. 22-4.
22. Budde H, Voelcker-Rehage C, Pietrabyk-Kendziorra S, Ribeiro P, Tidow G. Acute coordinative exercise improves attentional performance in adolescents. Neurosci Lett 2008;441:219-23.
23. Budde H, Brunelli A, Machado S, Velasques B, Ribeiro P, Arias-Carrión O, *et al*. Intermittent maximal exercise improves attentional performance only in physically active students. Arch Med Res 2012;43:125-31.
24. Chaddock L, Erickson KI, Prakash RS, VanPatter M, Voss MW, Pontifex MB, *et al*. Basal ganglia volume is associated with aerobic fitness in preadolescent children. Dev Neurosci 2010;32:249-56.
25. Park IS, Lee KJ, Han JW, Lee NJ, Lee WT, Park KA, *et al*. Basketball training increases striatum volume. Hum Mov Sci 2011;30:56-62.
26. Hänggi J, Langer N, Lutz K, Birrer K, Mérillat S, Jäncke L. Structural brain correlates associated with professional handball playing. PLoS One 2015;10:e0124222.
27. Wei G, Luo J, Li Y. Brain structure in diving players on MR imaging studied with voxel-based morphometry. Prog Natural Sci 2009;19:1397-402.
28. Taubert M, Wenzel U, Draganski B, Kiebel SJ, Ragert P, Krug J, *et al*. Investigating Neuroanatomical features in top athletes at the single subject level. PLoS One 2015;10:e0129508.
29. Karabekir HS, Akosman MS, Gocmen-Mas N, Aksu F, Edizer M, Lenger OF, *et al*. The volume of experimental design cerebellum: Stereological microanatomic study. J Craniofac Surg 2014;25:1492-4.
30. Gocmen Mas N, Cirpan S, Aksu F, Yonguc Demirci GN, Lafci Fahrioglu S, Durmaz O, *et al*. Comparison of three methods used for estimating area of foramen magnum. J Craniofac Surg 2018;29:792-5.
31. Gocmen-Mas N, Akosman MS, Karabekir S, Turan Isik A, Mas MR, Aksu F. The volume prediction on the experimental design hippocampus using stereological method. J Craniofac Surg 2014;25:1501-3.

Case Report

Accessory Abductor Pollicis Longus: An Anatomical Case Report

Abstract

An accessory abductor pollicis longus (APL) tendon is present in more than 80% of people, but a separate muscle belly is present in only 20% of people. The present article documented the atypical anatomical variation of APL found during routine dissection. The muscle had three bellies and three tendons with unique bifurcation and attachments in the right upper limb of a 52-year-old male cadaver. The variation of APL is clinically important for surgeons doing flap surgeries, tendon transfer, for surgeons dealing with De Quervain's tenosynovitis, and in any operative procedure involving the forearm and hand. Multiple APL tendons can be regarded as a functional advantage since injured tendons can be compensated by healthy ones. In addition, knowledge of the anatomy of the area is essential for treating this condition surgically by performing a tendon release after conservative treatment has failed.

Keywords: *Abductor pollicis longus, accessory abductor pollicis longus, case report, De Quervain's tenosynovitis*

Amarjeet Kaur

Department of Rachana Sharira, Sumandeep Ayurved Medical College and Hospital, Sumandeep Vidyapeeth Deemed to be University, Vadodara, Gujarat, India

Introduction

The abductor pollicis longus (APL) is one of the deep muscles of the extensor compartment of the forearm. APL arises from the posterior surface of shafts of the radius and ulna and gets inserted into the lateral side of the base of the first metacarpal bone.[1] Variation of APL with supernumerary tendons is common. Very few studies are found on aberrant bellies with accessory tendons of APL. The variation of APL is clinically important for surgeons doing flap surgeries, tendon transfer, for surgeons dealing with De Quervain's tenosynovitis, and in any operative procedure involving the forearm and hand. This study will help surgeons in identifying the cause of diseases related to pain in the thumb. This article reports a case of accessory APL (AAPL) with supernumerary bellies and tendons in the right upper limb of a 52-year-old male cadaver.

Case Report

An abnormal APL muscle was encountered during the dissection of the right upper limb of a 52-year-old male cadaver. Dead body donation NOC declared by relatives has been obtained.

Dissection is done using the standard protocol. A vertical incision is made with 22 number surgical blade at the back of the forearm. With the help of tooth forceps and 22 number surgical blade the skin, superficial fascia and deep fascia are removed to expose the extensor retinaculum (ER), superficial group of muscles and deep group of muscles of extensor compartment of the forearm.

The first compartment (C1) of ER is opened to expose the tendons of APL and extensor pollicis brevis (EPB). The EPB has its normal origin and insertion. While tracing the tendon of APL toward its origin, it is observed that it has three accessory tendons and three aberrant bellies [Figure 1].

Accessory APL had fleshy origin from the posterior surface of the shaft of the radius and ulna and the adjoining interosseous membrane. The muscle runs oblique and laterally from an apex formed by the origin of the anconeus and supinator. The measurements were taken with the help of vernier caliper and measuring tape.

The muscle in the midway bifurcates at a distance of 6.5 cm from its origin into two bellies – upper belly (UB) and lower belly (LB). The LB again divides at a distance of 11.5 cm from its origin into LB1 and LB2. The muscle gets inserted through three tendons – 1 arising from UB of length 9 cm inserts into trapezium and 2 slips from

How to cite this article: Kaur A. Accessory abductor pollicis longus: An anatomical case report. J Anat Soc India 2024;73:284-6.

This is an open access journal, and articles are distributed under the terms of the Creative Commons Attribution-NonCommercial-ShareAlike 4.0 License, which allows others to remix, tweak, and build upon the work non-commercially, as long as appropriate credit is given and the new creations are licensed under the identical terms.

For reprints contact: WKHLRPMedknow_reprints@wolterskluwer.com

Article Info

Received: 22 July 2024
Revised: 22 July 2024
Accepted: 11 August 2024
Available online: 25 September 2024

Address for correspondence:
Dr. Amarjeet Kaur,
E-18, Sumandeep Quarters, Sumandeep Vidyapeeth, At Post Piparia, Ta. Waghodia, Vadodara - 391 760, Gujarat, India.
E-mail: amarjeet94.k@gmail.com

Access this article online

Website: https://journals.lww.com/joai
DOI: 10.4103/jasi.jasi_93_24
Quick Response Code:

© 2024 Journal of the Anatomical Society of India | Published by Wolters Kluwer - Medknow

LB1 and LB2 of length 9.5 and 8.5, respectively, insert into the first metacarpal joint. As it proceeds distally, the three tendons pass from C1 of ER. The thickness is varying in the three tendons. The width of AAPL T1 is 0.4 cm, AAPL T2 is 0.2 cm and AAPL T3 is 0.4 cm, respectively. APL lies close to the radial nerve [Figures 2, 3 and Table 1].

EPB has its normal origin and insertion. It is noted that it has a very thin tendon as compared to APL and EPL. The left upper limb did not exhibit any obvious muscular variations. The three tendons of AAPL and EPB are crowded in a very confined space of the first compartment of ER.

The APL and EPB form the lateral boundary of the anatomical snuffbox. The tendon of APL can be seen and felt at the radial aspect of the anatomical snuffbox when the thumb and wrist are abducted against resistance at the carpometacarpal joint[2] [Figure 4].

Discussion

The effect of anatomical variation in the first compartment of ER can lead to the risk of developing De Quervain's Disease (DQD), research on these variations could help to explain why some people are predisposed to this disorder more than others. Further study can be done in finding a relation between DQD with the occupation of the diseased and the presence of any notable anatomical variation of AAPL.

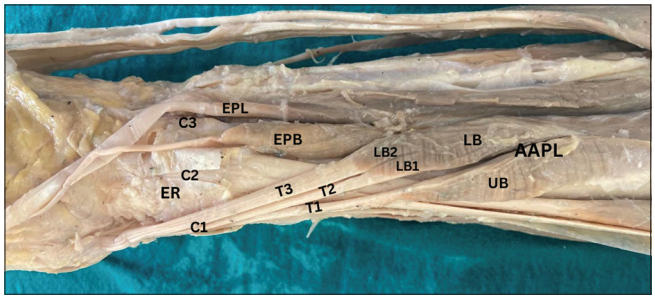

Figure 1: Bifurcation of accessory abductor pollicis longus with supernumerary bellies and tendons: UB: Upper belly, LB: Lower belly, LB1: Lower belly1, LB2: Lower belly 2, T1: Tendon 1, T1: Tendon 2, T1: Tendon 3, ER: Externsor retinaculum, C1: Compartment 1, C2: Compartment 2, C3: Compartment 3, EPB: Extensor pollicis brevis, EPL: Extensor pollicis longus

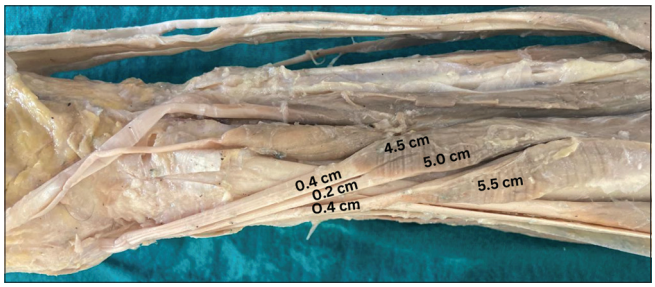

Figure 3: Width of tendons of accessory abductor pollicis longus (AAPL) (T1-0.4 cm, T2-0.2 cm, T3-0.4 cm) and Length of bellies of accessory abductor pollicis longus (UB-5.5 cm, LB1-5.0 cm, LB2-4.5 cm)

During embryological development, somites derived from skeletal muscle cells differentiate, proliferate, and migrate to limb buds. The associated connective tissue determines the muscle morphology and various attachments.[3,4]

During embryological development, the APL is divided into three separate slips of tendon mainly – dorsal, middle, and ventral.[5] The dorsal slip inserts on the first metacarpal bone, the middle slips interests to the trapezium bone, and the palmar slip inserts to opponens pollicis muscle.[6,7] As the length of the fetus increases to 50 mm, opponens pollicis is covered by fascia and thus loses contact with APL palmar slip. The dorsal tendon is attached to the first metacarpal bone. The middle tendon shows variation, it

Table 1: Parameter of bellies and tendons of accessory abductor pollicis longus

Parameter	Distance from origin (cm)	Length (cm)	Width (cm)
Upper belly	6.5	5.5	-
Lower belly 1	6.5	5.0	-
Lower belly 2	11.5	4.5	-
Tendon 1	-	9.0	0.4
Tendon 2	-	9.5	0.2
Tendon 3	-	8.5	0.4

Figure 2: Length of tendons of accessory abductor pollicis longus (AAPL), Black circle indicates the insertion of AAPL into trapezium and 1st metacarpal joint. EPL: Extensor pollicis longus, EPB: Extensor pollicis brevis

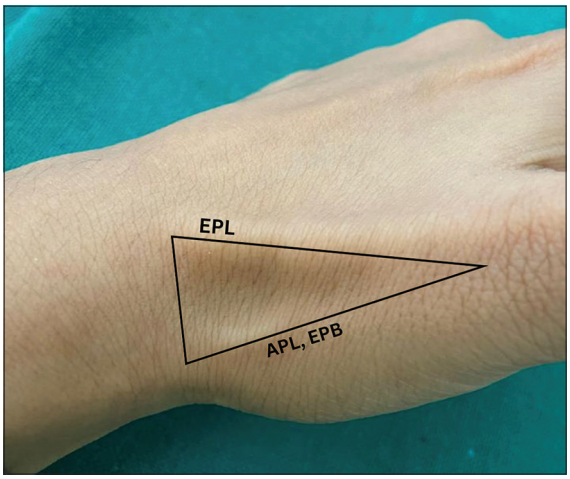

Figure 4: Anatomical snuff box: Lateral boundary is formed by abductor pollicis longus (APL) and extensor pollicis brevis, Medial boundary is formed by APL. EPL: Extensor pollicis longus, APL: Abductor pollicis longus, EPB: Extensor pollicis brevis

may completely regress or may fuse with the ventral or dorsal APL tendon having various insertion points.[8]

Normally it is seen that only one tendon of APL and EPB pass from the first compartment. But here, it was found that three tendons are passing from the first compartment resulting in compression and friction between these tendons resulting in swelling and inflammation developing DQD.

The prevalence of DQD is more common in women than in men mostly seen in people with occupations related to typing, gardening, knitting, or playing certain sports such as golf or tennis.[9] DQD causes pain and tenderness in the lateral aspect of the wrist which may radiate to the forearm. It also causes swelling and inflammation resulting in restricted movement of the thumb and grasping objects.[10]

Multiple APL tendons can be regarded as a functional advantage since injured tendons can be compensated by healthy ones. Awareness of variations of APL is helpful in reconstructive surgeries of the forearm and hand. The number and length of APL accessory tendons play an important role in the etiology of De Quervain's stenosing tenovaginitis. Movements of the thumb are carried by extrinsic and intrinsic muscles. Awareness of APL muscle variants could, therefore, offer an effective solution for the appropriate recognition of these accessory tendons.[11]

The presence of multiple tendons of AAPL can be considered functional advantage for people suffering from DQD. Variation of APL is important for surgeons doing flag surgeries and reconstructive surgeries in DQD. Knowledge of variations in the anatomy of AAPL will be helpful in doing surgeries, in which conservative treatment has failed.

Acknowledgment

I would like to acknowledge the Department of Anatomy.

Financial support and sponsorship

Nil.

Conflicts of interest

There are no conflicts of interest.

References

1. Chaurasia BD. Human Anatomy. Vol. 1. New Delhi: CBS Publishers & Distributers Pvt Ltd.; 2020. p. 149.
2. Standring S. Gray's Anatomy. China: Elsevier Limited; 2021. p. 947.
3. Moore KL, Persaud TV. The Developing Human: Clinically Oriented Embryology. Philadelphia: Saunders Elsevier; 2008.
4. Mathew SJ, Hansen JM, Merrell AJ, Murphy MM, Lawson JA, Hutcheson DA, *et al.* Connective tissue fibroblasts and Tcf4 regulate myogenesis. Development 2011;138:371-84.
5. Nayak SR, Krishnamurthy A, Pai MM, Prabhu LV, Ramanathan LA, Ganesh Kumar C, *et al.* Multiple variations of the extensor tendons of the forearm. Rom J Morphol Embryol 2008;49:97-100.
6. Cihák R. Connections of the abductor pollicis longus and brevis in the ontogenesis of the human hand. Folia Morphol (Praha) 1972;20:102-5.
7. Mehta V, Arora J, Suri RK, Rath G. A rare quadruplicate arrangement of abductor pollicis longus tendons: Anatomical and clinical relevance. Clinics (Sao Paulo) 2009;64:153-5.
8. El-Beshbishy RA, Abdel-Hamid GA. Variations of the abductor pollicis longus tendon: An anatomic study. Folia Morphol (Warsz) 2013;72:161-6.
9. Tendon trouble in the hands: De Quervain's tenosynovitis and trigger finger. Women are more likely than men to develop these painful conditions. Harv Womens Health Watch 2010;17:4-5.
10. Das S. A Manual on Clinical Surgery. Kolkata: Das S Publisher; 2019. p. 145.
11. Mehta V, Arora J, Suri RK, Rath G. A rare quadruplicate arrangement of abductor pollicis longus tendons: Anatomical and clinical relevance. Clinics (Sao Paulo) 2009;64:153-5.

Case Report

Circumaortic Left Renal Vein: An Uncommon Variation

Abstract

Circumaortic left renal vein is an uncommon developmental anomaly, usually detected incidentally however having significant clinical implications. It is important from surgical point of view as well as for any relevant endovascular intervention procedure. Here is a case of type-1 circumaortic renal vein detected incidentally on Computed Tomography angiography study which was primarily done for evaluation of extrahepatic portal vein obstruction in this patient.

Keywords: *Aortic collar, circumaortic, circumaortic left renal vein, computed tomography, left renal vein, preaortic, retroaortic*

Anil Kumar Singh

Department of Radiodiagnosis, Sanjay Gandhi Postgraduate Institute of Medical Sciences, Lucknow, Uttar Pradesh, India

Introduction

Different types of variations of the left renal vein have been described in the literature. Among these overall uncommon entities, more commonly seen include multiple left renal veins (LRVs), single retroaortic LRV, and circumaortic LRV. Circumaortic LRV (CLRV) forms a vascular ring (collar) around the abdominal aorta. Most of the time, these are detected unplanned on imaging studies and autopsies, and sometimes peroperatively. Initial studies were mainly cadaveric/autopsy based. These variations carry significant clinical implications from surgery as well as the interventional point of view. Furthermore, compression of the retroaortic LRV component may lead to renal venous hypertension, which may cause hematuria, and, in males, varicocele.[1-3] This patient did not have any urinary complaints. In this case report, incidentally detected type-1 CLRV is being described and discussed with its clinical implications.

Case Report

This case refers to a young female patient who came with complaints of progressively increasing abdominal distension with the feeling of a lump on the left side for 1 year, accompanied by continuous discomfort/unease in the abdomen. Ultrasonography revealed portal cavernoma with splenomegaly and no ascites. Further evaluation was done with computed tomography (CT) angiography, which revealed features of extrahepatic portal vein obstruction (EHPVO), including portal cavernoma, perigastric-splenic hilar collaterals, gastro-esophageal varices, and splenomegaly. There was no dominant gastrorenal shunt.

Apart from features of EHPVO, analysis of CT images also revealed two left renal veins instead of the single left renal vein (LRV), i.e., superior and inferior LRV. Superior LRV was larger in diameter (dominant) and was seen in the usual expected location of the left renal vein. It was coursing from the left renal hilum to the inferior vena cava, passing anterior to the aorta (preaortic course). Inferior LRV was seen coursing oblique inferiorly from the left renal hilum, passing between the aorta and vertebra, to join IVC at the lower level (retro-aortic course). At the left renal hilum, pre- and retro-aortic veins were joining together to form a common trunk of CLRV. Pre- and retroaortic LRV together formed a loop or collar around the abdominal aorta [Figures 1 and 2].

Discussion

Circumaortic LRV is a developmental anomaly. It is one of three well-described anomalies of LRV, the other two being multiple renal veins and retro-aortic renal veins. Embryologically, there are two primitive renal veins on the left side– ventral and dorsal. Normally, the dorsal vein regresses, and the ventral vein develops into LRV proper. Failure

How to cite this article: Singh AK. Circumaortic left renal vein: An uncommon variation. J Anat Soc India 2024;73:287-9.

This is an open access journal, and articles are distributed under the terms of the Creative Commons Attribution-NonCommercial-ShareAlike 4.0 License, which allows others to remix, tweak, and build upon the work non-commercially, as long as appropriate credit is given and the new creations are licensed under the identical terms.

For reprints contact: WKHLRPMedknow_reprints@wolterskluwer.com

Article Info

Received: 12 June 2024
Accepted: 11 August 2024
Available online: 25 September 2024

Address for correspondence:
Dr. Anil Kumar Singh, Department of Radiodiagnosis, Sanjay Gandhi Postgraduate Institute of Medical Sciences, Lucknow - 226 014, Uttar Pradesh, India.
E-mail: singh.anil.kr01@gmail.com

Access this article online

Website: https://journals.lww.com/joai
DOI: 10.4103/jasi.jasi_85_24
Quick Response Code:

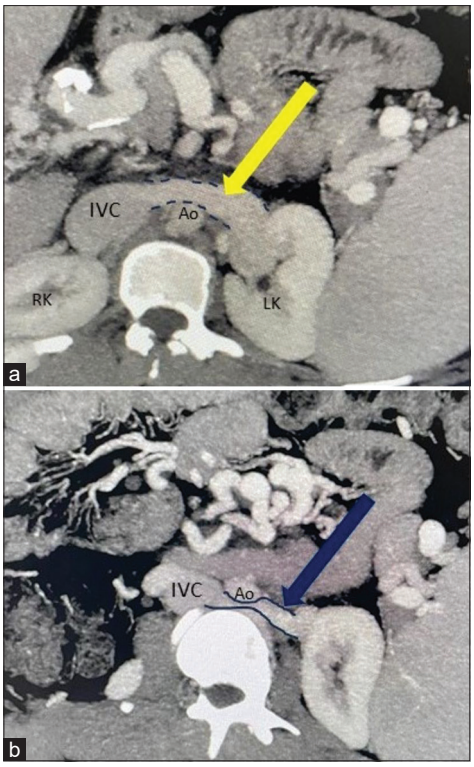

Figure 1: Axial images from the venous phase of computed tomography angiography study showing two left renal veins superior ([a] yellow arrow, dotted outline) and inferior ([b] blue arrow, solid outline) coursing anterior and posterior to aorta respectively. IVC: Inferior vena cava; Ao: Aorta; RK: Right kidney; LK: Left kidney

of regression of primitive dorsal renal vein leads to circumaortic LRV forming a vascular ring around the abdominal aorta.[1-3] There are three types of CLRV: Type-1 with a preaortic and a retro-aortic vein joining together at the renal hilum; Type-2 where preaortic and retro-aortic vein have parallel separate course till renal hilum without forming common trunk; Type-3 characterized by multiple anastomosis between pre- and retro-aortic vein or multiple veins.[3,4] In the case presented here, it was type-1 CLRV.

The varying prevalence of this developmental anomaly has been reported. Many studies have reported its prevalence <1%. Old cadaveric studies reported higher prevalence (0.2%–30%). Few studies in recent decades have reported a median prevalence of 5% to 7%. In cadaveric studies, prevalence has been found to be higher.[3-5]

Although most of the time, it is detected incidentally, it is important clinically. Both from the surgical point of view as well as for endovascular procedures, it is important to be aware of it if present in a given case. Compression of retro-aortic component of CLRV, may be the cause of hematuria due to venous hypertension, though it is more likely in other variants, i.e., isolated retroaortic LRV. Furthermore, if missed and injured inadvertently during retroperitoneal or renal surgery, it may lead to complications such as hematuria. Similarly, missing it may

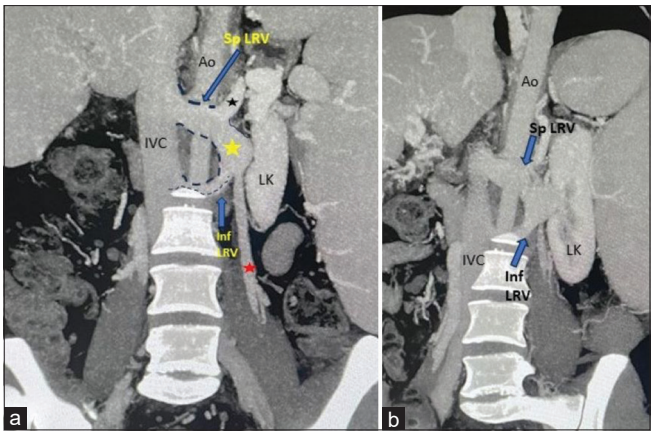

Figure 2: Coronal reformatted images (a and b) from the venous phase of computed tomography angiography study showing well outlined superior and inferior left renal vein (LRV) joining together to form the common trunk of circumaortic LRV (CLRV) at the renal hilum, i.e., type-1 CLRV) (yellow star). IVC: Inferior vena cava, Ao: Aorta, Sp LRV: Superior left renal vein, Inf LRV: Superior left renal vein, black star: left inferior phrenic vein joining Sp LRV, Red star: left gonadal vein joining common trunk of CLRV. LK: Left kidney

lead to a failed endovascular procedure. Preprocedural knowledge of its presence will avoid complications and misses.[6,7]

If a case of EHPVO suffers from variceal bleeding, endoscopic management of varices is one of the commonly offered treatment options. However, if such patients also have developed a dominant gastrorenal shunt, the endovascular procedure in the form of balloon occluded retrograde transvenous obliteration (BRTO) of varices offers an additional established treatment option.[8] BRTO procedure requires cannulation of LRV; if it is CLRV, cannulation of both pre- and retroaortic veins would be required to define shunt and avoid treatment failure. The case presented here did not have a dominant gastrorenal shunt.

Preoperative/preintervention contrast-enhanced CT or MRI studies should be analyzed in detail to look for variant vascular anatomy and the analysis for the primary disease process.

Conclusion

Anatomical variations in the left renal vein, including CLRV, though uncommon, have important clinical implications. Imaging studies such as CECT and MRI can provide information about their presence, and preprocedural knowledge about these variations has the potential to avoid complications and therapeutic failures.

Declaration of patient consent

The authors certify that they have obtained all appropriate patient consent forms. In the form, the patient(s) has/have given his/her/their consent for his/her/their images and other clinical information to be reported in the journal. The patients understand that their names and initials will not be published and due efforts will be made to conceal their identity, but anonymity cannot be guaranteed.

Financial support and sponsorship

Nil.

Conflicts of interest

There are no conflicts of interest.

References

1. Provenza CG, Boutrous M, Amankwah KS. Incidental finding of circumaortic left renal vein aneurysm on imaging. J Vasc Surg Cases Innov Tech 2022;8:711-4.
2. Haładaj R, Polguj M, Wysiadecki G, Żytkowski A, Topol M. Circumaortic left renal vein (circumaortic renal collar) associated with the presence of vascular anomalies: A case series and review of literature. Folia Morphol (Warsz) 2019;78:437-43.
3. İsmailoğlu P, Tanyeli E, Üzel M, Soyluoğlu Aİ, Kahraman Yildirim G. Double left renal vein encircling the aorta (renal collar). Cerrahpaşa Med J 2020;44:112-4.
4. Hashizume K, Taniguchi S, Ariyoshi T, Hisata Y, Tanigawa K, Miura T, *et al.* Circumaortic left renal vein associated with juxtarenal abdominal aortic aneurysm. Ann Vasc Dis 2013;6:658-61.
5. Satyapal KS, Kalideen JM, Haffejee AA, Singh B, Robbs JV. Left renal vein variations. Surg Radiol Anat 1999;21:77-81.
6. Nam JK, Park SW, Lee SD, Chung MK. The clinical significance of a retroaortic left renal vein. Korean J Urol 2010;51:276-80.
7. Wang W, Padilla R, Padilla E, Hernandez M, Kumar S, Lall C. Two rare cases of circumaortic left renal vein with double retroaortic limbs and its procedural implications. Radiol Case Rep 2024;19:48-52.
8. Sabri SS, Swee W, Turba UC, Saad WE, Park AW, Al-Osaimi AM, *et al.* Bleeding gastric varices obliteration with balloon-occluded retrograde transvenous obliteration using sodium tetradecyl sulfate foam. J Vasc Interv Radiol 2011;22:309-16.

The Editorial Process

A manuscript will be reviewed for possible publication with the understanding that it is being submitted to Journal of the Anatomical Society of India alone at that point in time and has not been published anywhere, simultaneously submitted, or already accepted for publication elsewhere. The journal expects that authors would authorize one of them to correspond with the Journal for all matters related to the manuscript. All manuscripts received are duly acknowledged. On submission, editors review all submitted manuscripts initially for suitability for formal review. Manuscripts with insufficient originality, serious scientific or technical flaws, or lack of a significant message are rejected before proceeding for formal peer-review. Manuscripts that are unlikely to be of interest to the Journal of the Anatomical Society of India readers are also liable to be rejected at this stage itself.

Manuscripts that are found suitable for publication in Journal of the Anatomical Society of India are sent to two or more expert reviewers. During submission, the contributor is requested to provide names of two or three qualified reviewers who have had experience in the subject of the submitted manuscript, but this is not mandatory. The reviewers should not be affiliated with the same institutes as the contributor/s. However, the selection of these reviewers is at the sole discretion of the editor. The journal follows a double-blind review process, wherein the reviewers and authors are unaware of each other's identity. Every manuscript is also assigned to a member of the editorial team, who based on the comments from the reviewers takes a final decision on the manuscript. The comments and suggestions (acceptance/ rejection/ amendments in manuscript) received from reviewers are conveyed to the corresponding author. If required, the author is requested to provide a point by point response to reviewers' comments and submit a revised version of the manuscript. This process is repeated till reviewers and editors are satisfied with the manuscript.

Manuscripts accepted for publication are copy edited for grammar, punctuation, print style, and format. Page proofs are sent to the corresponding author. The corresponding author is expected to return the corrected proofs within three days. It may not be possible to incorporate corrections received after that period. The whole process of submission of the manuscript to final decision and sending and receiving proofs is completed online. To achieve faster and greater dissemination of knowledge and information, the journal publishes articles online as 'Ahead of Print' immediately on acceptance.

Clinical trial registry

Journal of the Anatomical Society of India favors registration of clinical trials and is a signatory to the Statement on publishing clinical trials in Indian biomedical journals. Journal of the Anatomical Society of India would publish clinical trials that have been registered with a clinical trial registry that allows free online access to public. Registration in the following trial registers is acceptable: http://www.ctri.in/; http://www.actr.org.au/; http://www.clinicaltrials.gov/; http://isrctn.org/; http://www.trialregister.nl/trialreg/index.asp; and http://www.umin.ac.jp/ctr. This is applicable to clinical trials that have begun enrollment of subjects in or after June 2008. Clinical trials that have commenced enrollment of subjects prior to June 2008 would be considered for publication in Journal of the Anatomical Society of India only if they have been registered retrospectively with clinical trial registry that allows unhindered online access to public without charging any fees.

Authorship Criteria

Authorship credit should be based only on substantial contributions to each of the three components mentioned below:

1. Concept and design of study or acquisition of data or analysis and interpretation of data;
2. Drafting the article or revising it critically for important intellectual content; and
3. Final approval of the version to be published.

Participation solely in the acquisition of funding or the collection of data does not justify authorship. General supervision of the research group is not sufficient for authorship. Each contributor should have participated sufficiently in the work to take public responsibility for appropriate portions of the content of the manuscript. The order of naming the contributors should be based on the relative contribution of the contributor towards the study and writing the manuscript. Once submitted the order cannot be changed without written consent of all the contributors. The journal prescribes a maximum number of authors for manuscripts depending upon the type of manuscript, its scope and number of institutions involved (vide infra). The authors should provide a justification, if the number of authors exceeds these limits.

Contribution Details

Contributors should provide a description of contributions made by each of them towards the manuscript. Description should be divided in following categories, as applicable: concept, design, definition of intellectual content, literature search, clinical studies, experimental studies, data acquisition, data analysis, statistical analysis, manuscript preparation, manuscript editing and manuscript review. Authors' contributions will be printed along with the article. One or more author should take responsibility for the integrity of the work as a whole from inception to published article and should be designated as 'guarantor'.

© 2024 Journal of the Anatomical Society of India | Published by Wolters Kluwer - Medknow

Conflicts of Interest/ Competing Interests

All authors of must disclose any and all conflicts of interest they may have with publication of the manuscript or an institution or product that is mentioned in the manuscript and/or is important to the outcome of the study presented. Authors should also disclose conflict of interest with products that compete with those mentioned in their manuscript.

Submission of Manuscripts

All manuscripts must be submitted on-line through the website https://review.jow.medknow.com/jasi. First time users will have to register at this site. Registration is free but mandatory. Registered authors can keep track of their articles after logging into the site using their user name and password.

- If you experience any problems, please contact the editorial office by e-mail at editor@jasi.org.in

The submitted manuscripts that are not as per the "Instructions to Authors" would be returned to the authors for technical correction, before they undergo editorial/ peer-review. Generally, the manuscript should be submitted in the form of two separate files:

[1] Title Page/First Page File/covering letter:

This file should provide

1. The type of manuscript (original article, case report, review article, Letter to editor, Images, etc.) title of the manuscript, running title, names of all authors/ contributors (with their highest academic degrees, designation and affiliations) and name(s) of department(s) and/ or institution(s) to which the work should be credited, . All information which can reveal your identity should be here. Use text/rtf/doc files. Do not zip the files.
2. The total number of pages, total number of photographs and word counts separately for abstract and for the text (excluding the references, tables and abstract), word counts for introduction + discussion in case of an original article;
3. Source(s) of support in the form of grants, equipment, drugs, or all of these;
4. Acknowledgement, if any. One or more statements should specify 1) contributions that need acknowledging but do not justify authorship, such as general support by a departmental chair; 2) acknowledgments of technical help; and 3) acknowledgments of financial and material support, which should specify the nature of the support. This should be included in the title page of the manuscript and not in the main article file.
5. If the manuscript was presented as part at a meeting, the organization, place, and exact date on which it was read. A full statement to the editor about all submissions and previous reports that might be regarded as redundant publication of the same or very similar work. Any such work should be referred to specifically, and referenced in the new paper. Copies of such material should be included with the submitted paper, to help the editor decide how to handle the matter.
6. Registration number in case of a clinical trial and where it is registered (name of the registry and its URL)
7. Conflicts of Interest of each author/ contributor. A statement of financial or other relationships that might lead to a conflict of interest, if that information is not included in the manuscript itself or in an authors' form
8. Criteria for inclusion in the authors'/ contributors' list
9. A statement that the manuscript has been read and approved by all the authors, that the requirements for authorship as stated earlier in this document have been met, and that each author believes that the manuscript represents honest work, if that information is not provided in another form (see below); and
10. The name, address, e-mail, and telephone number of the corresponding author, who is responsible for communicating with the other authors about revisions and final approval of the proofs, if that information is not included on the manuscript itself.

[2] Blinded Article file: The main text of the article, beginning from Abstract till References (including tables) should be in this file. The file must not contain any mention of the authors' names or initials or the institution at which the study was done or acknowledgements. Page headers/ running title can include the title but not the authors' names. Manuscripts not in compliance with the Journal's blinding policy will be returned to the corresponding author. Use rtf/doc files. Do not zip the files. **Limit the file size to 1 MB.** Do not incorporate images in the file. If file size is large, graphs can be submitted as images separately without incorporating them in the article file to reduce the size of the file. The pages should be numbered consecutively, beginning with the first page of the blinded article file.

[3] Images: Submit good quality color images. **Each image should be less than 2 MB in size.** Size of the image can be reduced by decreasing the actual height and width of the images (keep up to 1600 x 1200 pixels or 5-6 inches). Images can be submitted as jpeg files. Do not zip the files. Legends for the figures/images should be included at the end of the article file.

[4] The contributors' / copyright transfer form (template provided below) has to be submitted in original with the signatures of all the contributors within two weeks of submission via courier, fax or email as a scanned image. Print ready hard copies of the images (one set) or digital images should be sent to the journal office at the time of submitting revised manuscript. High resolution images (up to 5 MB each) can be sent by email.

Contributors' form / copyright transfer form can be submitted online from the authors' area on https://review.jow.medknow.com/jasi.

Preparation of Manuscripts

Manuscripts must be prepared in accordance with "Uniform requirements for Manuscripts submitted to Biomedical Journals" developed by the International Committee of Medical Journal Editors (October 2008). The uniform requirements and specific requirement of Journal of the Anatomical Society of India are summarized below. Before submitting a manuscript, contributors are requested to check for the latest instructions available. Instructions are also available from the website of the journal (www.jasi.org.in) and from the manuscript submission site https://review.jow.medknow.com/jasi.

Journal of the Anatomical Society of India accepts manuscripts written in American English.

Copies of any permission(s)

It is the responsibility of authors/ contributors to obtain permissions for reproducing any copyrighted material. A copy of the permission obtained must accompany the manuscript. Copies of any and all published articles or other manuscripts in preparation or submitted elsewhere that are related to the manuscript must also accompany the manuscript.

Types of Manuscripts

Original articles:

These include randomized controlled trials, intervention studies, studies of screening and diagnostic test, outcome studies, cost effectiveness analyses, case-control series, and surveys with high response rate. The text of original articles amounting to up to 3000 words (excluding Abstract, references and Tables) should be divided into sections with the headings Abstract, Key-words, Introduction, Material and Methods, Results, Discussion and Conclusion, References, Tables and Figure legends.

An abstract should be in a structured format under following heads: **Introduction, Material and Methods, Results,** and **Discussion and Conclusion.**

Introduction: State the purpose and summarize the rationale for the study or observation.

Material and Methods: It should include and describe the following aspects:

Ethics: When reporting studies on human beings, indicate whether the procedures followed were in accordance with the ethical standards of the responsible committee on human experimentation (institutional or regional) and with the Helsinki Declaration of 1975, as revised in 2000 (available at http://www.wma.net/e/policy/17-c_e.html). For prospective studies involving human participants, authors are expected to mention about approval of (regional/ national/ institutional or independent Ethics Committee or Review Board, obtaining informed consent from adult research participants and obtaining assent for children aged over 7 years participating in the trial. The age beyond which assent would be required could vary as per regional and/ or national guidelines. Ensure confidentiality of subjects by desisting from mentioning participants' names, initials or hospital numbers, especially in illustrative material. When reporting experiments on animals, indicate whether the institution's or a national research council's guide for, or any national law on the care and use of laboratory animals was followed. Evidence for approval by a local Ethics Committee (for both human as well as animal studies) must be supplied by the authors on demand. Animal experimental procedures should be as humane as possible and the details of anesthetics and analgesics used should be clearly stated. The ethical standards of experiments must be in accordance with the guidelines provided by the CPCSEA and World Medical Association Declaration of Helsinki on Ethical Principles for Medical Research Involving Humans for studies involving experimental animals and human beings, respectively). The journal will not consider any paper which is ethically unacceptable. A statement on ethics committee permission and ethical practices must be included in all research articles under the 'Materials and Methods' section.

Study design:

Selection and Description of Participants: Describe your selection of the observational or experimental participants (patients or laboratory animals, including controls) clearly, including eligibility and exclusion criteria and a description of the source population. *Technical information*: Identify the methods, apparatus (give the manufacturer›s name and address in parentheses), and procedures in sufficient detail to allow other workers to reproduce the results. Give references to established methods, including statistical methods (see below); provide references and brief descriptions for methods that have been published but are not well known; describe new or substantially modified methods, give reasons for using them, and evaluate their limitations. Identify precisely all drugs and chemicals used, including generic name(s), dose(s), and route(s) of administration.

Reports of randomized clinical trials should present information on all major study elements, including the protocol, assignment of interventions (methods of randomization, concealment of allocation to treatment groups), and the method of masking (blinding), based on the CONSORT Statement (http://www.consort-statement.org).

Reporting Guidelines for Specific Study Designs

Initiative	Type of Study	Source
CONSORT	Randomized controlled trials	http://www.consort-statement.org
STARD	Studies of diagnostic accuracy	http://www.consort-statement.org/stardstatement.htm
QUOROM	Systematic reviews and meta-analyses	http://www.consort- statement.org/Initiatives/MOOSE/moose.pdf statement.org/Initiatives/MOOSE/moose.pdf
STROBE	Observational studies in epidemiology	http://www.strobe-statement.org
MOOSE	Meta-analyses of observational studies in epidemiology	http://www.consort- statement.org/Initiatives/MOOSE/moose.pdf

Statistics: Whenever possible quantify findings and present them with appropriate indicators of measurement error or uncertainty (such as confidence intervals). Authors should report losses to observation (such as, dropouts from a clinical trial). When data are summarized in the Results section, specify the statistical methods used to analyze them. Avoid non-technical uses of technical terms in statistics, such as 'random' (which implies a randomizing device), 'normal', 'significant', 'correlations', and 'sample'. Define statistical terms, abbreviations, and most symbols. Specify the computer software used. Use upper italics (*P* 0.048). For all *P* values include the exact value and not less than 0.05 or 0.001. Mean differences in continuous variables, proportions in categorical variables and relative risks including odds ratios and hazard ratios should be accompanied by their confidence intervals.

Results: Present your results in a logical sequence in the text, tables, and illustrations, giving the main or most important findings first. Do not repeat in the text all the data in the tables or illustrations; emphasize or summarize only important observations. Extra- or supplementary materials and technical detail can be placed in an appendix where it will be accessible but will not interrupt the flow of the text; alternatively, it can be published only in the electronic version of the journal.

When data are summarized in the Results section, give numeric results not only as derivatives (for example, percentages) but also as the absolute numbers from which the derivatives were calculated, and specify the statistical methods used to analyze them. Restrict tables and figures to those needed to explain the argument of the paper and to assess its support. Use graphs as an alternative to tables with many entries; do not duplicate data in graphs and tables. Where scientifically appropriate, analyses of the data by variables such as age and sex should be included.

Discussion: Include summary of *key findings* (primary outcome measures, secondary outcome measures, results as they relate to a prior hypothesis); *Strengths and limitations* of the study (study question, study design, data collection, analysis and interpretation); *Interpretation and implications* in the context of the totality of evidence (is there a systematic review to refer to, if not, could one be reasonably done here and now?, what this study adds to the available evidence, effects on patient care and health policy, possible mechanisms); *Controversies* raised by this study; and *Future research directions* (for this particular research collaboration, underlying mechanisms, clinical research).

Do not repeat in detail data or other material given in the Introduction or the Results section. In particular, contributors should avoid making statements on economic benefits and costs unless their manuscript includes economic data and analyses. Avoid claiming priority and alluding to work that has not been completed. New hypotheses may be stated if needed, however they should be clearly labeled as such. About 30 references can be included. These articles generally should not have more than six authors.

Review Articles:

These are comprehensive review articles on topics related to various fields of Anatomy. The entire manuscript should not exceed 7000 words with no more than 50 references and two authors. Following types of articles can be submitted under this category:

- Newer techniques of dissection and histology
- New methodology in Medical Education
- Review of a current concept

Please note that generally review articles are by invitation only. But unsolicited review articles will be considered for publication on merit basis.

Case reports:

New, interesting and rare cases can be reported. They should be unique, describing a great diagnostic or therapeutic challenge and providing a learning point for the readers. Cases with clinical significance or implications will be given priority. These communications could be of up to 1000 words (excluding Abstract and references) and should have the following headings: Abstract (unstructured), Key-words, Introduction, Case report, Discussion and Conclusion, Reference, Tables and Legends in that order.

The manuscript could be of up to 1000 words (excluding references and abstract) and could be supported with up to 10 references. Case Reports could be authored by up to four authors.

Letter to the Editor:

These should be short and decisive observations. They should preferably be related to articles previously published in the Journal or views expressed in the journal. They should not be preliminary observations that need a later

paper for validation. The letter could have up to 500 words and 5 references. It could be generally authored by not more than four authors.

Book Review: This consists of a critical appraisal of selected books on Anatomy. Potential authors or publishers may submit books, as well as a list of suggested reviewers, to the editorial office. The author/publisher has to pay INR 10,000 per book review.

Other:

Editorial, Guest Editorial, Commentary and Opinion are solicited by the editorial board.

References

References should be *numbered* consecutively in the order in which they are first mentioned in the text (not in alphabetic order). Identify references *in text*, tables, and legends by Arabic numerals in superscript with square bracket after the punctuation *marks. References cited only* in tables or figure legends should be numbered in accordance with the sequence established by the first identification in the text of the particular table or figure. Use the style of the examples below, which are based on the formats used by the NLM *in Index Medicus*. The titles of journals *should be abbreviated* according to the style used in Index Medicus. Use complete name of the journal for non-indexed journals. Avoid using abstracts as references. Information from manuscripts submitted but not accepted should be cited in the text as "unpublished observations" with written permission from the source. Avoid citing a "personal communication" unless it provides essential information not available from a public source, in which case the name of the person and date of communication should be cited in parentheses in the text. The commonly cited types of references are shown here, for other types of references such as newspaper items please refer to ICMJE Guidelines (http://www.icmje.org or http://www.nlm.nih.gov/bsd/uniform_requirements.html).

Articles in Journals

1. Standard journal article (for up to six authors): Parija S C, Ravinder PT, Shariff M. Detection of hydatid antigen in the fluid samples from hydatid cysts by co-agglutination. Trans. R.Soc. Trop. Med. Hyg.1996; 90:255–256.
2. Standard journal article (for more than six authors): List the first six contributors followed by *et al*.

Roddy P, Goiri J, Flevaud L, Palma PP, Morote S, Lima N. *et al*., Field Evaluation of a Rapid Immunochromatographic Assay for Detection of Trypanosoma cruzi Infection by Use of Whole Blood. J. Clin. Microbiol. 2008; 46: 2022-2027.

3. Volume with supplement: Otranto D, Capelli G, Genchi C: Changing distribution patterns of canine vector borne diseases in Italy: leishmaniosis vs. dirofilariosis. Parasites & Vectors 2009; Suppl 1:S2.

Books and Other Monographs

1. Personal author(s): Parija SC. Textbook of Medical Parasitology. 3rd ed. All India Publishers and Distributors. 2008.
2. Editor(s), compiler(s) as author: Garcia LS, Filarial Nematodes In: Garcia LS (editor) Diagnostic Medical Parasitology ASM press Washington DC 2007: pp 319-356.
3. Chapter in a book: Nesheim M C. Ascariasis and human nutrition. In Ascariasis and its prevention and control, D. W. T. Crompton, M. C. Nesbemi, and Z. S. Pawlowski (eds.). Taylor and Francis,London, U.K.1989, pp. 87–100.

Electronic Sources as reference

Journal article on the Internet: Parija SC, Khairnar K. Detection of excretory *Entamoeba histolytica* DNA in the urine, and detection of *E. histolytica* DNA and lectin antigen in the liver abscess pus for the diagnosis of amoebic liver abscess. *BMC Microbiology* 2007, **7**:41. doi:10.1186/1471-2180-7-41. http://www.biomedcentral.com/1471-2180/7/41

Tables

- Tables should be self-explanatory and should not duplicate textual material.
- Tables with more than 10 columns and 25 rows are not acceptable.
- Number tables, in Arabic numerals, consecutively in the order of their first citation in the text and supply a brief title for each.
- Place explanatory matter in footnotes, not in the heading.
- Explain in footnotes all non-standard abbreviations that are used in each table.
- Obtain permission for all fully borrowed, adapted, and modified tables and provide a credit line in the footnote.
- For footnotes use the following symbols, in this sequence: *, †, ‡, §, ‖,¶ , **, ††, ‡‡
- Tables with their legends should be provided at the end of the text after the references. The tables along with their number should be cited at the relevant place in the text

Illustrations (Figures)

- Upload the images in JPEG format. The file size should be within 1024 kb in size while uploading.
- Figures should be numbered consecutively according to the order in which they have been first cited in the text.
- Labels, numbers, and symbols should be clear and of uniform size. The lettering for figures should be large enough to be legible after reduction to fit the width of a printed column.
- Symbols, arrows, or letters used in photomicrographs

should contrast with the background and should be marked neatly with transfer type or by tissue overlay and not by pen.
- Titles and detailed explanations belong in the legends for illustrations not on the illustrations themselves.
- When graphs, scatter-grams or histograms are submitted the numerical data on which they are based should also be supplied.
- The photographs and figures should be trimmed to remove all the unwanted areas.
- If photographs of individuals are used, their pictures must be accompanied by written permission to use the photograph.
- If a figure has been published elsewhere, acknowledge the original source and submit written permission from the copyright holder to reproduce the material. A credit line should appear in the legend for such figures.
- Legends for illustrations: Type or print out legends (maximum 40 words, excluding the credit line) for illustrations using double spacing, with Arabic numerals corresponding to the illustrations. When symbols, arrows, numbers, or letters are used to identify parts of the illustrations, identify and explain each one in the legend. Explain the internal scale (magnification) and identify the method of staining in photomicrographs.
- Final figures for print production: Send sharp, glossy, un-mounted, color photographic prints, with height of 4 inches and width of 6 inches at the time of submitting the revised manuscript. Print outs of digital photographs are not acceptable. If digital images are the only source of images, ensure that the image has minimum resolution of 300 dpi or 1800 x 1600 pixels in TIFF format. Send the images on a CD. Each figure should have a label pasted (avoid use of liquid gum for pasting) on its back indicating the number of the figure, the running title, top of the figure and the legends of the figure. Do not write the contributor/s' name/s. Do not write on the back of figures, scratch, or mark them by using paper clips.
- The Journal reserves the right to crop, rotate, reduce, or enlarge the photographs to an acceptable size.

Protection of Patients' Rights to Privacy

Identifying information should not be published in written descriptions, photographs, sonograms, CT scans, etc., and pedigrees unless the information is essential for scientific purposes and the patient (or parent or guardian, wherever applicable) gives informed consent for publication. Authors should remove patients' names from figures unless they have obtained informed consent from the patients. The journal abides by ICMJE guidelines:

1. Authors, not the journals nor the publisher, need to obtain the patient consent form before the publication and have the form properly archived. The consent forms are not to be uploaded with the cover letter or sent through email to editorial or publisher offices.
2. If the manuscript contains patient images that preclude anonymity, or a description that has obvious indication to the identity of the patient, a statement about obtaining informed patient consent should be indicated in the manuscript.

Sending a revised manuscript

The revised version of the manuscript should be submitted online in a manner similar to that used for submission of the manuscript for the first time. However, there is no need to submit the "First Page" or "Covering Letter" file while submitting a revised version. When submitting a revised manuscript, contributors are requested to include, the 'referees' remarks along with point to point clarification at the beginning in the revised file itself. In addition, they are expected to mark the changes as underlined or colored text in the article.

Reprints and proofs

Journal provides no free printed reprints. Authors can purchase reprints, payment for which should be done at the time of submitting the proofs.

Publication schedule

The journal publishes articles on its website immediately on acceptance and follows a 'continuous publication' schedule. Articles are compiled in issues for 'print on demand' quarterly.

Copyrights

The entire contents of the Journal of the Anatomical Society of India are protected under Indian and international copyrights. The Journal, however, grants to all users a free, irrevocable, worldwide, perpetual right of access to, and a license to copy, use, distribute, perform and display the work publicly and to make and distribute derivative works in any digital medium for any reasonable non-commercial purpose, subject to proper attribution of authorship and ownership of the rights. The journal also grants the right to make small numbers of printed copies for their personal non-commercial use under Creative Commons Attribution-Noncommercial-Share Alike 4.0 Unported License.

Checklist

Covering letter

- Signed by all contributors
- Previous publication / presentations mentioned
- Source of funding mentioned
- Conflicts of interest disclosed

Authors

- Last name and given name provided along with Middle name initials (where applicable)
- Author for correspondence, with e-mail address provided
- Number of contributors restricted as per the instructions
- Identity not revealed in paper except title page (e.g. name of the institute in Methods, citing previous study as 'our study', names on figure labels, name of institute in photographs, etc.)

Presentation and format

- Double spacing
- Margins 2.5 cm from all four sides
- Page numbers included at bottom
- Title page contains all the desired information
- Running title provided (not more than 50 characters)
- Abstract page contains the full title of the manuscript
- Abstract provided (structured abstract of 250 words for original articles, unstructured abstracts of about 150 words for all other manuscripts excluding letters to the Editor)
- Key words provided (three or more)
- Introduction of 75-100 words
- Headings in title case (not ALL CAPITALS)
- The references cited in the text should be after punctuation marks, in superscript with square bracket.
- References according to the journal's instructions, punctuation marks checked
- Send the article file without 'Track Changes'

Language and grammar

- Uniformly American English
- Write the full term for each abbreviation at its first use in the title, abstract, keywords and text separately unless it is a standard unit of measure. Numerals from 1 to 10 spelt out
- Numerals at the beginning of the sentence spelt out
- Check the manuscript for spelling, grammar and punctuation errors
- If a brand name is cited, supply the manufacturer's name and address (city and state/country).
- Species names should be in italics

Tables and figures

- No repetition of data in tables and graphs and in text
- Actual numbers from which graphs drawn, provided
- Figures necessary and of good quality (colour)
- Table and figure numbers in Arabic letters (not Roman)
- Labels pasted on back of the photographs (no names written)
- Figure legends provided (not more than 40 words)
- Patients' privacy maintained (if not permission taken)
- Credit note for borrowed figures/tables provided
- Write the full term for each abbreviation used in the table as a footnote

Journal of
The Anatomical Society of India

Salient Features:

- Publishes research articles related to all aspects of Anatomy and Allied medical/surgical sciences.
- Pre-Publication Peer Review and Post-Publication Peer Review
- Online Manuscript Submission System
- Selection of articles on the basis of MRS system
- Eminent academicians across the globe as the Editorial board members
- Electronic Table of Contents alerts
- Available in both online and print form.

The journal is registered with the following abstracting partners:
Baidu Scholar, CNKI (China National Knowledge Infrastructure), EBSCO Publishing's Electronic Databases, Ex Libris – Primo Central, Google Scholar, Hinari, Infotrieve, Netherlands ISSN center, ProQuest, TdNet, Wanfang Data

The journal is indexed with, or included in, the following:
SCOPUS, Science Citation Index Expanded, IndMed, MedInd, Scimago Journal Ranking, Emerging Sources Citation Index.

Impact Factor® as reported in the 2022 Journal Citation Reports® (Clarivate Analytics, 2023): 0.4

Editorial Office:
Dr. Vishram Singh, Editor-in-Chief, JASI
B5/3 Hahnemann Enclave, Plot No. 40, Sector 6,
Dwarka Phase – 2, New Delhi - 110 075, India.
Email: editorjasi@gmail.com
(O) | Website: www.asiindia.in

The journal is owned and run by The Anatomical Society of India